Pathophysiological role of Pyk2 in the nervous system

Benoit De Pins

Thèse de doctorat - Sorbonne Université
Ecole doctorale Cerveau Cognition Comportement

Présentée par
Benoit de Pins

Pathophysiological role of Pyk2 in the nervous system

Soutenue le 12 septembre 2019

Devant le jury composé de :

Dr. Jocelyne Caboche	Présidente
Dr. Véronique Sgambato	Rapporteur
Dr. Emmanuel Valjent	Rapporteur
Pr. Jean-Christophe Corvol	Examinateur
Dr. Jean-Antoine Girault	Directeur de thèse

Acknowledgments

Ce manuscrit conclue quatre années de travail dans un environnement aussi riche qu'agréable, entouré de collègues qui sont finalement devenus mes amis. Il est normal que je le commence par un remerciement à tous ceux sans qui ce travail n'aurait pu être réalisé.

A vous tout d'abord Jean-Antoine, pour m'avoir reçu dans votre bureau il y a exactement cinq ans. Je suis très fier d'avoir été votre étudiant. Vous m'avez encadré tout en me donnant toujours beaucoup de liberté. J'ai aimé nos discussions et « faire de la science » avec vous.

Denis, merci pour tous les précieux conseils que tu m'as donnés au cours de ces cinq années. Merci pour ta gentillesse et ton accessibilité.

Je voudrais remercier tout particulièrement les Dr. Jocelyne Caboche, Dr. Véronique Sgambato, Dr. Emmanuel Valjent ainsi que le Pr. Jean-Christophe Corvol d'avoir accepté d'être membre de mon jury et de relire ce manuscrit.

Au 5ème étage : Merci les amis, j'ai passé cinq années formidables autour de vous. Vous allez tous beaucoup me manquer.

A mes amis, de Versailles, de prépa, de l'ENS, de Roscoff, de l'IFM : je me suis senti bien entouré pendant ces quelques années. Je sais à quel point je suis chanceux de vous connaitre.

Papa, Maman, Ronan, Solène, Amicie, Peyo, Antoine, Pierre, Olivier, Gilles, Chantal, Xavier, Christine et toute la famille, merci pour votre présence et votre soutien quotidiens. Je vous aime très fort.

A toi Albert, bien évidemment, un énorme merci. Sans toi, tout cela n'est rien. Merci de m'avoir fait rentrer dans ton monde. Ens tornarem a trobar !

Enrica, je termine évidemment par toi. Tu sais déjà tout, merci beaucoup.

Contents

List of abbreviations

AAV-Cre	Cre-expressing adeno-associated virus
AD	Alzheimer's disease
APP	amyloid precursor protein
ArgBP2	Arg kinase binding protein 2
ASAP2	ArfGAP with SH3 domain, ankyrin repeat and PH domain 2
ATP	adenosine triphosphate
Aβ	amyloid β peptide
Aβo	Aβ oligomers
BDNF	brain-derived neurotrophic factor
BK	"big potassium" large conductance voltage-gated K^+ channel
BY-kinase	bacterial tyrosine kinase
CADTK	calcium dependent-protein tyrosine kinase
CAKβ	cell adhesion kinase-β
cAMP	3',5'-cyclic adenosine monophosphate
CSPG	chondroitin sulphate proteoglycan
CUMS	chronic unpredictable mild stress
DHPG	(S)-3,5-dihydroxy-phenylglycine
DNA	deoxyribonucleic acid
EGFR	epidermal growth factor receptor
eNOS	endothelial nitric oxide synthase
EOAD	early onset AD
ePK	eukaryotic protein kinase
ERK	extracellular signal-regulated kinase
FAK	focal adhesion kinase
FAT	focal adhesion targeting
FERM	four-point-one, ezrin, radixin, moesin
FIP200	FAK family kinase-interacting protein of 200 kDa
FNRK	FAK-related non-kinase
GluN2A	NMDAR subunit 2A
GWAS	genome-wide association studies
HD	Huntington's disease
HTT	huntingtin (human gene)
Htt	huntingtin (protein)
JNK	c-Jun NH2-terminal kinase
KIR	kinase inhibitory region
LOAD	late onset AD
LTP	long-term potentiation
LTP-IE	long-term potentiation of intrinsic excitability
MAPK	mitogen activated protein kinase
MAP4K4	mitogen-activated protein kinase kinase kinase kinase 4
MECP2	methyl-CpG-binding protein 2
MKK3	mitogen-activated protein kinase kinase 3
mGluR5	metabotropic glutamate receptor 5
mRNA	messenger RNA
NAc	nucleus accumbens

NAPOR	neuroblastoma apoptosis-related RNA-binding protein
NES	nuclear export signal
NLS	nuclear localization sequence
NMDAR	NMDA receptor
nRTK	non-receptor tyrosine kinases
NTS	nuclear targeting sequence
PARP	poly(adenosine diphosphate ribose)polymerase
PD	Parkinson's disease
PDGFR	platelet-derived growth factor receptor
PITPNMs	membrane-associated phosphatidylinositol transfer proteins
PKC	protein kinase C
PR	proline-rich
PRAP	proline-rich acidic protein
PRNK	Pyk2-related non-kinase
PrPc	prion protein cellular precursor
Prx2	peroxiredoxin 2
PSTPs	protein serine-threonine phosphatases
PTP	protein tyrosine phosphatase
pTyr	phosphotyrosine
Pyk2	proline-rich tyrosine kinase 2
RAFTK	related adhesion focal tyrosine kinase
RB1CC1	retinoblastoma 1-inducible coiled-coil 1
RNA	ribonucleic acid
ROS	reactive oxygen species
RTK	receptors having a tyrosine kinase activity
SAP102	synapse-associated protein 102
SFKs	Src-family kinases
SH2	Src homology 2
SH3	Src homology 3
SNP	single nucleotide polymorphism
SPN	striatal projection neuron
STEP	striatal-enriched protein-tyrosine phosphatase
STK	serine/threonine kinase
TK	tyrosine kinases
TRPM2	transient receptor potential melastatin 2

Context and objectives

Protein function regulation by phosphorylation is implicated in the great majority of cellular processes in eukaryotes, and to a lesser extent in prokaryotes. Regulatory phosphorylation of proteins is a post-translational modification in which a phosphoryl group is transferred from a donor, usually adenosine triphosphate (ATP), to the substrate, a residue of an amino acid: either serine, threonine or tyrosine in metazoans. Protein phosphorylation is a reaction catalyzed by protein kinases, usually reversible due to the action of protein phosphatases which catalyze dephosphorylation. Protein kinases and phosphatases contribute to the cellular adaptation to the environment in response to extra and intra-cellular signals and often act as integrators.

Genes coding for protein kinases represent about 2% of eukaryotes protein coding genes and embody one of the major classes. Protein kinases and protein phosphatases are both comprised of different families. In the human, on the ~540 genes coding for protein kinases, 90 code for "real" tyrosine kinases (TK) of which 32 are non-receptor tyrosine kinases (nRTK) and 58 are transmembrane receptors having a tyrosine kinase activity (RTK) (Manning et al., 2002b; Wilson et al., 2018). Our laboratory is particularly interested in the nRTK group named focal adhesion kinase (FAK) family containing only two members: FAK and the proline-rich tyrosine kinase 2 (Pyk2).

FAK and Pyk2 share roughly 45% amino acid sequence identity and 65% similarity (Avraham et al., 1995, 2000; Sasaki et al., 1995) but display very distinct expression patterns. Two products of alternative splicing characterized by the presence or absence of an alternative exon were described for Pyk2. The variant lacking this exon is highly expressed in hematopoietic cells whereas the complete form is enriched in the brain. Pyk2 has a key role in numerous cellular physiological and pathological processes such as cell migration, proliferation, survival and death. In the nervous system, it could participate in learning and memory. The major step initiating Pyk2 activation is its autophosphorylation on Tyr-402. This phosphorylation allows the recruitment and the activation of Src family members, the phosphorylation of other residues of Pyk2 and the recruitment of other partners leading to the activation of several pathways.

Works of many laboratories, including ours, have shown that Pyk2 is involved in NMDA receptor regulation and synaptic plasticity in the hippocampus, suggesting maybe a participation of Pyk2 in neurological diseases. However, Pyk2 function remains unclear and the mechanism of action of Pyk2 is still poorly understood. The objective of my thesis was to clarify the role of Pyk2 in the central nervous system and its implication in several neurological pathologies.

We studied the involvement of Pyk2 in cognitive deficits associated to Huntington's disease (**Article 1**). We also investigated a putative role of Pyk2 in the resilience of mice to a model of depression (**Article 2**) and in a mouse model of Alzheimer's disease (AD) (**Article 3**). In parallel with this last study, we used the same mouse model of AD to investigate the potential benefit of astrocyte-targeted delivery of BDNF in this disease (**Article 4**). We finally characterized the expression of Pyk2 in the striatum and its role in cocaine response (**Article 5**, submitted).

In the bibliographic introduction, I will address several topics associated to my subject: the presentation of FAK family kinases, the characterization of Pyk2, and the specific role of Pyk2 in the central nervous system.

INTRODUCTION

I. Tyrosine kinase signaling and the FAK family

In animals, phosphotyrosine (pTyr) signaling is an essential system that regulates hormone, growth factor, immune, and adhesion-based signaling, therefore allowing cell-cell communication (Hunter and Cooper, 1981; Shattil and Brugge, 1991; Myers et al., 1994; Weiss and Littman, 1994).

This signaling relies on a simple mechanism: a TK phosphorylates certain tyrosine residues on the substrate protein (or itself). Then, an effector protein recognize the pTyr by its Src homology 2 (SH2) domain or other pTyr-binding domains, and activates downstream signaling. The pathway can be stopped by a protein tyrosine phosphatase (PTP) which dephosphorylates the pTyr (**Figure 1**).

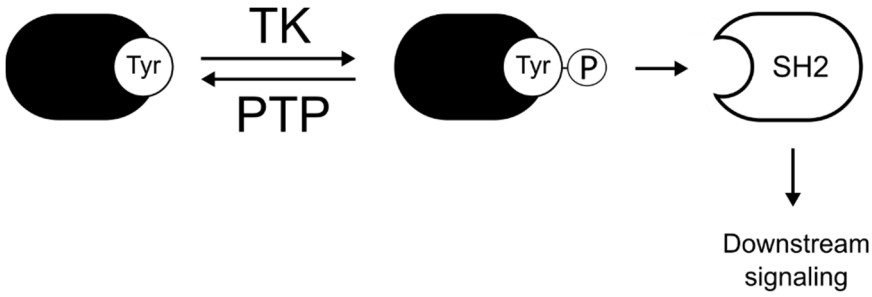

Figure 1. Mechanism of TK signaling. Tyrosines are phosphorylated by TKs and dephosphorylated by PTPs. The phosphorylated tyrosine is then recognized by an SH2-containing effector.

1. The origin of TKs and FAK family

The eukaryotic protein kinase (ePK) superfamily is divided into two kinase families according to their substrate specificity: the TKs and the serine/threonine kinases (STKs) families. TKs originally evolved from STKs. Although some STKs can phosphorylate tyrosine residues and are referred to as dual specificity protein kinases (Lindberg et al., 1992), TKs are discriminated from STKs by their overall sequence similarity and also notably by their characteristic catalytic loop motif (Hanks and Hunter, 1995; Manning et al., 2008).

The evolutionary history of TK family has been specifically studied and discussed for many years (Miller, 2012; Tong et al., 2017). It was initially believed that tyrosine kinases were specific to metazoans. In contrast with the high diversity of TKs in many metazoan phyla, they were initially not found in plants, fungi and other analyzed eukaryotes (Hanks and Hunter, 1995; Manning et al., 2002a). Although some bacteria evolved unique tyrosine kinases known as bacterial tyrosine kinases (BY-kinases), metazoan-like TKs were not found in bacteria (Grangeasse et al., 2012). Accordingly, TK were hypothesized to be a metazoan-specific evolutionary innovation that permitted cell-cell communication and thus contributed to the origin of metazoan multicellularity.

However, in 2001, King and Carroll discovered the first TK (a receptor tyrosine kinase designated MBRTK1) outside of the metazoan taxon (King and Carroll, 2001). This TK was found in *Monosiga brevicollis*, a unicellular member of choanoflagellates that are the closest known living relatives of metazoans (Richter and King, 2013). Successive papers

then confirmed the existence of multiple active tyrosine kinases in this organism (King et al., 2003) and in several other choanoflagellate species (Segawa et al., 2006; Suga et al., 2008).

Genomic analyses then revealed that choanoflagellates contain a rich and complex repertoire of TKs that is comparable to those observed in the most complex multicellular animals (King et al., 2008; Manning et al., 2008; Pincus et al., 2008). Many choanoflagellates can form colonies, suggesting that their common ancestor with the metazoan could be a transitional form between unicellular and multicellular organisms and that these unicellular tyrosine kinases may have facilitated the evolution of multicellular animals (King, 2004).

Afterward, new genome/transcriptome sequencing has uncovered TKs in other eukaryotes thus forcing to reconsider every time the apparition date of TKs during evolution. In this way, in addition to the metazoans and the choanoflagellates, tyrosine kinases were discovered in three other sister lineages: the filastereans, the ichthyosporeans and the corallochytreans (forming, with the metazoans and the choanoflagellates, the holozoans) (Shalchian-Tabrizi et al., 2008; Suga et al., 2012, 2014; Fairclough et al., 2013; Sebé-Pedrós et al., 2016). TKs were also found in two amoebozoans (Clarke et al., 2013; Schaap et al., 2015) and in the apusozoan *Thecamonas trahens* (Suga et al., 2012). Moreover, TKs were discovered in some bikonts such as the green alga *Chlamydomonas reinhardtii* or the higher plants *Arabidopsis thaliana* and *Oryza sativa* (Shiu and Li, 2004; Miranda-Saavedra and Barton, 2007; Kerk et al., 2008; Wheeler et al., 2008) but also the oomycete *Phytophthora infestans* (Shiu and Li, 2004; Judelson and Ah-Fong, 2010). Nevertheless and so far, TKs were not found in the non-holozoan opistokonts (the fungi (Shiu and Li, 2004; Miranda-Saavedra and Barton, 2007; Suga et al., 2012, 2014), and the fungi relatives cristidiscoideans (Suga et al., 2014)), and in many other species (Shiu and Li, 2004; Miranda-Saavedra and Barton, 2007; Suga et al., 2008; Liu et al., 2011; Clarke et al., 2013) (**Figure 2**).

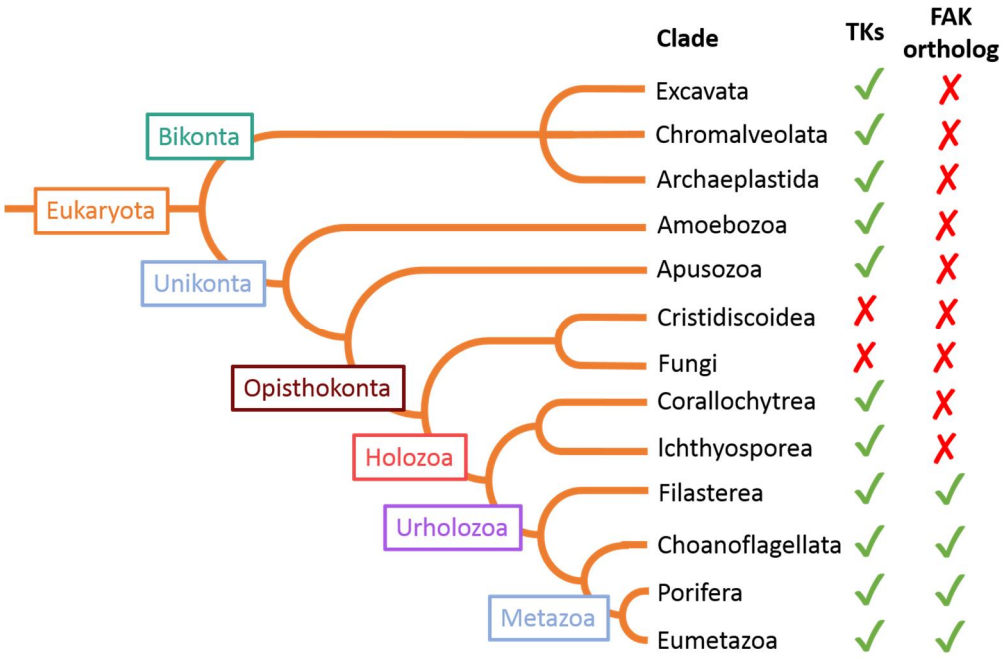

Figure 2. Distribution of tyrosine kinases and FAK family within eukaryotic evolution. The branches in the phylogenetic tree are not proportional to the divergence time. Presence or absence of tyrosine kinases or FAK orthologs in a clade is marked by a green tick or a red cross respectively.

One can thus hypothesize that the appearance of TKs dates back up to the beginning of eukaryotic evolution and that some species then lost these enzymes (Shiu and Li, 2004;

Miranda-Saavedra and Barton, 2007; Kerk et al., 2008; Wheeler et al., 2008; Schaap et al., 2015). However, one cannot exclude absolutely the possibility of multiple independent appearance of TKs or eventually some horizontal gene transfers. In any case, the prime hypothesis of a phosphotyrosine signaling at the origin of metazoan multicellularity is invalidated by these recent findings. Nevertheless, it is worth noting that the number of TKs underwent a great expansion in the holozoans (Manning et al., 2008; Suga et al., 2012, 2014; Fairclough et al., 2013; Sebé-Pedrós et al., 2016) suggesting a more prominent role of phosphotyrosine signaling in this monophyletic group. This expansion is the result of several gene duplications and domain shuffling (Shiu and Li, 2004; Suga et al., 2008, 2012, 2014; Liu et al., 2011; Jin and Pawson, 2012; Liu and Nash, 2012) and, as reviewed in Tong et al., it was certainly allowed by the fact that holozoan pTyr signaling had little cross-interference with pre-existing signaling systems such as pSer/Thr signaling and had therefore liberty to evolve novel functions (Tong et al., 2017).

Within holozoan lineage, a central set of TK families rapidly arose and remained conserved throughout the evolution. Among them, orthologs of the focal adhesion kinase (FAK) family have been discovered in filastereans and choanoflagellates but not in more evolutionary-distant clades (Sebe-Pedros et al., 2010; Fairclough et al., 2013; Suga et al., 2014) (**Figure 2**). This suggests an urholozoan origin of the FAK family.

However, the appearance of paralogs within FAK family seems to have occurred early in the vertebrate lineage. FAK family is composed of FAK and the proline rich kinase 2 (Pyk2) sharing together around 45% amino acid identity. Sequence alignments from different species suggests that gene duplication leading to the appearance of FAK and Pyk2 occurred after the urochordate branch and is consequently specific to vertebrates (Corsi et al., 2006) (**Figure 3**). Besides, the aforementioned alignments showed that FAK genes are more closely related to the common unique ancestor than Pyk2 genes. This gives rise to the idea that Pyk2 probably underwent less evolutionary pressures and had thus more possibilities to evolve.

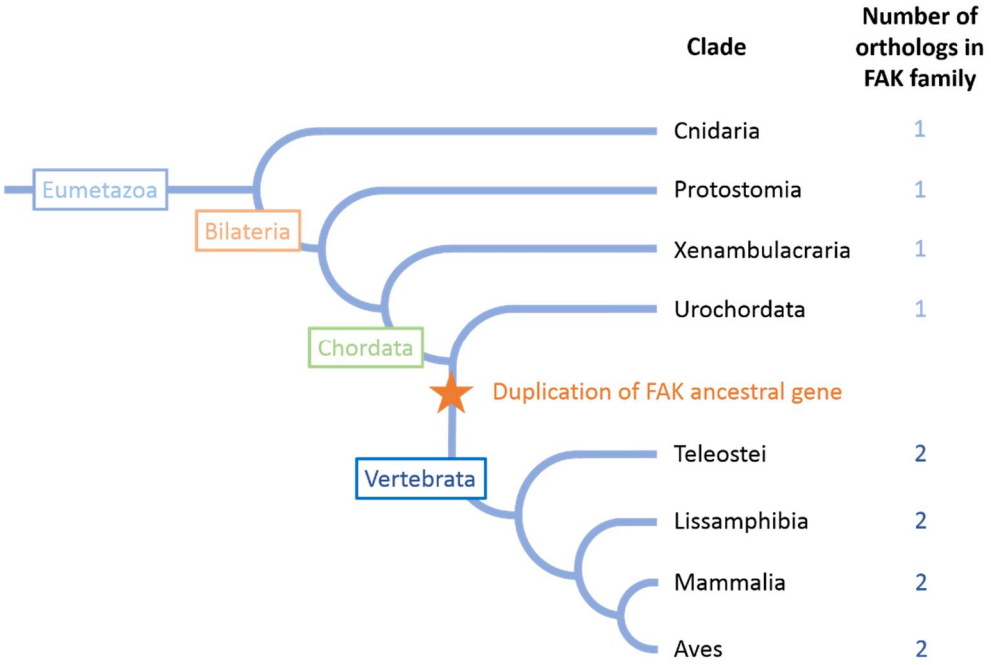

Figure 3. Evolution of FAK family within eumetazoan clade. The branches in the phylogenetic tree are not proportional to the divergence time. The dendrogram summarizes the results obtained in Corsi et al., 2006.

2. FAK family

2.1. Identification of FAK family kinases

FAK was first identified in the beginning of the 90's as a 120-kDa protein that is phosphorylated on tyrosine in cells attached to fibronectin-coated surfaces (Guan et al., 1991). It was then cloned independently by two laboratories from chicken embryo cells infected with v-Src (Schaller et al., 1992) and by sequence homology in mouse (Hanks et al., 1992). As its name implies, FAK is located to focal adhesions which are interaction sites mediated by integrins, between extracellular matrix and actin cytoskeleton through the plasma membrane (Carragher and Frame, 2004). FAK was then cloned in multiples vertebrate and invertebrate species including human (Whitney et al., 1993), xenope (Hens and DeSimone, 1995; Zhang et al., 1995), zebrafisch (Henry et al., 2001; Crawford et al., 2003), sea urchin (García et al., 2004) and drosophila (Fox et al., 1999; Fujimoto et al., 1999; Palmer et al., 1999).

Pyk2 (Lev et al., 1995), also known as cell adhesion kinase-β (CAKβ) (Sasaki et al., 1995), calcium dependent-protein tyrosine kinase (CADTK) (Yu et al., 1996) or related adhesion focal tyrosine kinase (RAFTK) (Avraham et al., 2000) was initially described in PC12 cells as an nRTK activated by cytosolic calcium increase and stimulation of protein kinase C (PKC) (Lev et al., 1995). These two signaling pathways can be, in some case, independently activated by the same stimulus but can have an additive effect on Pyk2 activation (Brinson et al., 1998). As mentioned above, Pyk2 is a vertebrates-specific protein.

2.2. Structure of FAK family kinases

FAK and Pyk2 are composed of three conserved domains (**Figure 4**): an amino-terminal four-point-one, ezrin, radixin, moesin (FERM) domain, a central kinase domain and carboxy-terminal focal adhesion targeting (FAT) domain (Girault et al., 1999b; Lipinski and Loftus, 2010; Hall et al., 2011; Walkiewicz et al., 2015). These three domains are connected by two linker regions which contain proline-rich (PR) motifs. Unlike many nRTKs, neither FAK nor Pyk2 encompass Src-homology domains 2 and 3 (SH2 and SH3). FERM and FAT domains both contribute to the regulation of the enzymatic activity of FAK and Pyk2 and allow their interaction with many proteins playing a key role in signal transduction.

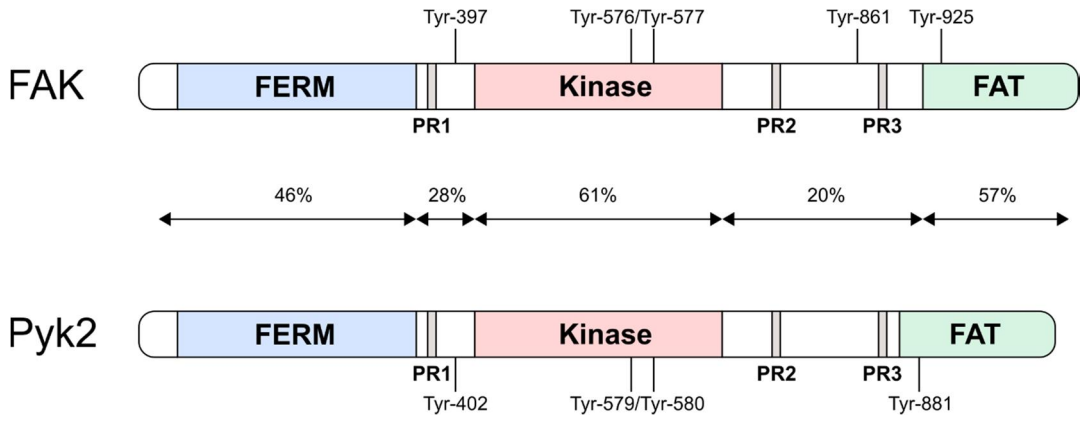

Figure 4. Comparison of human FAK and Pyk2 structures. FERM, kinase, FAT and PR domains, as well the main phosphorylated tyrosines are indicated. Percentages of identity (aminoacids) of each domain are specified.

2.2.1. FERM domain

FERM domains are roughly 300 amino-acids domains commonly found in proteins that bind cytoplasmic regions of transmembrane proteins and often act as linker between the cytoskeleton and plasma membrane (Chishti et al., 1998; Girault et al., 1999b; Riggs et al., 2011). Besides, FERM domains can also mediate intramolecular interactions. For instance, the functional activity of the prototypical FERM domain proteins ezrin, radixin, and moesin is regulated by FERM domain mediated intramolecular associations (Pearson et al., 2000; Edwards and Keep, 2001).

The FERM domain has three lobes, namely: F1, F2 and F3, together forming a cloverleaf-shaped structure that mediates both protein-membrane targeting as well as protein-protein interactions (**Figure 5**). It is worth noting FAK FERM domain shares only 12–15% identity with the sequences of other FERM domains but they adopt a quite similar tertiary structure as shown by hydrophobic cluster analysis (Girault et al., 1999b).

FERM proteins are targeted to the membrane due to the interaction between basic residues in a cleft between subdomains F1 and F3 and PIP2 (Hirao et al., 1996; Hamada et al., 2000). This interaction further induces conformational changes of FERM proteins that would stimulate their interaction with the cytoplasmic tails of transmembrane proteins (Hamada et al., 2003).

The FERM domain also appears be a domain of interaction with various cytosolic and nuclear proteins. Among them, the three membrane-associated phosphatidylinositol transfer proteins (PITPNMs), a family of protein associated with metastasized cancers, interact with the FERM domain of Pyk2 but not FAK (Lev et al., 1999). In contrast, the transcription factor p53 was shown to interact with the FERM domain of both FAK (Golubovskaya and Cance, 2011) and Pyk2 (Lim et al., 2010). The mitogen-activated protein kinase kinase kinase kinase 4 (MAP4K4) was shown to interact with the FERM domain of Pyk2 but not of FAK (Loftus et al., 2013).

Another function of the FERM domain is a potential autoregulatory role due to interactions with the kinase domain. This autoinhibitory interaction has been described in FAK (Lietha et al., 2007), and also, more recently, in Pyk2 (Loving and Underbakke, 2019). Moreover, in both FAK and Pyk2, the FERM domain is supposed to be mandatory for the activation-induced homodimerization (Kohno et al., 2008; Riggs et al., 2011; Brami-Cherrier et al., 2014).

Finally, a nuclear localization sequence (NLS) and a nuclear export signal (NES) were found in the F2 and F1 subdomain respectively of both FAK and Pyk2 showing a particular standing of this region for FAK family kinases nucleocytoplasmic shuttling (Lim et al., 2008a; Ossovskaya et al., 2008).

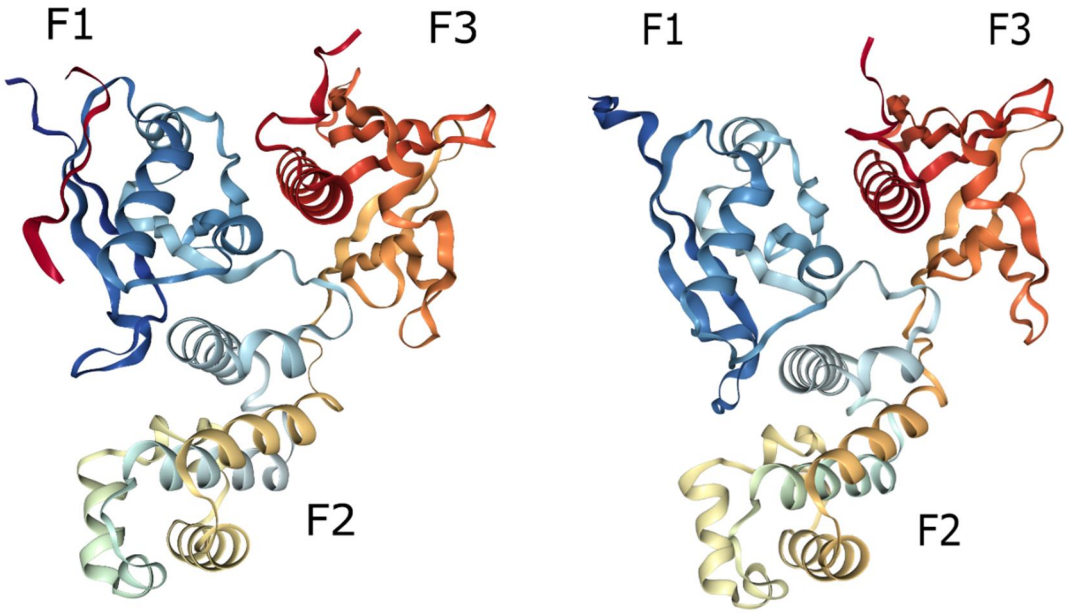

Figure 5. Cartoon structure of FAK (left) and Pyk2 (right) FERM domain. FAK FERM structure was taken from Ceccarelli et al., 2006. Pyk2 FERM structure was taken from PDB ID: 4EKU Savarimuthu et al.

2.2.2. Linker 1

The FERM domain of FAK family kinases is followed by a linker of approximately 70 aminoacids which precedes the kinase domain. This sequence is poorly conserved with the exception of PR1 and the Tyr-397/Tyr-402 (FAK /Pyk2) whose phosphorylation plays a key role in the activation of FAK and Pyk2 and in the recruitment of Src-family kinases (SFKs) (Dikic et al., 1996; Hall et al., 2011). Indeed, this recruitment is based on a two-point interaction between: 1. the SH2 domain of the SFK and the phospho-tyrosine (pTyr-397 of FAK/pTyr-402 of Pyk2) 2. The SH3 domain of the SFK and the PR1 of FAK/Pyk2 (Schaller et al., 1994; Thomas et al., 1998; Arold et al., 2001).

In FAK specifically, this linker also contains the Tyr-407, which phosphorylation was shown to negatively regulate FAK activity (Lim et al., 2007).

2.2.3. Kinase domain

The central region is the kinase domain which is highly conserved between FAK and Pyk2 (Sasaki et al., 1995). This domain adopts a typical bi-lobal structure, very similar to that of other kinase domains, surrounding the catalytic site and the ATP binding pocket (Han et al., 2009) (**Figure 6**). The N-lobe contains a five-stranded beta-sheet and one alpha-helix whereas the C-lobe is mainly composed of alpha-helixes and the activation loop. Phosphorylation of Tyr-579 and Tyr-580 (Tyr-576 and Tyr-577 for FAK) within this activation loop is crucial to maximize Pyk2 kinase activity.

This kinase domain was also shown to interact directly with the retinoblastoma 1-inducible coiled-coil 1 (RB1CC1) which is supposed to be an inhibitor of Pyk2 kinase activity (Ueda et al., 2000).

Moreover, a NES was found in the C-lobe of both FAK and Pyk2 suggesting an unexpected role of the kinase domain in nucleocytoplasmic shuttling of FAK family kinases (Ossovskaya et al., 2008).

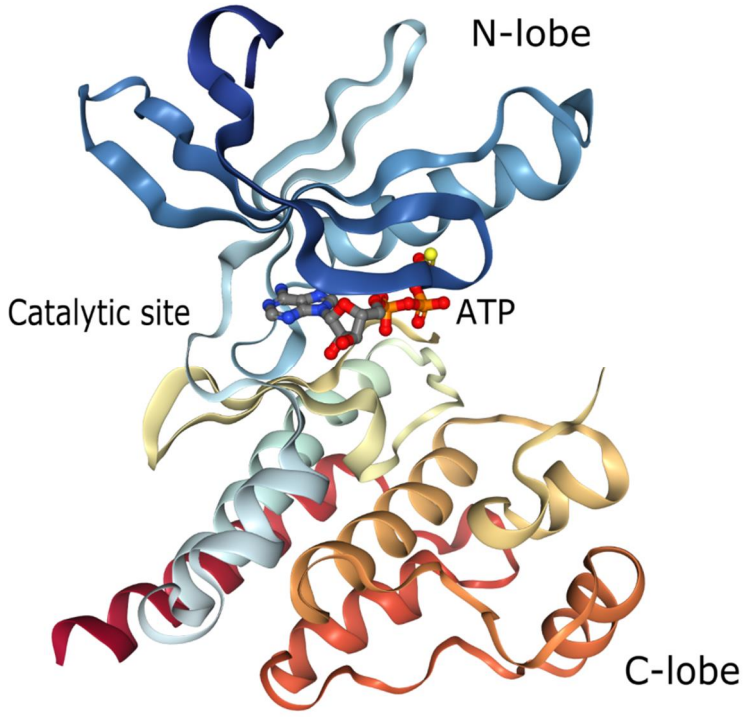

Figure 6. Cartoon structure of Pyk2 kinase domain co-crystalized with ATPgS. (From Han et al., 2009a).

2.2.4. Linker 2

The linker 2 is located between the kinase domain and the FAT domain. This sequence contains two PR sequences, named PR2 (residues 713 to 720 in Pyk2) and PR3 (residues 855 to 860, ibid.), that mediate the interaction of Pyk2 with a number of SH3 domain-containing proteins that also interact with FAK such as p130Cas (Astier et al., 1997; Xiong et al., 1998; Lakkakorpi et al., 1999), SAPAP3, and Graf (Ohba et al., 1998; Xiong et al., 1998). More specifically in Pyk2, these PR sequences were also shown to interact with PSD-95 (Seabold et al., 2003), synapse-associated protein 102 (SAP102) (Seabold et al., 2003), ArfGAP with SH3 domain, ankyrin repeat and PH domain 2 (ASAP2) (Andreev et al., 1999), Arg kinase binding protein 2 (ArgBP2) (Haglund et al., 2004), nephrocystin (Benzing et al., 2001) and proline-rich acidic protein (PRAP) (Takahashi et al., 2003).

Additionally, a NES and a nuclear targeting sequence (NTS) were found in the linker 2 of Pyk2, playing an important role in subcellular trafficking of Pyk2 (Faure et al., 2013).

2.2.5. FAT domain

The C-terminal FAT domain of FAK family kinases is highly conserved between Pyk2 and FAK. It exhibits an anti-parallel four-helix bundle structure in both FAK (Hayashi et al., 2002; Liu et al., 2002) and Pyk2 (Lulo et al., 2009) (**Figure 7**). In FAK, this domain is consubstantially linked to focal adhesion targeting (Hildebrand et al., 1993; Shen and Schaller, 1999). It was reported to interact with talin (Chen et al., 1995) and paxillin (Tachibana et al., 1995; Brown et al., 1996), two proteins highly enriched in focal adhesions. Conversely, Pyk2 FAT domain was shown to interact with paxillin (Lulo et al., 2009) but not talin (Zheng et al., 1998). Moreover, it was demonstrated that the binding mechanism between Pyk2 and FAK for paxillin was different and that paxillin thus formed a much

more stable complex with the FAT domain of FAK than with the FAT domain of Pyk2 (Vanarotti et al., 2014). Instead of paxillin, Pyk2 FAT domain showed a preferential interaction with some proteins from the same paxillin superfamily such as leupaxin (Vanarotti et al., 2016) or the molecular scaffold and transcription co-regulator Hic-5 (Matsuya et al., 1998). These differences between FAK and Pyk2 perhaps explain why only a small proportion of Pyk2 is localized in focal contacts in most cell types.

Moreover, the FAT domain of FAK and Pyk2 associates with gelsolin, an actin binding protein, showing a common regulatory role of FAK and Pyk2 in actin cytoskeleton organization (Wang et al., 2003; Chan et al., 2009). Finally, within the FAT domain, Tyr-925 in FAK and Tyr-881 in Pyk2, when phosphorylated by Src, constitute a binding site for the adaptor Grb2 leading to the initiation of the MAP kinase signaling pathway (Schlaepfer and Hunter, 1996; Blaukat et al., 1999). In Pyk2, this phosphorylated tyrosine was also reported to be an anchoring site for the oncogenic TK c-Abl (Zrihan-Licht et al., 2004).

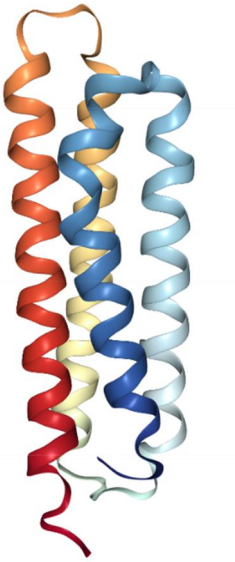

Figure 7. Cartoon structure of Pyk2 FAT domain. (From Lulo et al. 2009).

The structural differences between FAK and Pyk2 highlighted in this part constitute a basis for the explanation of the many differences between these two proteins.

2.3. Expression of FAK and Pyk2

FAK and Pyk2 are encoded by *PTK2* and *PTK2B* genes, respectively, in humans (*Ptk2* and *Ptk2b* in mice). These genes are localized, in human, on chromosome 8 and, in mouse, on chromosomes 15 and 14 respectively (Fiedorek and Kay, 1995; Herzog et al., 1996). Their regulation mechanisms are not well understood yet. However, FAK promotor characterization allowed to highlight regulations by several transcription factors. FAK transcription is positively regulated by NF-κB and N-Myc, and negatively regulated by p53 (Golubovskaya et al., 2004; Beierle et al., 2007). FAK is ubiquitously expressed during development and in the adult (Hanks et al., 1992; André and Becker-André, 1993; Furuta et al., 1995; Ilic et al., 1995; Kanazawa et al., 1995; Zachary, 1997). The highest expression of FAK is observed in the brain, lung, testis and osteoclasts (Hanks et al., 1992; André and Becker-André, 1993; Barry and Critchley, 1994; Burgaya et al., 1995; Grant et al., 1995).

In fetus, Pyk2 is mostly, although modestly, expressed in the brain. In adult, it is expressed in the brain but also in the lung, kidney, spleen and thymus (Avraham et al., 1995; Sasaki et al., 1995; Menegon et al., 1999). In adult brain, Pyk2 is mainly concentrated in forebrain neurons but it is also present in astrocytes (Cazaubon et al., 1997) and microglial cells (Combs et al., 1999; Tian et al., 2000).

2.4. Cellular localization of FAK family kinases

In adhering non-neuronal cells, FAK is located in focal adhesions which are sub-cellular complexes forming mechanical links between intracellular actin bundles and the extracellular matrix (Schaller et al., 1992). Pyk2 is essentially located in the perinuclear region (Sieg et al., 1998; Avraham et al., 2000) but can be found, to a lesser extent than FAK, in focal adhesions (Du et al., 2001).

In neurons, FAK is enriched is cellular body, growth cones and dendrites (Renaudin et al., 1999). Moreover, FAK can be enriched along perinuclear microtubules associated to centrosomes (Xie et al., 2003). In neurons, Pyk2 is enriched in cell body and dendritic shafts (Menegon et al., 1999; Corvol et al., 2005).

However, FAK and Pyk2 can also shuttle to the nucleus. Indeed, FAK was observed in the nucleus of cardiomyocytes under some pathological conditions (Lobo and Zachary, 2000; Yi et al., 2003). Pyk2 was also observed in the nucleus of various cell types including keratinocytes (Schindler et al., 2007), chondrocytes (Arcucci et al., 2006), and in depolarized neurons or PC12 cells (Faure et al., 2007). The dynamic of nucleocytoplasmic shuttling of FAK and Pyk2 results from the presence of multiple regulatory sequences detailed above. For instance, in the case of Pyk2, it was shown that the NES located on linker 2 was regulated by phosphorylation at residue Ser-778, a substrate of 3',5'-cyclic adenosine monophosphate (cAMP)-dependent protein kinase and calcineurin, a Ca^{2+}/calmodulin-activated protein phosphatase. The detailed mechanism of this regulation will be discussed in III.1.2.

2.5. Isoforms of FAK family kinases

Both FAK and Pyk2 present various isoforms resulting from alternative splicing of their messenger ribonucleic acid (mRNA) or from alternative transcription initiation sites (**Figure 8**).

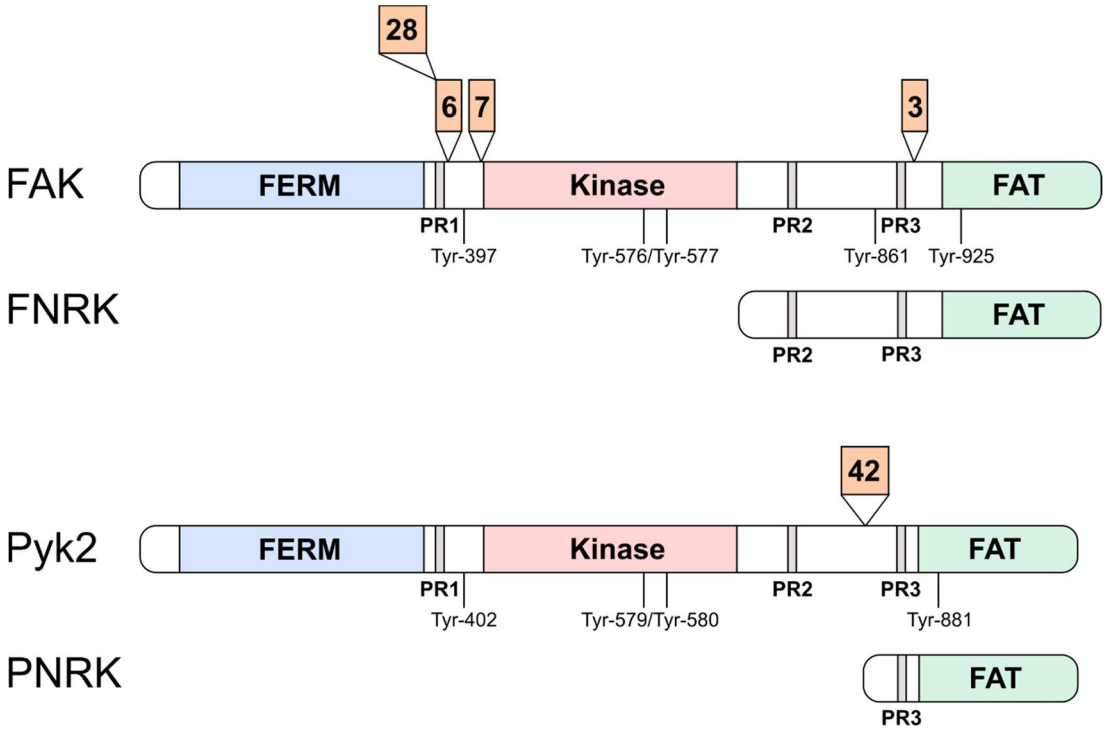

Figure 8. FAK and Pyk2 isoforms.

2.5.1. FAK isoforms

To date, FAK possesses four additional peptides (called boxes) which can be included or not to the sequence and are named according to the number of aminoacids contained in the box: box 28, box 6, box 7 and box 3 (or PWR, based on the single letter amino acid code for three residues of this box, Pro, Trp, and Arg; FAK isoform containing this exon is termed FAK^{+}).

These inserts provide biological differences between isoform. Besides, every isoform present a specific expression pattern. For instance the isoform containing the boxes 3, 6 and 7 (called $FAK^{+6,7}$) is predominant in neurons (Burgaya et al., 1997).

Moreover, FAK gene possesses a second promotor located in the intron following the last exon coding for the catalytic domain. Expression of the C-ter domain from this promotor produces the so-called FAK-related non-kinase (FNRK). This variant is an in vitro inhibitor of FAK as it competes with FAK for the localization to focal adhesions by its intact FAT domain (Schaller, 2010). FRNK was shown to have physiological functions. Increased expression of FRNK prevented metastatic adhesion of hepatocellular carcinoma cells (von Sengbusch et al., 2005). Moreover, FRNK negatively regulates IL-4-mediated inflammation by attenuating eosinophil recruitment in a way that seems independent of FAK pathway (Sharma et al., 2015).

2.5.2. Pyk2 isoforms

Pyk2 has an isoform lacking 42 amino acids in the linker 2 (Dikic et al., 1998; Xiong et al., 1998; Keogh et al., 2002; Kacena et al., 2012). This isoform, called Pyk2-H (hematopoietic) or Pyk2-S (short), is abundantly expressed in hematopoietic cells where it is implied in cell response to some chemokines.

As for FAK, another isoform of Pyk2 results from the expression of the C-terminal domain only and is termed Pyk2-related non-kinase (PRNK) (Xiong et al., 1998). This variant also inhibits Pyk2 function and was tested for this reason in many experiments. Thus, exogenous expression of PRNK could prevent myocardial fibrosis (You et al., 2015), impair CD11b/CD18-mediated phagocytosis in macrophages (Paone et al., 2016), and could reduce squamous carcinoma cells viability, migration, invasiveness and adhesion ability (Yue et al., 2015). However, PRNK may act as an inhibitor of Pyk2 only in some cell types as it does not interact with the Pyk2 partner p130Cas or Graf (Xiong et al., 1998).

Finally, Arcucci et al discovered a nuclear fragment of Pyk2 of 68 kDa in chick embryo epiphyseal chondrocytes which is not recognized by an antibody raised against the N-terminal region of Pyk2 suggesting that this fragment lacks the N-terminal region (Arcucci et al., 2006). However, neither the mechanism of formation of this fragment nor its biological function is known.

2.6. Biological functions of FAK

2.6.1. Cellular functions of FAK

Among the adhesion sites mediated by integrins, the focal adhesions are long flat structures often located in the periphery of cells (Sastry and Burridge, 2000). They are mainly composed of integrin, paxillin, vinculin, talin and FAK.

Upon engagement of integrins by extracellular matrix, FAK is recruited to the focal adhesions and rapidly phosphorylated on tyrosine (Hanks et al., 1992; Kirchner et al., 2003; Zaidel-Bar et al., 2003). Activated FAK can interact with Src which phosphorylate many partners such as α-actinin which then recruits vinculin and regroups the actin bundles to the focal adhesions (Mitra et al., 2005) (**Figure 9**). $FAK^{-/-}$ fibroblasts have reduced and immature focal adhesions with a default of binding to the actin bundles showing that FAK is essential to the function of these structures (Ilić et al., 1995; Katoh, 2017). Particularly, loss of FAK results in the persistence of old focal adhesions and in the inability to form new ones showing the importance of FAK in focal adhesion turnover (Ren et al., 2000).

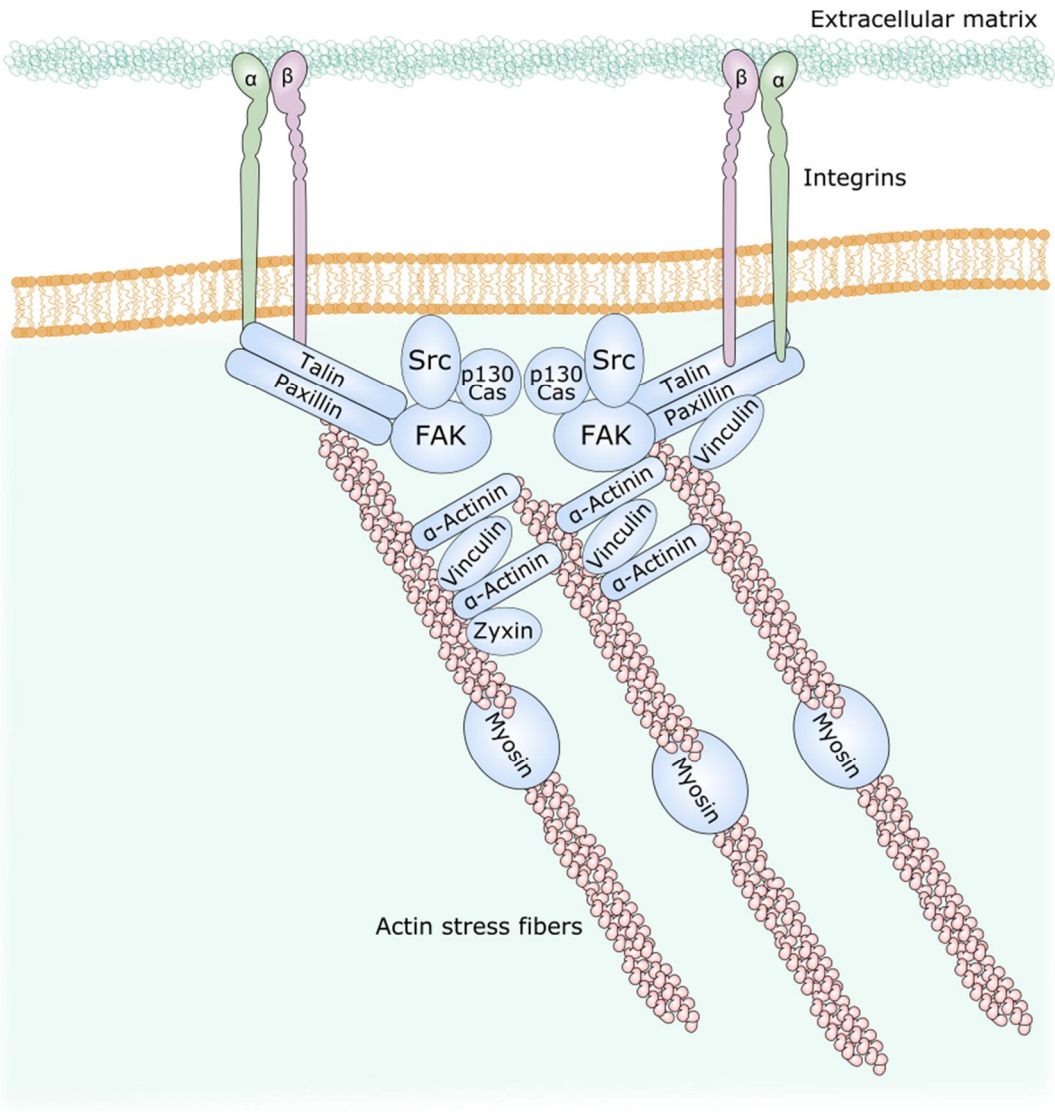

Figure 9. Structure of focal adhesions. Adapted from Mitra et al., 2005.

FAK$^{-/-}$ fibroblasts also show decreased motility (Ilić et al., 1995) whereas FAK overexpression in many cell types stimulates migration (Schlaepfer and Mitra, 2004). Cell migration can be defined as the ability of a cell to move in response to a stimulus. It participates in many physiological processes such as embryogenesis, wound healing, angiogenesis, inflammation, or in some pathological processes such as tumorigenesis and metastasis formation. Several studies demonstrated the importance of FAK in many steps of cell migration such as stimuli sensing (Katsumi et al., 2004; Schlaepfer and Mitra, 2004), lamellipodia (Tilghman et al., 2005) and filipodia (Wu et al., 2004) formation and microtubules stabilization (Siegrist and Doe, 2007). FAK thus functions as a biosensor or integrator to control cell motility by influencing the cytoskeleton and the renewing of focal adhesion and membrane protrusions (Mitra et al., 2005).

FAK was also shown to contribute to cell proliferation. Inhibition of FAK results in cell proliferation inhibition (Parsons, 2003; Owen et al., 2011; Mierke et al., 2017) whereas FAK overexpression in fibroblasts speeds it up (Zhao et al., 1998). FAK would particularly promote cyclin D expression and cyclin-dependent kinases activation during G1/S transition allowing a faster transition (Zhao et al., 2003; Bond et al., 2004; Owen et al., 2011).

Finally, FAK is involved in cell survival and was shown to be an anti-apoptotic kinase. In response to some pro-apoptotic stimuli such as oxidative stress, FAK can activate the PI3K/Akt pathway (Chen et al., 1996) thereby inhibiting many actors of the apoptotic machinery such as BAD or caspase-9 (Hanks et al., 2003). FAK would also be an inhibitor of the pro-apoptotic p53 (Golubovskaya and Cance, 2013). Furthermore, FAK was shown to undergo cleavage during apoptosis thereby stopping its anti-apoptotic function (Manzur et al., 2018). This function is particularly engaged for the inhibition of anoikis, a form of programmed cell death that occurs in anchorage-dependent cells when they detach from the surrounding extracellular matrix (Duxbury et al., 2004). Integrin interaction with the extracellular matrix activates FAK thereby preventing cell from anoikis (Beauséjour et al., 2012).

2.6.2. Physiological functions of FAK

FAK knockout mice is embryonic lethal around E8.5 showing a major role in development (Furuta et al., 1995). This phenotype principally results of a migration defect as detailed in the previous part (Ilić et al., 1995). Interestingly the function of FAK during early development involves more than its autophosphorylation mechanism. For example mice homozygous for a deletion of the exon that codes for Tyr-397 have a normal development up to E12.5 and die later (Corsi et al., 2009).

FAK is also important in the nervous system *in vivo* as shown by several studies. It is highly expressed during brain development whereas its levels decrease in the adult (Burgaya et al., 1995). Conditional deletion of FAK in the cortex demonstrated its major role in basal lamina formation (Beggs et al., 2003) and in dendritic shaft formation (Gorski et al., 2002). Conforming to its role in focal adhesion turnover, FAK was shown to be a negative regulator of axonal branching and synapse formation (Rico et al., 2004). FAK is also critical for neuronal migration and axon guidance during development (Xie et al., 2003; Li et al., 2004b; Bechara et al., 2008; Chacón et al., 2012; Kerstein et al., 2017) as well as for the control of cortical dendrite arborization (Garrett et al., 2012). Additionally, conditional deletion of FAK in Schwann cells proved the requirement of FAK for axonal myelination (Grove and Brophy, 2014).

According to these various physiological functions, FAK is involved in many diseases such as cancer (Naser et al., 2018), ischemia (Bikis et al., 2015; Gao et al., 2018), beta peptide accumulation (Zhang et al., 1996; Williamson et al., 2002) and cardiac hypertrophy (Mohanty and Bhatnagar, 2018) and is thus studied as a potential target for many molecular therapies.

II. Pyk2: a nRTK of FAK family

1. Regulation of Pyk2 activity in non-neuronal cells

1.1. Activation and phosphorylation of Pyk2

1.1.1. Canonical activation of Pyk2

Canonically, Pyk2 is activated in response to increases in intracellular calcium levels (Lev et al., 1995; Girault et al., 1999a; Alier and Morris, 2005; Cao et al., 2007; Schaller, 2008). Calmodulin appears to play an important role in this activation. However the mechanism

proposed for this activation is still not well understood. Kohno et al. proposed that Ca^{2+}/CaM binds to the FERM domain of Pyk2 allowing dimerization and trans-autophosphorylation of Pyk2 (Kohno et al., 2008). Conversely, Xie et al. suggested that the interaction site of Pyk2 with Ca^{2+}/CaM was located in the kinase domain of Pyk2 (Hens and DeSimone, 1995). This binding would enhance Pyk2 homodimerization. In 2011, Riggs et al. demonstrated that EGTA could not dissociate Pyk2 homodimers leading to the hypothesis that Ca^{2+}/CaM is required for Pyk2 homodimer formation but that this dimer undergoes a conformational change in another state which does not include Ca^{2+}/CaM (Riggs et al., 2011). Following this dimerization, Pyk2 is phosphorylated on Tyr-402. Several enzyme can catalyze this reaction. In 2004, Park et al. transfected Pyk2 in SYF cells which are deprived of the Src, Yes and Fyn kinases and they observed phosphorylation of Pyk2 on Tyr-402 supporting the hypothesis of an autophosphorylation independent of Src. They also provided evidence for an autophosphorylation acting in a trans (and not cis) manner by transfecting various mutant forms of Pyk2 and observing that a kinase dead mutant form of Pyk2 was phosphorylated by Pyk2 with an active kinase domain (Park et al., 2004). However in 2016, Zhao et al. reassessed this question by proving that Src was necessary to adhesion-induced phosphorylation of Pyk2 in vitro (Zhao et al., 2016). They proposed that the phosphorylation of Pyk2 observed by Park et al. in SYF cells was due to the overexpression of Pyk2 and that, in physiological conditions, Src would be needed for the initial phosphorylation of Tyr-402 of Pyk2 and that this pre-activated form of Pyk2 could then auto-trans-phosphorylate the other Pyk2 proteins thus bringing back together the two hypothesis.

This latter mechanism may nonetheless be limited to the activation of Pyk2 upon integrin ligation. Additionally, in some cell types, Pyk2 activation seems to be independent of CaM. In cytotoxic T lymphocytes, Pyk2 phosphorylation was not inhibited by the calmodulin inhibitor W7 (Lysechko 2010). In these cells, increased intracellular Ca^{2+} induces the production of reactive oxygen species, which activate the mitogen activated protein kinase (MAPK)/extracellular signal-regulated kinase (ERK) pathway, leading to Src-family kinase-dependent Pyk2 phosphorylation (Lysechko 2010). In human sperm, calmodulin inhibition even enhances Pyk2 phosphorylation by an unknown mechanism (Battistone 2014).

The mechanisms leading to the phosphorylation of Pyk2 on Tyr-402 are thus likely to be different according to the stimulus activating Pyk2. The specific mechanism of activation of Pyk2 in neurons will be discussed in III.1.1.

The phosphorylated tyrosine then constitutes a binding site for the SH2 domain of the SFKs which phosphorylate Tyr-579 and Tyr-580 within the activation loop of Pyk2 kinase domain triggering full activation (Li et al., 1999; Schlaepfer et al., 1999). SFKs also phosphorylate Tyr-881 which recruits the Grb2/Sos complex thus leading to the ERK pathway activation (Blaukat et al., 1999; Lev et al., 1999).

Other residues of Pyk2 can be phosphorylated but the biological function of these phosphorylation sites still remains unclear (Oppermann et al., 2009).

1.1.2. Regulation of Pyk2 activation by Ca^{2+}-activated kinases

1.1.2.1. PKC

The role of PKC in Pyk2 activation is still not clear. In 1995, Lev et al. demonstrated that PKC activation was able to activate Pyk2 (Lev et al., 1995). Many studies then confirmed the involvement of PKC in Pyk2 activation. Pharmacological inhibition of PKC by

staurosporine and Ro31-8220 in platelet cells inhibited Pyk2 phosphorylation in response to thrombin (Ohmori et al., 1999). In accordance with this, inhibition of PKC in neurons also blocked depolarization-induced Pyk2 phosphorylation (Siciliano et al., 1996; Corvol et al., 2005). Although, the precise mechanism of PKC function in Pyk2 activation is unknown, residue(s) phosphorylated by PKC on Pyk2 have not been identified so far, and one can hypothesize that it acts indirectly by favoring Ca^{2+} elevation in cells.

1.1.2.2. CaMKII

Another enzyme involved in Pyk2 regulation is CaMKII. Pharmacological inhibition by KN-62 reduced Pyk2 phosphorylation induced by depolarization but not by bradykinin (Zwick et al., 1999). Ribonucleic acid (RNA) interference of CaMKII in PC12 cells blocked KCl-induced phosphorylation of Pyk2 (Banno et al., 2008). Treatment of vascular smooth muscle cells with the inhibitor KN-93 also inhibited H_20_2 induced Pyk2 phosphorylation (Bouallegue et al., 2009). Specific knockdown of CaM kinase IIδ2 in cultured hypothalamic neurons and CaM kinase IIβ'e in cultured gonadotroph cells both inhibited the GnRH-induced activation of Pyk2 (Okitsu-Sakurayama et al., 2019). Although the specific mechanism of Pyk2 activation by CaM kinases remains unknown, these results clearly show a direct or indirect role for Ca^{2+}-dependent kinases in Pyk2 regulation.

1.2. Dephosphorylation of Pyk2

Pyk2 signaling can also be regulated by dephosphorylation. The protein phosphatases involved are divided in two groups according to their substrates: the PTPs and the protein serine-threonine phosphatases (PSTPs).

1.2.1. Tyrosine phosphatases

1.2.1.1. SHP-1

Pyk2 is a substrate of SHP-1 (Kumar et al., 1999; Ganju et al., 2000). SHP-1 associates with Pyk2 (Ganju et al., 2000) and overexpression of SHP-1 inhibits Pyk2 phosphorylation (Kumar et al., 1999).

1.2.1.2. SHP-2

Pyk2 is also a substrate of SHP-2 (Chauhan et al., 2000; Tang et al., 2000). An interaction between SHP-2 and Pyk2 was shown in some cell types. This interaction was constitutive (Tang et al., 2000), induced by interleukins (Chauhan et al., 2000) or by platelets engagement (Wiiger and Prydz, 2004). The domain involved in this interaction is unknown but it does not involved SH2 (Chauhan et al., 2000; Tang et al., 2000).

1.2.1.3. PTP-PEST

The Tyr-402 and Tyr-579/580 of Pyk2 were shown to be substrates of PTPN12, also known as PTP-PEST (Davidson and Veillette, 2001; Lyons et al., 2001). PTP-PEST interacts with Pyk2 by its N-terminal PR domain (Gupta et al., 2003; Chellaiah et al., 2007). PTP-PEST deficiency results in Pyk2 hyperphosphorylation and increased cell motility in endothelial (Souza et al., 2012), cancer (Sahu et al., 2007; Li et al., 2015) and dendritic cells (Rhee et al., 2014). A PTP-PEST/Pyk2 pathway is also involved in the response of T cells (Davidson et al., 2010), macrophages fusion (Rhee et al., 2013) and osteoclasts function (Eleniste et al., 2012).

1.2.1.4. STEP

PTPN5, also known as striatal-enriched protein-tyrosine phosphatase (STEP) binds to and dephosphorylates Pyk2 at Tyr-402 (Xu et al., 2012). The role of this brain-specific PTP in Pyk2 regulation will be discussed further in III.

1.2.2. Ser/Thr phosphatases

In 2002, Lin et al. described the implication of Pyk2 and calcineurin, also known as PP2B, in the carbachol-induced signaling pathway (Lin et al., 2002). Treatment of cells with cyclosporine A, a calcineurin inhibitor, was shown to decrease Pyk2 phosphorylation suggesting a role of calcineurin in Pyk2 activation (Xia et al., 2006). Calcineurin dephosphorylates Pyk2 at Ser-778, a residue phosphorylated by PKA and involved in the regulation of the nuclear export motif of Pyk2 (Faure et al., 2007, 2013). This dephosphorylation leads to Pyk2 nuclear accumulation but mutation of Ser-778 do not.

1.3. SUMOylation of Pyk2

Recently, Uzoma et al. discovered that four lysines of Pyk2 could be SUMOylated thus promoting autophosphorylation of Pyk2 at Tyr-402 (Uzoma et al., 2018). This result suggests a crosstalk between phosphorylation and SUMOylation and enriches the spectrum of Pyk2 regulatory mechanisms.

1.4. S-nitrosylation of Pyk2

In 2015, Yan et al. demonstrated that oxidative stress induced S-nitrosylation of Cys-534 of Pyk2 (Yan et al., 2015). The Cys-534 mutant Pyk2 overexpression in cells reduced Pyk2 S-nitrosylation and decreased the oxygen glucose deprivation-induced Pyk2 phosphorylation suggesting a role for this post-translational modification in the regulation of Pyk2 phosphorylation.

The principal post-translational modifications of Pyk2 are compiled in **Figure 10**.

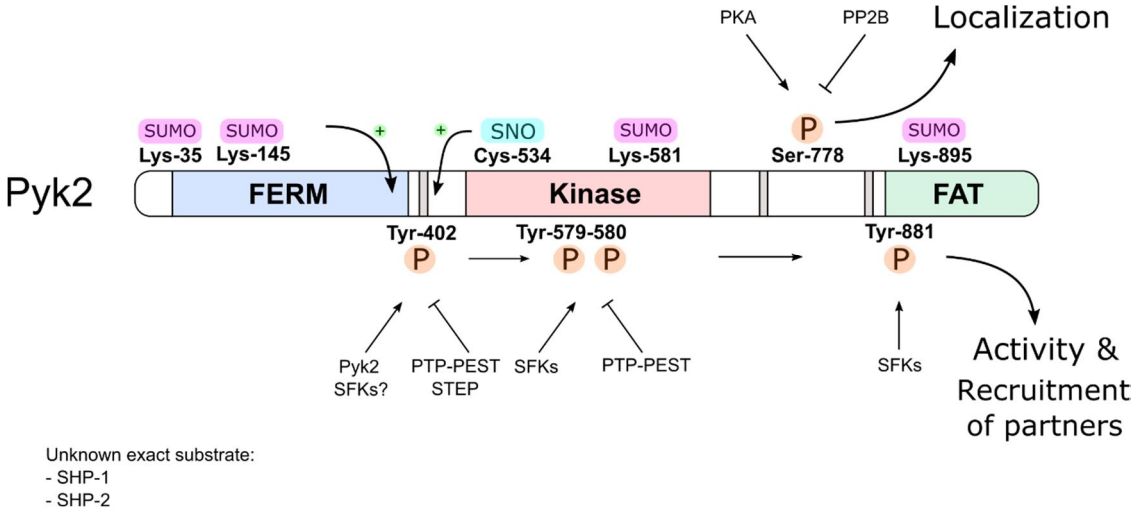

Figure 10. Pyk2 post-translational modifications. SUMOylation and S-nitrosylation of Pyk2 promote phosphorylation. Tyr-402 phosphorylation recruits SFKs which phosphorylate Tyr-579 and Tyr-580 leading to full activation of Pyk2, and Tyr-881 inducing the recruitment of the Grb2/Sos complex. Ser-778 phosphorylation/dephosphorylation regulate Pyk2 cytonuclear shuttling.

2. Pyk2 functions in non-neuronal cells

2.1. Pyk2 cellular functions

2.1.1. Cell adhesion

As FAK, Pyk2 possesses a FAT domain which targets it to the membrane and the focal adhesions. In fibroblasts, Pyk2 localizes at focal adhesions and microinjection of Pyk2 in these cells leads to reorganization of focal adhesions and cell rounding (Du et al., 2001). In macrophages as well, Pyk2 localizes within F-actin-rich membrane ruffles (Williams and Ridley, 2000). Pyk2 deletion in macrophages resulted in a delay in the formation of the leading edge lamellipodia in response to chemokine stimulation and the incapacity to detach from the substrate at the trailing edge thus reducing cell migration (Okigaki et al., 2003). Latter, Hashido et al. showed that Pyk2 was involved in cell repulsion by promoting focal adhesion disassembly (Hashido et al., 2006). In T-cells, Pyk2 activation leads to the separation of the cell with dendritic cells (Raab et al., 2017). It is thus likely that Pyk2 promotes the turnover of focal adhesions in cells. This may involve the activation of Rho, a GTPase controlling cytoskeletal morphology (Lim et al., 2008b).

2.1.2. Cell migration

In concordance with its role in focal adhesions turnover, Pyk2 also regulates migration in different cell types including vascular smooth muscle cells (Soe et al., 2009), PC-12 cells (Park et al., 2007), B-2 cells and marginal zone B cells (Tse et al., 2012), macrophages (Okigaki et al., 2003), cytotoxic T lymphocytes (Cheung and Ostergaard, 2016a), eosinophils(Zhu et al., 2008), monocytes (Watson et al., 2001) and neutrophils (Allingham et al., 2007).

Rho family of GTPases are crucial in this molecular process with Rho acting in cytoskeletal reorganization in stress fibers and Rac stimulating formation of lamellipodia (Lawson and Ridley, 2018). Pyk2 was shown to interact with these two signaling proteins. PLC-gamma1 activates Pyk2 which then activates Rac thus upregulating the formation of lamellipodia and cell migration (Choi et al., 2007). Pyk2-Rac pathway is also involved in macrophages migration (Miao et al., 2016). Rho is activated by Pyk2 in vascular smooth muscles cells (Ohtsu et al., 2005) and Pyk2 deficient macrophages were shown to have decreased Rho activation and lamellipodia contraction (Okigaki et al., 2003). By stimulating both Rac and Rho, Pyk2 thus embodies a pro-migratory role.

However, in osteoblasts, Pyk2 was shown to have an anti-migratory role as Pyk2 deletion increases osteoblast migration (Eleniste et al., 2016). Such contradictory results need further study to be understood precisely.

One should note that FAK loss is accompanied by a compensatory increase of Pyk2 expression and function (Sieg et al., 1998; Lim et al., 2008b; Weis et al., 2008) suggesting that FAK can be partly replaced by Pyk2 for the regulation of cellular migration. On the contrary, FAK does not compensate for Pyk2 in Pyk2-deficient B cells and macrophages suggesting that Pyk2 developed particular features during evolution (Guinamard et al., 2000).

2.1.3. Cell division

Pyk2 is also involved in the control of the cell cycle and cell proliferation. Expression of inactive Pyk2 decreases lymphocytes (Miyazaki et al., 1998) and prostatic cells (Picascia et al., 2002) proliferation.

The Wnt/β-catenin pathway is known for promoting cellular proliferation by initiating the transcription of cyclin D1 and cMyc (Klaus and Birchmeier, 2008). Pyk2 increases nuclear accumulation of β-catenin by phosphorylating β-catenin on tyrosine residues (Otero et al., 2009), associating with the Wnt5a/Frizzled/LRP5 complex which also activates β-catenin (Despeaux et al., 2012), and protecting β-catenin from GSK3β-induced degradation (Zhang et al., 2014).

Pyk2 thus promotes cell proliferation and is the object of many studies focusing of its oncogenic function (Shen and Guo, 2018).

2.1.4. Cell survival

Pyk2 plays a dual role in cell survival as it can be either pro or anti-apoptotic depending on the cell type and the conditions.

In mammary epithelial cells, Pyk2 activates an anti-apoptotic pathway involving epidermal growth factor receptor (EGFR), Akt and the inhibition of p53 in response to benzo[a]pyrene exposure (Burdick et al., 2006). In thymocytes, Pyk2 is activated by interleukine-7 in an anti-apoptotic pathway involving Jak activation (Benbernou et al., 2000). In pathological conditions, Pyk2 is also associated with pathways preventing cell death. In breast cancer cells for instance, Pyk2 activates an EGFR/Akt signaling inhibiting apoptosis (Burdick et al., 2006). Inhibition of the Pyk2/β-catenin pathway in multiple myeloma cells leads to increased cell death, showing an anti-apoptotic role of Pyk2-activated pathway in this situation (Kamihara et al., 2016). After ischemia/reperfusion, Pyk2 is involved in the activation of the prosurvival signaling molecules ERK and Akt, thereby preventing excessive increases in reactive oxygen species and providing protection from injury (Miller et al., 2019).

Pyk2 also has a pro-apoptotic role. In 1997, Xiong and Parsons induced apoptosis in fibroblasts by inducing the expression of Pyk2 (Xiong and Parsons, 1997). Latter, Ueda et al. reported this effect *in vitro* and prevented apoptosis by the expression of the FAK family kinase-interacting protein of 200 kD (FIP200), which is a natural inhibitor of Pyk2 (Ueda et al., 2000). Inhibition of Pyk2 by the expression of its C-terminal domain also improved survival of ventricular myocytes *in vivo* following myocardial infarction suggesting a role of Pyk2 in cell death (Hart et al., 2008). In osteoblasts as well, kinase-deficient or phosphorylation-defective Pyk2 mutations were shown to inhibit the glucocorticoid-induced apoptosis (Plotkin et al., 2007). In the bone marrow, Pyk2 deletion increases the number of monocytes suggesting a pro-apoptotic role of Pyk2 in these cells thus regulating the turnover of these cells (Llewellyn et al., 2017). Pharmacological blockade of Pyk2 or inhibition of Pyk2 activation by Na_2S reduced myocardial infarct size in mice (Bibli et al., 2017).

The molecular mechanisms involved may be different depending on the cell type and the environmental condition. In fibroblasts, Pyk2 may function as an inhibitor of the anti-apoptotic PI3K/Akt pathway (Xiong and Parsons, 1997). Pyk2 was also shown to phosphorylates and inhibits endothelial NO synthase (eNOS) which produces protective amounts of NO (Bibli et al., 2017). The effect of Pyk2 on cell survival is also often related to the activation of MAPKs. As mentioned in II.1.1.1, Pyk2 can recruit the Grb2/Sos

complex which activates the ERK pathway (Blaukat et al., 1999; Lev et al., 1999). Pyk2 also act as an upstream regulator of the c-Jun NH_2-terminal kinase (JNK) pathway through the phosphorylation, by Src, of p130Cas and subsequent recruitment of Crk, C3G and DOCK180, leading to JNK activation (Blaukat et al., 1999). Furthermore, p38 was shown to be activated by Pyk2 through a pathway involving mitogen-activated protein kinase kinase 3 (MKK3) (Pandey et al., 1999; Sorokin et al., 2001). These signaling pathways regulate a variety of cellular activities including cell survival and death. In osteoblasts, the apoptotic effect of Pyk2 in appears to be due to the activation of JNK (Plotkin et al., 2007). In cardiomyocytes, Pyk2 activates p38 leading to the cleavage of PARP, the activation of caspase-3 and deoxyribonucleic acid (DNA) degradation (Melendez et al., 2004). Conversely, in these same cells but following ischemia/reperfusion, Pyk2 has a protective role through the activation of the ERK pathway notably (Miller et al., 2019).

2.1.5. Cell differentiation

Pyk2 is involved in keratinocytes differentiation by increasing the expression of transcription factors promoting the expression of differentiation markers (Schindler et al., 2007).

However, Pyk2 is more often associated with de-differentiation of cells. Pyk2 inhibits the differentiation of myeloid progenitors (Dylla et al., 2004) and of osteoprogenitors (Buckbinder et al., 2007). Recently, Pyk2 was confirmed to inhibit osteoblast differentiation (Posritong et al., 2018). Besides, Pyk2 inhibition promotes differentiation of vascular smooth muscle cells into a contractile phenotype thus promoting the integrity of the vascular wall (Grossi et al., 2017). This aspect of Pyk2 also contributes to its involvement in many cancers.

2.2. Physiological role of Pyk2

2.2.1. Bone physiology

Bone mass regulation results from the equilibrium between the actions of osteoblastic cells which produce bone matrix and osteoclasts which induce matrix resorption.

$Pyk2^{-/-}$ mice have increased bone-mass due to increased osteoblast proliferation, migration and activity and decreased osteoclast function (Buckbinder et al., 2007; Gil-Henn et al., 2007; Eleniste et al., 2016).

In osteoclasts, Pyk2 is involved in the assembly and disassembly of podosomes which are conical, actin-rich membrane protrusions which serve as both sites of attachment and degradation along the extracellular matrix. Pyk2 interacts with structural proteins surrounding the actin ring of the podosome such as vinculin, talin, α-actinin and gelsolin (Shyu et al., 2007). Pyk2 is activated by the attachment of osteoclasts on different substrates (Duong et al., 1998). One should note that the role of Pyk2 appears to be dependent on its autophosphorylation site (Tyr-402) but not on its kinase activity. Pyk2 appears to recruit Src which then activates Cbl and PI3K allowing the development of osteoclasts polarity and function (Lakkakorpi et al., 2003; Horne et al., 2005; Buckbinder et al., 2007).

In osteoblasts, mechanical stimulations were shown to activate and re-localize Pyk2 (Guignandon et al., 2006). Pyk2 has an inhibitory function on osteoblast activity (Posritong et al., 2018). Accordingly, a research team developed a PEGDA-gelatin hydrogel containing an inhibitor of Pyk2 which promoted, *in vitro*, increased osteoblast activity and mineral

deposition possibly constituting a suitable treatment of skeletal defect (Posritong et al., 2019).

2.2.2. Vascular system integrity

In endothelial cells, Pyk2 is activated upon stimulation by different signals from integrin binding to growth factors or mechanical stimulations (Orr and Murphy-Ullrich, 2004). Neovessel formation after hind-limb ischemia is impaired in Pyk2-/- mice. Pyk2 is involved in Src/PLCgamma1 and Src/PI3-kinase/Akt pathways, leading to endothelial NO synthase phosphorylation, and modulation of vasoactive function and angiogenic response (Matsui et al., 2007). Pyk2 would actually have an inhibitory action on eNOS thus blocking its vasodilatation activity (Fisslthaler et al., 2008).

Pyk2 is an important determinant of thrombin-induced endothelial inflammation. Thrombin stimulation of endothelial cells was shown to activate IKK, through Pyk2, and to promote the release and the transcriptional capacity of RelA/p65 (Soni et al., 2017).

Pyk2 may also have a role in endothelial integrity by modulating cell adhesion. VE-cadherin loss of function was shown to induce tyrosine phosphorylation of β-catenin by Pyk2 (van Buul et al., 2005). Pyk2 phosphorylation of VE-PTP constitutes a docking site for Src which phosphorylates VE-cadherin leading to endothelial barrier dysfunction (Soni et al., 2017).

2.2.3. Immune system function

Pyk2 is expressed in cells of hematopoietic origin where it controls the molecular mechanisms of migration and activation.

In macrophages, Pyk2 is activated by FcγR stimulation during phagocytosis (Kedzierska et al., 2001). Both FAK and Pyk2 are involved in phagocytosis (Bruce-Staskal et al., 2002; Hudson et al., 2005). However, the two proteins do not display the same function. Pyk2 activation is sufficient for phagocytosis of YadA expressing bacteria whereas FAK is sufficient for phagocytosis of invasin expressing bacteria (Owen et al., 2007).

Pyk2 is also involved in cytokines secretion by macrophages such as IL-1β and IL-18 (Välimäki et al., 2013). Pyk2 phosphorylates the inflammasome adaptor protein ASC which participates in speck formation that leads to caspase-1 activation and secretion of IL-1β and IL-18 (Chung et al., 2016). Pyk2 might thus be involved in HIV-associated dementia characterized by the infiltration of macrophages in perivascular sites of the central nervous system and the production of IL-1β in the brain (Cheung et al., 2008).

As detailed above, Pyk2 is implicated in cell migration. Particularly, Pyk2 plays a crucial role in the migration of macrophages (Owen et al., 2007), T cells (Cheung and Ostergaard, 2016b), marginal zone B cells (Tse et al., 2009), platelets (Cipolla et al., 2013), eosinophils (Zhu et al., 2008), and neutrophils (Kamen et al., 2011). The role of Pyk2, probably involving the RhoA-ROCK signaling pathway, is underlined by the inability of Pyk2 deficient cells to detach form the rear (Okigaki et al., 2003; Cheung and Ostergaard, 2016a).

The production of reactive oxygen species (ROS) by macrophages (Lin et al., 2008) and neutrophils (Zhao and Bokoch, 2005) also involves Pyk2 activity and is necessary to inflammatory response of these cells.

2.2.4. Kidney function

Pyk2 plays an important role in acidobasic homeostasis. Acidosis activates Pyk2 in kidney cells, promoting MAPK- and JNK-dependent transcription and activation of the NHE3

transporter, thus increasing acid secretion by these cells (Gluck, 2004; Li et al., 2004a; Preisig, 2007).

Pyk2 is also involved in the acid-stimulated citrate reuptake by NaDC-1 cotransporter in kidney cells (Zacchia et al., 2018).

Diabetes was also shown to induce a Pyk2-dependent inactivation of GSK3β thus causing elevated protein synthesis and kidney hypertrophy (Mariappan et al., 2014).

2.2.5. Sperm capacitation

Northern blot and immunoprecipitation analysis demonstrate that, among germinal cells, Pyk2 is more abundant in spermatocytes and spermatids (Chieffi et al., 2003). Inhibition of Pyk2 results in decreased sperm motility, acrosome reaction and ability to penetrate eggs (Battistone et al., 2014). Pyk2 may phosphorylate CatSper, a Ca^{2+} channel, thus promoting the Ca^{2+} wave necessary to sperm capacitation (Brukman et al., 2019).

2.2.6. Generation of Pyk2 knockout mice

Genetic knockout is a useful approach to better study the physiological function of a protein in an organism.

The Schlessinger group was the first to develop Pyk2 knockout mice by inserting a Neo expression cassette into the 5' portion of Pyk2 sequence encoding for the protein tyrosine kinase domain as shown in **Figure 11** (Okigaki et al., 2003). In contrast to the embryonic lethality in FAK-deficient mice, Pyk2 knockout mice are viable and fertile (Guinamard et al., 2000; Okigaki et al., 2003). They display a mild immunological phenotype with reported defects in immune cells activation and mobility as described in II.2.2.3 (Guinamard et al., 2000; Okigaki et al., 2003; Cipolla et al., 2013).

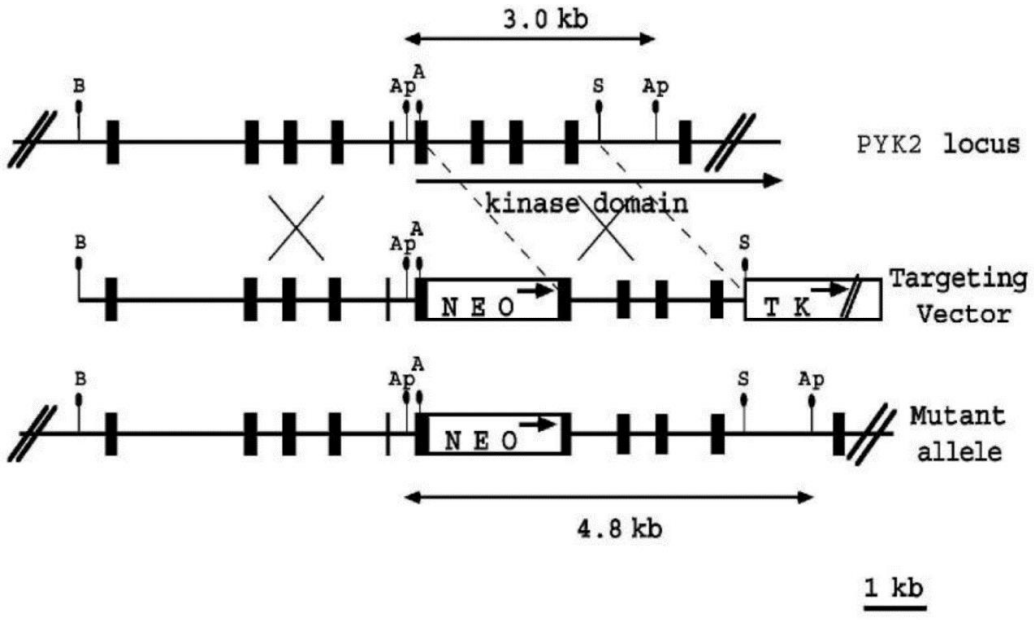

Figure 11. Generation of Pyk2 knockout by Okigaki et al., 2003. Schematic diagrams and partial restriction maps of Pyk2 locus, the Pyk2 targeting vector, and the predicted structure of the Pyk2 locus after homologous recombination with targeting vector. The filled box represents Pyk2 coding sequence, the open box indicates the Neo expression cassette and thymidine kinase (TK) expression cassette. The arrows in open box indicate the direction of transcription. A, Ap, B, and S represent AccI, ApaI, BamHI, and SacI, respectively. From Okigaki et al., 2003.

More recently, our group generated Pyk2 knockout mice in collaboration with Gen-O-way (Lyon, France) (Giralt et al., 2016). First, the *Ptk2b* exons 15b-18 were flanked with LoxP sequences to generate Pyk2$^{f/f}$ C57Bl/6 mice (**Figure 12**). Pyk2$^{f/f}$ mice were then crossed with an expressing Cre line to delete exons 15b-18 thereby resulting in Pyk2 genetic knockout (Giralt et al., 2016). These Pyk2 knockout mice were used to study the involvement of Pyk2 in astrocytes migration as will be detailed further in III.2.5.

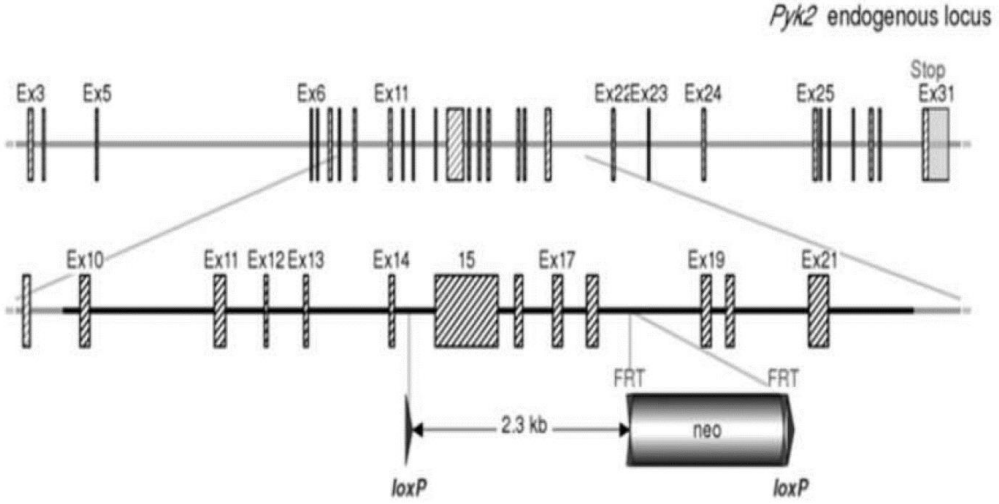

Figure 12. Generation of Pyk2$^{f/f}$ C57Bl/6 mice by Giralt et al., 2016. Hatched rectangles represent Pyk2 coding sequences, grey rectangles indicate non-coding exon portions and solid lines represent chromosome sequences. The neomycin positive selection cassette is indicated. LoxP sites are represented by triangles and FRT sites by double triangles. From Giralt et al., 2016.

3. Pathological role of Pyk2

3.1. Pyk2 and inflammatory diseases

As shown in II.2.2.3, Pyk2 is an important actor of the immune system. Pyk2 is also associated with the dysregulation of this system characterizing inflammatory diseases (Zhu et al., 2018). Pyk2, which is essential for inflammatory cell migration *in vitro*, regulates airway inflammation, Th2 cytokine secretion, and airway hyper-responsiveness in a mouse model of asthma (Duan et al., 2010). In the development of peritonitis, Pyk2 was shown to phosphorylate ASC, an inflammasome adaptor protein thus leading to its dimerization and to NLRP3 activation (Chung et al., 2016). Pyk2 inhibition blocks lung inflammation in a mouse model of acute lung injury (Duan et al., 2012). As detailed in 2.2.1, Pyk2 is also targeted in a recent therapy directed against osteoporosis (Posritong et al., 2019).

3.1. Pyk2 and cancers

Given its many roles in cell survival, differentiation and migration, Pyk2 rapidly appeared as a putative oncogenic factor (Shen and Guo, 2018). Pyk2 acts as the crossroads of multiple signaling pathways promoting cancer progression.

Pyk2 induces cell proliferation and tumor growth via activation of ERK pathway in breast (Behmoaram et al., 2008), prostate (Picascia et al., 2002), lung (Roelle et al., 2008; Zhang et al., 2008b) and liver cancers (Sun et al., 2008) and in glioma (van der Horst et al., 2005). In lung cancer cells, SOCS3, a tumor suppressor, binds to Pyk2 via its SH2 and kinase inhibitory region (KIR) domains, and decreases cell migration through inhibiting

Pyk2-associated ERK activity (Zhang et al., 2008a). A Pyk2/ERK pathway was also shown to mediate the EGF-inducted telomerase activity in malignant ovarian cells (Bermudez et al., 2008). In urothelial carcinoma cells as well, Pyk2 regulates IGF-I-induced ERK activation leading to cell motility and invasion (Genua et al., 2012).

Pyk2 is also an activator of the EGFR/PI3K/Akt pathway promoting survival of multiple myeloma (Zhang et al., 2014) and breast cancer cells (Burdick et al., 2006). In 2015, Datta et al. targeted this pathway with alpha-naphthoflavone, a chemopreventive agent promoting the sensitivity of breast cancer cells to doxorubicin and abrogating doxorubicin resistance via inhibiting phospho-Pyk2, phospho-FAK and EGF-induced Akt activation (Datta et al., 2015). In liver cancer as well, Pyk2 activates Akt thus promoting cell survival, drug resistance (Geng et al., 2011) and VEGF production leading to angiogenesis and metastasis (Cao et al., 2013). In urothelial carcinoma cells, Akt activation by Pyk2 also contributes to the IGF-I-induced cell motility and invasion evoked previously (Genua et al., 2012).

Pyk2 also contributes to the activation of the Rho GTPases pathway leading to increased cell motility in prostate (Sahu et al., 2007) and in liver cancer (Sun et al., 2011).

At the intersection of these pathways, Pyk2 appears to have an oncogenic role, promoting proliferation, survival, invasion, metastasis, and chemo-resistance of tumor cells as reviewed in **Figure 13**. However, two exceptions were interestingly reported. A tumor-suppressive role of Pyk2 has indeed been observed in both neuroblastoma (Nakagawa-Yagi et al., 2001) and androgen-dependent prostate cancers (Stanzione et al., 2001; Wang et al., 2002; Wiese et al., 2015). The differences between cell types studied in this section may explain this apparent contradiction.

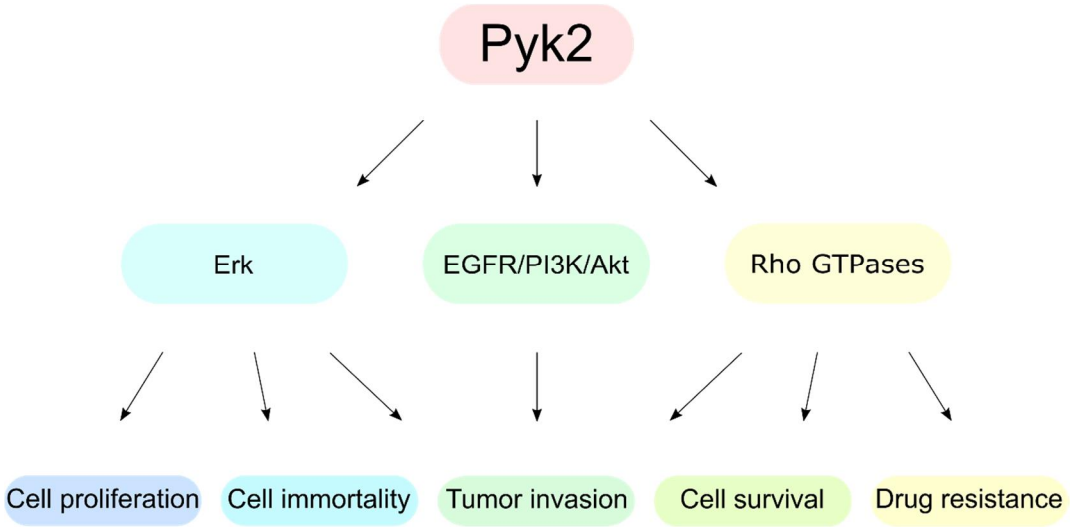

Figure 13. Schematic model of the oncogenic role of Pyk2.

3.1. Pharmacological inhibitors of Pyk2

The involvement of Pyk2 in many diseases created expectation for the discovery or the development of an efficient and specific chemical inhibitor.

Malononitrile, 3,5-di-tert-butyl-4-hydroxybenzylidene, also referred as tyrphostin A9, or AG 17 has been shown to inhibit Pyk2 activation in cultured cells (Fuortes et al., 1999). This inhibitor was used for showing the role of Pyk2 in neutrophils (Fuortes et al., 1999; Evangelista et al., 2007), platelets (Kim et al., 2013) and chondrocytes (Ding et al.,

2009) activation, in T-cells chemotaxis (Saitoh et al., 2017), in the production of interleukin-10 by macrophages (Okenwa et al., 2013) and in zebrafish oocyte fertilization (Sharma and Kinsey, 2013). However, this chemical inhibitor is not selective against Pyk2 as it was shown to inhibits other kinases including Cdk2 (Palumbo et al., 1997) and the platelet-derived growth factor receptor (PDGFR) (Marhaba et al., 1996). Hence, the effects of this inhibitor may be only partially due to Pyk2 inhibition.

During the 2000s, the Pfizer group got particularly interested in some diaminopyrimidines and derivatives for their ability to compete with the ATP binding site of FAK and/or Pyk2. Diaminopyrimidines are a class of organic chemical compounds that include two amine groups on a pyrimidine ring. Among them, PF-562271 is a potent reversible inhibitor of FAK and Pyk2 with an IC50 of 1.5 and 14 nmol/L respectively (Roberts et al., 2008). In accordance with the oncogenic role of both FAK and Pyk2, this compound displays an antitumor activity (Roberts et al., 2008; Bagi et al., 2009; Stokes et al., 2011). In 2008, Walker et al. used a combination of library and chemistry techniques to transform the FAK-selective inhibitor PF-431396 into compounds with good Pyk2 potency and up to 10- to 20-fold selectivity over FAK (Walker et al., 2008). Thereafter, Han et al. described a novel Pyk2 conformation which led to the development of strong Pyk2-targeted inhibitors PF-4618433 (Han et al., 2009) and PF-4594755 (Bonnette et al., 2010) interacting with allosteric sites outside of the ATP binding pocket which are poorly conserved between Pyk2 and FAK. PF-4618433 was recently used in a PEGDA-gelatin hydrogel as a promising treatment for skeletal defect (Posritong et al., 2019).

Another study reported the screening of a diverse collection of ~250,000 small molecule compounds to identify inhibitors of Pyk2 with potential osteogenic activity in osteoblast cells (Allen et al., 2009). This screening identified compounds that showed strong biochemical potency against Pyk2 and up to 3700-fold selectivity over FAK (Allen et al., 2009).

In 2017, Meirson et al. used an *in silico* systematic screening approach to discover Pyk2-selective inhibitors in an original way: four different Pyk2 kinase domain crystal structures were generated and prepared for screening. A virtual library of six million compounds was docked in silico against these four domains and ligand selectivity for Pyk2 over FAK was then evaluated to identify promising Pyk2 inhibitors with high specificity (Meirson et al., 2017).

A distinct strategy for the inhibition of Pyk2 consists in the expression of recombinant proteins which prevent Pyk2 activation. The dominant-negative inhibitor of Pyk2, TAT-mediated protein transduction of dominant-negative C-terminal Pyk2 (TAT-Pyk2-CT), results from the fusion of TAT peptide to the C-terminal Pyk2 (Han et al., 2003). This inhibitor was used to show the involvement of Pyk2 in the regulation of leucocytes activation (Han et al., 2003) and migration (Zhu et al., 2008; Wang et al., 2010a), in platelets activation (Kim et al., 2013), and more generally in lung inflammation (Duan et al., 2010, 2012). Alternatively, a GST-FERM fusion protein was shown to block Pyk2 oligomerization and activation (Riggs et al., 2011). This fusion protein was used to demonstrate the role of Pyk2 in zebrafish oocyte fertilization (Sharma and Kinsey, 2013).

Finally, it is interesting to note that the anti-inflammatory effects of salicylate may be due, at least partially, to the inhibition of Pyk2 and Src and not solely to the inhibition of cyclooxygenase activity (Wang and Brecher, 2001). Particularly, the vasodilator effect of salicylate would results from the inhibition of the Pyk2-mediated RhoA/Rho-kinase activation (Ying et al., 2009; Mills et al., 2015).

III. Roles of Pyk2 in the CNS

1. Specific regulation of Pyk2 in the CNS

1.1. Activation of Pyk2 in neurons

We have seen above that, in most non-neuronal cells, Pyk2 is thought to be activated through a Ca^{2+}/calmodulin-dependent homodimerization and transphosphorylation (Kohno et al., 2008; Schaller, 2008; Riggs et al., 2011; Walkiewicz et al., 2015).

In neurons, it was also suggested that intermolecular Pyk2 autophosphorylation results from the Ca^{2+}-induced dimerization of the associated post-synaptic density protein PSD-95 (Bartos et al., 2010). In 2003, Seabold et al. discovered that the PR sequences-containing linker 2 of Pyk2 interacts with the SH3 domain of PSD-95 (Seabold et al., 2003). However, the GK domain of PSD-95 also interacts with this SH3 domain thus inhibiting PSD-95 interaction with Pyk2 at basal state (Seabold et al., 2003). Following this study, Bartos et al. demonstrated that Ca^{2+}/calmodulin but not calmodulin alone associates with the SH3 domain of PSD-95 thereby releasing this autoinhibitory interaction and allowing PSD-95 to interact with Pyk2 (Bartos et al., 2010). In this model, Ca^{2+} influx through NMDAR induces post-synaptic Pyk2 clustering through Ca^{2+}/CaM:PSD-95. Clustered Pyk2 then autophosphorylates in trans, leading to full activation of Pyk2. In this cluster, Pyk2 can modify neuronal excitability by inducing the phosphorylation of ion channels (Lev et al., 1995; Felsch et al., 1998; Huang et al., 2001) (**Figure 14**).

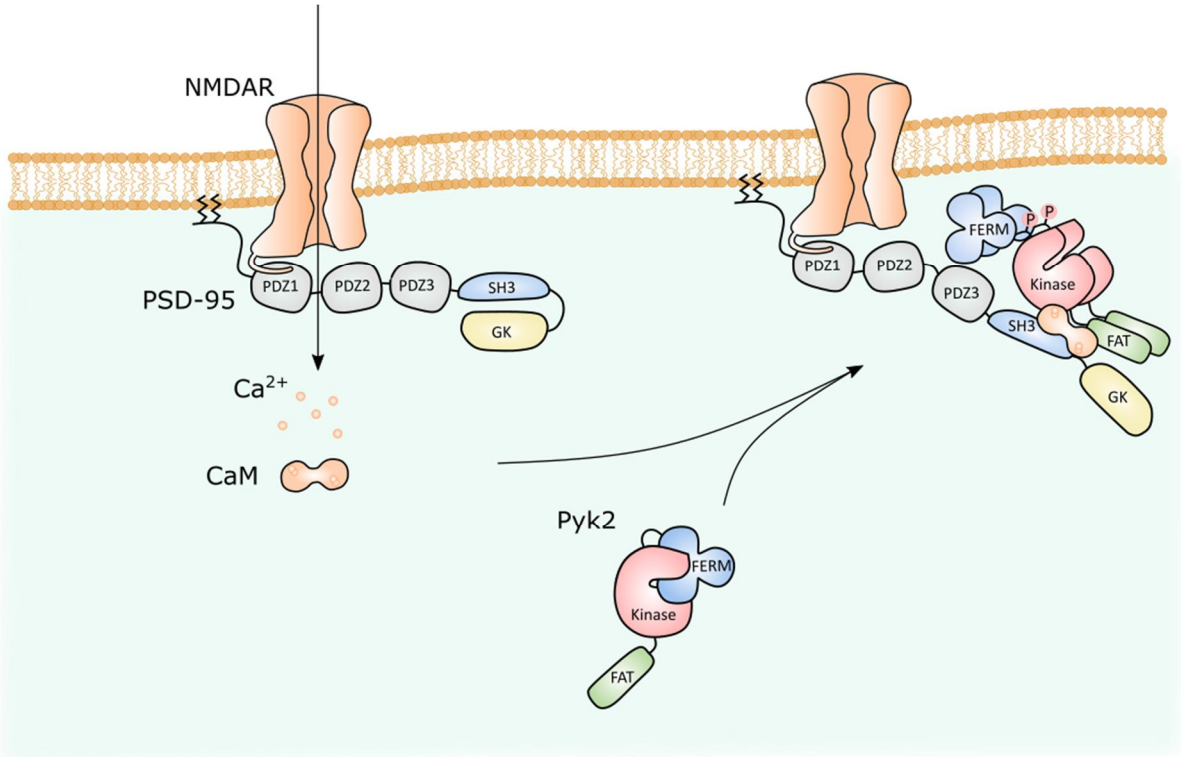

Figure 14. Model of the activation of the neuronal activation Pyk2.

1.2. Regulation of Pyk2 localization

In addition to its postsynaptic translocation, Pyk2 can also shuttle between the nucleus and cytoplasm in neurons as described in I.2.4 and II.1.2.2 (Faure et al., 2007, 2013). In hippocampal slices and PC12 cells, depolarization induces a calcineurin-dependent nuclear translocation of Pyk2 (Faure et al., 2007). This translocation depends on the regulation of the NES by the phosphorylation/dephosphorylation of residue Ser-778. At basal state, this residue is phosphorylated by PKA and positively regulates this nuclear export motif thereby leading to nuclear exclusion of Pyk2. Upon neuronal stimulation and Ca^{2+} increase, calcineurin dephosphorylates Ser-778 leading to the inactivation of the nuclear export motif and the accumulation of Pyk2 in the nucleus mediated by the NLS and NES located in the FERM domain and the linker 2 respectively (**Figure 15**) (Faure et al., 2013).

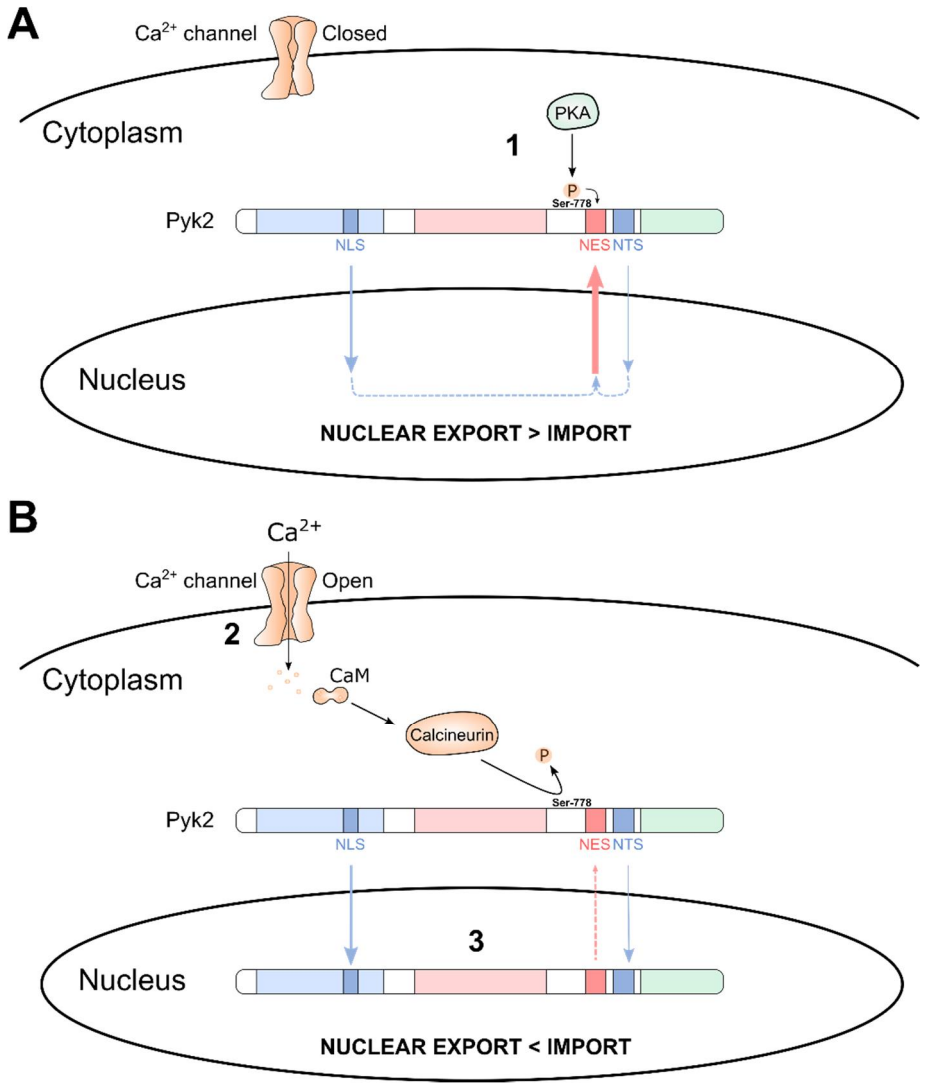

Figure 15. Model of Pyk2 intracellular localization regulation in neurons proposed in Faure et al., 2013. a In basal conditions, the phosphorylation of S778 positively regulates the NES of Pyk2 contributing to its nuclear exclusion. **b** Upon neuronal depolarization, Ca^{2+}/calmodulin (CaM) activates calcineurin which dephosphorylates S778 leading to the inactivation of the NES and the nuclear accumulation of Pyk2 due to the predominant activity of the NLS and possibly the NTS.

This property may contribute to specific long-term adaptations in neurons, given the possible effects of Pyk2 on chromatin and transcription observed in other cell types. Indeed, in osteocytes, after translocation to the nucleus, Pyk2 was shown to interact with methyl-CpG-binding protein 2 (MECP2), a protein involved in the mediation of the biological consequences of methylation signals in DNA (Hum et al., 2014). In fibroblasts, it was shown that nuclear accumulation of Pyk2 was accompanied by the accumulation of Hic-5, a coactivator of nuclear receptors, thereby regulating transcription (Aoto et al., 2002). However and despite this elucidated mechanism, any direct implication of Pyk2 in the regulation of transcription in neurons still remains to be elucidated.

2. Pyk2 biological functions in the CNS

2.1. Ionic channels regulation

2.1.1. Kv1.2

In 1995, Pyk2 was identified as a Kv1.2 regulator (Lev et al., 1995). This channel is highly expressed in the brain and in cardiac muscle and it is negatively regulated by tyrosine phosphorylation which induces its endocytosis (Williams et al., 2007). In 1998, Felsch et al. transfected Xenopus oocytes with truncated forms of the channel and revealed that the C-terminus was phosphorylated by Pyk2 (Felsch et al., 1998).

2.1.2. BK channels

"Big potassium" large conductance voltage-gated K+ channel (BK) channels are potassium channels activated by membrane depolarization and increases in intracellular Ca^{2+} concentration (Contet et al., 2016). Pyk2 regulates and co-immunoprecipitates with BK channel (Ling et al., 2004; Florio et al., 2005; Massa et al., 2006). BK channel activity was reduced by Pyk2 inhibitors indicating an activating role of Pyk2 (Florio et al., 2005; Massa et al., 2006).

More recently, Pyk2 was also shown to be positively regulated by BK channels in astrocytes (Hsieh et al., 2016; Liou et al., 2019).

2.1.3. NMDA receptor (NMDAR)

In 2001, Huang et al. demonstrated a physical interaction of Pyk2 but not FAK with the NMDAR in CA1 hippocampus, without determining whether the interaction was direct or indirect (Huang et al., 2001). In this study, Pyk2 was shown to enhance NMDAR currents via sequential activation of Src (Huang et al., 2001). In cortical neurons, selective activation of group I mGluRs with (S)-3,5-dihydroxy-phenylglycine (DHPG) induced a Ca^{2+}/calmodulin-dependent activation of Pyk2 and the SFKs Src and Fyn leading to tyrosine phosphorylation of the NMDAR (Heidinger et al., 2002). After transient cerebral ischemia and reperfusion, tyrosine phosphorylation of NMDAR subunit 2A (GluN2A) is also mediated via the Pyk2/Src pathway (Liu et al., 2003, 2005). In human neuroblastoma cells, NRG1 signaling, through activation of Fyn and Pyk2, stimulates phosphorylation of Tyr-1472 on the GluN2B subunit of the NMDAR (Bjarnadottir et al., 2007). Pyk2 and the SFKs are also involved in the potentiation of the NMDAR by insulin (Jones and Leonard, 2005).

PSD-95 and SAP102 constitute a potential link between Pyk2 and the NMDAR, allowing, upon Pyk2 activation, its recruitment to the NMDAR via their SH3 domains

(Seabold et al., 2003). More recently, tyrosine phosphorylation of PSD-95 by Src was shown to facilitate the recruitment of Pyk2 to the complex, leading to the idea of a positive loop in which Pyk2 recruited at PSD-95 clusters can activate Src, which phosphorylates PSD-95 and thereby supports the maintained recruitment of Pyk2 and the subsequent tyrosine phosphorylation of GluN2A, which ultimately results in the upregulation of NMDAR function and synaptic transmission (Zhao et al., 2015).

2.2. Development

Pyk2 is a key component of signaling pathways involved in neurite growth and synapse formation (Wang et al., 2010b). In 2000, Ivankovic-Dikic et al. showed that the expression of the C-terminal domain of Pyk2 or FAK blocked neurite outgrowth indicating the possible implication of the FAK family in neurite outgrowth regulation (Ivankovic-Dikic et al., 2000). Blocking intracellular Ca^{2+} mobilization and thereby Pyk2 activation in PC12 cells prevents cell attachment and spreading indicating a role for Pyk2 in morphogenesis and cytoskeletal reorganization that provide the subcellular framework for neurite outgrowth during NGF-induced neuronal differentiation (Park et al., 2000). The role of Pyk2 in neurite formation is likely to involve paxillin, a protein expressed at focal adhesions and interacting with Pyk2 (Park et al., 2000). In PC-12 cells, S85A mutation of paxillin, a residue phosphorylated by the p38 MAPK, was shown to decrease its association with Pyk2 and to inhibit NGF-induced neurite extension (Huang et al., 2004). Pyk2 was also shown to form, with Cbl, a signaling complex that is translocated to lipid rafts and is enriched in growth cones of differentiating PC12 cells following growth factor stimulation (Haglund et al., 2004). Pyk2 may also be involved in pathways leading to the regulation of the expression of genes promoting neurite outgrowth (Banno et al., 2008).

Conversely, activation of GSK3β by Pyk2 was shown to cause neurite retraction in a mechanism depending on microtubules destabilization (Sayas et al., 2006) and, in 2012, Suo et al. demonstrated an inhibitory function of Pyk2 on Rac1 activity and dendritic development (Suo et al., 2012). It is thus likely that Pyk2 activity may be implicated in both retraction and outgrowth of developing neurites, maybe depending on its subcellular localization and specific binding partners.

2.3. Synaptic plasticity

Pyk2 and the Src family kinases were rapidly proposed and then shown to be involved in synaptic plasticity (Girault et al., 1999a; Huang et al., 2001; Bartos et al., 2010; Hsin et al., 2010).

Several studies highlighted the importance of Pyk2 clustering with PSD-95 and NMDAR in the induction of long-term potentiation (LTP). NMDAR was already known to be regulated by phosphorylation on tyrosine, particularly by Src kinase (Yu et al., 1997). In 2001, Huang et al. demonstrated that Pyk2 regulates NMDAR function and LTP by overexpressing Pyk2 in hippocampal slices (Huang et al., 2001). In 2010, Bartos et al. showed that the disruption of the interaction between Pyk2 and PSD-95 abolished LTP in the CA1 (Bartos et al., 2010). In 2013, Yang et al. discovered that Pyk2 activation was accompanied by increased surface expression of NMDAR (Yang et al., 2013). It is thus likely that Pyk2 regulates NMDAR activity, in response to calcium increase, thereby leading to LTP expression.

In addition to its interaction with NMDAR complex, Pyk2 may also regulate the MAPK/ERK pathway, a critical player in synaptic and neuronal plasticity (Derkinderen et al., 1999; Adams and Sweatt, 2002). Pyk2 and ERK are required for LTP induction and/or maintenance in some cell types (Huang et al., 2001; Salter and Kalia, 2004) but it remains unclear if Pyk2 contributes to MAPK activation (Lev et al., 1995; Dikic et al., 1996; Blaukat et al., 1999; Pandey et al., 1999) or if they both participate independently to LTP (Yan et al., 1999; Ivankovic-Dikic et al., 2000; Corvol et al., 2005).

Interestingly, some studies using a heterologous expression system have revealed that the internalization of the Kv1.2 potassium channels is regulated by Pyk2 and its downstream Src-family kinases (Lev et al., 1995; Felsch et al., 1998; Nesti et al., 2004). This mechanism could be involved in a long-term potentiation of intrinsic excitability (LTP-IE) in hippocampal CA3 pyramidal neurons (Hyun et al., 2013).

Pyk2 is also involved in LTD (Hsin et al., 2010). Small hairpin RNA-mediated knockdown of Pyk2 blocks LTD in hippocampal slice cultures. Therefore it is possible that Pyk2 plays a dual role in synaptic plasticity, being involved in both depression and potentiation.

2.4. Neuronal survival

As seen in II.2.1.4, Pyk2 exhibits dual role in non-neuronal cell survival as it can be either pro or anti-apoptotic according to the cell type and the conditions.

In neurons, Pyk2 appears to have an important role in neurogenesis and survival. Overexpression of Pyk2 increases cerebellar granule neurons survival while silencing Pyk2 activity by expressing a dominant-negative form decreases neuronal viability (Strappazzon et al., 2007). Pyk2 may be involved in the brain-derived neurotrophic factor (BDNF) pathway which promotes the growth and differentiation of new neurons and synapses (Xu et al., 2016). Indeed, BDNF was shown to activate Pyk2 through STEP inhibition (Xu et al., 2016) and to induce synaptic synthesis of Pyk2 in the same time (Afonso et al., 2019). In PC12 cells, Pyk2 activates the survival signaling pathway PI3K/Akt/p70S6K in response to H_2O_2 exposure (Banno et al., 2005). Pyk2 was also shown to be involved, with PKCα, in a neuroprotective pathway activated by an enzymatic degradation product of chondroitin sulphate proteoglycan (CSPG) (Rolls et al., 2004). More recently, a neuroprotective role of Pyk2 has also been described in rats receiving a moderate ethanol preconditioning. This preconditioning induces neuroprotection against oxidative stress possibly involving a Pyk2/NMDAR pathway leading to the elevation of an antioxidant protein, peroxiredoxin 2 (Prx2) (Mitchell et al., 2016).

In contrast, a pro-apoptotic role of Pyk2 was described in the chicken spinal cord where overexpression of Pyk2 induces apoptosis. In these cells, alpha- and gamma-protocadherins, by binding and inhibiting Pyk2, prevent this pro-apoptotic effect of Pyk2 and thereby promote cell survival. (Chen et al., 2009). In human differentiating neuroblastoma SH-SY5Y cells as well, Pyk2 may be involved in a pro-apoptotic pathway induced by colchicine and implicating the formation of an 85-kDa poly(adenosine diphosphate ribose)polymerase (PARP) fragment and the induction of the neuroblastoma apoptosis-related RNA-binding protein (NAPOR) gene (Nakagawa-Yagi et al., 2001).

2.5. Pyk2 in glial cells

As evoked in I.2.3, Pyk2 in the brain is mainly expressed by forebrain neurons but it is also present in astrocytes (Cazaubon et al., 1997) and microglial cells (Combs et al., 1999; Tian et al., 2000).

Pyk2 is notably involved in the regulation of astrocytes migration after physical lesion: Pyk2 deficient astrocytes migrate slower and are characterized by an impaired actin re-polymerization after treatment with latrunculin B, a depolymerizing drug (Giralt et al., 2016). This function possibly involves an interaction between Pyk2 and gelsolin (Wang et al., 2003; Giralt et al., 2016).

In microglia, Pyk2 is implicated in the neurotoxic response to amyloidogenic fragments of beta-amyloid and prion proteins (Combs et al., 1999). Pyk2 was also shown to be phosphorylated and to colocalize with phospho-p38MAPK in microglia around the necrotic infarcted area, 24-72 hours following ischemia (Tian et al., 2000).

Such studies corroborate the already evoked functions of Pyk2 (cell migration, response to stress-signals, etc.) in other cell types.

3. Pyk2 in CNS diseases

Given the involvement of Pyk2 in many cellular functions in the central nervous system, an increasing number of studies focus on the pathophysiological role of Pyk2 in the central nervous system and possible therapeutic strategies targeting this protein.

3.1. Alzheimer's disease

Many genome-wide association studies (GWAS) identified *PTK2B* as a susceptibility locus of late onset AD (LOAD) (Kamboh et al., 2012; Lambert et al., 2013; Beecham et al., 2014; De Jager et al., 2014; Wang et al., 2014; Chan et al., 2015; Jiao et al., 2015; Li et al., 2016; Nettiksimmons et al., 2016; Lin et al., 2017). *PTK2B* appears to be associated with hippocampal sclerosis (Beecham et al., 2014), disease progression (Wang et al., 2014), and cognitive decline (Nettiksimmons et al., 2016). The identified risk-associated single nucleotide polymorphism (SNP) rs28834970C was associated with increased *PTK2B* mRNA expression in monocytes, suggesting that Pyk2 is overexpressed in patients carrying this allele (Chan et al., 2015).

Particular proteolysis of amyloid precursor protein (APP) leads to the production and accumulation of β-amyloid peptide (Aβ), which is a hallmark of AD (Benilova et al., 2012). Accumulated Aβ can form both various neurotoxic oligomers and extracellular insoluble plaques (Mucke and Selkoe, 2012). The prion protein (PrPc), which is a receptor of Aβ oligomers (Aβo), associates with metabotropic glutamate receptor 5 (mGluR5) and through it with Homer1b/c, Pyk2, and CamKII (Haas and Strittmatter, 2016; Haas et al., 2016, 2017). Signaling by PrPc and mGluR5, which includes Pyk2 activation, is disrupted by Aβo (Haas and Strittmatter, 2016). This PrPc -mGluR5 signaling pathway involves Fyn since a Fyn inhibitor blocked Pyk2 activation and improved learning and memory in Alzheimer mice (Kaufman et al., 2015).

Another molecular hallmark of AD is aberrant phosphorylation of Tau (Mandelkow and Mandelkow, 2012). Pyk2 is also likely to be involved in tauopathy since Tau is a substrate of both Fyn (Lee et al., 1998, 2004, Bhaskar et al., 2005, 2010) and Pyk2 (Li and Götz, 2018). Pyk2 colocalizes with hyperphosphorylated Tau in the brain of AD patients

and in Tau transgenic pR5 mouse model (Köhler et al., 2013; Dourlen et al., 2017). Pyk2 can also activate GSK3, which phosphorylates Tau (Hooper et al., 2008). Moreover, in drosophila, dFAK, the single orthologue of FAK and Pyk2 in invertebrates, is a modulator of Tau toxicity (Dourlen et al., 2017).

Taken together, these results suggest that Pyk2 can be part of a signaling cascade downstream of mGluR5 that is altered by Aβo interaction with PrPc, while it could also contribute to tauopathy by regulating Tau phosphorylation on several sites.

In contrast, inhibition of the tyrosine phosphatase STEP was shown to enhance Pyk2 phosphorylation *in vivo* and to improve some cognitive deficits in 3xTg-AD mouse model of AD with no change in Aβ and phospho-Tau levels (Xu et al., 2014).

Pyk2 may thus contribute to different parts in the course of the disease. However, further work would be needed to better characterize its precise role.

3.2. Parkinson's disease

Just like in AD, STEP levels were shown to be elevated in brains from patients with Parkinson's disease (PD) (Lombroso et al., 2016) and STEP61, the membrane-associated isoform of STEP, is upregulated in PD (Kurup et al., 2015). These results could suggest a decrease in Pyk2 function in PD but this subject remains unexplored.

3.3. Huntington's disease

Pyk2 may also be involved in Huntington's disease (HD), a neurodegenerative condition caused by an expansion of a CAG repeat in the huntingtin (HTT) gene characterized by motor and behavioral symptoms, and cognitive decline. Expression of polyglutamine-expanded huntingtin (Htt) increases tyrosine phosphorylation of NMDA receptors via PSD-95 and SFKs (Sun et al., 2001; Song et al., 2003). It was also shown that wild-type Htt and Pyk2 interact with the same SH3 domain of PSD-95 (Sun et al., 2001; Seabold et al., 2003). Pyk2 could thus be involved in the Htt-dependent phosphorylation of NMDA receptors leading to HD progression.

3.4. Neuroinflammation

Transient receptor potential melastatin 2 (TRPM2) is a ROS-sensitive calcium channel involved in many neurological diseases (Belrose and Jackson, 2018). In monocytes, TRPM2 was shown to activate a Pyk2/ERK pathway leading to generation of chemokines and ulcerative inflammation (Yamamoto et al., 2008). More recently, Alawieyah Syed Mortadza et al. studied the role of this pathway in Aβ-induced AD-related neuroinflammation (Alawieyah Syed Mortadza et al., 2018). They discovered that a TRPM2-dependent activation of the Pyk2/ERK signaling pathway was critical for microglial activation and generation of tumor necrosis factor-α (Alawieyah Syed Mortadza et al., 2018). In the same way, it must be noted that the Pyk2-activated kinase GSK3 is also involved in neuroinflammation (Weng et al., 2014) contributing to the idea of a pro-inflammatory role of Pyk2 in the brain.

3.5. Glioma and neuroblastoma

Protein levels of Pyk2 were shown to be upregulated in glioma cells (Hoelzinger et al., 2005). In 2003, Lipinski et al. discovered that the overexpression of Pyk2 in human

glioblastoma cells stimulated migration (Lipinski et al., 2003). siRNA knockdown of Pyk2 further confirmed the central role of Pyk2 in the migration of glioblastoma cells (Lipinski et al., 2005; Rolón-Reyes et al., 2015). Especially, the interaction between Pyk2 and MAP4K4 was shown to be decisive in this function (Loftus et al., 2013). In 2015, Xu et al. demonstrated that melatonin could be a potential therapeutic molecule which is able to reduce Pyk2 activation and, thus, inhibit tumor cell migration/invasion (Xu et al., 2015). In neuroblastoma, Pyk2 may also play an important role as it was shown that TRPM2 expression protects the viability of neuroblastoma through a pathway involving Pyk2 activation (Hirschler-Laszkiewicz et al., 2018). Taken together, these results indicate that Pyk2 could be a potential target for glioma and neuroblastoma therapies.

3.6. Cerebral ischemia

Pyk2 is activated in cortical neurons following cerebral ischemia (Tian et al., 2000) and in SH-SY5Y cells following oxygen-glucose deprivation, a widely used in vitro model for stroke (Yan et al., 2015). Pyk2 would be involved in the modulation of NMDA receptor activity after ischemia as it was shown that suppression of Pyk2 attenuates the increased tyrosine phosphorylation of NR2A after brain ischemia in rat hippocampus (Liu et al., 2005). Moreover, chronic lithium is neuroprotective during ischemia by inhibiting the phosphorylation of Pyk2 and the interactions of Pyk2 and PSD-95 with NR2A, thus decreasing NR2A activity (Ma et al., 2004). Pyk2 appears here as well as a good candidate for therapies aiming to protect the brain after ischemia.

3.7. Psychiatric disorders

Several studies associated Pyk2 with chronic stress damage and depressive disorders. In the lateral septum, Pyk2 phosphorylation decreases following stress exposure and the enhancement of Pyk2 expression prevented behavioral deficit caused by exposure to inescapable shock, indicating an antidepressant role (Sheehan et al., 2003). Accordingly, in rat prefrontal cortex, imipramine, an antidepressant drug that counteracts depressive disorders, activates a pathway involving Pyk2 activation and ERK phosphorylation also suggesting a possible antidepressant function of Pyk2 (Zalewska et al., 2016). In 2014, Kinoshita et al. discovered a role of Pyk2 in the deficit of the nuclear pore protein NUP62 in CA3 hippocampal neurons following chronic stress, possibly leading to a decreased dendritic complexity (Kinoshita et al., 2014). Besides, genome-wide association studies identified *PTK2B* as a gene associated with subjective well-being, depressive symptoms, and neuroticism (Okbay et al., 2016).

Thus, Pyk2 is probably playing different roles but still appears as an element of stress response.

Another brain disorder which may involve Pyk2 is addiction. Chronic exposure to cocaine was shown to increase Pyk2 levels in primate nucleus accumbens (NAc) (Freeman et al., 2001) and rat frontal cortex (Freeman et al., 2002) leading here again to the idea of a possible implication of Pyk2 in these troubles.

To conclude this introduction, Pyk2 is an isoform of FAK which appeared early in vertebrate ancestors. It is regulated by Ca^{2+} through several mechanisms which are not fully understood at the molecular level. It can also be recruited following SFKs activation and have non-enzymatic scaffolding functions. Pyk2 role has been described in many cellular

functions, some being similar to those of FAK with which there is some degree of redundancy, but mostly in other original functions. It appears to have sometimes opposing effects depending on cell types and experimental conditions. Pyk2 knockout mice are viable and show little or no phenotype showing that Pyk2 function is not essential and/or can be compensated by other genes. In the nervous system it may play a role in development, synaptic function and plasticity and in non-neuronal cells including astrocytes and microglial cells. Its implication in multiple pathological conditions has also been suggested but very little has been actually demonstrated or shown to be important in vivo. In this thesis the aim was to use Pyk2 KO mice to address these points.

RESULTS

In the following section, I will present the experimental results of my PhD, grouping articles to which I contributed and a preliminary manuscript of my main project.

Works from many laboratories, including our, have shown that Pyk2 is involved in many pathologies and, notably, in neurologic diseases. For its reported implication in synaptic signaling and plasticity amongst other, the involvement of Pyk2 in such neurological disorders may rely on signaling abnormalities and synaptic plasticity defects. The aim of my PhD was to dissect out the involvement and function of Pyk2 in pathological conditions of the brain and particularly, in neurodegenerative diseases.

Our experimental approach is based on constitutive and conditional genetic deletion of Pyk2 in mice. To do so, $Pyk2^{f/f}$ C57Bl/6 mice were generated as described in II.2.2.6 and then crossed with an expressing Cre line (under a constitutive promotor or under a promotor specific to a neuronal population), or injected in a part of the brain with a Cre-expressing adeno-associated virus (AAV-Cre).

I first participated in the characterization of the biochemical and cellular consequences of Pyk2 deficit in the hippocampus of mice and described the possible involvement of Pyk2 in Huntington's disease cognitive impairments (**Article 1**).

In the prolongation of this work focused on hippocampus, I participated in a study of Pyk2 role in chronic stress-induced depression in mice (**Article 2**).

Given the identification of *PTK2B* as a gene associated with increased risk for LOAD, we then explored the putative role of Pyk2 in a mouse model of Alzheimer's disease (**Article 3**).

In parallel with these experiments I used the same mouse model of AD to investigate the potential benefit of astrocyte-targeted delivery of BDNF in this disease (**Article 4**). Since some studies described relations between Pyk2 and the BDNF pathway (Xu et al., 2016; Afonso et al., 2019), we will discuss the results of this paper in light of our previous findings.

The last study (**Article 5**, submitted) dealt with the putative role of Pyk2 in the striatum of mice and, particularly, in the locomotor response to cocaine.

I. Pyk2 modulates hippocampal excitatory synapses and contributes to cognitive deficits in a Huntington's disease model

Albert Giralt, Veronica Brito, Quentin Chevy, Clémence Simonnet, Yo Otsu, Carmen Cifuentes-Díaz, Benoit de Pins, Renata Coura, Jordi Alberch, Sílvia Ginés, Jean-Christophe Poncer and Jean-Antoine Girault

Nature Communication
30 May 2017, 8:15592

1. Context and objectives

Although several studies have investigated the regulation and the role of Pyk2 in the brain including in hippocampus *in vitro* and demonstrated its possible implication in synaptic plasticity, nothing was known about the importance of Pyk2 *in vivo*.

In this paper, we used Pyk2 heterozygous and homozygous knockout mice generated in the laboratory to investigate the functional consequences of Pyk2 deficiency in hippocampal physiology. To rule out the role of developmental defects in the phenotype, we also used $Pyk2^{f/f}$ mice to induce a targeted deletion in the adult by injecting AAV Cre in the hippocampus. We also studied the morphology of $Pyk2^{-/-}$ hippocampal neurons in culture and tried to rescue the phenotype by expressing various forms of Pyk2 to determine the role of its various domains, kinase activity, and autophosphorylated residue.

HD is an autosomal dominant neurodegenerative disorder associated with the development of mood alterations, mental disabilities, coordination problems, and jerky body movements. Although the lesions of the striatum and cerebral cortex are the most prominent and at the forefront of the clinical manifestations, hippocampal alterations have also been reported (Murphy et al., 2000; Milnerwood et al., 2006). Since the hippocampal phenotype of Pyk2 KO mice had some similarities with that of R6/1 mice, a model of Huntington's disease (HD), we examined the levels of Pyk2 in these mice and in the hippocampus of patients with HD. We then investigated whether overexpressing Pyk2 in the hippocampus of R6/1 mice could restore some behavioral, histological, physiological or biochemical defects.

2. Contribution to the work

In this work, I personally contributed to the molecular biology works and to tissue imaging.

3. Article

nature COMMUNICATIONS

ARTICLE

Received 18 Aug 2016 | Accepted 11 Apr 2017 | Published 30 May 2017

DOI: 10.1038/ncomms15592 OPEN

Pyk2 modulates hippocampal excitatory synapses and contributes to cognitive deficits in a Huntington's disease model

Albert Giralt[1,2,3], Veronica Brito[4,5,6,7], Quentin Chevy[1,2,3,†], Clémence Simonnet[1,2,3], Yo Otsu[1,2,3], Carmen Cifuentes-Díaz[1,2,3], Benoit de Pins[1,2,3], Renata Coura[1,2,3], Jordi Alberch[4,5,6,7], Sílvia Ginés[4,5,6,7], Jean-Christophe Poncer[1,2,3] & Jean-Antoine Girault[1,2,3]

The structure and function of spines and excitatory synapses are under the dynamic control of multiple signalling networks. Although tyrosine phosphorylation is involved, its regulation and importance are not well understood. Here we study the role of Pyk2, a non-receptor calcium-dependent protein-tyrosine kinase highly expressed in the hippocampus. Hippocampal-related learning and CA1 long-term potentiation are severely impaired in Pyk2-deficient mice and are associated with alterations in NMDA receptors, PSD-95 and dendritic spines. In cultured hippocampal neurons, Pyk2 has autophosphorylation-dependent and -independent roles in determining PSD-95 enrichment and spines density. Pyk2 levels are decreased in the hippocampus of individuals with Huntington and in the R6/1 mouse model of the disease. Normalizing Pyk2 levels in the hippocampus of R6/1 mice rescues memory deficits, spines pathology and PSD-95 localization. Our results reveal a role for Pyk2 in spine structure and synaptic function, and suggest that its deficit contributes to Huntington's disease cognitive impairments.

[1] Inserm UMR-S 839, 75005 Paris, France. [2] Université Pierre & Marie Curie, Sorbonne Universités, 75005 Paris, France. [3] Institut du Fer a Moulin, 75005 Paris, France. [4] Departament de Biomedicina, Facultat de Medicina, Universitat de Barcelona, 08036 Barcelona, Spain. [5] Institut d'Investigacions Biomèdiques August Pii Sunyer (IDIBAPS), 08036 Barcelona, Spain. [6] Centro de Investigación Biomédica en Red Sobre Enfermedades Neurodegenerativas (CIBERNED), 28031 Madrid, Spain. [7] Institut de Neurociencies, Universitat de Barcelona, 08036 Barcelona, Spain. † Present address: Cold Spring Harbor Laboratory, 1 Bungtown Road, Cold Spring Harbor, New York 11724, USA. Correspondence and requests for materials should be addressed to J.-A.G. (email: jean-antoine.girault@inserm.fr).

Synaptic function and plasticity, as well as spine morphology are regulated by multiple signalling pathways that integrate the diversity of signals converging on synapses. Receptors for neurotransmitters, as well as numerous other post-synaptic proteins are phosphorylated by a variety of serine/threonine protein kinases, many of which have been extensively investigated, especially in the context of synaptic plasticity. Tyrosine kinases have also been reported to contribute to the regulation of post-synaptic proteins, including regulation of NMDA (*N*-methyl-D-aspartate) glutamate receptors by Src family kinases (SFKs) and proline-rich tyrosine kinase 2 (Pyk2)[1,2]. However, the functional importance of these regulations *in vivo* is unknown.

Pyk2 is a non-receptor tyrosine kinase that can be activated by Ca^{2+} and is highly expressed in forebrain neurons, especially in the hippocampus[3,4]. Previous findings indicated a role for Pyk2 in synaptic plasticity[1,5–7] and its gene, *PTK2B*, is a susceptibility locus for Alzheimer's disease[8]. Pyk2 is activated by Ca^{2+}, and although the mechanism has not been fully elucidated, it probably involves dimer assembly[9], which triggers its autophosphorylation at Tyr402 and the recruitment of SFKs[10]. Tyr402 phosphorylation is increased by neuronal depolarization[11] and tetanic stimulation[7] in hippocampal slices, and by activation of NMDA[5] or group I metabotropic[12] glutamate receptors in cultured hippocampal neurons. Pyk2 and SFKs are part of the NMDA receptor complex[7,13] and Pyk2 interacts directly with post-synaptic density (PSD) proteins PSD95 (ref. 14), SAP102 (ref. 14) and SAPAP3 (ref. 15). Long-term potentiation (LTP) of CA1 synapses requires protein tyrosine phosphorylation[16,17] and is prevented by a kinase-dead Pyk2 (ref. 7) or by competition of Pyk2:PSD95 interaction[5]. These results led to the suggestion of a role of Ca^{2+}-induced activation of Pyk2 in regulating NMDA receptor function and synaptic plasticity, likely through recruitment of SFKs[1,2]. However, the functional relevance of these findings *in vivo* is not known and the role of Pyk2 in hippocampal physiology or pathology has not been investigated. Pyk2 knockout mice display a mild immunological phenotype but their nervous system has not been studied[18].

Here we show that the inactivation of one or two alleles of the *Ptk2b* gene in mice does not alter hippocampal development but prevents hippocampal-dependent memory tasks and LTP. We provide evidence for multiple roles of Pyk2 in spine morphology and post-synaptic structure. Moreover, we show that Pyk2 is decreased in the hippocampus of patients with Huntington's disease (HD), an inherited neurodegenerative disorder, which results from the expansion of a CAG trinucleotide repeat in the huntingtin (Htt) gene[19]. Pyk2 is also decreased in R6/1 mice, which express a mutated form of Htt, and these mice display a hippocampal phenotype similar to that observed in Pyk2 mutant mice. This phenotype is partly rescued by restoring Pyk2 levels in R6/1 mice, suggesting a reversible role of Pyk2 deficit in the HD mouse model.

Results

Pyk2 knockout impairs hippocampal-dependent memory and LTP. To study the role of Pyk2 in the brain, we used a knockout mouse line[20] that we recently generated. As previously observed for a similar line[18], these mice bred normally and there were no differences between $Pyk2^{+/+}$, $Pyk2^{+/-}$ and $Pyk2^{-/-}$ mice in body weight, muscular strength, general locomotor activity or anxiety levels evaluated in the elevated plus-maze (Supplementary Fig. 1a–d). We tested $Pyk2^{+/+}$, $Pyk2^{+/-}$ and $Pyk2^{-/-}$ littermate mice in two simple tasks that depend on hippocampus-mediated spatial memory[21,22]. In the Y-maze spontaneous alternation task, $Pyk2^{+/+}$ mice showed a significant preference for the new arm 2 h after exposure to the other arm, whereas both $Pyk2^{+/-}$ and $Pyk2^{-/-}$ littermates explored equally both arms (Fig. 1a). In the novel object location (NOL) test, 24 h after a first exposure, wild-type mice spent more time exploring the object placed at a new location (Fig. 1b). In contrast, both $Pyk2^{+/-}$ and $Pyk2^{-/-}$ mice did not display any preference for either object (Fig. 1b). These results revealed spatial memory deficits in both heterozygous and homozygous mutant mice.

We next examined whether these behavioural deficits were accompanied by altered synaptic plasticity in hippocampal slices. We restricted our study to CA1, a hippocampal region extensively implicated in spatial learning. High-frequency conditioning tetanus of Schaffer collaterals (5×1 s at 100 Hz) induced LTP in CA1 of wild-type mice (Fig. 1c). In contrast, no LTP was observed in slices from $Pyk2^{+/-}$ or $Pyk2^{-/-}$ mice (Fig. 1c,d). We also examined a form of short-term plasticity at the same synapses. Paired-pulse facilitation was observed in wild-type mice but was markedly decreased in both homozygous and heterozygous Pyk2 mutant mice (Fig. 1e and Supplementary Fig. 1e), suggesting the existence of a presynaptic role of Pyk2. Taken together, these results show that deletion of Pyk2 impairs hippocampus-dependent memory and synaptic plasticity in CA1. Importantly, the heterozygous mutation of Pyk2 was as severe as the full deletion, indicating that Pyk2 levels may be limiting for hippocampal plasticity.

Alteration in NMDA receptors and PSD-95 in Pyk2 mutant mice. To explore the molecular consequences of Pyk2 deficit, we examined the levels of proteins previously associated with the Pyk2 pathway at synapses by immunoblotting. In hippocampal tissue of $Pyk2^{+/-}$ mice, Pyk2 protein was decreased by about 50% as compared to wild-type littermates, and was not detectable in $Pyk2^{-/-}$ mice (Fig. 2a,b). No N-terminal truncated fragment was detected in the knockout mice (Supplementary Fig. 2a), showing that deletion of exons 15–18 in the *Pyk2* gene[20] destabilized the resulting mRNA and/or protein. There was no compensatory alteration of the related focal adhesion kinase (FAK, Fig. 2a,b). In both $Pyk2^{+/-}$ and $Pyk2^{-/-}$ mice, the activated form of SFKs (pY-SFK, pTyr420 in Fyn) was markedly reduced, whereas Fyn levels were unchanged (Fig. 2a,b), underlining the contribution of Pyk2 in regulating SFKs phosphorylation. In contrast, there was no change in the basal phosphorylation (activation) of ERK1/2 (Supplementary Fig. 2b,c), reported to be downstream of Pyk2 in some cell systems[10], including in hippocampal neurons in culture[6], but not in adult slices[23]. We then focused on glutamate receptors. We found no consistent change between genotypes in GluA1 and GluA2 AMPA receptors subunits, or in their phosphorylated forms pSer831-GluA1 and pTyr876-GluA2 (Supplementary Fig. 2d,e). NMDA receptors GluN1 levels were not changed either (Fig. 2d,e). In contrast, we observed marked alterations of NMDA receptor N2 subunits. The phosphorylated forms of GluN2A and GluN2B, pTyr1246- and pTyr1325-GluN2A, and pTyr1472-GluN2B were decreased in $Pyk2^{-/-}$ compared to wild-type mice. Total GluN2B was not changed indicating deficient tyrosine phosphorylation in the absence of Pyk2 (Fig. 2d,e). In contrast, total GluN2A was decreased (Fig. 2d,e). We also examined PSD-95, a post-synaptic scaffolding protein that interacts with both NMDA receptors and Pyk2 (refs 5,14). The levels of PSD-95 were markedly decreased in homozygous mutant mice (Fig. 2d,e). Thus, in contrast with the behavioural and physiological deficits, which appeared as pronounced in heterozygous as in homozygous mutant mice (see Fig. 1), the protein alterations in $Pyk2^{+/-}$ mice were intermediate between wild type and $Pyk2^{-/-}$, indicating some proportionality between the decrease in Pyk2 and its consequences on other proteins. To determine the changes in receptors that took place at

synapses, we carried out subcellular fractionation and isolated postsynaptic densities (PSDs). The amounts of GluN1, GluN2A, GluN2B and PSD-95 were decreased in the PSD fraction of Pyk2$^{-/-}$ mice as compared to wild type (Fig. 2e,f). These results showed that the lack of Pyk2 signalling resulted in decreased tyrosine phosphorylation of SFKs and GluN2B subunits as well as decreased levels of GluN2A and PSD95 total protein. The enrichment of all these proteins in PSDs was markedly decreased, indicating a key role of Pyk2 in regulating the recruitment of post-synaptic proteins to PSDs.

Spines are altered in the hippocampus of Pyk2 mutant mice. To explore how Pyk2 deficit could induce alterations of synaptic proteins, we first determined its localization in CA1. Pyk2 immunofluorescence in the neuropil was punctate and appeared to surround MAP2-positive dendritic processes (Fig. 3a). Some Pyk2-positive puncta co-localized with PSD-95-positive puncta, identifying them as PSDs (Fig. 3b). We then examined Pyk2 immunoreactivity by electron microscopy. Pyk2-positive immunogold particles were found in both presynaptic elements and dendritic spines (Fig. 3c and Supplementary Fig. 3a). Pyk2 was enriched in asymmetric (presumably excitatory) synapses as compared to symmetric (presumably inhibitory) synapses (Supplementary Fig. 3a–d). Because of Pyk2 co-localization with PSD-95 and of the marked decrease in PSD-95 in Pyk2$^{-/-}$ mice, we quantified PSD-95-positive puncta in CA1 *stratum radiatum* of wild-type and mutant mice. The number of PSD-95-positive puncta was significantly reduced in Pyk2$^{+/-}$ and even more so in Pyk2$^{-/-}$ as compared to Pyk2$^{+/+}$ mice (Fig. 3d,e).

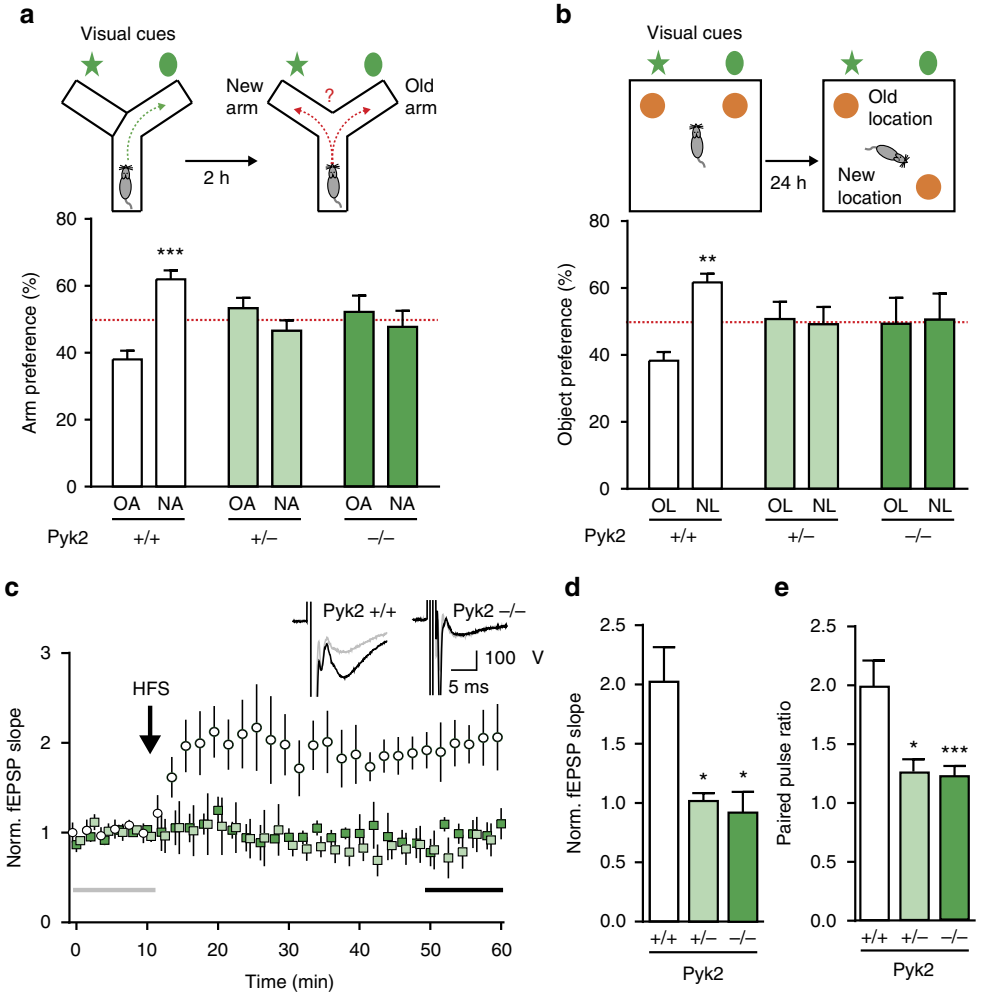

Figure 1 | Spatial learning and memory and CA1 LTP deficits in Pyk2 mutant mice. (**a**) In the spontaneous alternation test, Pyk2$^{+/+}$, Pyk2$^{+/-}$ and Pyk2$^{-/-}$ 3-month-old mice were placed for 10 min in a Y-maze with one arm closed (upper left panel). Two hours later, they were put in the same maze with the new arm (NA) open and the percentage of time exploring the NA and the previously explored (old arm, OA) was compared (upper right panel). Two-way ANOVA interaction $F_{(2,48)}=11.6$, $P<0.0001$, OA versus NA Holm-Sidak's test, Pyk2$^{+/+}$, $t=4.6$, $P<0.0001$, Pyk2$^{+/-}$, $t=1.58$, Pyk2$^{-/-}$, $t=0.81$. (**b**) In the NOL test, the percentage of time exploring the displaced object (new location, NL, 24 h after first exposure) and the unmoved object (old location, OL) was compared (upper panels). Two-way ANOVA interaction $F_{(2,50)}=3.41$, $P=0.041$, OL versus NL Holm-Sidak's test, Pyk2$^{+/+}$, $t=3.1$, $P<0.01$, Pyk2$^{+/-}$, $t=0.23$, Pyk2$^{-/-}$, $t=0.14$. In **a**,**b**, 7-12 mice were used per genotype; the red dotted line indicates the chance level. (**c**,**d**) Schaffer collaterals were stimulated in hippocampal slices (one-three slices per animal) from 3-4-week-old Pyk2$^{+/+}$ ($n=5$), Pyk2$^{+/-}$ ($n=6$) and Pyk2$^{-/-}$ ($n=4$) mice, and fEPSP were recorded in CA1, before and after HFS (5 × 1 s at 100 Hz). (**c**) Time course of fEPSP slope. Insets show typical traces before (grey) and 40 min after (black) HFS in Pyk2$^{+/+}$ and Pyk2$^{-/-}$ slices. (**d**) Ten-min average of fEPSP slope 40 min after HFS, normalized to the mean of 10- min baseline (corresponding time points are indicated in **c** by grey and black horizontal lines). Kruskal–Wallis = 9.37, $P=0.0024$, *post hoc* analysis with Dunn's multiple comparisons test. (**e**) Paired-pulse ratio (50-ms interval, see Supplementary Fig. 1e) at the same synapses. $n=3$–5 mice per group, two-four slices per mouse. Kruskal–Wallis = 15.62, $P=0.0004$. In **a**–**e**, values are means + s.e.m., $^{*}P<0.05$, $^{**}P<0.01$, $^{***}P<0.001$.

This effect appeared consistent throughout CA1 depth (Supplementary Fig. 3e).

To determine the consequences of these alterations on spines, we analysed spine density and morphology in CA1 pyramidal neurons, using the Golgi-Cox method (Fig. 3f). The apical dendritic spines density was decreased in Pyk2$^{+/-}$ (−8%) and Pyk2$^{-/-}$ (−16%) mice as compared to wild type (Fig. 3g). The decrease in spine number was less pronounced than the decrease in PSD-95 puncta, possibly due to an immunofluorescence detection threshold and/or an increased number of spines lacking PSD-95. To determine whether the absence of Pyk2 also affected spine morphology, we quantified the spine head diameter and spine neck length. Spine head size did not change between genotypes (Fig. 3h), whereas spine neck length was decreased in Pyk2 mutant mice (Fig. 3i). Altogether, these data show that the lack of Pyk2 leads to a decrease in PSD-95 at synapses and a decreased number of PSDs and spines.

Adult hippocampal Pyk2 deletion recapitulates the phenotype. Although Pyk2 expression in the hippocampus is mostly postnatal[4], the severe alterations observed in Pyk2$^{+/-}$ and Pyk2$^{-/-}$ mice could result from developmental effects. To rule out this possibility, we used 3-month-old mice bearing floxed Pyk2 alleles (Pyk2$^{f/f}$ mice). Mice received a bilateral stereotaxic injection in CA1 of adeno-associated virus expressing Cre recombinase and GFP (AAV-Cre) or expressing GFP alone (AAV-GFP), as a control (Fig. 4a). Three weeks after AAV-Cre injection, Pyk2 expression disappeared in CA1, whereas the injection of

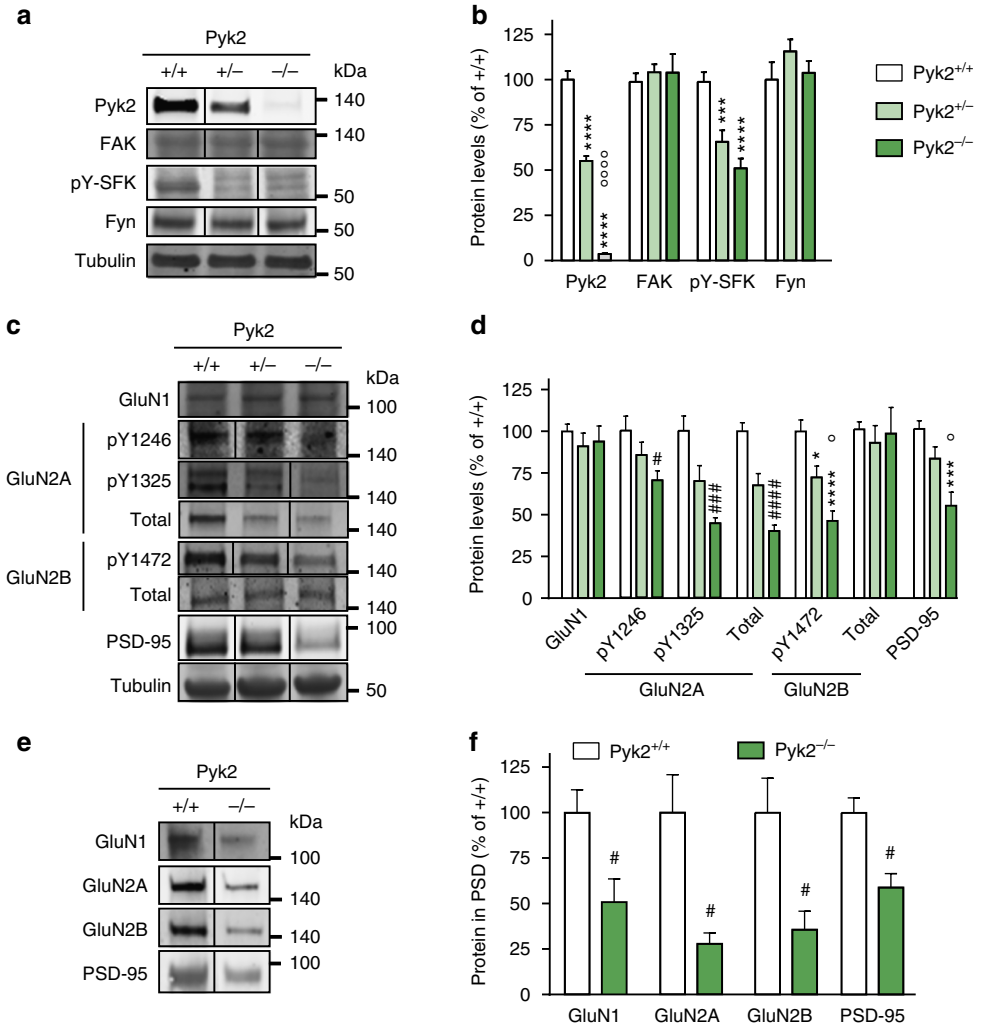

Figure 2 | Hippocampal proteins phosphorylation and levels in Pyk2-deficient mice. (**a**) Immunoblotting analysis of Pyk2, the related tyrosine kinase FAK, the active autophosphorylated form of Src-family kinases (pY-SFK, pTyr-420 in Fyn), Fyn and tubulin as a loading control in 3-month-old Pyk2$^{+/+}$, Pyk2$^{+/-}$ and Pyk2$^{-/-}$ littermates. (**b**) Densitometry quantification of results as in **a**. Data were normalized to tubulin for each sample and expressed as percentage of wild type. (**c**) NMDA receptors subunits phosphorylated residues, total levels and PSD-95 were analysed by immunoblotting. (**d**) Results as in **c** were quantified and analysed as indicated in **b**. In **b** and **d**, statistical analysis was done with one-way ANOVA and Holm-Sidak's multiple comparisons test or Kruskal–Wallis and Dunn's test depending on the normality of distribution (see Supplementary Table 1 for tests used, values and number of mice). (**e**) PSD fraction was prepared from hippocampus of Pyk2$^{+/+}$ and Pyk2$^{-/-}$ mice and NMDA receptor subunits and PSD-95 were analysed in this fraction by immunoblotting. (**f**) Quantification of immunoblots as in **e**. Data are expressed as a percentage of the mean values in wild-type PSDs. Two-tailed Mann and Whitney test ($n=7^{+/+}$ and $5^{-/-}$): GluN1, $t_{10}=3.52$, $P=0.0056$, GluN2A, $t_{10}=2.68$, $P=0.023$, GluN2B, $t_{10}=2.69$, $P=0.022$, PSD-95, $t_{10}=2.66$, $P=0.024$. In **a**,**c**,**e**, molecular weight markers positions are indicated in kDa. In **b**,**d**, Holm-Sidak's versus wild type, $^{*}P<0.05$, $^{**}P<0.01$, $^{***}P<0.001$ and $^{****}P<10^{-4}$; significant differences between $-/-$ and $-/+$ are indicated with $^{\circ}P<0.05$, $^{\circ\circ}P<0.01$ and $^{\circ\circ\circ\circ}P<10^{-4}$. In Dunn's test (**d**) and Mann and Whitney's test (**f**), significant differences versus wild type are indicated with # $P<0.05$, ### $P<0.01$ and #### $P<10^{-4}$. In all graphs, data are means + s.e.m. Uncropped blots for **a**,**c** and **e** are shown in Supplementary Figs 5, 6 and 7, respectively.

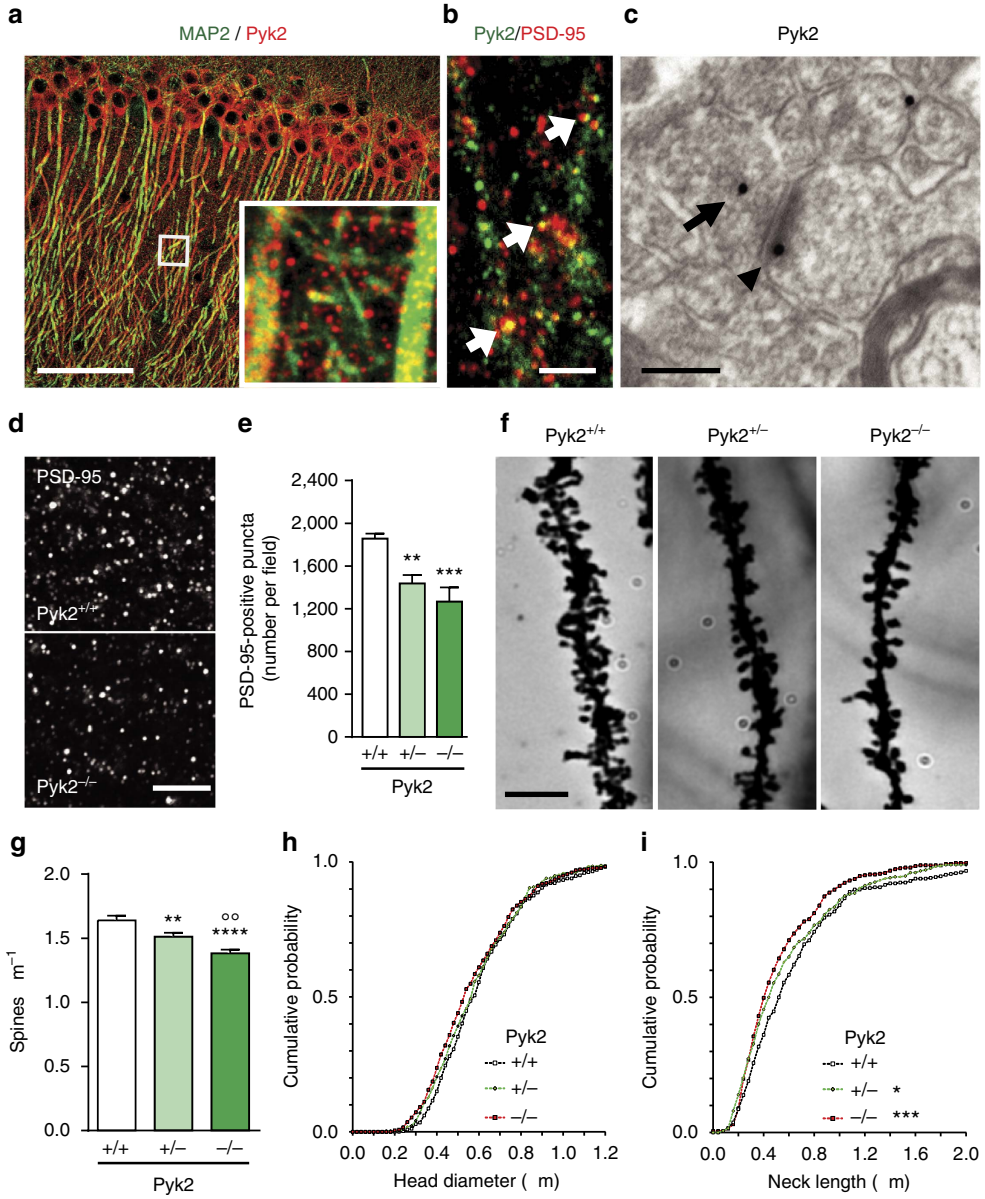

Figure 3 | Pyk2 localization and dendritic spine density and morphology in Pyk2-deficient mice. (**a**,**b**) Confocal microscopy images of CA1 *stratum radiatum* immunostained for (**a**) Pyk2 (red) and MAP2 (green; inset, higher magnification of the indicated white box) and for (**b**) Pyk2 (green) and PSD-95 (red; white arrows, double-labelled puncta). Scale bars, 80 µm (**a**) and 3 µm (**b**). (**c**) Electron microscopy in the same region showing of Pyk2 immunoreactive gold particles in a presynaptic terminal (arrow) and a PSD (arrowhead). Scale bar, 0.2 µm. (**d**) Immunofluorescence PSD-95-positive puncta in the CA1 *stratum radiatum* from Pyk2$^{+/+}$ and Pyk2$^{-/-}$ mice. Scale bar, 5 µm. (**e**) Quantification of puncta as in **d**. Data are means + s.e.m. (7–10 mice per genotype, three quantified sections per mouse). One-way ANOVA $F_{(2,21)} = 10.23$, $P = 0.0008$. Holm-Sidak's multiple comparisons test versus +/+, $^{**}P < 0.01$, $^{***}P < 0.001$. (**f**) Golgi-Cox-stained apical dendrites of CA1 *stratum radiatum* pyramidal neuron from Pyk2$^{+/+}$, Pyk2$^{+/-}$ and Pyk2$^{-/-}$ mice. Scale bar, 3 µm. (**g**) Quantification of spine density in dendrites as in **f**, three–four animals per genotype, one-way ANOVA, $F_{(2,146)} = 14.95$, $P < 10^{-4}$ ($n = 47$–54 dendrites per group), *post hoc* analysis with Holm-Sidak's multiple comparisons test versus +/+, $^{**}P < 0.01$, $^{****}P < 10^{-4}$ and −/− versus −/+, $^{\circ\circ}P < 0.01$. (**h**,**i**) Cumulative probability of spine head diameter (**h**, $n = 80$) and spine neck length (**i**, $n = 115$) in ~60 dendrites from three–four animals per genotype. Distributions were compared with the Kolmogorov–Smirnov test: spine head diameter no significant difference, neck length +/+ versus +/−, $D = 0.108$, $P = 0.04$, +/+ versus −/−, $D = 0.154$, $P = 0.0005$. In **e**,**g**, data are means + s.e.m. All mice were 3–4-month old.

AAV-GFP had no effect (Fig. 4a). In the NOL test, AAV-GFP-injected mice showed increased preference for the object placed at the new location, whereas AAV-Cre-injected mice did not (Fig. 4b). We analysed spine density in CA1 apical dendrites and found it was significantly reduced in AAV-Cre-injected mice as compared to AAV-GFP-injected mice (Fig. 4c,d). We also quantified a reduced number of PSD-95-positive puncta in CA1 *stratum radiatum* of AAV-Cre-injected mice as compared to AAV-GFP-injected mice (Fig. 4e,f). Altogether these results show that local deletion of Pyk2 in CA1 of adult mice recapitulates behavioural and morphological deficits observed in Pyk2$^{+/-}$ and Pyk2$^{-/-}$ mice, ruling out a developmental effect in the phenotype of Pyk2 mutant mice.

Pyk2 is needed for NMDA-induced PSD-95 recruitment in spines. PSD-95 undergoes rapid activity-dependent relocalization[24].

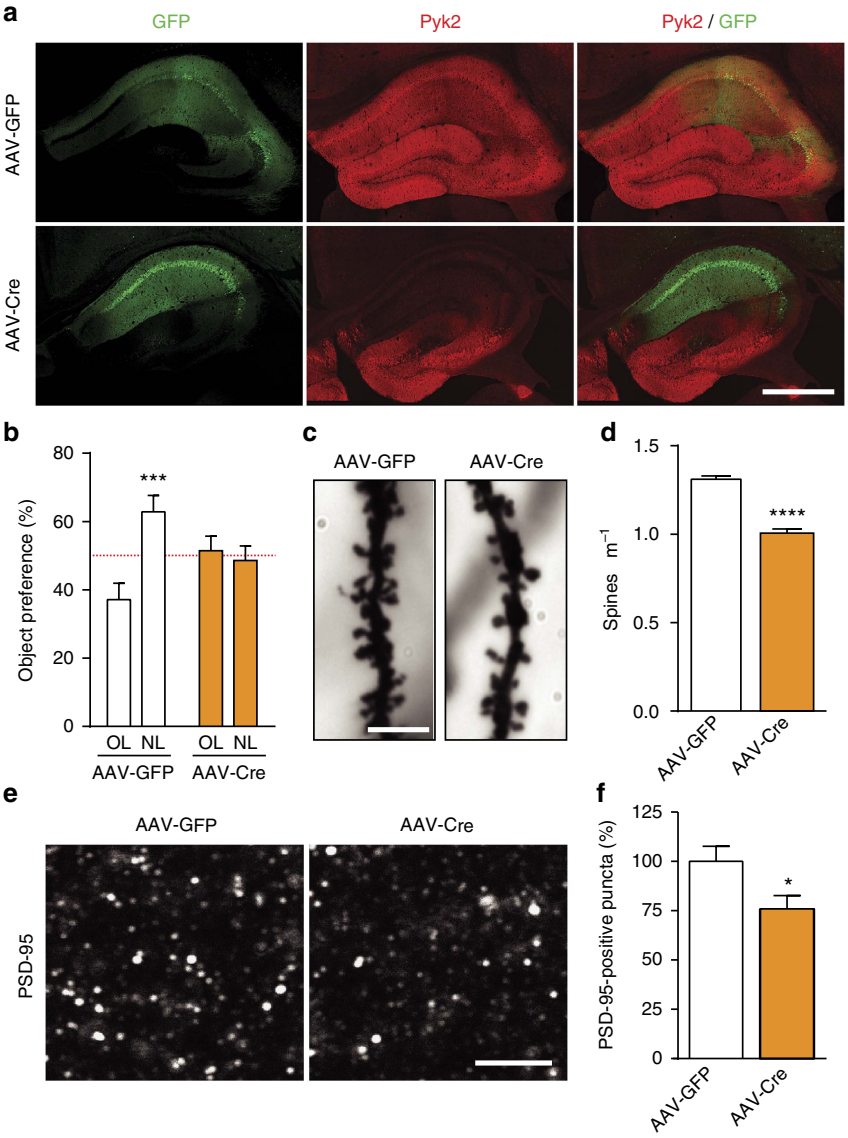

Figure 4 | Pyk2 ablation in CA1 from adult mice induces spatial learning deficits and spine alterations. (**a**) Mice with floxed Pyk2 alleles ($Pyk2^{f/f}$, 4-week-old) were bilaterally injected in dorsal hippocampus CA1 with AAV expressing GFP (AAV-GFP) or GFP-Cre (AAV-Cre). GFP fluorescence (green) and Pyk2 immunoreactivity (red) were detected with confocal microscope (stitched pictures). With both viruses widespread, GFP expression is present in CA1 and Pyk2 is reduced in CA1 of AAV-Cre-injected mice. Scale bar, 200 µm. (**b**) AAV-GFP and AAV-Cre mice were subjected to the NOL test as in Fig. 1b and the percentage of time exploring the displaced object (NL) compared to that exploring the unmoved object (OL). Two-way ANOVA interaction $F_{(1,44)}=9.94$, $P=0.003$, OL versus NL Holm-Sidak's test, AAV-GFP, $t=4.0$, $P<0.001$, AAV-Cre, $t=0.45$, ns (12 mice per group). The red dotted line indicates the chance level. (**c**) Representative Golgi-Cox-stained apical dendrites from CA1 pyramidal neurons of AAV-GFP and AAV-Cre mice. Scale bar, 4 µm. (**d**) Quantification of spine density in dendrites stained as in **c**, 81–86 dendrites from four mice per genotype. Student's *t*-test $t_{165}=10.1$, $P<10^{-4}$. (**e**) PSD-95 immunoreactive puncta in CA1 *stratum radiatum* of AAV-GFP and AAV-Cre mice. Scale bar, 4 µm (**c**,**e**). (**f**) Quantification of PSD-95-positive puncta density as in **e**, three sections per mouse, six–eight mice per genotype, Student's *t*-test $t_{12}=2.36$, $P<0.5$. In **a**,**d**,**f**, data are means + s.e.m., $^{*}P<0.05$, $^{***}P<0.001$ and $^{****}P<10^{-4}$.

Although neuronal stimulation decreases PSD-95 palmitoylation-dependent synaptic targeting[25] and increases its ubiquitination and degradation[26], prolonged neuronal activity was shown to increase PSD-95 synaptic concentration[27]. PSD-95 is phosphorylated on multiple tyrosine residues and this phosphorylation can increase its synaptic clustering[28,29]. Since PSD-95 synaptic clustering was decreased in the absence of Pyk2 (Figs 3d,e and 4e,f), we hypothesized Pyk2 may influence the synaptic localization of PSD-95. We tested this hypothesis using hippocampal neurons in primary culture at ~21–22 DIV. As expected, glutamate treatment (40 µM, 15 min) increased Pyk2 phosphorylation at Tyr402 in hippocampal neurons in culture and this effect was prevented by an NMDA receptor antagonist, MK801 (10 µM, Fig. 5a,b). The size of PSD-95-positive puncta measured 3 h after glutamate treatment was increased and this effect was also prevented by MK801 (Fig. 5c,d). We then compared the effects of glutamate on the size of PSD-95 puncta in neurons from wild-type and Pyk2-KO mice (Fig. 5e,f). In the absence of Pyk2, the effects of glutamate on the size of PSD-95 puncta were lost (Fig. 5e,f). Taken together, these results reveal a role for Pyk2 in NMDA receptor-induced PSD-95 recruitment at post-synaptic sites.

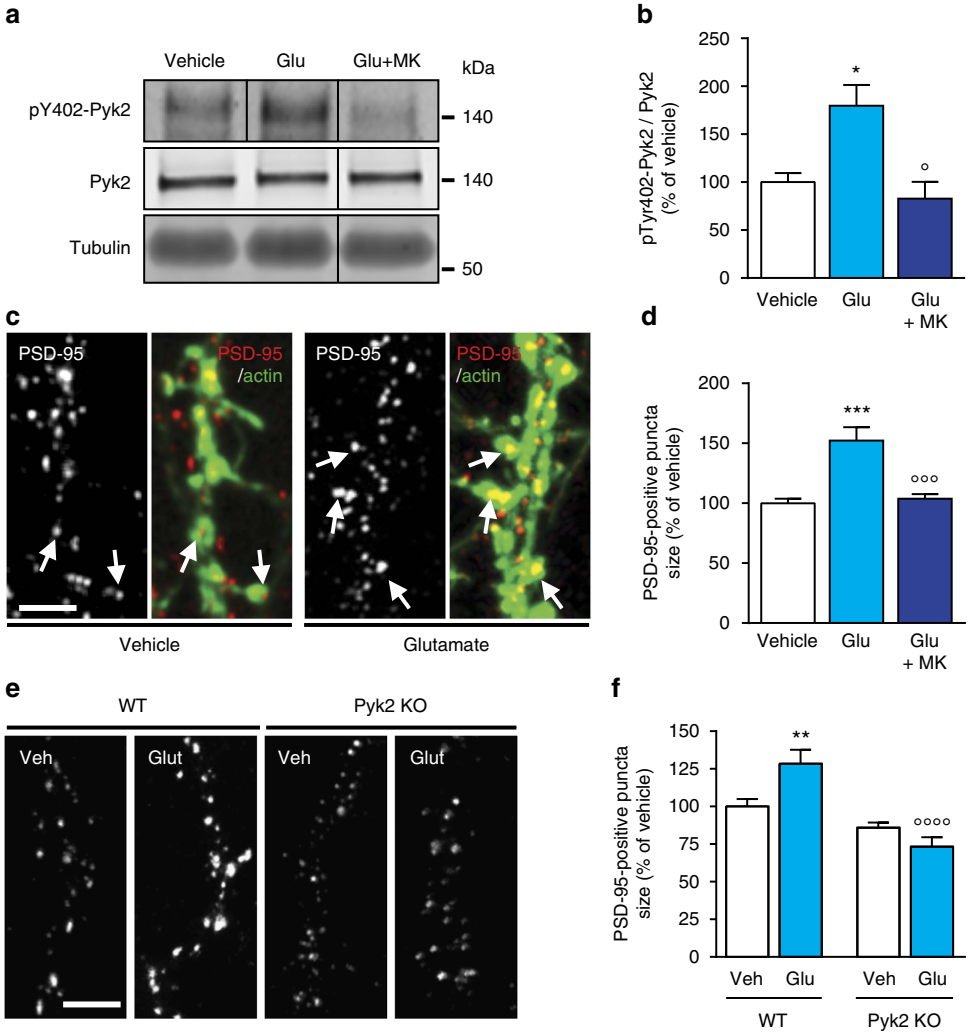

Figure 5 | Pyk2 modulates glutamate-induced PSD-95 accumulation in dendritic spines. (**a**) Hippocampal neurons were cultured for 3 weeks and treated for 15 min with vehicle or glutamate (Glu, 40 μM) without or with MK801 (MK, 10 μM), added 30 min before. PhosphoTyr402-Pyk2 (pY402-Pyk2), Pyk2 and α-tubulin as a loading control were analysed by immunoblotting. Molecular weight markers position is indicated in kDa. (**b**) Densitometric quantification of results as in **a**. One-way ANOVA ($F_{(2,13)}=8.02$, $P=0.005$, $n=4$–7 per group) and *post hoc* Holm-Sidak's test for multiple comparisons. (**c**) Cultured hippocampal neurons were treated with vehicle or glutamate (40 μM) without or with MK801 (10 μM) for 3 h, fixed and labelled for PSD-95 immunoreactivity and rhodamine-phalloidin (an F-actin marker) to identify PSD-95-positive puncta localized in dendritic spines (arrows). (**d**) The size of these PSD-95-positive puncta was measured and analysed with one-way ANOVA ($F_{(2,30)}=15.37$, $P<0.0001$, $n=10$–12 per group) and Holm-Sidak's test. (**e**) Hippocampal neurons from wild-type (WT) or Pyk2 KO mice were treated for 3 h with vehicle (Veh) or glutamate (40 μM) and immunostained for PSD-95. (**f**) The size of spine-associated PSD-95-positive puncta was measured in $Pyk2^{+/+}$ and $Pyk2^{-/-}$ hippocampal cultures treated as in **e** and quantified ($n=18$–27 per group). Statistical analysis with two-way ANOVA (interaction $F_{(1,89)}=12.42$, $P=0.0007$, glutamate effect, $F_{(1,89)}=1.84$, $P=0.18$, genotype effect, $F_{(1,89)}=35.29$, $P<10^{-4}$) and *post hoc* multiple comparisons Holm-Sidak's test. In **b**,**d**,**f**, one-two dendrites per neuron from two to three independent experiments were measured. In **b**,**d**,**f**, data are means + s.e.m., $^{*}P<0.05$, $^{**}P<0.01$, $^{***}P<0.001$, as compared to vehicle-treated $Pyk2^{+/+}$ cultures; $^{\circ}P<0.05$, $^{\circ\circ\circ}P<0.001$ and $^{\circ\circ\circ\circ}P<10^{-4}$, as compared to glutamate-treated $Pyk2^{+/+}$ cultures. Scale bars, 5 μm (**c** and **e**). Uncropped blots for **a** are shown in Supplementary Fig. 8.

Pyk2 function in spines is partly phosphorylation dependent. Since Pyk2 is a large protein that has tyrosine kinase activity, including functionally important autophosphorylation activity, and interactions with multiple partners[9], we examined which of its molecular properties were required for regulation of PSD-95 and spines. We transfected wild-type and Pyk2-KO hippocampal cultures with GFP or GFP fused to either Pyk2, or $Pyk2_{1-840}$, unable to bind to PSD-95 (ref. 5), or $Pyk2_{Y402F}$ with a point mutation of the autophosphorylation site or to kinase-dead Pyk2 (Pyk2-KD) with a K457A mutation[30]. We first analysed the size of PSD-95-positive puncta in these various conditions (Fig. 6a). As in untransfected neurons (see Fig. 5c–f), glutamate treatment increased the size of PSD-95-positive puncta in wild-type cultures transfected with either GFP or GFP:Pyk2, used as controls (Fig. 6a,b). Glutamate effects were absent in KO cultures transfected with GFP, but were rescued by Pyk2:GFP transfection (Fig. 6a,b). In contrast, glutamate treatment did not increase PSD-95-positive puncta size in $Pyk2^{-/-}$ cultures transfected with GFP:$Pyk2_{1-840}$, GFP:$Pyk2_{Y402F}$ or GFP:Pyk2-KD (Fig. 6a,b). These results show that the autophosphorylation site, Tyr-402, the kinase activity and the C-terminal domain of Pyk2 are all essential for glutamate-induced PSD-95 synaptic translocation.

We then examined if the spine density could be rescued in cultured hippocampal neurons. Dendritic spine density was reduced in Pyk2-KO neurons as compared to wild type (Fig. 6c,d), as observed *in vivo* (Fig. 3f,g). Transfection of

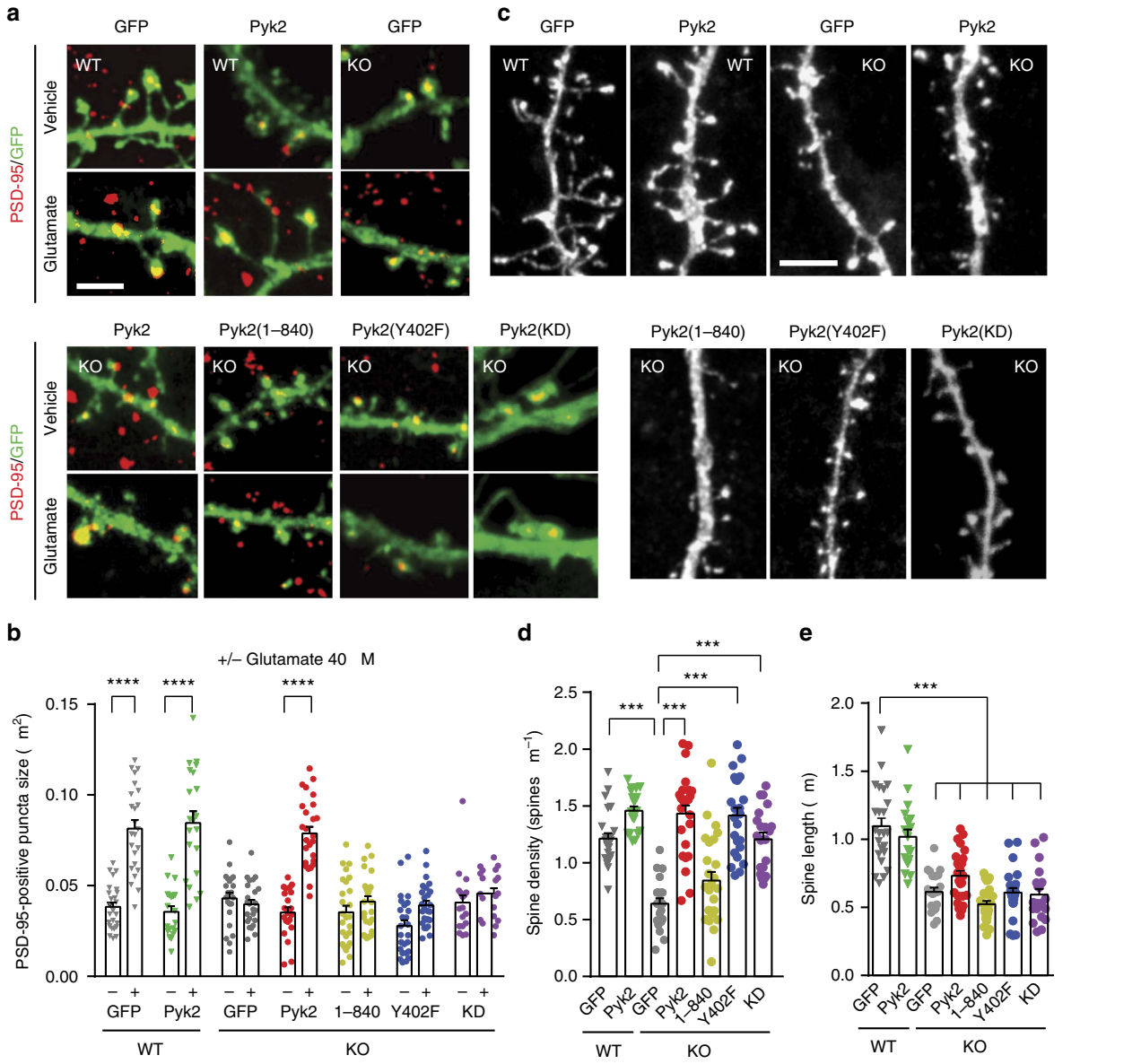

Figure 6 | Autophosphorylation-dependent and -independent roles of Pyk2 in dendritic spines. (**a**) Hippocampal neurons from wild-type (WT) and Pyk2 KO mice were cultured for 21–22 days, transfected with plasmids coding GFP or GFP fused to wild-type Pyk2, to Pyk2(1-840), Pyk2(Y402F) or Pyk2-KD (as indicated), and treated with vehicle or glutamate (Glu, 40 μM, 3 h). Neurons were imaged for GFP fluorescence (green) and PSD-95 immunoreactivity (red). (**b**) Quantification of GFP/PSD-95 double-positive puncta size (that is, yellow puncta) as in **a**. Two-way ANOVA: interaction, $F_{(6,312)}=19.07$, $P<10^{-4}$, glutamate effect, $F_{(1,312)}=134.3$, $P<10^{-4}$, Pyk2 expression effect, $F_{(6,312)}=20.06$, $P<10^{-4}$. (**c**) Spine density and length were studied in similar conditions as in **a**, in the absence of treatment, using GFP or Pyk2:GFP fluorescence. (**d**) Quantification of spine density. One-way ANOVA: $F_{(6,155)}=24.90$, $P<10^{-4}$. (**e**) Quantification of spine length. One-way ANOVA: $F_{(6,157)}=30.68$, $P<10^{-4}$ and. In **b**,**d**,**e**, individual data points and means + s.e.m. are shown, 15–20 dendrites per condition (one-two dendrites per neuron) from two to three independent experiments. *Post hoc* multiple comparisons were done with Holm-Sidak's test (**b**,**d**,**e**), ***$P<0.001$, ****$P<10^{-4}$. Scale bars, 3 μm (**a**) and 1 μm (**c**).

GFP:Pyk2 rescued spine density in KO neurons *in vitro* (Fig. 6c,d). Transfection of GFP:Pyk2$_{1-840}$ had no significant effect, but, in contrast to what we observed for PSD-95 puncta rescue (see Fig. 6b), both GFP:Pyk2$_{Y402F}$ and GFP:Pyk2-KD fully restored spine density (Fig. 6c,d), revealing a role for Pyk2 independent of its autophosphorylation and kinase activity. We also quantified the effects of Pyk2 deletion on spine length (Fig. 6e). In the absence of Pyk2, spines were shorter, as observed *in vivo* (see Fig. 3i), but this effect was not rescued by re-expression of wild type or mutated Pyk2 (Fig. 6e). This lack of rescue of spine length deficits *in vitro* may indicate a contribution of presynaptic Pyk2 in spine length regulation since with the low transfection rate in our culture system, concomitant transfection of pre- and post-synaptic neurons was very rare. Taken together, these results show that Pyk2 is important for PSD-95 synaptic enrichment and that this function requires both the C-terminal region involved in PSD-95 interaction and the autophosphorylation site and tyrosine kinase activity. In contrast, Tyr402 or kinase activity is not necessary for Pyk2 effects on spine density, revealing the existence of autophosphorylation/kinase activity-dependent and -independent roles of Pyk2 in spines.

Hippocampal Pyk2 is altered in HD. Since our results emphasized the high sensitivity of hippocampal function to Pyk2 protein

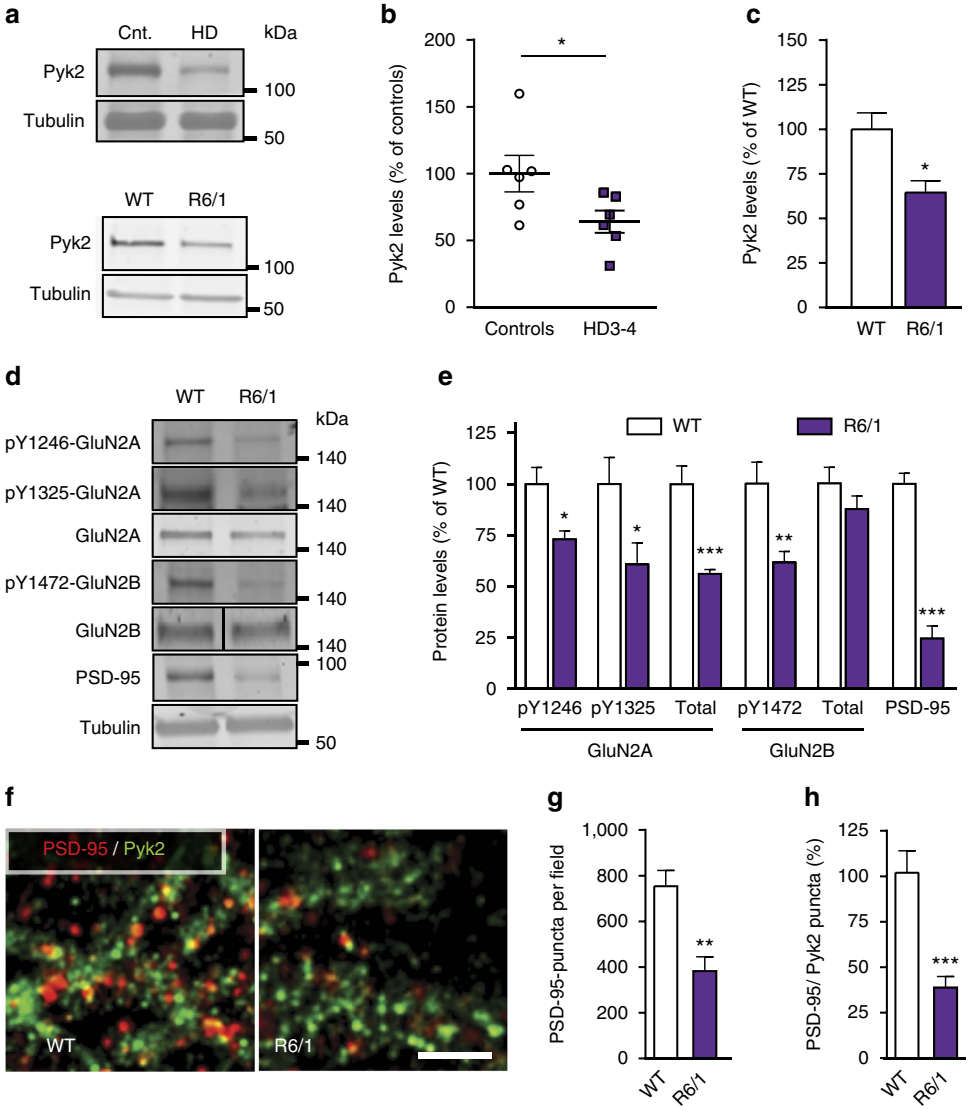

Figure 7 | Hippocampal alterations of Pyk2 and synaptic markers in Huntington's disease. (**a**) Hippocampal post-mortem samples from human patients grades 3–4 (HD3-4) and controls (Cnt., top panel) and from wild-type (WT) mice and R6/1 transgenic mice (lower panel) were analysed by immunoblotting for Pyk2 and α-tubulin as a loading control. Molecular weight marker positions are indicated in kDa. (**b**) Densitometric quantification of results as in **a**, for human samples expressed as a percentage of the mean in controls ($n=6$ per group, Student's t-test, $t_{10}=2.25$, $P<0.05$). (**c**) Quantification of results as in **a** for WT and R6/1 mice (percentage of WT mean, $n=4$–6 mice per group, Student's t-test, $t_8=3.23$, $P=0.012$). (**d**) Immunoblotting for phosphorylated forms and total GluN2A and GluN2B, and PSD-95 in hippocampus of WT and R6/1 mice. (**e**) Quantification of results as in **d** (percentage of WT mean), Student's t-test, pY1246-GluN2A, $t_9=3.10$, $P=0.013$, pY1325-GluN2A, $t_9=2.37$, $P=0.04$, GluN2A, $t_9=5.21$, $P=0.0006$, pY1472-GluN2B, $t_8=3.64$, $P=0.0066$, GluN2B, $t_8=1.22$, $P=0.26$, PSD-95, $t_9=9.18$, $P<10^{-4}$. (**f**) Confocal images of the *stratum radiatum* of CA1hippocampal sections from WT and R6/1 mice immunolabelled for PSD95 (red) and Pyk2 (green). Scale bar, 10 μm. (**g**,**h**) Quantification of results as in **f** in (three slices per mouse, five–six mice per genotype. (**g**) Number of PSD95-positive puncta, Student's t-test, $t_9=3.98$, $P=0.003$. (**h**) Number of Pyk2/PSD-95-double-positive puncta, expressed as a percentage of WT mean, Student's t-test, $t_{10}=4.66$, $P=0.0009$. All data are means + s.e.m. $^*P<0.05$, $^{**}P<0.01$ and $^{***}P<0.001$. R6/1 mice were 5-month old. Uncropped blots for **a** and **d** are shown in Supplementary Figs 9 and 10, respectively.

expression levels, we hypothesized that any alteration in Pyk2 levels in pathological conditions might have deleterious consequences. HD appeared as an interesting condition since Pyk2 and wild-type Htt interact with the same SH3 domain of PSD-95 (refs 14,31). This interaction is altered in mutant Htt with a pathological polyglutamine expansion[31], resulting in PSD-95 mislocalization to extrasynaptic sites[32]. We noticed that the hippocampal phenotype of Pyk2 KO mice resembled that of HD mouse models, which display spatial learning impairments[33], decreased PSD-95 (ref. 34), dendritic spines loss[35] and shorter dendritic spine necks[33]. To test the possible involvement of Pyk2 in HD, we first measured Pyk2 protein levels in post-mortem hippocampal samples from human patients. In patients with intermediate or late HD (grades 3–4 (ref. 36)) Pyk2 levels were reduced to 64 ± 8% of controls (mean ± s.e.m., Fig. 7a,b), whereas in patients at prodromal or early stage (grades 1–2) there was no significant change (Supplementary Fig. 4a,b). Pyk2 was also diminished in the hippocampus of R6/1 mice, an HD mouse model, transgenic for the first exon of the human *Htt* gene with amplified CAG repeats[37] (64 ± 6% of control levels, mean ± s.e.m., Fig. 7a,c). Since Pyk2 can traffic between cytoplasm and nucleus[38], and since R6/1-mutated Htt accumulates in the nucleus[39] we looked for the existence of altered cytonuclear distribution of Pyk2 or its possible

sequestration in nuclear aggregates. Although Pyk2 was predominantly decreased in the cytoplasm (Supplementary Fig. 4c,d) it was not sequestered in intra-nuclear aggregates and did not co-localize with EM48-immunolabelled nuclear aggregates (Supplementary Fig. 4e). These results indicated a reduced Pyk2 function in the cytoplasm of HD mice. Indeed, in R6/1 mice we observed changes similar to those in Pyk2 mutant mice, including a decrease in total GluN2A but no change in GluN2B, a decrease in tyrosine phosphorylated GluN2A and GluN2B, and a marked decrease in total PSD-95 (Fig. 7d,e). Double immunostaining for Pyk2 and PSD-95 in CA1 of wild-type and R6/1 mice showed a decreased number of

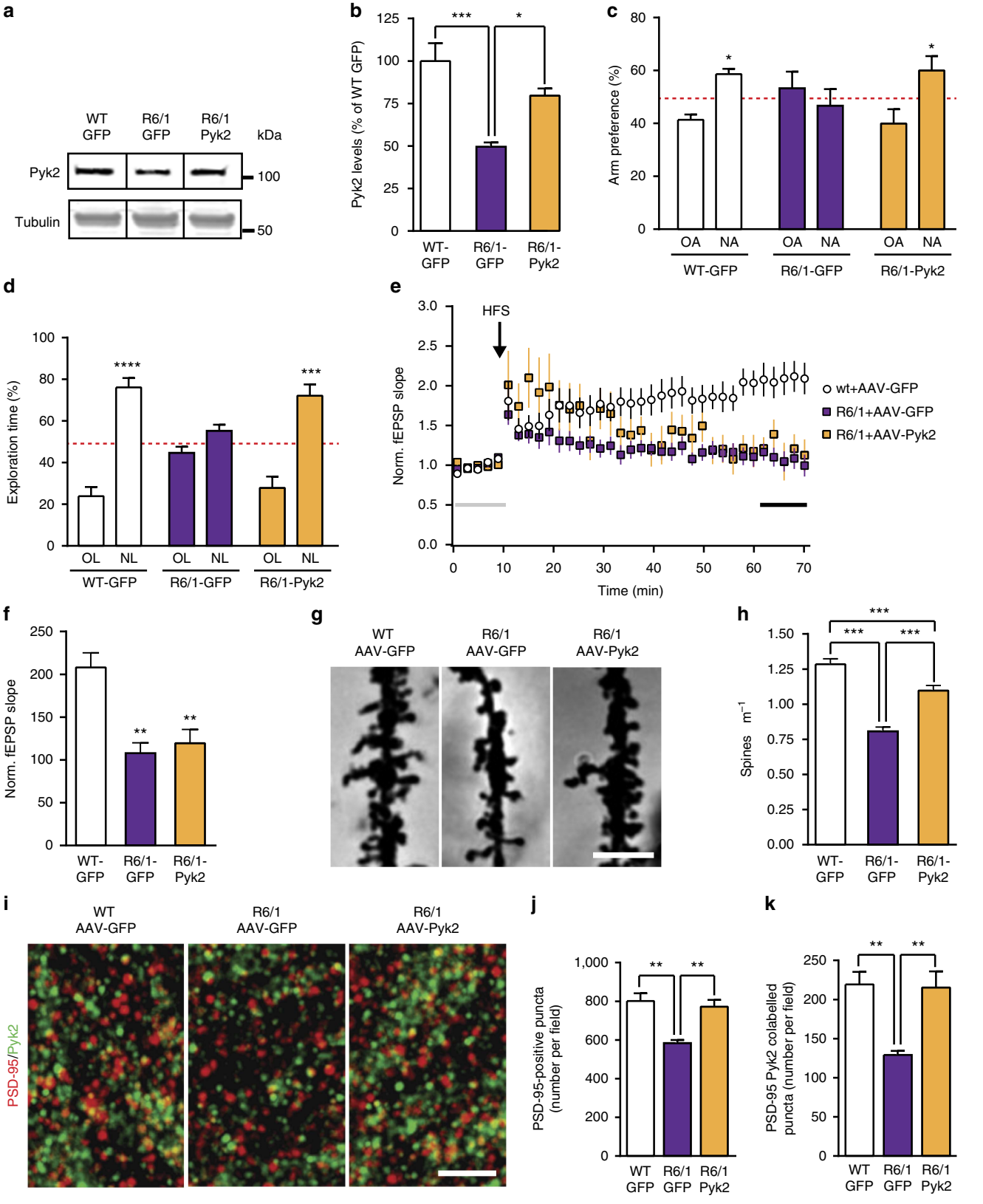

PSD-95-positive puncta in R6/1 mice as compared to wild-type mice (Fig. 7f,g), and less co-localization of PSD-95-positive and Pyk2-positive puncta in mutant mice (Fig. 7h). The similarity in the modifications observed in R6/1 mice and Pyk2 mutant mice suggested that the decreased levels of Pyk2 might contribute to PSD-95 and NMDA receptors subunits alterations.

Pyk2 partly rescues the hippocampal phenotype of R6/1 mice. Since the levels of Pyk2 in the hippocampus of HD patients and R6/1 mice (Fig. 7a–c) were close to those in Pyk2$^{+/-}$ mice, which displayed a similar phenotype, we asked whether correcting this defect in R6/1 mice could rescue some of their deficits. We stereotaxically injected AAV expressing either Pyk2 and GFP or GFP alone in the dorsal hippocampus of R6/1 mice (R6/1-Pyk2 and R6/1-GFP mice, respectively) or GFP alone in wild-type mice (WT-GFP) as a control. Three weeks after the injection, GFP expression demonstrated a wide spreading of viral transduction within the dorsal hippocampus, but restricted to this brain structure (Supplementary Fig. 4f). Immunoblotting showed that Pyk2 levels in R6/1-GFP mice, which were 50 ± 3% of those in WT-GFP mice, were raised to 80 ± 4% in R6/1-Pyk2 mice (Fig. 8a,b). The recovery of Pyk2 expression restored R6/1 mice performance in the Y-maze spontaneous alternation task (Fig. 8c) and corrected the deficit in the novel object recognition task (Fig. 8d). We also examined LTP in these mice at the same age as for behavioural experiments (4–5 months). In WT-GFP mice, we observed a robust LTP in CA1 after stimulation of Schaffer collaterals (Fig. 8e,f). In contrast, in R6/1-GFP and R6/1-Pyk2 mice, synaptic potentiation was not stable (Fig. 8e,f). One hour after high frequency stimulation (HFS), potentiation was observed only in WT-GFP mice (Fig. 8f), revealing that restoration of Pyk2 levels was not sufficient to correct the LTP impairment.

To assess the cellular effects of Pyk2 recovery possibly underlying the behavioural improvements, we analysed spine density in CA1 apical dendrites by the Golgi-Cox method (Fig. 8g). Spine density, which was decreased in R6/1-GFP compared to WT-GFP mice, was partly restored by Pyk2 viral expression in R6/1-Pyk2 mice (Fig. 8g,h). We also analysed PSD-95- and Pyk2-positive puncta in CA1 *stratum radiatum* of the three groups of mice (Fig. 8i). R6/1-GFP mice displayed a reduced number of PSD-95-positive puncta (Fig. 8j) and fewer double-positive PSD-95/Pyk2 puncta (Fig. 8k) compared to WT-GFP mice, consistent with the results shown in Fig. 7g–i. The numbers of PSD-95-positive puncta (Fig. 8j) and PSD-95/Pyk2 double-positive puncta (Fig. 8k) were both completely rescued in R6/1-Pyk2, reaching values similar to those in WT-GFP mice. These results strongly indicate that Pyk2 deficit contributes to the hippocampal phenotype of the R6/1 HD mouse model, including cognitive deficits, dendritic spine loss and PSD-95 alteration. Moreover, they show that these deficits can be improved by Pyk2-induced expression, although this expression was not sufficient to restore synaptic plasticity in our experimental conditions.

Discussion

Here we show the functional importance of the Ca^{2+}-activated non-receptor tyrosine kinase Pyk2 for hippocampal function and spines physiology. We also provide evidence that Pyk2 deficit contributes to the hippocampal impairments in a mouse model of HD, a severe genetic neurodegenerative disorder. Although Pyk2$^{+/-}$ and Pyk2$^{-/-}$ mice develop and breed normally in standard animal facility conditions, and show no gross behavioural defects, they appear strongly deficient in hippocampal-related memory tasks. These behavioural impairments were accompanied by impaired synaptic plasticity, decreased levels and/or tyrosine phosphorylation of NMDA receptor subunits, and alterations in PSDs composition and in spines density and morphology.

A previous study in hippocampal slices using overexpression or interfering constructs, reported that Pyk2 can regulate NMDA receptor function and LTP induction[7]. Here we show that in Pyk2 mutant mice LTP was not induced in standard conditions at Schaffer collaterals synapses on CA1 pyramidal neurons. A number of biochemical alterations at the post-synaptic level are likely to participate in this deficit. Both GluN2A and GluN2B were altered with a decreased total and tyrosine phosphorylated GluN2A and a decreased tyrosine phosphorylation of GluN2B. Moreover, subcellular fractionation revealed a decrease in the three NMDA receptor subunits (GluN1, GluN2A and GluN2B) in the PSD fraction. The reduction of GluN2B in PSDs may result from its decreased tyrosine phosphorylation, which is known to promote surface expression of GluN2B-containing NMDA receptors and their recruitment to PSDs[40,41]. This phosphorylation deficit was in agreement with the decreased active form of SFKs we observed in Pyk2 mutant mice, supporting their role in mediating NMDA receptors phosphorylation downstream from Pyk2 (ref. 7). In the case of GluN2A, the total protein and the phosphorylated form were decreased. Since tyrosine phosphorylation of GluN2A increases NMDA receptor currents[42,43], reduction of both forms of GluN2A may contribute to synaptic defects of Pyk2 knockout mice. These alterations seemed to be specific for the NMDA receptor complex since AMPA receptors levels and phosphorylation were not affected. These combined alterations in NMDA receptor subunits provide a first basis for the functional deficit in LTP induction. Many other aspects of synaptic function and plasticity remain to be investigated in Pyk2 mutant mice, and

Figure 8 | Pyk2 protein levels restoration in the hippocampus partly rescues R6/1 mice phenotype. (**a**) Pyk2 and α-tubulin (loading control) immunoblotting in 3-month WT mice injected with AAV-GFP (WT-GFP), or R6/A injected with AAV-GFP (R6/1-GFP) or AAV-Pyk2 and GFP (R6/1-Pyk2). Uncropped blots in Supplementary Fig. 11. (**b**) Quantification of results as in **a** (six–nine mice per group). One-way ANOVA: $F_{(2,18)} = 4.39$, $P < 0.05$, Holm-Sidak's test versus R6/1-GFP. (**c**) Y-maze spontaneous alternation test (10–11 mice per group). Two-way ANOVA interaction $F_{(2,56)} = 4.39$, $P < 0.05$, OA versus NA, Holm-Sidak's test WT-GFP $t = 2.64$, $P < 0.05$, R6/1-GFP, $t = 0.97$, ns, R6/1-Pyk2, $t = 2.93$, $P < 0.05$. (**d**) NOL test (9–12 mice per group). Two-way ANOVA interaction $F_{(2,54)} = 11.9$, $P < 0.0001$, OL versus NL, Holm-Sidak's test WT-GFP $t = 9.08$, $P < 0.0001$, R6/1-GFP, $t = 1.60$, ns, R6/1-Pyk2, $t = 6.66$, $P < 0.0001$. (**e**) LTP studied as in Fig. 1c in hippocampal slices from 5-month WT-GFP, R6/1-GFP and R6/1-Pyk2 mice ($n = 3$–4 mice per group, 2–3 slices per mouse, 10–11 slices total). (**f**) Ten-min average of fEPSP slope 40 min after HFS, normalized to the mean of 10-min baseline (corresponding time points are indicated in **e** by an horizontal line). Kruskal–Wallis = 15.63, $P < 0.05$, *post hoc* analysis with Dunn's multiple comparisons test. (**g**) Golgi-Cox-stained apical dendrites from CA1 pyramidal neurons. Scale bar, 3 µm. (**h**) Quantitative analysis of dendritic spine density as in **e** (59–62 dendrites from four mice per group). One-way ANOVA: $F_{(2,177)} = 46.7$, $P < 10^{-4}$, Holm-Sidak's test versus R6/1-GFP. (**i**) Hippocampal sections of WT and R6/1 mice injected with AAV-GFP or AAV-Pyk2 as indicated, and double-immunostained for PSD-95 and Pyk2. High magnification in CA1 *stratum radiatum* is shown. Scale bar, 5 µm. (**j**) Quantification of PSD-95-positive puncta density. One-way ANOVA $F_{(2,14)} = 10.81$, $P = 0.0014$, Holm-Sidak's multiple comparisons test. (**k**) Quantification of PSD-95/Pyk2 double-positive puncta density. One-way ANOVA $F_{(2,14)} = 9.76$, $P = 0.0022$, Holm-Sidak's multiple comparisons test. In **j**,**k**, five–seven mice per group. In all graphs values are means + s.e.m. $^{*}P < 0.05$, $^{**}P < 0.01$, $^{***}P < 0.001$ and $^{****}P < 10^{-4}$.

the modifications induced by the absence of Pyk2 clearly extend beyond NMDA receptors.

A marked alteration observed in Pyk2 mutant mice concerned PSD-95. PSD-95 SH3 domain is known to bind Pyk2 C-terminal Pro-rich motif[14], thereby clustering and activating Pyk2 in response to Ca^{2+} increase[5,14]. In contrast, effects of Pyk2 on PSD-95 have not been described. Our study reveals that Pyk2 has a critical influence on PSD-95, regulating its levels, its localization at PSDs in basal conditions and its clustering in response to stimulation of NMDA receptors. The decreased PSD-95 expression cannot explain, by itself, the absence of LTP in Pyk2 mutant mice, since PSD-95 knockout mice display an enhanced LTP[44]. Therefore, the functional deficit is likely to result from its combination with dysregulation of NMDA receptors and possibly other proteins. PSD-95 is phosphorylated by c-Abl and SFKs on several tyrosine residues, which can favour PSD-95 aggregation and GluN2A activation[28,45]. Thus, there appears to be a reciprocal interaction between Pyk2 and PSD-95, each enhancing the function of the other, thereby directly and indirectly regulating NMDA receptors and PSD organization. In support of this functional association, it has been reported that in hippocampal neurons in culture, corticosterone-induced recruitment of Pyk2, PSD-95 and GluN1 to spines requires Pyk2 activation[46]. NMDA receptor activation recruits Pyk2 to spines through its interaction with PSD-95 (ref. 5), whereas it also rapidly destabilizes PSD-95 and removes it from PSDs[47]. Our study shows that Pyk2 is required for the later recruitment of PSD-95 to spines revealing its contribution in the coordinated Ca^{2+}-dependent dynamics of PSD proteins, a key aspect of synaptic function and plasticity. Importantly, GluN2A, GluN2B and PSD-95 co-assemble together with PSD-93 into 1.5 MDa 'supercomplexes'[48]. PSD-93 is phosphorylated by Fyn[49], which is altered in PyK2 mutant mice. Since both PSD-93 and PSD-95 promote Fyn-mediated tyrosine phosphorylation of GluN2A and/or GluN2B[50,51], it appears that Pyk2 is potentially placed at a strategic location to regulate NMDA receptor supercomplexes. Since these supercomplexes have been proposed to be functionally important, with mutations in their key components resulting in abnormal LTP and learning[48], it will be particularly interesting to investigate whether their alteration accounts for LTP and other synaptic deficits in Pyk2 mutant mice.

Dendritic spine density and length were also altered in Pyk2 mutant mice. Our study of the requirement of Pyk2 protein domains and functions for its various roles reveals the complexity of its contribution. The kinase activity of Pyk2 and its autophosphorylation site, Tyr402, which is critical for the recruitment of SFKs, were both necessary for the rescue of PSD-95 clustering in spines in Pyk2 KO neurons. The C-terminal region, which allows interaction with PSD-95 (ref. 14), was also required for PSD-95 clustering. In contrast, rescue of spine density required the C-terminal region but neither Tyr402 nor the kinase activity, indicating a phosphorylation-independent role of Pyk2 in the regulation of spine number. Such an autophosphorylation/kinase activity-independent function of Pyk2 is reminiscent of those reported for the closely related FAK[52,53] in non-neuronal cells. This alternate signalling is presumably SFK-independent and may be linked to scaffolding properties of Pyk2 and/or its interaction with specific partners.

The current study also suggests a role for Pyk2 at the presynaptic level. Our electron microscopy experiments show the presence of Pyk2 in nerve terminals, confirming previous biochemical observations[54]. Its functional role is indicated by the alteration in paired-pulse facilitation, a form of short-term plasticity that is considered to be mostly presynaptic[55,56], although post-synaptic mechanisms are also possible[57]. Finally, in the absence of Pyk2, spine length was decreased both *in vivo* and in culture. A possible explanation for this lack of rescue could be a dual role of Pyk2 at the pre- and post-synaptic levels, which were not simultaneously restored at the same synapses in the culture conditions in which the transfection rate was low. At any rate, the mechanisms by which Pyk2 controls spine length are likely to be complex since both positive and negative effects of Pyk2 and FAK on spine growth have been previously reported[58–60] and their elucidation will require further investigation. The important aspect of the present results is the overall deficit in spine number and length in the absence of Pyk2. Interestingly, it has been shown that chronic stress induces a redistribution of activated Pyk2 to the perinuclear region of CA3 neurons, contributing to a deficit in the nuclear pore protein NUP62 and its potential negative consequences on dendritic complexity[61]. The present study suggests that Pyk2 redistribution could also directly contribute to dendritic or synaptic alterations by reducing its local levels.

Our observations thus reveal an essential and complex role of Pyk2 in the regulation of spines, PSDs and NMDA receptors, whose alterations impair synaptic plasticity and hippocampal-dependent memory in Pyk2-deficient mice. The importance of Pyk2 expression levels is underlined by the unexpected severity of the functional deficits in heterozygous mutant mice. Their behavioural and physiological phenotype was as severe as in homozygous mutant mice, whereas a clear gene dosage effect was observed at the molecular level. This suggests that Pyk2 expression levels are a limiting factor for excitatory synapses function in hippocampus and raises the question of the possible implications of decreased Pyk2 protein levels in pathological conditions. This hypothesis was supported by our results in a mouse model of HD. Pyk2 was decreased in the R6/1 mouse, to a level comparable to that observed in $Pyk2^{+/-}$ heterozygous mutant mice, which displayed a clear behavioural phenotype. Several alterations in R6/1 mice were similar to those in Pyk2 mutant mice including the alterations in NMDA receptors, PSD-95 distribution and spines. Of course, such alterations could potentially result from different mechanisms in the two types of mutant mice, but our results provide strong evidence that Pyk2 deficit contributes to some of the abnormalities observed in R6/1 mice. Although enhancing Pyk2 expression by AAV transduction in R6/1 mice was not sufficient to restore a normal LTP in CA1, it corrected several behavioural, molecular and cellular deficits. Interestingly, the deleterious consequences of Pyk2 deficit are likely to synergize with other factors including increased activity of STEP[62], a tyrosine phosphatase active on Pyk2 (ref. 63), which is expected to aggravate the functional consequences of Pyk2 insufficiency. In patients, the role of Pyk2 deficiency remains to be determined since it was detected in grades 3–4 when there is a loss of other synaptic proteins but not at earlier stages (grades 1–2). Nevertheless, our results suggest that strategies for enhancing Pyk2 expression or activity, or for inhibiting STEP phosphatase activity[64] could have a potential therapeutic interest in HD. Further work will determine whether Pyk2 deficiency could play a role in other neurodegenerative conditions, such as Alzheimer disease[8], besides its possible role as modulator of Tau toxicity[65].

Our study reveals that the absence of Pyk2 impairs synaptic functions and hippocampal-dependent learning and memory. We show that Pyk2 plays critical roles in spines and PSD organization and in the regulation of PSD-95 and NMDA receptors. Although we focused our investigations on hippocampus where Pyk2 expression is the highest, it is likely that it is also important in other neurons, especially in neocortical areas where it is highly expressed and which are known to undergo intense synaptic plasticity. We also reveal the contribution of Pyk2 in hippocampal dysfunction in a HD model and its potential

reversibility. Our results should stimulate research on the role of Pyk2 in other pathological conditions in which NMDA receptor dysfunction is thought to be directly or indirectly involved.

Methods

Animals. For Pyk2 deletion, $Pyk2^{f/f}$ C57Bl/6 mice were generated in which the *PTK2B* exons 15b-18 were flanked with LoxP sequences (Gen-O-way, Lyon, France) leading to a deletion that disrupts the protein kinase domain when crossed with a expressing Cre line[20]. $Pyk2^{-/-}$ mice and $Pyk2^{f/f}$ mice were genotyped from a tail biopsy (Charles River, Saint-Germain-Nuelles, France) using for DNA amplification of floxed *PTK2B* as forward primer 5′-GAGAGTGCTGGGT ACTCCAGACTCAGATAG-3′ and as reverse primer 5′-TTCAGGAACACCAG AGAACTAGGGTGG-3′ and previously reported primers[20] for $Pyk2^{-/-}$ mice. Heterozygous mice were crossed to generate $+/+$, $+/-$ and $-/-$ mice. Male R6/1 transgenic mice[37] (4–5-month-old) expressing exon-1 mutant Htt with 145 glutamines under the HD human promoter and their wild-type littermates were obtained from Jackson Laboratory (Bar Harbor, ME, USA). Housing room was kept at 19–22 °C and 40–60% humidity, under a 12:12 h light/dark cycle and mice had ad libitum access to food and water. Animal experiments and handling was in accordance with ethical guidelines of Declaration of Helsinki and NIH, (1985-revised publication no. 85-23, European Community Guidelines), and French Agriculture and Forestry Ministry guidelines for handling animals (decree 87849, licence A 75-05-22) and approval of the Charles Darwin ethical committee. All mice used in this study were males and the ages are indicated in the figure legends.

Behavioural phenotyping. Wire hanging, plus maze and open-field paradigms were carried out as described elsewhere[66]. In brief, for wire hanging, mice were placed on a standard wire cage lid, which was then turned upside down for 60 s and the number of falls was recorded. The elevated plus maze consisted of two opposing 30 × 8 cm open arms, and two opposing 30 × 8 cm arms enclosed by 15 cm high walls. The maze was raised 50 cm from the floor and lit with dim light. Each mouse was placed in the central square, facing an open arm and the time spent in the open arms was recorded for 5 min. The open field apparatus was a dimly lit white circular arena (40 cm diameter, 40 cm high wall). Mice were placed in the arena centre and free exploration was recorded for 10 min. NOL test and spontaneous alternation in a Y-maze task (Y-SAT) were performed as previously described[33]. Briefly, for NOL an open-top arena (45 × 45 × 45 cm) was used. Mice were first habituated to the arena (2 days, 15 min per day). On day 3 of the acquisition phase, two identical objects (A1 and A2) were placed in the arena and explored for 10 min. Twenty-four hour later, one object was moved from its original location to the diagonally opposite corner and mice were allowed to explore the arena for 5 min. The object preference was measured as the time exploring each object × 100/time exploring both objects. For Y-SAT, a Y-maze apparatus, made of clear Perspex, was used (Y-maze dimensions: arms, 35 cm length, 25 cm height, 15 cm width). For the training session, mice were placed in the stem arm of the Y and allowed to explore for 10 min only one accessible arm (familiar arm) for 10 min. They were then returned to their home cage. After an inter-trial interval of 2 h, mice were placed in the stem arm of the T-maze and allowed to freely explore all three arms for 5 min. Big and highly perceptible objects were situated surrounding the maze at 20–40 cm. The arm preference was measured as the time exploring each arm × 100/time exploring both arms. Animals were tracked and recorded with Smart junior software (Panlab).

Viral constructs and stereotaxic injection. For specific deletion of Pyk2 in dorsal hippocampus expression, 4-week-old $Pyk2^{f/f}$ mice were stereotaxically injected with AAV expressing Cre recombinase and (AV-9-PV2521, AAV9.CamKII.HI.eGFP-Cre.WPRE.SV40 (AAV-Cre)) (from Perelman School of Medicine, University of Pennsylvania, USA). To overexpress Pyk2, we used AAV1-CamKIIa0.4-GFP-2A-mPTK2B (AAV-Pyk2) with a T2A cleavable link (Vector Biolabs Malvern, PA, USA). As a control, we injected AAVs expressing GFP (AV-9-PV1917, AAV9.CamKII0.4.eGFP.WPRE.rBG (AAV-GFP) from Perelman). Following anaesthesia with pentobarbital (30 mg kg^{-1}), we performed bilateral injections of AAV-GFP, AAV-Cre or AAV-Pyk2 (2.6×10^9 GS per injection) in the dorsal hippocampus following coordinates from the bregma (millimetres); anteroposterior, –2.0; lateral, ± 1.5; and dorsoventral, ± 0.8. For R6/1 mice, we performed an additional injection at dorsoventral ± 1.2. AAV injection was carried out in 2 min. The cannula was left in place for 5 min for complete virus diffusion before being slowly pulled out of the tissue. After 2 h of careful monitoring, mice were returned to their home cage for 3 weeks before starting analyses of behaviour, biochemistry and morphology.

Electrophysiology. Littermate mice (1–2 months) received an injection of ketamine/xylazine (75/10 mg kg^{-1}, i.p.) and intracardially perfused with an ice-cold solution ((all mM) 25 $NaHCO_3$, 1.25 NaH_2PO_4, 2.5 KCl, 0.5 $CaCl_2$, 7 $MgCl_2$, 110 choline chloride, 25 glucose, 11.6 ascorbic acid, and 3.1 pyruvic acid). The brain was rapidly removed and horizontal slices (350 µm thick) cut with a vibratome (Microm, Thermo Fisher). Slices were placed in an interface chamber containing artificial CSF (ACSF) ((all mM) 124 NaCl, 1 NaH_2PO_4, 26.2 $NaHCO_3$, 2.5 KCl, 1.6 $CaCl_2$, 1.2 $MgCl_2$, 11 glucose) at 37 °C, saturated with 5% (vol/vol) CO_2 in O_2, and allowed to recover for 1 h. Slices were then transferred to a submerged recording chamber, a cut was made between the CA3 and CA1, and bicuculline-supplemented ACSF used for superfusion. An ACSF-filled recording borosilicate glass pipette (2–4 MΩ) was inserted in the *stratum radiatum* of CA1 region. Schaffer collaterals were stimulated (HFS, 5 × 1 s at 100 Hz) with a tungsten bipolar electrode (0.5 MΩ). Field excitatory post-synaptic potentials (fEPSPs) were recorded using a multiclamp 700B amplifier (Molecular Devices) low-pass filtered at 5 kHz and digitized at 20 kHz. Offline analysis of fEPSP slopes was done with Clampfit software (Molecular Devices). Baseline potential was set to zero and recordings were low-pass filtered at 1 kHz with Bessel filter. A 1-ms time-window was manually positioned at the onset of the fEPSP and its initial slope automatically measured. LTP was investigated in AAV-injected R6/1 mice in similar conditions except that mice were 5-month old at the time of the recording. Paired pulse ratio was determined at a 50 ms interval. In all cases, the experimenter carrying out the acquisition and analysis of electrophysiological data was blind to the mice genotype and/or AAV type.

Electronic microscopy. Mice were transcardially perfused with a solution containing 40 g l^{-1} paraformaldehyde and 1 ml l^{-1} glutaraldehyde in 0.1 M sodium phosphate buffer (PB), pH 7.4. Brains were then immersed in the same fixative 12 h at 4 °C. Tissue blocks containing the hippocampus were dissected and washed in 0.1 M PB, cryoprotected in 10 and 20% sucrose in 0.1 M PB, freeze thawed in isopentane and liquid nitrogen. Samples were post fixed in 25 ml l^{-1} glutaraldehyde in 0.1 M PB for 20 min, washed and treated with 20 g l^{-1} osmium tetroxide in PB for 20 min. They were dehydrated in a series of ethanol and flat embedded in epoxy resin (EPON 812 Polysciences). After polymerization, blocks from the CA1 region were cut at 70 nm thickness using an ultramicrotome (Ultracut E Leica). Sections were cut with a diamond knife, picked up on formvar-coated 200 mesh nickel grids. For etching resin and remove osmium, sections were treated with saturated aqueous sodium periodate ($NaIO_4$). They were then immunostained for Pyk2 with rabbit antibodies (see below) by indirect immunolabelling protein A-gold probes (20 nm) (CMC Utrecht; Netherlands) following a published method[67]. The sections were then double stained with uranyl acetate and lead citrate before observation with a Philips (CM-100) electron microscope. Digital images were obtained with a CCD camera (Gatan Orius). To test the immunostaining specificity, the primary antibody was omitted.

Tissue preparation and immunofluorescence. Mice were anaesthetized (pentobarbital, 60 mg kg^{-1} i.p.) and intracardially perfused with a 40 g l^{-1} paraformaldehyde solution in 0.1 M sodium phosphate, pH 7.2. Brains were removed and post-fixed overnight in the same paraformaldehyde solution, cryoprotected with 300 g l^{-1} sucrose in PBS with 0.2 g l^{-1} NaN_3 and frozen in dry-ice cooled isopentane. All the following steps were done with gentle shaking. Serial 30-µm coronal cryostat-free floating sections were washed three times in PBS, permeabilized in PBS with 3 ml l^{-1} Triton X-100 and 30 ml l^{-1} normal goat serum (Pierce Biotechnology, Rockford, IL, USA) for 15 min at room temperature, and washed three times. Brain slices were then incubated overnight at 4 °C in the presence of primary antibodies in PBS with 0.2 g l^{-1} NaN_3: rabbit Pyk2 antibody (1:500, #07M4755) and mouse MAP2 antibody (1:500) from Sigma, Chemical Co. (St Louis, MO, USA), mouse antibodies for Htt (clone EM48 1:150, #2026373, Chemicon, Temecula, CA, USA), mouse anti-PSD-95 1:500 (#QA210648, Thermo Scientific, MA, USA). Sections were then washed three times and incubated for 2 h at room temperature with fluorescent secondary antibodies: Cy3 goat anti-rabbit (1:200) and/or AlexaFluor 488 goat anti-mouse (1:200; both from Jackson ImmunoResearch, West Grove, PA, USA). No signal was detected in control sections incubated in the absence of the primary antibody.

Primary hippocampal neurons culture and immunofluorescence. Hippocampal neurons were prepared from E17 C57Bl/6 mouse embryos (pregnant mice from Charles River, Saint Germain Nuelles, France) or from our Pyk2 mice colony as previously described[33]. The neuronal cell suspension was seeded (70,000 cells cm^{-2}) on coverslips precoated with poly-D-lysine (0.1 mg ml^{-1}, Sigma) in 24-well plates or in 6-well plates without coverslips. Neurobasal medium (GIBCO, Renfrewshire, Scotland, UK) containing 1 ml per 50 ml of B27 supplement (Gibco-BRL) and 50 ml of GlutaMAX (100 ×) (Gibco-BRL) was used to grow the cells in serum-free medium conditions and maintained at 37 °C in 5% CO_2. At DIV 21–22, cells were treated with vehicle or 10 µM MK801 (Sigma) for 30 min. Then, cells were treated with vehicle or 40 µM glutamate (Sigma) for 15 min and samples were collected for immunoblot analysis or the glutamate was washed out and cells further incubated for 3 h before being fixed for 10 min with 40 g l^{-1} paraformaldehyde in PB 0.2 M for immunostaining. Fixed cells were permeabilized in 1 ml l^{-1} Triton X-100 for 10 min and then blocking was performed with 10 g l^{-1} BSA in PBS for 1 h. Cells were incubated with mouse monoclonal antibodies for PSD-95, (1:500, #QA210648, Millipore) or MAP2 (1:800, #073M4774, Sigma) or rabbit Pyk2 antibodies (1:500, #074M4755, Sigma, XX) at 4 °C overnight. After three washes with PBS, cells were incubated with the

corresponding fluorescent secondary antibodies, Cy3 or Cy2 (1:200; Jackson ImmunoReseach, West Grove, PA). Then, cells were rinsed twice with PBS and incubated with phalloidin–rhodamine 1:1,000 (Sigma) for 45 min in PBS. After washing twice with PBS, the coverslips were mounted with Vectashield (Vector Laboratories Burlingam, UK). Hippocampal neuron staining was observed with a confocal SP5-II (see below).

Cell transfection and constructs. Pyk2$^{+/+}$ and Pyk2$^{-/-}$ hippocampal neurons at DIV 18 were transfected using transfectin (Bio-Rad, Hercules, CA, USA) following the manufacturer's instructions and left for 48–72 h. Cells were transfected with previously described constructs[38]: GFP (control), GFP-Pyk2, GFP-Pyk2$^{1\text{-}840}$ (Pyk2 deleted from the FAT domain and the third proline-rich motif) and GFP-Pyk2^{Y402F} (Pyk2 with a point mutation of the autophosphorylated tyrosine-402). GFP was fused to the N terminus of Pyk2.

Confocal imaging and analysis. Immunostained neurons in culture or tissue sections were imaged using a Leica Confocal SP5-II (63 × numerical aperture lens, 5 × digital zoom, 1-Airy unit pinhole. Four frames were averaged per *z*-step throughout the study. Confocal *z*-stacks were taken at 1,024 × 1,024 pixel resolution, every 2 µm for brain sections and every 0.2 µm for cultured cells. The labelled PSD95-positive clusters number and size were quantified with NIH ImageJ freeware (Wayne Rasband, NIH) as described[68] with minor changes. For tissue sections, at least three 30-µm slices containing dorsal hippocampus were analysed per mouse and up to three representative CA1 *stratum radiatum* images were obtained from each slice. For cultured hippocampal neurons, PSD95-positive clusters co-localized with F-actin clusters (stained with phalloidin–rodhamine) or GFP-enriched spines were quantified as described[69] with minor changes using ImageJ. The number of neurites analysed was >20 neurites (one–two neurites per neuron) per condition from two–three different cultures.

Golgi staining and spine analysis. Fresh brain hemispheres were processed following the Golgi-Cox method as described elsewhere[70]. Essentially, mouse brain hemispheres were incubated in the dark for 14–17 days in filtered dye solution (10 g l^{-1} $K_2Cr_2O_7$, 10 g l^{-1} $HgCl_2$ and 8 g l^{-1} K_2CrO_4). The tissue was then washed 3 × 2 min in water and 30 min in 90% EtOH (v/v). Two hundred-µm sections were cut in 70% EtOH on a vibratome (Leica) and washed in water for 5 min. Next, they were reduced in 16% ammonia solution for 1 h before washing in water for 2 min and fixation in 10 g l^{-1} $Na_2S_2O_3$ for 7 min. After a 2- min final wash in water, sections were mounted on superfrost coverslips, dehydrated for 3 min in 50%, then 70, 80 and 100% EtOH, incubated for 2 × 5 min in a 2:1 isopropanol:EtOH mixture, followed by 1 × 5 min in pure isopropanol and 2 × 5 min in xylol. Bright-field images of Golgi-impregnated *stratum radiatum* dendrites from hippocampal CA1 pyramidal neurons were captured with a Nikon DXM 1200F digital camera attached to a Nikon Eclipse E600 light microscope (× 100 oil objective). Only fully impregnated pyramidal neurons with their soma entirely within the thickness of the section were used. Image *z*-stacks were taken every 0.2 µm, at 1,024 × 1,024 pixel resolution, yielding an image with pixel dimensions of 49.25 × 49.25 µm. *Z*-stacks were deconvolved using the Huygens software (Scientific volume imaging, Hilversum, the Netherlands) to improve voxel resolution and to reduce optical aberration along the *z* axis. Segments of proximal apical dendrites were selected for the analysis of spine density and spine morphology according to the following criteria: (a) segments with no overlap with other branches that would obscure visualization of spines and (b) segments either 'parallel' to or 'at acute angles' relative to the coronal surface of the section to avoid ambiguous identification of spines. Only spines arising from the lateral surfaces of the dendrites were included in the study; spines located on the top or bottom of the dendrite surface were ignored. Given that spine density increases as a function of the distance from the soma, reaching a plateau 45 µm away from the soma, we selected dendritic segments of basal dendrites 45 µm away from the cell body. The total number of spines was obtained using the cell counter tool in the ImageJ software. At least 60 dendrites per group from at least three mice per genotype were counted. For a more precise description of the dendritic shape changes, the spine head diameter was analysed as a continuous distribution (between 368 and 418 spines per group were analysed) using the ImageJ software. Then, a distribution analysis of head diameter was performed. Then, head diameter analysis was performed manually using ImageJ for all the spines in control mice. Spine neck was measured in all spines as the distance from the dendritic shaft to the head of the spine using the ImageJ.

Subcellular fractionation. Hippocampus from 20-week-old R6/1 mice was homogenized with a Teflon-glass potter in lysis buffer (4 mM HEPES, 0.32 M sucrose, 1 mM phenylmethylsulfonyl fluoride (PMSF), 10 mg l^{-1} aprotinin, 1 mg l^{-1} leupeptin, 2 mM sodium orthovanadate, 0.1 g l^{-1} benzamidine) and centrifuged at 3,000 *g* for 10 min. The supernatant was taken as 'cytosolic' fraction and the pellet as 'nuclear' fractions. The latter was resuspended in 10 mM Tris-HCl (pH 7.5), 0.25 M sucrose, 2 mM PMSF, 10 mg l^{-1} aprotinin, 1 mg l^{-1} leupeptin, 2 mM Na_3VO_4 and sonicated. For PSD preparation, the two hippocampi (30–50 mg) of each mouse were homogenized using a Dounce Homogenizer in 1 ml of homogenization buffer (320 mM sucrose, 1 mM Hepes pH 7.4). Samples were centrifuged at 1,000 x g for 10 min, 4 °C. The pellet was resuspended in 1 ml of homogenization buffer and centrifuged at 1,000 x g for 10 min, 41°C. The two supernatants were pooled and centrifuged at 18,600 x g for 15 min, 4 °C. The pellet was then resuspended in 1 ml of 1.5 M sucrose, 50 mM Tris-HCl pH 7.4) and transferred in a 4 ml. Thinwall, ultra-clear Beckman Coulter tube and centrifuged on a 0.3–0.85 sucrose gradient at 25,000 r.p.m. for 85 min, 4 °C (SW60 Ti rotor in Optima L90K Ultracentrifuge). The synaptosomal fraction was collected at the interface, resuspended in 2 ml 50 mM Tris-HCl, pH 7.4 and centrifuged at 32,000 r.p.m. for 18 min, 4 °C (MLA-80 rotor, Optima Max Ultracentrifuge). The pellet was resuspended in 1 ml Tris-HCl, 25 mM pH 7.4, 30 ml l-1 Triton X100 and left on ice for 30 min. Then the sample was loaded onto 2 ml of Tris buffer with 0.85 M sucrose in a Thinwall, ultra-clear tube and centrifuged at 32,000 r.p.m. for 40 min, 4 °C (SW60 Ti rotor in Optima L90K Ultracentrifuge). The pellet corresponding to the PSD fraction was resuspended in 50 mM Tris-HCl, pH 7.4. Until the gradient buffers contained 30 mM NaF, 5 mM sodium-orthovanadate, and cOmpleteTM ULTRA protease inhibitor cocktail (Roche).

Post-mortem human brain tissues. Hippocampal brain tissues were supplied by the Banc de Teixits Neurològics (Biobanc-HC-IDIBAPS), Barcelona, Spain. They included six controls (mean ± s.e.m.; two females, four males, age 53.5 ± 6.8 years, post-mortem intervals, 4–18 h), four patients with HD grades 1–2 (four males, age 72.2 ± 1.7 years post-mortem intervals, 6–14 h) and seven patients with HD grades 3–4 (three females, four males, age 54.5 ± 6.5 years, post-mortem intervals of 4–17 h).

Immunoblot analysis. Animals were killed by cervical dislocation. The hippocampus was dissected out, frozen using CO_2 pellets and stored at −80 °C until use. Briefly, the tissue was lysed by sonication in 250 µl of lysis buffer (PBS, 10 ml l^{-1} Nonidet P-40, 1 mM PMSF, 10 mg l^{-1} aprotinin, 1 mg l^{-1} leupeptin and 2 mg l^{-1} sodium orthovanadate). After lysis, samples were centrifuged at 12,000 r.p.m. for 20 min. Supernatant proteins (15 µg) from total brain regions extracts were loaded in SDS–PAGE and transferred to nitrocellulose membranes (GE Healthcare, LC, UK). Membranes were blocked in TBS-T (150 mM NaCl, 20 mM Tris-HCl, pH 7.5, 0.5 ml l^{-1} Tween 20) with 50 g l^{-1} phospho-Blocker (Cell Biolabs, San Diego, CA) or 50 g l^{-1} non-fat dry milk and 5 g l^{-1} BSA. Immunoblots were probed with the following antibodies (all diluted 1:1,000): rabbit polyclonal antibodies: Pyk2 (#074M4755, Sigma), Pyk2 (#ab32571, Abcam, epitope within the first 100 residues), phosphoY402-Pyk2 (#5), PSD-95 (#QA210648), phosphoY876-GluA2 (#2), and phosphoY1246-GluN2A (#1, Cell Signaling Technology, Danvers, MA, USA), GluA1 (#JBC1830522, Upstate Biotechnology, NY, USA), phosphoY1472-GluN2B (#04242010009761, Cayman antibodies, Ann Arbor, MI, USA), phosphoY418-Src reacting with all phosphoSFKs (#GR144140-2), and phosphoY1325-GluN2A (#GR14161032, Abcam, Cambridge, UK), phosphoS831-GluA1 (#2726818), GluN2B (#2697434), GluA2 (#2280905), and GluN2A (#NRG1815904, Millipore Bedford, MA, USA), mouse monoclonal antibodies: phosphoERK1/2 (#26,Cell Signaling Technology, Danvers, MA, USA), FAK (#JBC1900835, Santa Cruz Biotechnology, Santa Cruz, CA, USA), GluN1 (#225310,Millipore, Bedford, MA, USA). All blots were incubated with the primary antibody overnight at 4 °C by shaking in PBS with 0.2 g l^{-1} sodium azide. After several washes in TBS-T, blots were incubated with secondary anti-rabbit or anti-mouse IgG IRdye800CW-coupled or anti-mouse IgG IRdye700DX-coupled antibodies (1:2,000, Rockland Immunochemicals, USA). Secondary antibody binding was detected by Odyssey infrared imaging apparatus (Li-Cor Inc., Lincoln, NE). For loading control a mouse monoclonal antibody for α-tubulin was used (#083M4847V, 1:10,000; Sigma).

Statistical analysis. Statistical analyses were carried out using the GraphPad Prism 6.0 software. Data sets were tested for normality distribution with d'Agostino–Pearson and Shapiro–Wilk tests. When distribution was not different from normal, they were analysed with parametric using Student's *t*-test (95% confidence), one-way ANOVA or two-way ANOVA, with Holm–Sidak *post hoc* multiple comparisons test. Two by two comparisons were two-tailed. In cases in which the distribution was significantly different from normal ($P<0.05$), non-parametric tests were used including Mann and Whitney for two groups comparisons and Kruskal–Wallis for more than two groups and Dunn's test for *post hoc* multiple comparisons. Kolmogorov–Smirnov test was used as indicated in the figure legends. Values of $P<0.05$ were considered as statistically significant.

Data availability. The authors declare that the data supporting the findings of this study are available within the paper and its Supplementary Information files or available on request from the corresponding author.

References

1. Girault, J. A., Costa, A., Derkinderen, P., Studler, J. M. & Toutant, M. FAK and PYK2/CAKbeta in the nervous system: a link between neuronal activity, plasticity and survival? *Trends Neurosci.* **22,** 257–263 (1999).
2. Salter, M. W. & Kalia, L. V. Src kinases: a hub for NMDA receptor regulation. *Nat. Rev. Neurosci.* **5,** 317–328 (2004).

3. Lev, S. *et al.* Protein tyrosine kinase PYK2 involved in Ca(2+)-induced regulation of ion channel and MAP kinase functions. *Nature* **376,** 737–745 (1995).
4. Menegon, A. *et al.* FAK^{+} and PYK2/CAKbeta, two related tyrosine kinases highly expressed in the central nervous system: similarities and differences in the expression pattern. *Eur. J. Neurosci.* **11,** 3777–3788 (1999).
5. Bartos, J. A. *et al.* Postsynaptic clustering and activation of Pyk2 by PSD-95. *J. Neurosci.* **30,** 449–463 (2010).
6. Hsin, H., Kim, M. J., Wang, C. F. & Sheng, M. Proline-rich tyrosine kinase 2 regulates hippocampal long-term depression. *J. Neurosci.* **30,** 11983–11993 (2010).
7. Huang, Y. *et al.* CAKbeta/Pyk2 kinase is a signaling link for induction of long-term potentiation in CA1 hippocampus. *Neuron* **29,** 485–496 (2001).
8. Lambert, J. C. *et al.* Meta-analysis of 74,046 individuals identifies 11 new susceptibility loci for Alzheimer's disease. *Nat. Genet.* **45,** 1452–1458 (2013).
9. Walkiewicz, K. W., Girault, J. A. & Arold, S. T. How to awaken your nanomachines: site-specific activation of focal adhesion kinases through ligand interactions. *Prog. Biophys. Mol. Biol.* **119,** 60–71 (2015).
10. Dikic, I., Tokiwa, G., Lev, S., Courtneidge, S. A. & Schlessinger, J. A role for Pyk2 and Src in linking G-protein-coupled receptors with MAP kinase activation. *Nature* **383,** 547–550 (1996).
11. Siciliano, J. C., Toutant, M., Derkinderen, P., Sasaki, T. & Girault, J. A. Differential regulation of proline-rich tyrosine kinase 2/cell adhesion kinase beta (PYK2/CAKbeta) and pp125(FAK) by glutamate and depolarization in rat hippocampus. *J. Biol. Chem.* **271,** 28942–28946 (1996).
12. Heidinger, V. *et al.* Metabotropic glutamate receptor 1-induced upregulation of NMDA receptor current: mediation through the Pyk2/Src-family kinase pathway in cortical neurons. *J. Neurosci.* **22,** 5452–5461 (2002).
13. Husi, H., Ward, M. A., Choudhary, J. S., Blackstock, W. P. & Grant, S. G. Proteomic analysis of NMDA receptor-adhesion protein signaling complexes. *Nat. Neurosci.* **3,** 661–669 (2000).
14. Seabold, G. K., Burette, A., Lim, I. A., Weinberg, R. J. & Hell, J. W. Interaction of the tyrosine kinase Pyk2 with the N-methyl-D-aspartate receptor complex via the Src homology 3 domains of PSD-95 and SAP102. *J. Biol. Chem.* **278,** 15040–15048 (2003).
15. Bongiorno-Borbone, L., Kadare, G., Benfenati, F. & Girault, J. A. FAK and PYK2 interact with SAP90/PSD-95-associated protein-3. *Biochem. Biophys. Res. Commun.* **337,** 641–646 (2005).
16. Grant, S. G. *et al.* Impaired long-term potentiation, spatial learning, and hippocampal development in fyn mutant mice. *Science* **258,** 1903–1910 (1992).
17. O'Dell, T. J., Kandel, E. R. & Grant, S. G. Long-term potentiation in the hippocampus is blocked by tyrosine kinase inhibitors. *Nature* **353,** 558–560 (1991).
18. Okigaki, M. *et al.* Pyk2 regulates multiple signaling events crucial for macrophage morphology and migration. *Proc. Natl Acad. Sci. USA* **100,** 10740–10745 (2003).
19. The Huntington's Disease Collaborative Research Group. A novel gene containing a trinucleotide repeat that is expanded and unstable on Huntington's disease chromosomes. *Cell* **72,** 971–983 (1993).
20. Giralt, A., Coura, R. & Girault, J. A. Pyk2 is essential for astrocytes mobility following brain lesion. *Glia* **64,** 620–634 (2016).
21. Assini, F. L., Duzzioni, M. & Takahashi, R. N. Object location memory in mice: pharmacological validation and further evidence of hippocampal CA1 participation. *Behav. Brain Res.* **204,** 206–211 (2009).
22. Cunningham, J. I., Raudensky, J., Tonkiss, J. & Yamamoto, B. K. MDMA pretreatment leads to mild chronic unpredictable stress-induced impairments in spatial learning. *Behav. Neurosci.* **123,** 1076–1084 (2009).
23. Corvol, J. C. *et al.* Depolarization activates ERK and proline-rich tyrosine kinase 2 (PYK2) independently in different cellular compartments in hippocampal slices. *J. Biol. Chem.* **280,** 660–668 (2005).
24. Gray, N. W., Weimer, R. M., Bureau, I. & Svoboda, K. Rapid redistribution of synaptic PSD-95 in the neocortex *in vivo*. *PLoS Biol.* **4,** e370 (2006).
25. El-Husseini Ael, D. *et al.* Synaptic strength regulated by palmitate cycling on PSD-95. *Cell* **108,** 849–863 (2002).
26. Colledge, M. *et al.* Ubiquitination regulates PSD-95 degradation and AMPA receptor surface expression. *Neuron* **40,** 595–607 (2003).
27. Ehlers, M. D. Activity level controls postsynaptic composition and signaling via the ubiquitin-proteasome system. *Nat. Neurosci.* **6,** 231–242 (2003).
28. Perez de Arce, K. *et al.* Synaptic clustering of PSD-95 is regulated by c-Abl through tyrosine phosphorylation. *J. Neurosci.* **30,** 3728–3738 (2010).
29. Zhang, J., Petit, C. M., King, D. S. & Lee, A. L. Phosphorylation of a PDZ domain extension modulates binding affinity and interdomain interactions in postsynaptic density-95 (PSD-95) protein, a membrane-associated guanylate kinase (MAGUK). *J. Biol. Chem.* **286,** 41776–41785 (2011).
30. Faure, C. *et al.* Calcineurin is essential for depolarization-induced nuclear translocation and tyrosine phosphorylation of PYK2 in neurons. *J. Cell Sci.* **120,** 3034–3044 (2007).
31. Sun, Y., Savanenin, A., Reddy, P. H. & Liu, Y. F. Polyglutamine-expanded huntingtin promotes sensitization of N-methyl-D-aspartate receptors via post-synaptic density 95. *J. Biol. Chem.* **276,** 24713–24718 (2001).
32. Fan, J. *et al.* P38 MAPK is involved in enhanced NMDA receptor-dependent excitotoxicity in YAC transgenic mouse model of Huntington disease. *Neurobiol. Dis.* **45,** 999–1009 (2012).
33. Brito, V. *et al.* Neurotrophin receptor p75(NTR) mediates Huntington's disease-associated synaptic and memory dysfunction. *J. Clin. Invest.* **124,** 4411–4428 (2014).
34. Nithianantharajah, J., Barkus, C., Murphy, M. & Hannan, A. J. Gene-environment interactions modulating cognitive function and molecular correlates of synaptic plasticity in Huntington's disease transgenic mice. *Neurobiol. Dis.* **29,** 490–504 (2008).
35. Miguez, A. *et al.* Fingolimod (FTY720) enhances hippocampal synaptic plasticity and memory in Huntington's disease by preventing p75NTR up-regulation and astrocyte-mediated inflammation. *Hum. Mol. Genet.* **24,** 4958–4970 (2015).
36. Vonsattel, J. P. *et al.* Neuropathological classification of Huntington's disease. *J. Neuropathol. Exp. Neurol.* **44,** 559–577 (1985).
37. Mangiarini, L. *et al.* Exon 1 of the HD gene with an expanded CAG repeat is sufficient to cause a progressive neurological phenotype in transgenic mice. *Cell* **87,** 493–506 (1996).
38. Faure, C., Ramos, M. & Girault, J. A. Pyk2 cytonuclear localization: mechanisms and regulation by serine dephosphorylation. *Cell Mol. Life Sci.* **70,** 137–152 (2013).
39. Van Raamsdonk, J. M., Murphy, Z., Slow, E. J., Leavitt, B. R. & Hayden, M. R. Selective degeneration and nuclear localization of mutant huntingtin in the YAC128 mouse model of Huntington disease. *Hum. Mol. Genet.* **14,** 3823–3835 (2005).
40. Prybylowski, K. *et al.* The synaptic localization of NR2B-containing NMDA receptors is controlled by interactions with PDZ proteins and AP-2. *Neuron* **47,** 845–857 (2005).
41. Hallett, P. J., Spoelgen, R., Hyman, B. T., Standaert, D. G. & Dunah, A. W. Dopamine D1 activation potentiates striatal NMDA receptors by tyrosine phosphorylation-dependent subunit trafficking. *J. Neurosci.* **26,** 4690–4700 (2006).
42. Köhr, G. & Seeburg, P. H. Subtype-specific regulation of recombinant NMDA receptor- channels by protein tyrosine kinases of the *src* family. *J. Physiol.* **492,** 445–452 (1996).
43. Taniguchi, S. *et al.* Involvement of NMDAR2A tyrosine phosphorylation in depression-related behaviour. *EMBO J.* **28,** 3717–3729 (2009).
44. Migaud, M. *et al.* Enhanced long-term potentiation and impaired learning in mice with mutant postsynaptic density-95 protein. *Nature* **396,** 433–439 (1998).
45. Zhao, C. *et al.* The upregulation of NR2A-containing N-methyl-D-aspartate receptor function by tyrosine phosphorylation of postsynaptic density 95 via facilitating Src/proline-rich tyrosine kinase 2 activation. *Mol. Neurobiol.* **51,** 500–511 (2015).
46. Yang, S., Roselli, F., Patchev, A. V., Yu, S. & Almeida, O. F. Non-receptor-tyrosine kinases integrate fast glucocorticoid signaling in hippocampal neurons. *J. Biol. Chem.* **288,** 23725–23739 (2013).
47. Sturgill, J. F., Steiner, P., Czervionke, B. L. & Sabatini, B. L. Distinct domains within PSD-95 mediate synaptic incorporation, stabilization, and activity-dependent trafficking. *J. Neurosci.* **29,** 12845–12854 (2009).
48. Frank, R. A. *et al.* NMDA receptors are selectively partitioned into complexes and supercomplexes during synapse maturation. *Nat. Commun.* **7,** 11264 (2016).
49. Nada, S. *et al.* Identification of PSD-93 as a substrate for the Src family tyrosine kinase Fyn. *J. Biol. Chem.* **278,** 47610–47621 (2003).
50. Sato, Y., Tao, Y. X., Su, Q. & Johns, R. A. Post-synaptic density-93 mediates tyrosine-phosphorylation of the N-methyl-D-aspartate receptors. *Neuroscience* **153,** 700–708 (2008).
51. Tezuka, T., Umemori, H., Akiyama, T., Nakanishi, S. & Yamamoto, T. PSD-95 promotes Fyn-mediated tyrosine phosphorylation of the N-methyl-D-aspartate receptor subunit NR2A. *Proc. Natl Acad. Sci. USA* **96,** 435–440 (1999).
52. Corsi, J. M. *et al.* Autophosphorylation-independent and -dependent functions of focal adhesion kinase during development. *J. Biol. Chem.* **284,** 34769–34776 (2009).
53. Zhao, X., Peng, X., Sun, S., Park, A. Y. & Guan, J. L. Role of kinase-independent and -dependent functions of FAK in endothelial cell survival and barrier function during embryonic development. *J. Cell Biol.* **189,** 955–965 (2010).
54. Bongiorno-Borbone, L. *et al.* The translocation of focal adhesion kinase in brain synaptosomes is regulated by phosphorylation and actin assembly. *J. Neurochem.* **81,** 1212–1222 (2002).
55. Regehr, W. G. Short-term presynaptic plasticity. *Cold Spring Harb. Perspect. Biol.* **4,** a005702 (2012).
56. Zucker, R. S. Short-term synaptic plasticity. *Annu. Rev. Neurosci.* **12,** 13–31 (1989).
57. Yang, S., Santos, M. D., Tang, C. M., Kim, J. G. & Yang, S. A postsynaptic role for short-term neuronal facilitation in dendritic spines. *Front. Cell Neurosci.* **10,** 224 (2016).

58. Bourgin, C., Murai, K. K., Richter, M. & Pasquale, E. B. The EphA4 receptor regulates dendritic spine remodeling by affecting beta1-integrin signaling pathways. *J. Cell Biol.* **178,** 1295–1307 (2007).
59. Shi, Y., Pontrello, C. G., DeFea, K. A., Reichardt, L. F. & Ethell, I. M. Focal adhesion kinase acts downstream of EphB receptors to maintain mature dendritic spines by regulating cofilin activity. *J. Neurosci.* **29,** 8129–8142 (2009).
60. Suo, L., Lu, H., Ying, G., Capecchi, M. R. & Wu, Q. Protocadherin clusters and cell adhesion kinase regulate dendrite complexity through Rho GTPase. *J. Mol. Cell Biol.* **4,** 362–376 (2012).
61. Kinoshita, Y. *et al.* Role for NUP62 depletion and PYK2 redistribution in dendritic retraction resulting from chronic stress. *Proc. Natl Acad. Sci. USA* **111,** 16130–16135 (2014).
62. Gladding, C. M. *et al.* Calpain and STriatal-enriched protein tyrosine phosphatase (STEP) activation contribute to extrasynaptic NMDA receptor localization in a Huntington's disease mouse model. *Hum. Mol. Genet.* **21,** 3739–3752 (2012).
63. Xu, J. *et al.* Striatal-enriched protein-tyrosine phosphatase (STEP) regulates Pyk2 kinase activity. *J. Biol. Chem.* **287,** 20942–20956 (2012).
64. Xu, J. *et al.* Inhibitor of the tyrosine phosphatase STEP reverses cognitive deficits in a mouse model of Alzheimer's disease. *PLoS Biol.* **12,** e1001923 (2014).
65. Dourlen, P. *et al.* Functional screening of Alzheimer risk loci identifies PTK2B as an *in vivo* modulator and early marker of Tau pathology. *Mol. Psychiatry.* doi: 10.1038/mp.2016.59 (2016).
66. Giralt, A., Carreton, O., Lao-Peregrin, C., Martin, E. D. & Alberch, J. Conditional BDNF release under pathological conditions improves Huntington's disease pathology by delaying neuronal dysfunction. *Mol. Neurodegener.* **6,** 71 (2011).
67. Slot, J. W. & Geuze, H. J. Cryosectioning and immunolabeling. *Nat. Protoc.* **2,** 2480–2491 (2007).
68. Prange, O., Wong, T. P., Gerrow, K., Wang, Y. T. & El-Husseini, A. A balance between excitatory and inhibitory synapses is controlled by PSD-95 and neuroligin. *Proc. Natl Acad. Sci. USA* **101,** 13915–13920 (2004).
69. Shao, C. Y., Sondhi, R., van de Nes, P. S. & Sacktor, T. C. PKMzeta is necessary and sufficient for synaptic clustering of PSD-95. *Hippocampus* **22,** 1501–1507 (2012).
70. Engmann, O. *et al.* DARPP-32 interaction with adducin may mediate rapid environmental effects on striatal neurons. *Nat. Commun.* **6,** 10099 (2015).

Acknowledgements

This work was supported in part by Inserm, the Université Pierre et Marie Curie (UPMC, Paris 6), and an ERC advanced investigator grant (#250349) to J.-A.G. A.G. was partly supported by the King Abdullah University of Science and Technology (KAUST) Office of Sponsored Research award (#OSR-2015-CRG4-2602) to J.-A.G. and Stefan Arold. J.-C.P. lab is supported by grants from the Human Frontier Science Program (RGP0022/2013) and the Fondation pour la Recherche Médicale (DEQ20140329539). Q.C. and C.S. were recipients of doctoral fellowships of UPMC. Equipment at the IFM was also supported by DIM NeRF from Région Ile-de-France and by the FRC/Rotary 'Espoir en tête'. Microscopy was carried out at the Institut du Fer à Moulin Cell and Tissue Imaging facility. Labs of J.-A.G. and J.-C.P. are affiliated with the Paris School of Neuroscience (ENP) and the Bio-Psy Laboratory of excellence. Work in S.G. and J.A. labs was supported by Ministerio de Ciencia e Innovación (SAF2015-67474-R; MINECO/FEDER to S.G. and SAF2014-57160 to J.A.), Fundacio La Marato TV3, and Centro de Investigación Biomédica en Red sobre Enfermedades Neurodegenerativas (CIBERNED, R006/0010/0006). We thank Ana López and Maria Teresa Muñoz for technical assistance, and Teresa Rodrigo Calduch and the staff of the animal care facility (Facultat de Psicologia, Universitat de Barcelona) for their help.

Author contributions

A.G. conceived and carried out most experiments, analysed and interpreted results and wrote the manuscript. V.B. carried out experiments related to HD and mouse model. Q.C. and Y.O. carried out and analysed electrophysiological experiments. C.S. carried out cell fractionation experiments. C.C.-D. carried out electron microscopy. B.d.P. and R.C. contributed to behavioural and biochemical experiments. J.A. and S.G. supervised Huntington-related experiments. J.-C.P. supervised and analysed electrophysiological experiments. J.-A.G. conceived and supervised the study, analysed results and wrote the manuscript.

Additional information

Supplementary Information accompanies this paper at http://www.nature.com/naturecommunications

Competing interests: The authors declare no competing financial interests.

Reprints and permission information is available online at http://npg.nature.com/reprintsandpermissions/

How to cite this article: Giralt, A. *et al.* Pyk2 modulates hippocampal excitatory synapses and contributes to cognitive deficits in a Huntington's disease model. *Nat. Commun.* **8,** 15592 doi: 10.1038/ncomms15592 (2017).

Publisher's note: Springer Nature remains neutral with regard to jurisdictional claims in published maps and institutional affiliations.

4. Summary of the findings and conclusions

In this paper, we reconfirmed the importance of Pyk2 in hippocampal LTP by showing an impairment of CA1 LTP and hippocampal-related learning in Pyk2-deficient mice. We observed that these deficits were associated with alterations in NMDA receptors, PSD-95 and dendritic spines. We revealed in vitro, that the role of Pyk2 in determining PSD-95 enrichment appeared to be autophosphorylation-dependent whereas its effect on spine density was not likely to involve the autophosphorylation of Pyk2 neither its kinase activity. We finally described a decrease of Pyk2 levels in the hippocampus of HD patients and in the R6/1 mouse model of the disease and observed that normalizing Pyk2 levels in the hippocampus of R6/1 mice could rescue, to some extent, the molecular and behavioral deficits of these mice.

We thus revealed for the first time, a role for Pyk2 in Huntington's disease cognitive impairments. We also described *in vivo*, the importance of Pyk2 in spine structure and synaptic function.

II. Pyk2 in the amygdala modulates chronic stress sequelae via PSD-95-related micro-structural changes

Enrica Montalban, Omar Al-Massadi, Anna Sancho-Balsells, Verónica Brito, Benoit de Pins, Jordi Alberch, Silvia Ginés, Jean-Antoine Girault and Albert Giralt

Translational Psychiatry
15 January 2019, 9(1):3

1. Context and objectives

At the cellular level, chronic stress is closely associated to microstructural alterations in dendritic spines morphology and spine density. Identifying master molecules regulating these alterations would give a better understanding of the molecular mechanisms underlying stress-induced depression.

Given our previous study showing the importance of Pyk2 in spine morphology and in synaptic biochemistry in general, we intended here to investigate the role of Pyk2 in the development of depressive-like symptoms induced by a model of chronic unpredictable mild stress (CUMS).

To do so we compared anxiety-like and anhedonia-like phenotypes induced by CUMS in Pyk2$^{-/-}$ mice and several region-specific knockout as compared to wild type control mice. We then analyzed the spine morphology and biochemical features of synapses in these different conditions.

2. Contribution to the work

In this work, I personally contributed to the management of mice lines and to the redaction of the final manuscript.

3. Article

Montalban et al. *Translational Psychiatry* (2019)9:3
https://doi.org/10.1038/s41398-018-0352-y

Translational Psychiatry

ARTICLE Open Access

Pyk2 in the amygdala modulates chronic stress sequelae via PSD-95-related micro-structural changes

Enrica Montalban[1,2,3], Omar Al-Massadi[1,2,3,4,5], Anna Sancho-Balsells[6,7,8], Verónica Brito[6,7,8], Benoit de Pins[1,2,3], Jordi Alberch[6,7,8], Silvia Ginés[6,7,8], Jean-Antoine Girault[1,2,3] and Albert Giralt[1,2,3,6,7,8]

Abstract

Major depressive disorder (MDD) is a common disorder with a variety of symptoms including mood alterations, anhedonia, sleep and appetite disorders, and cognitive disturbances. Stressful life events are among the strongest risk factors for developing MDD. At the cellular level, chronic stress results in the modification of dendritic spine morphology and density. Here, we study the role of Pyk2 in the development of depressive-like symptoms induced by a model of chronic unpredictable mild stress (CUMS). Pyk2 is a non-receptor calcium-dependent protein-tyrosine kinase highly expressed in the forebrain principal neurons and involved in spine structure and density regulation. We show that Pyk2 knockout mice are less affected to anxiety-like and anhedonia-like phenotypes induced by the CUMS paradigm. Using region-specific knockout, we demonstrate that this phenotype is fully recapitulated by selective Pyk2 inactivation in the amygdala. We also show that in the absence of Pyk2 the spine alterations, PSD-95 clustering, and NMDA receptors changes induced by the CUMS paradigm are prevented. Our results reveal a possible role for Pyk2 in the response to stress and in synaptic markers expression and spine density regulation in the amygdala. We suggest that Pyk2 contributes to stress-induced responses through micro-structural changes and that its deficit may contribute to the resilience to chronic stress.

Introduction

Major depressive disorder (MDD) is a debilitating disease characterized by low mood, loss of interest in outside stimuli, impaired cognitive function, and vegetative symptoms, such as disturbed sleep or appetite[1]. MDD is a multifactorial and clinically heterogenous mental disorder with a percentage of heritability estimated around 35% and yearly incidence of 6% of affected individuals among the adult worldwide population[2]. Chronic life stressors are among the main risk factors for developing a major depressive syndrome[3]. Notably, a clear association between stressors and the emergence of major depressive episodes has been demonstrated among dysthymic patients[4]. The impact of stressors depends on the characteristics of the stressor itself (e.g. severity, chronicity, predictability), coping ability, and individuals' stressor history (including early life trauma)[3,5–7].

A large body of evidence shows that in animal models depression is closely associated to microstructural alterations in dendritic spines morphology and spine density[8]. Indeed, chronic stress results in decreased dendritic spine density in hippocampus and prefrontal cortex, and an increased spine density in amygdala and nucleus accumbens[9–12]. Therefore, understanding dendritic spines dynamics and turnover and identifying master molecules regulating this phenomenon is crucial for uncovering the mechanisms underlying stress-induced depression.

Pyk2 could be one of these master molecules. Pyk2 is a non-receptor tyrosine kinase that can be activated by

Correspondence: Albert Giralt (albertgiralt@ub.edu)
[1]Inserm UMR-S 839, 75005 Paris, France
[2]Sorbonne Université, Faculté des Sciences et d'Ingénierie, 75005 Paris, France
Full list of author information is available at the end of the article.

Ca^{2+} and is highly expressed in cortex, amygdala, striatum, and hippocampus[13,14]. Previous findings indicated a role for Pyk2 in the regulation of hippocampal synaptic plasticity[15–17]. Our recent work with Pyk2 mutant mice showed its importance in vivo for spatial learning and memory, synaptic plasticity and spine density, and morphology[18]. Yet, the role of Pyk2 in the physiopathology of MDD remains largely unexplored as only two reports have pointed out a possible role of Pyk2 in this context. First, it has been reported that a model chronic stress in mice increases the colocalization of Pyk2 with NUP62, a nucleoprotein involved in chromatin organization and transcription[19]. The increased colocalization results in an increased phosphorylation of NUP62[19] suggesting a potential role of Pyk2 in mediating depressive-like symptomatology after chronic stress via the indirect regulation of gene transcription. A second study demonstrated that, in a model of chronic stress in rats, the overexpression of Pyk2 in the lateral septal nucleus has a positive effect on the forced swimming test's performance[20], a common paradigm to evaluate behavioral despair in rodents, one of the symptoms of MDD[21]. Finally, a recent genome wide association study (GWAS) indicated that the *PTK2B* gene is significantly associated with neuroticism[22] which in turn is a common risk factor to develop MDD[23]. Despite these early results, the relevance of the tyrosine kinase Pyk2 in the pathophysiology of MDD is not known. Understanding in which brain region and through which molecular mechanism Pyk2 regulates depressive symptoms would provide important insights on the possible role of PyK2 in MDD.

We recently generated full knockout mice for the *PTKB2* gene, as well as mice with floxed *PTK2B* alleles, which permit to inactivate the gene in discrete brain regions or cell types[13,18]. Mice were exposed to the chronic unpredictable mild stress (CUMS) paradigm to induce depressive-like symptoms. The CUMS protocol overcomes the stress habituation and has been widely used to model depression-like behaviors[8,24]. As expected, we observed that CUMS induced a severe depressive-like performances in the stressed mice as compared to non-stressed controls. Observed phenotypes included; decreased time spent in the open arms in the plus maze, decreased time struggling in the forced swimming test, and decreased preference for sweet water in the sucrose preference test as described previously[25]. Surprisingly, compared to WT mice, Pyk2-deficient mice showed reduced behavioral sequelae induced by the CUMS paradigm in several tests. Region-specific KO studies showed a major role of Pyk2 in the basolateral nuclei of the amygdala. We also examined spine density in this brain region and found that stress-induced spine alterations were absent in Pyk2-deficient mice. These results underline the possible role of Pyk2 in depressive states induced by stress.

Materials and methods

Detailed descriptions and procedures for genetically modified mice, CUMS paradigm, open field test, elevated plus maze test, forced swimming test, sucrose preference test, viral constructs and stereotaxic injection, tissue preparation and immunofluorescence, confocal imaging and analysis, Golgi staining and spines analysis, immunoblot analysis and statistical analysis are provided in the Supplementary Methods section.

Results

Effects of CUMS paradigm in mice lacking *PTK2B* gene (Pyk2$^{-/-}$ mice)

Pyk2$^{+/+}$ and Pyk2$^{-/-}$ mice were exposed for 28 days to randomized and unpredictable aversive stimuli (CUMS protocol, see Materials and methods and supplementary figure 1a). After the CUMS protocol all mice were evaluated for behavioral alterations. Naive mice from both genotypes (Pyk2$^{+/+}$ and Pyk2$^{-/-}$) were used as controls. First, as a general health index, we also monitored the body weight and we observed no difference in any group as compared to Pyk2$^{+/+}$ controls (Fig. 1a). Next, we used the open field to evaluate time spent in the center of the arena and pathlengths in Pyk2$^{+/+}$ and Pyk2$^{-/-}$ mice exposed (Pyk2$^{+/+}$:CUMS and Pyk2$^{-/-}$:CUMS) or not to CUMS (control Pyk2$^{+/+}$ and Pyk2$^{-/-}$ mice). All groups of mice habituated well and showed no difference in pathlengths (Fig. 1b) during the 30-min session. However, Pyk2$^{+/+}$:CUMS but not Pyk2$^{-/-}$:CUMS mice displayed significantly reduced time in the center in the open field paradigm (Fig. 1c). We then subjected the mice to the forced swimming test (FST). We measured the time during which mice were mobile to escape from the water: stressed mice showed lower levels of time struggling as compared to their respective controls without CUMS. No difference was observed when comparing Pyk2$^{+/+}$ and Pyk2$^{-/-}$ control mice or Pyk2$^{+/+}$:CUMS and Pyk2$^{-/-}$:CUMS mice (Fig. 1d). We also analyzed the two first minutes of the assay and no changes were observed when comparing Pyk2$^{+/+}$ and Pyk2$^{-/-}$ control mice or Pyk2$^{+/+}$:CUMS and Pyk2$^{-/-}$:CUMS mice (Fig. 1e). Next, we used an elevated plus maze to evaluate the effect of the CUMS paradigm on time spent in the open arms in the four groups of mice (Fig. 1f, g). We found a significant preference for the open arms of the Pyk2$^{+/+}$ control mice as compared to the Pyk2$^{+/+}$:CUMS (Fig. 1f). Interestingly this difference was lost when comparing control Pyk2$^{-/-}$ mice to Pyk2$^{-/-}$:CUMS, which all spent a comparable amount of time as the Pyk2$^{+/+}$ controls in exploring the open arm. Importantly the locomotor activity (measured

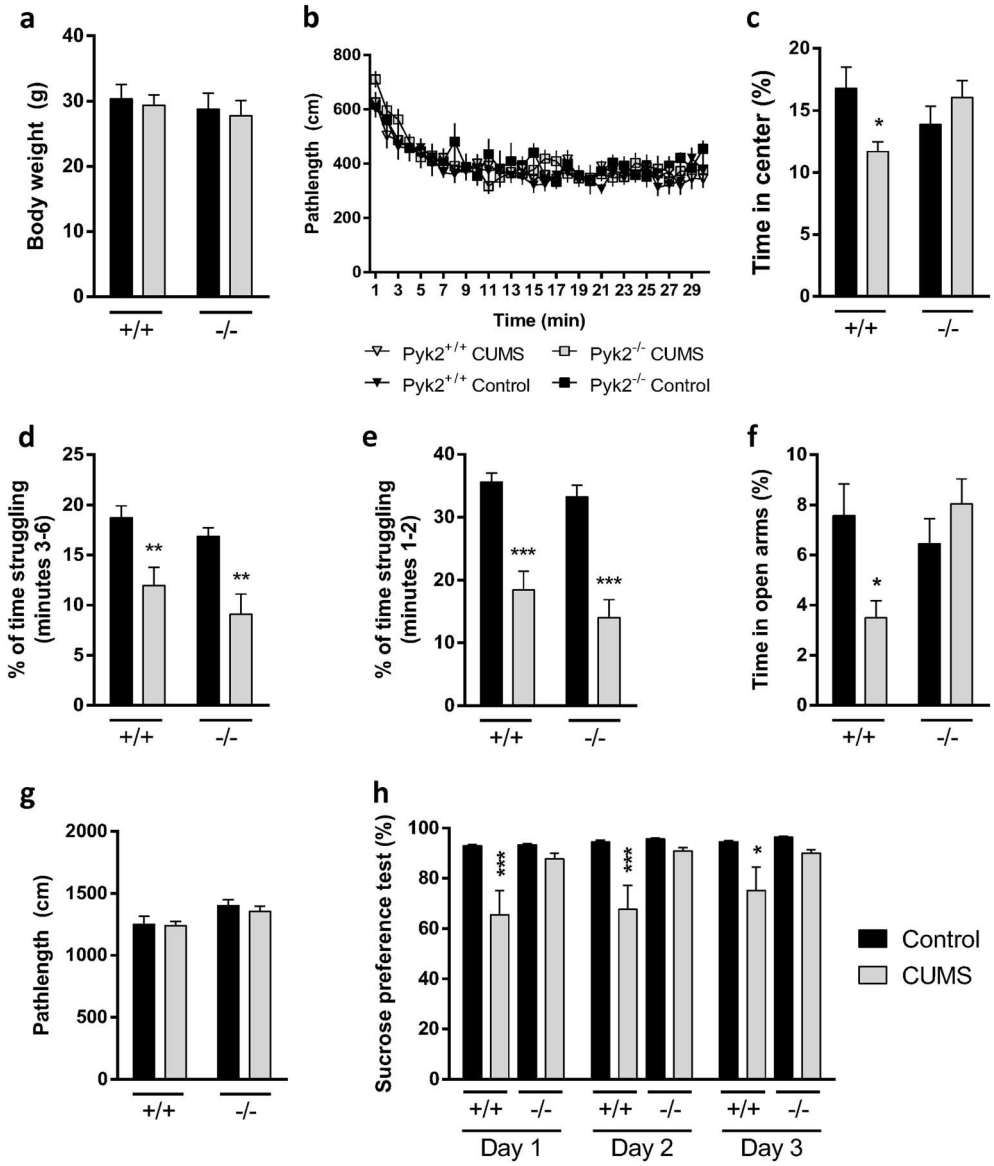

Fig. 1 Behavioral effects of CUMS in Pyk2$^{+/+}$ and Pyk2$^{-/-}$ mice. a Body weight was monitored as a measure of general health. Two-way ANOVA, genotype effect: $F_{(1, 51)} = 2.19$, $p = 0.09$. **b** Pathlength traveled in an open field apparatus during 30 min. Two-way ANOVA, genotype effect: $F_{(3, 52)} = 0.303$, $p = 0.82$. **c** Time in the center in an open field apparatus during 30 min. Two-way ANOVA, interaction effect: $F_{(1, 52)} = 6.956$, $p = 0.011$. **d** Forced swimming test: % of time struggling from the 3rd to the 6th minute in a 6-min long session. Two-way ANOVA, genotype effect: $F_{(1, 52)} = 21.72$, $p < 0.0001$. **e** Forced swimming test: % of time struggling from the 1st to the 2nd minute in a 6-min long session. Two-way ANOVA, genotype effect: $F_{(1, 52)} = 54.33$, $p < 0.0001$. **f** Time spent in the open arms of an elevated plus maze. Two-way ANOVA, genotype effect: $F_{(1, 52)} = 4.14$, $p = 0.01$. **g** Path length traveled in the elevated plus maze. Two-way ANOVA, genotype effect: $F_{(1, 52)} = 2.24$, $p = 0.078$. **h** Sucrose preference test. Preference for sweet water over plain water (%). Three consecutive days of testing were evaluated in the sucrose preference test. Two-way ANOVA genotype effect: day 1, $F_{(1, 52)} = 11.20$, $p = 0.0015$; day 2, $F_{(1, 52)} = 10.73$, $p = 0.0019$; day 3, $F_{(1, 52)} = 7.42$, $p = 0.008$. Data are means + SEM. Control Pyk2$^{+/+}$ ($n = 14$); control Pyk2$^{-/-}$ ($n = 14$); Pyk2$^{+/+}$:CUMS ($n = 13$) and Pyk2$^{-/-}$:CUMS ($n = 15$). Tukey's post hoc test was used in all experiments. **c–h**: *$p < 0.05$, **$p < 0.01$, and ***$p < 0.001$ compared to Pyk2$^{+/+}$ controls. CUMS Chronic unpredictable mild stress group

as a pathlength) tested in the plus maze was similar in all groups (Fig. 1g). Finally, we evaluated the effect of the genotype on potential CUMS-induced changes in the sucrose preference test. Animals were tested for 3 consecutive days for their preference for sweet water (2% sucrose) versus plain water (Fig. 1h). Control Pyk2$^{+/+}$ mice displayed high levels of preference towards sweet water as compared to normal water. In contrast, although they still had some preference for sweet water, Pyk2$^{+/+}$:CUMS mice displayed a significantly reduced preference

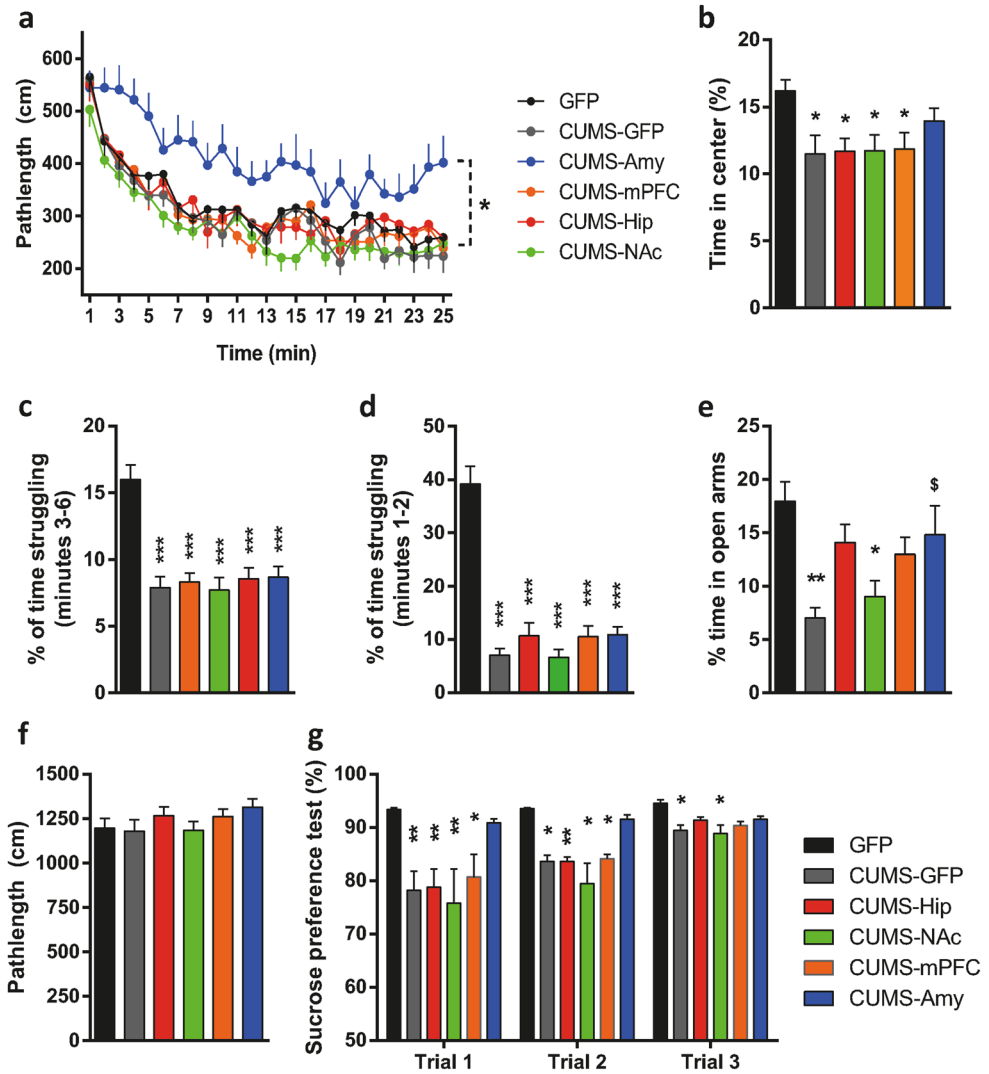

Fig. 2 Consequences of the regional-specific ablation of Pyk2 on the behavioral effects of CUMS. a Pathlength traveled in an open field apparatus during a 30 min session. Two-way ANOVA, genotype effect: $F_{(5,\ 74)} = 5.42$, $p = 0.0003$. **b** Time in the center in an open field apparatus during 30 min. One-way ANOVA, genotype effect: $F_{(5,\ 76)} = 2.349$, $p = 0.0488$. **c** Forced swimming test: % of time struggling from the 3rd to the 6th minute in a 6-min long session. One-way ANOVA: $F_{(5,\ 76)} = 20.83$, $p < 0.0001$. **d** Forced swimming test: % of time struggling from the 1st to the 2nd minute in a 6-min long session. One-way ANOVA: $F_{(5,\ 76)} = 45.34$, $p < 0.0001$. **e** Elevated plus maze test, time spent in open arms, One-way ANOVA and Tukey's post hoc test: $F_{(5,\ 76)} = 4.396$, $p = 0.001$. **f** Pathlength traveled in the elevated plus maze. One-way ANOVA and Tukey's post hoc test: $F_{(5,\ 76)} = 1.19$, $p = 0.32$. **g** Sucrose preference test: Preference for sweet water over plain water (%). Three consecutive days of testing were evaluated in the sucrose preference test. One-way ANOVA: day 1, $F_{(5,\ 79)} = 2.91$, $p = 0.018$; day 2: $F_{(5,\ 79)} = 7.34$, $p < 0.0001$; day 3: $F_{(5,\ 79)} = 3.86$, $p = 0.003$. Post-hoc Tukey's test. Data are means + SEM. **a–g** GFP group ($n = 10$); CUMS-GFP group ($n = 13$); CUMS-mPFC group ($n = 15$); CUMS-Nacc group ($n = 15$); CUMS-Hipp group ($n = 15$); CUMS-Amy group ($n = 14$). *$p < 0.05$ and **$p < 0.01$ compared to unstressed GFP group and $^{\$}p < 0.05$ compared to CUMS-GFP group

as compared to Pyk2$^{+/+}$ unstressed controls. Intriguingly, Pyk2$^{-/-}$ and Pyk2$^{-/-}$:CUMS groups of mice showed a comparable preference for sweet water, with no difference from that observed in control Pyk2$^{+/+}$ mice. This set of results indicates that behavioral alterations induced by the CUMS paradigm in Pyk2$^{+/+}$ mice were almost completely absent in Pyk2$^{-/-}$ mice in the same conditions. In contrast, the performance in the forced swimming test was not affected.

Pyk2 inactivation in the amygdala is sufficient to mimic the Pyk2$^{-/-}$ mice phenotype after CUMS

To gain insight on the brain region that could mediate such behavioral changes we knocked out Pyk2 in the neurons of selected brain regions by injecting Pyk2$^{f/f}$ mice with AAV expressing a Cre recombinase under the control of CaMKII promoter (AAV-CaMKII-Cre-GFP). Control AAVs expressed only GFP (AAV-CaMKII-GFP). AAV-CaMKII-Cre-GFP and control viruses were

bilaterally injected either in the amygdala (CUMS-Amy group), or the medial prefrontal cortex (CUMS-mPFC group), or the nucleus accumbens (CUMS-NAc group), or the hippocampus (CUMS-Hip group). Three weeks after surgery, all the groups of mice were exposed to the CUMS protocol. The GFP group of mice was injected in one of the four aforementioned brain regions with AAV-CaMKII-GFP, but not exposed to CUMS. For more clarity see supplementary figure 1b. First, we verified the correct coordinates of the injection sites (supplementary figure 2a), and the effects of to the local deletion of the *PTK2B* gene on reduction of Pyk2 protein levels in the injection site by immunofluorescence (supplementary figure 2b–e). Our results showed a clear decrease or disappearance of Pyk2 immunoreactivity in the AAV-Cre-targeted brain regions.

Next, after 28 days of CUMS all groups of mice were evaluated in a battery of behavioral tests namely open field test, plus maze test, forced swimming test, and sucrose preference test. Concerning the general locomotor activity, all groups of mice habituated well and showed equal levels of locomotor activity in the open field except for the CUMS-Amy group which showed increased pathlengths but normal habituation (Fig. 2a). Regarding to the parameter time in the center, all the groups of mice displayed reduced time in the center of the arena when compared with the GFP group with the exception of the CUMS-Amy group (Fig. 2b). We then used the forced swimming test in all the groups (Fig. 2c). Regardless of the regional deletion, all groups of mice exposed to CUMS struggled much less than the unstressed GFP group confirming that the changes in the levels of Pyk2 in any tested brain region had no effect on the performance in the forced swimming test. We also analyzed the two first minutes of the assay and again all groups of mice exposed to CUMS struggled much less than the unstressed GFP group (Fig. 2d). Then, the elevated plus maze was performed in all groups of mice (Fig. 2e). As compared to all the other groups, the CUMS-GFP group spent the lowest time in the open arms. The CUMS-NAc group displayed reduced time in the open arms similar to those of CUMS-GFP mice. In contrast, the CUMS-Amy group had levels of open arms exploration close to those of unstressed GFP controls, and significantly different from those of the CUMS-GFP group. Finally, the CUMS-mPFC and CUMS-Hip groups showed intermediate alterations regarding to the time spent in open arms. These results did not appear to depend on general locomotor activity in the plus maze as shown in Fig. 2f. This was a discrepancy from the CUMS-Amy group when comparing the locomotor activity parameter in the elevated plus maze and in the open field test. The CUMS-Amy group showed hyper locomotion only in the latter. This discrepancy with the elevated plus maze is likely due to the fact that the open field is more useful for locomotor measurements than it is to anxiety and elevated plus maze is more useful for anxiety-like measurements than it is to locomotor behavior[26,27]. Altogether, these results indicate that the CUMS-Amy group was the less affected by the CUMS protocol in parameters evaluated by the elevated plus maze and open field test. Finally, we tested in all six groups of mice their preference for sweet (2% sucrose) or plain water, as in Fig. 1h (Fig. 2g). As expected, control GFP mice exhibited the highest level of preference towards palatable water in the presence of both plain and sucrose-water. In contrast, although the CUMS-GFP mice had some preference for sweet water, this preference was significantly reduced as compared to GFP CUMS-naive controls. CUMS-mPFC, CUMS-Hip, and CUMS-NAc displayed similarly low levels of sucrose preference as compared to CUMS-GFP and significantly reduced preference when compared with the GFP group during the first 2 days of testing. Interestingly the CUMS-Amy group was the only group showing indistinguishable levels of sucrose preference as compared to GFP mice indicating that CUMS did not affect the preference towards the sweet water in this group of mice. In summary, the present results show that the reduced sequelae displayed by full $Pyk2^{-/-}$ knockout mice after the CUMS protocol was completely mimicked when Pyk2 expression was specifically removed in the amygdala.

Pyk2 levels and its activation are not altered by stress in the amygdala

To address the molecular mechanisms underlying the phenotype showed by the mice lacking PyK2 in the amygdala, we measured Pyk2 total protein levels and its phosphorylation at Tyr-402, the autophosphorylation site[28], a good indicator of its kinase activity, in the amygdala of $Pyk2^{+/+}$ mice subjected to 28 days of CUMS vs. naive control $Pyk2^{+/+}$. When animals were sacrificed 24 h after the end of the CUMS protocol, we did not observe any change either in the total levels of Pyk2 (Fig. 3a, b) nor in phosphoTyr-402-Pyk2 (Fig. 3a, c). We then hypothesized that the changes in the total or phospho-Pyk2 levels might be more acute and/or transient or that they could take place earlier after the exposure of the mice to stress. Thus, we designed a new experiment in which $Pyk2^{+/+}$ mice were acutely stressed by subjecting them to an hour restrain. Mice were sacrificed 0 or 3 h after the restrain protocol and the amygdala was quickly dissected out. Unstressed $Pyk2^{+/+}$ mice were used as controls. Again, no change in either total Pyk2 (Fig. 3d and e) or phosphoTyr-402-Pyk2 (Fig. 3d, f) was observed in the stressed $Pyk2^{+/+}$ mice as compared to control mice. In summary, these results show that neither acute stress nor CUMS alter Pyk2 levels or autophosphorylation in a manner that is detectable at the tissue level.

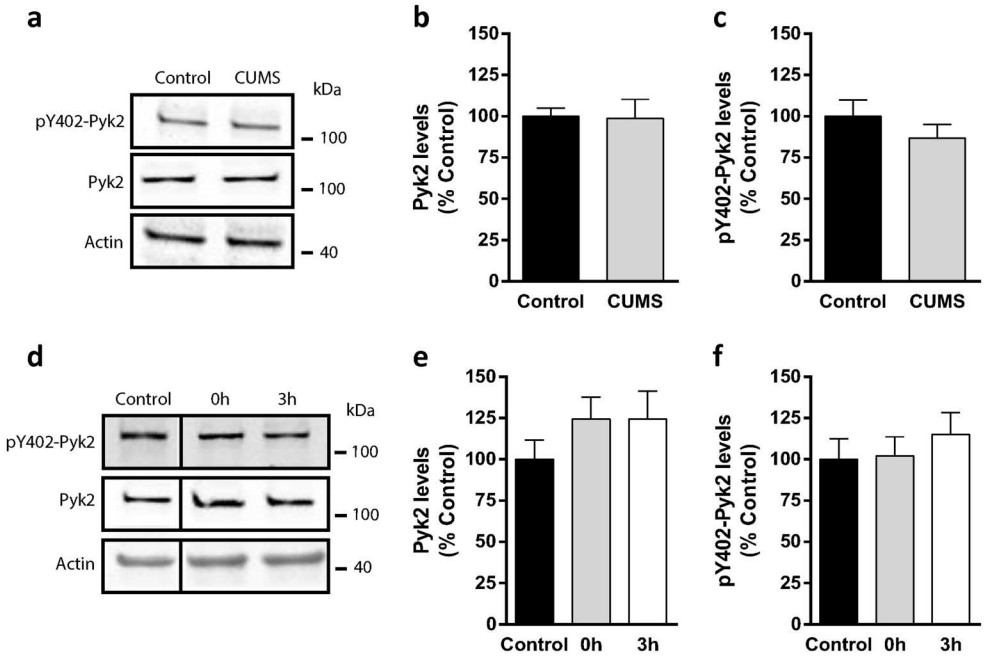

Fig. 3 Lack of effect of stress on the total levels and phosphorylation of Pyk2. a–c Wild type mice subjected or not to a 28-day CUMS protocol (from Fig. 1) and sacrificed 10 days later (after the behavioral assessment was ended). **a** Immunoblotting analysis of Pyk2 and its activated form autophosphorylated on Tyr402 (pY402-Pyk2) and tubulin as a loading control. **b** Densitometric quantification of total Pyk2 as in **a**. Two-tailed Student's *t*-test: $t_{17} = 1.24$, $p = 0.23$. **c** Densitometric quantification of pY402-Pyk2 as in **a**. Two-tailed Student's *t*-test: $t_{17} = 1.31$, $p = 0.19$. In **b** and **c** data were normalized to tubulin for each sample and expressed as percentage of $Pyk2^{+/+}$ controls. **d–f** Another set of wild type mice were subjected or not to acute restraint stress and sacrificed immediately (0 h) or 3 h later. **d** Immunoblotting analysis of Pyk2, pY402-Pyk2, and tubulin as a loading control. **e** Densitometric quantification of total Pyk2 results as in **d**. One-way ANOVA: $F_{(2, 14)} = 0.88$, $p = 0.43$. **e** Densitometric quantification of pY402-Pyk2 as in **d**. One-way ANOVA: $F_{(2, 14)} = 0.44$, $p = 0.66$. Data are means + SEM. Tukey's post hoc test was used in **e** and **f**. In **b**, **c**, **e**, and **f**, data were normalized to tubulin and expressed as percentage of $Pyk2^{+/+}$ unstressed controls. In **a**–**c** $n = 9$ mice/group; in **d**–**f** $n = 5$–6 mice per group. In **a** and **d** molecular weight markers position is indicated in kDa

Excitatory synapses in principal neurons of the basolateral amygdala (BLA) are increased during CUMS in $Pyk2^{+/+}$ but not in $Pyk2^{-/-}$ mice

Pyk2 has functions that are dependent on its kinase activity and others that are more related to other properties, such as scaffolding[15,18,19]. In our previous work we observed that the decreased spine density in $Pyk2^{-/-}$ hippocampal neurons is rescued by Pyk2 re-expression independently of its kinase activity[18]. Chronic stress and subsequent depression-like phenotype correlate with an increase in dendritic spines in the principal neurons of the BLA nuclei[8]. We therefore investigated whether the lack of Pyk2 in the amygdala could prevent the formation of these new dendritic spines. We used Golgi staining in a sub-set of $Pyk2^{+/+}$, $Pyk2^{-/-}$ control mice, as well as in $Pyk2^{+/+}$:CUMS and $Pyk2^{-/-}$:CUMS mice that were sacrificed 24 h after the last day of CUMS to study the spine density in the principal projection neurons of the BLA. First, our analysis confirmed the previous reports showing that dendritic spine density was significantly increased in $Pyk2^{+/+}$ mice, 10 days after the CUMS protocol, as compared to $Pyk2^{+/+}$ controls (Fig. 4a, b). In contrast, this stress-induced effect was completely absent in $Pyk2^{-/-}$:CUMS mice compared to $Pyk2^{-/-}$ control mice (Fig. 4a, b). To further explore the role of Pyk2 we performed a double immunofluorescence in $Pyk2^{+/+}$ and $Pyk2^{+/+}$:CUMS mice to study whether Pyk2 translocates and colocalizes with PSD-95 after chronic stress as previously published in stimulated pyramidal neurons of the hippocampus[15]. CUMS induced a clear increase in Pyk2 and PSD-95 colocalization (Fig. 4c–e). We then evaluated the PSD-95 dynamics in response to CUMS and counted the number of PSD-95 clusters, which correspond to post-synaptic densities, in the BLA of wild type and $Pyk2^{-/-}$ mice. In $Pyk2^{+/+}$ mice CUMS increased the number of PSD-95-positive clusters per field as compared to $Pyk2^{+/+}$ controls (Fig. 4f, g). In $Pyk2^{-/-}$ mice the CUMS protocol also increased the number of PSD-95-positive particles, but this effect was significantly less pronounced as compared to $Pyk2^{+/+}$:CUMS mice (Fig. 5f, g)

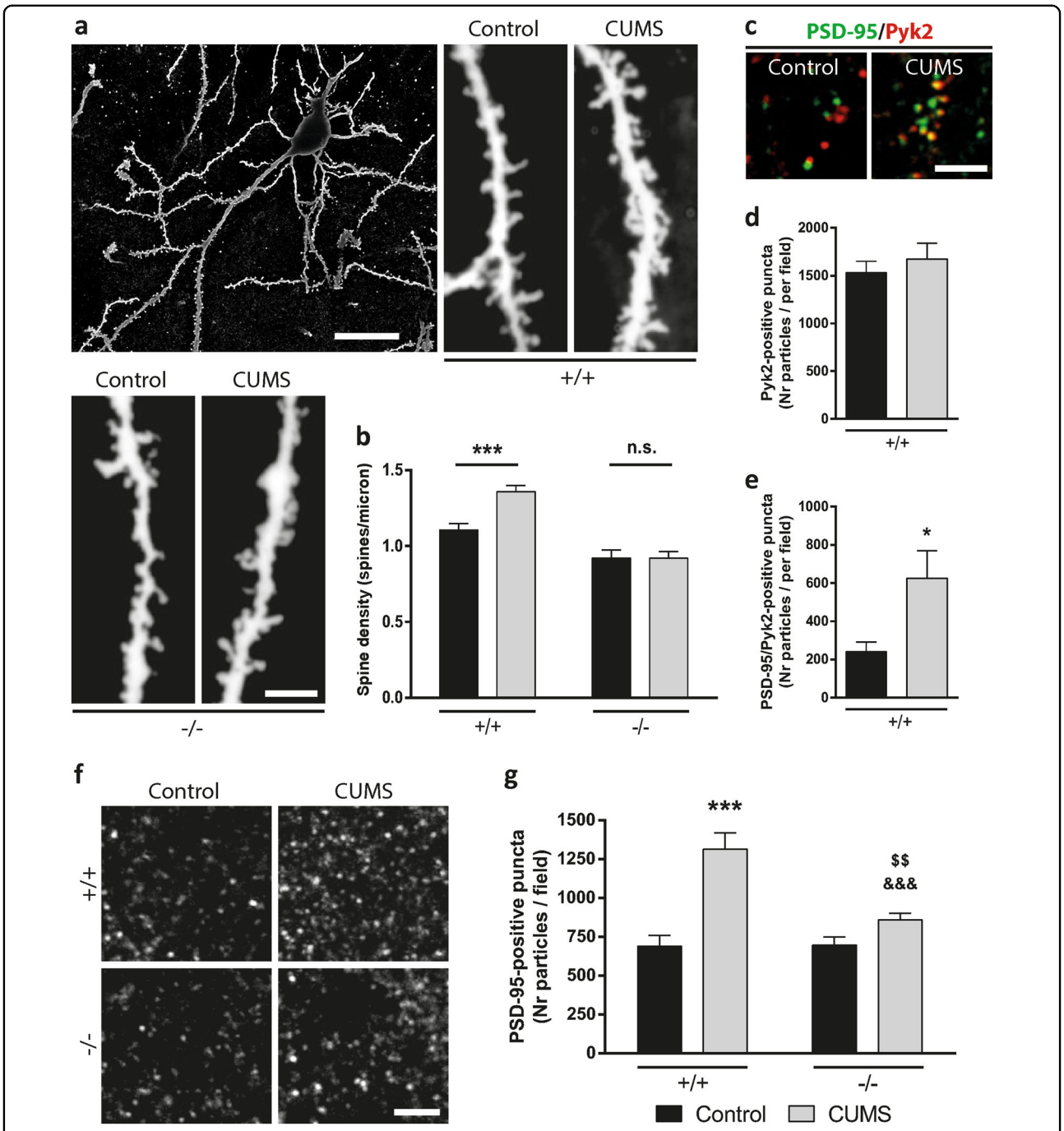

Fig. 4 Pyk2 knockout prevents the changes in dendritic spines and PSD-95 induced by chronic stress in the amygdala. a Golgi-Cox-stained apical dendrites of a basolateral amygdala principal neuron from Pyk2$^{+/+}$ and Pyk2$^{-/-}$ unstressed control mice and in Pyk2$^{+/+}$:CUMS and Pyk2$^{-/-}$:CUMS mice. The images are negatives for better visualization. Scale bars, 15 and 3 µm, respectively. **b** Quantification of spine density in dendrites as in **a**. Two-way ANOVA, interaction, $F_{(1,\ 261)} = 17.92$, $p < 0.0001$, Bonferroni's post hoc test (55–60 dendrites from 5 mice per group). **c** Confocal images of the basolateral nucleus of the amygdala sections from Pyk2$^{+/+}$ controls and Pyk2$^{+/+}$ mice after CUMS immunolabelled for PSD-95 (green) and Pyk2 (red). We analyzed 1 image per slice, three slices per mouse, seven mice per group. Scale bar, 4 µm. **d** and **e** Quantification of results as in **c**. **d** Number of Pyk2-positive puncta per field, Student's *t*-test; $t = 0.69$, $p = 0.5$. **e** Number of Pyk2/PSD-95-double-positive puncta per field, Student's *t*-test, $t = 2.52$, $p = 0.026$. **f** PSD-95-positive puncta in the basolateral nucleus in Pyk2$^{+/+}$ and Pyk2$^{-/-}$ control mice and in Pyk2$^{+/+}$:CUMS and Pyk2$^{-/-}$:CUMS mice. Scale bar, 3 µm. **g** Quantification of PSD-95-positive puncta in basolateral nucleus as in **f**. Two-way ANOVA, interaction, $F_{(1,\ 33)} = 9.53$, $p < 0.004$; stress effect $F_{(1,\ 33)} = 27.71$, $p < 0.0001$, Bonferroni's post hoc test (1 image per slice, three slices per mouse, 8–9 mice per group). Data are means + SEM. ***$p < 0.001$ compared to Pyk2$^{+/+}$ unstressed controls, $^{\&\&\&}p < 0.001$ compared to Pyk2$^{+/+}$:CUMS, and $^{\$\$}p < 0.01$ compared to Pyk2$^{-/-}$ controls

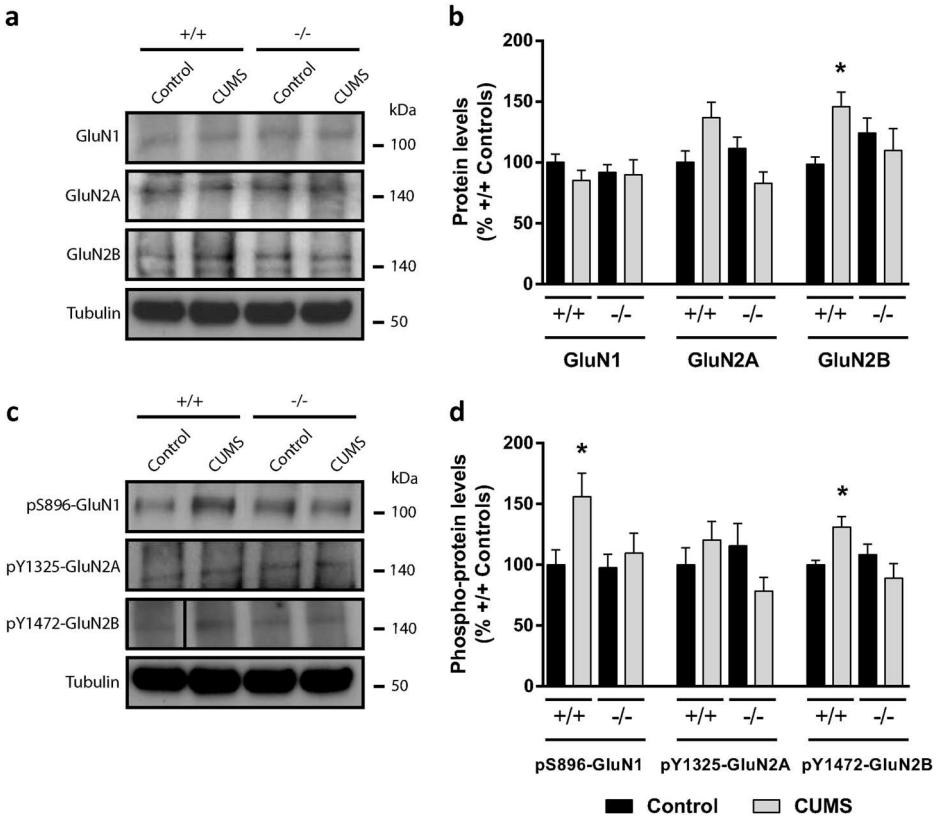

Fig. 5 Pyk2 knockout prevents the changes in NMDA receptors levels and phosphorylation induced by chronic stress in the amygdala. NMDARs were studied by immunoblotting in Pyk2$^{+/+}$ and Pyk2$^{-/-}$ mice unstressed (Control) or 10 days after being subjected to a CUMS paradigm. **a** Immunoblotting analysis of GluN1, GluN2A, GluN2B, and tubulin as a loading control. **b** Densitometric quantification of results as in **a**. Two-way ANOVA interaction, GluN1, $F_{(1,\ 30)} = 0.33$, $p = 0.95$, GluN2A, $F_{(1,\ 30)} = 1.14$, $p = 0.70$, GluN2B, $F_{(1,\ 30)} = 6.04$, $p = 0.02$, Tukey's post hoc test. **c** Immunoblotting analysis of pS896-GluN1, pY1325-GluN2A, pY1472-GluN2B, and tubulin as a loading control. **d** Densitometric quantification of results as in **c**. Two-way ANOVA interaction, pS896-GluN1, $F_{(1,\ 29)} = 5.75$, $p = 0.02$; pY1325-GluN2A, $F_{(1,\ 29)} = 0.42$, $p = 0.51$, pY1472-GluN2B, $F_{(1,\ 29)} = 7.35$, p = 0.01, Tukey's post hoc test. Data are means + SEM. In all experiments $n = 8$–9 mice per group. From **a** to **d**: *$p < 0.05$ compared to Pyk2$^{+/+}$ unstressed controls. In **a** and **c** molecular weight markers position is indicated in kDa

confirming the hypothesis that the increase in PSD-95 clusters due to chronic stress is significantly weaker in Pyk2$^{-/-}$ mice.

N-methyl-D-aspartate receptors (NMDARs) alterations in the amygdala after CUMS are Pyk2-dependent

The increase of Pyk2/PSD-95 colocalization in the BLA after CUMS was coincident with both the clustering of PSD-95 at excitatory synapses and the increase in spine density in the BLA. We therefore hypothesized that the increase in the post-synaptic density scaffold could correspond to changes in the NMDARs in the principal neurons of the BLA. To test this hypothesis, we evaluated by immunoblotting the total and phosphorylated levels of several NMDAR subunits in the amygdala of Pyk2$^{+/+}$:CUMS and Pyk2$^{-/-}$:CUMS mice and we compared the results with those obtained in Pyk2$^{+/+}$ and Pyk2$^{-/-}$ controls. First, total NMDA receptors GluN1 and GluN2A levels were not changed in mice subjected to CUMS as compared to control mice (Fig. 5a, b). In contrast, we observed an increase in GluN2B total protein levels in Pyk2$^{+/+}$:CUMS as compared to Pyk2$^{+/+}$ mice. The increase in GluN2B was negligible when comparing Pyk2$^{-/-}$:CUMS with Pyk2$^{-/-}$ mice. The phosphorylated forms, pS896-GluN1 and pY1472-GluN2B were also increased in Pyk2$^{+/+}$:CUMS compared to Pyk2$^{+/+}$ control mice (Fig. 5c, d). When we calculated the ratio pY1472-GluN2B/GluN2B the increase disappeared (data not shown) indicating that increased pY1472-GluN2B levels were due to a general up-regulation of the GluN2B protein subunit. In Pyk2$^{-/-}$:CUMS mice however, these changes were completely abolished when compared to Pyk2$^{-/-}$ mice. These results indicate that, in wild type mice, CUMS induced a long-lasting change in the properties of excitatory synapses in the BLA, which was apparent as an increase in the Ser896 phosphorylation of GluN1 and in the GluN2B protein levels. In contrast these changes were prevented in the absence of Pyk2, revealing

the key role of this protein in synaptic adaptations in response to chronic stress.

Discussion

Here, we show the role of Pyk2 in the response to a model of chronic stress. We showed that although in basal conditions (i.e. in the absence of stress) the absence of Pyk2 does not modify the responses in anxiety-like and depression-like behavioral tests, PyK2 ablation in the adult confers a marked resistance to the sequelae induced by CUMS, as shown by the normal performances in the plus maze and sucrose preference tests. We also identified the amygdala as a core structure in the modulation of the observed phenotype in Pyk2-deficient mice. Importantly, we provide evidence for a key role of Pyk2 in the regulation of dendritic spine density in the projection neurons of the BLA, with a concomitant PSD-95 stabilization at synapses. Accordingly, the modifications of NMDARs were prevented in the amygdala of Pyk2-deficient mice exposed to the CUMS paradigm. The ensemble of those results strongly indicates a role of Pyk2 in regulating the structural plasticity upon chronic stress.

Interestingly, we observed a dissociation in the Pyk2-dependence of different components of the behavioral alterations induced by CUMS. We observed that in full Pyk2 knockout mice the CUMS protocol failed to induce a reduction of sucrose preference, as well as a decrease on the exploratory behavior in the open arms of the elevated plus maze. In order to identify the regions mainly implicated in the reduced alterations induced by CUMS we focused on the brain areas showing the highest levels of Pyk2 expression, and that are associated to chronic stress and major depression: medial prefrontal cortex, nucleus accumbens, hippocampus, and amygdala[8,13,20,29–31]. We identified the amygdala as the brain region mostly implicated in the absence of alterations (detected by the plus maze and sucrose preference tests) after CUMS in Pyk2-deficient mice. In other words, Pyk2 deletion in amygdala neurons was sufficient to prevent the sequelae induced by the CUMS paradigm.

It is well known that a history of repeated or prolonged stress often leads to hyperactivity of the amygdala[32–34]. Furthermore, human studies show that depression and anxiety are also associated with amygdala hyperactivity[35–38]. In animal models, the BLA has emerged as a target for the effects of repeated stress in a range of anxiety and depressive behaviors. Furthermore, these behavioral abnormalities are associated with hyperactivity of BLA neurons resulting from an increased excitatory input to those neurons[39–43]. The increase in the excitatory synaptic inputs to BLA after repeated stress correlates with an increase in dendritic spines and dendritic length[44–46]. Pyk2, is a tyrosine kinase involved in both the induction and maintenance of synaptic plasticity, in the regulation of dendritic spines density and morphology, and in the formation of memory traces[17,18]. Our results show that Pyk2 plays an important role in the structural plasticity induced by the CUMS paradigm in the neurons of the BLA, including the increase in dendritic spines. Importantly, the amygdala can sense a stressful event and generate an appropriate response to it; however, the dysfunction of this mechanism might lead to the development of a major depression[31]. Thus, our hypothesis is that the inactivation of Pyk2, principally in the amygdala, would lead to the alteration of the processing of the stressful stimuli turning the animal "resistant" to anhedonia-like and anxiety-like phenotypes.

Regarding to the unchanged levels of phosphorylation of Pyk2 in the amygdala after CUMS or acute stressful stimuli, we hypothesize that there could be different interpretations. First, Pyk2 could be transiently activated in few dozens of minutes following stress and return to a basal activity after 1 h. If so, our methods were unsuitable for the detection of such activity. A second interpretation is that the role of Pyk2 that we observed in the stress-activated pathway could rely on the phosphorylation/dephosphorylation of another residue than the Tyr-402. Our group has already shown in hippocampal slices that depolarization induces a calcineurin-dependent nuclear translocation of Pyk2 involving the dephosphorylation of Ser-778[47]. Finally, one can also hypothesize that the function of Pyk2 in response to stress does not need an increased activation of itself compared to basal level. If so, we can imagine the involvement of interactors of Pyk2 which regulate its substrate specificity or limit its accessibility towards a subset of its substrates by anchoring Pyk2 in a specific subcellular localization. As an example, cyclin-dependent kinases (CDKs) perfectly illustrate this type of regulation. Interaction of CDKs with cyclins can help to target their activity toward precise substrates, or to limit their accessibility by shuttling them to a cellular compartment, such as the Golgi apparatus or nucleus[48]. In this line, we hypothesize that there is a necessary role of Pyk2 at synapses without a need for an increased activation. It can also be related to kinase-independent functions of Pyk2, which we previously showed to be sufficient for regulating spine number in hippocampal neurons in culture in response to glutamate stimulation[18,19]. In the hippocampus Pyk2 interacts with PSD-95[15,49]. We did show that Pyk2 stabilizes PSD-95 in the excitatory synapses and regulates synaptic plasticity[18]. PSD-95 anchors essential proteins, including NMDARs, which are implicated in the regulation of excitatory synapses plasticity[50], and in the control of the number and morphology of dendritic spines[51]. We showed an increased Pyk2/PSD-95 colocalization in the amygdala of the chronically stressed mice concomitant with an increase in the number of puncta positive for PSD-95. We also

observed an increase in GluN2B and pSer896-GluN1 induced by CUMS and prevented in the absence of Pyk2. Since Pyk2 is a tyrosine kinase, which cannot be directly responsible for Ser896-GluN1 phosphorylation, these changes rather indicate the role of Pyk2 in the maintenance or function of excitatory synapses during the processes described here. The role of Pyk2 is likely to be, in part, related to its interaction with PSD-95.

Supporting our results, several studies showed that PSD-95 is essential for the maintenance of long-lasting fear memories via remodeling excitatory synapses[52] and that both NMDARs subunits and PSD-95 are increased in the amygdala of postmortem samples from patients with MDD[53]. The increase in GluN1 Ser896 phosphorylation and in the number of GluN2B subunits phosphorylated on Tyr1472 we observed after CUMS suggests an enhanced NMDAR function with increased channel opening probability, calcium influx, and receptor recruitment to the membrane[54]. NMDAR was shown to play an essential role in the aforementioned hyperactivation of the amygdala upon chronic stress and in the subsequent formation of new excitatory synapses[55,56]. Since the synaptic changes in the amygdala were prevented in the absence of Pyk2, this kinase appears to be a core molecule mediating the effects of chronic stress.

Intriguingly, we show that the Pyk2-deficient mice behaved as the non-stressed controls in the sucrose preference test but not in the forced swimming test. It is known that a missing response to a reward stimulus is the behavioral correlate of the anhedonia, a core clinical symptom of the depression. When looking at our results we should consider that, although the amygdala is widely accepted as important for the recognition of negative emotions such as fear[57,58], several works in animal models, as well as in humans point out the involvement of this region in processing of positive emotions[59,60]. There is evidence that the amygdala has a role in the processing stimulus—reward learning by interacting with the cortico-limbic and meso-limbic systems. This is particularly true for the lateral amygdala that seems to be especially important for the association of a value to the reward. For example, in animals lesioned in basolateral but not central amygdala[61] we can prevent the normal loss of the response to a stimulus predicting a food reward when paired to a malaise-induced injections of lithium chloride[62]. We could hypothesize that one possible explanation of our results could be a preferential effect of the deletion of PTK2B in the amygdala in tests tracking the effect of chronic stress of more reward-related symptoms rather than measuring the behavioral despair, that in the other hand could be more related to other regions of the brain. Partially supporting this idea one study showed that in rodents, the level of 5-HT release following a forced swim test is reduced in hippocampus, nucleus accumbens, and cortex but not in the amygdala[63]. However, the most obvious explanation for this lack of changes in the forced swimming test is that Pyk2 might not be important for its principal and underlying molecular/physiological processes. Another divergence in our work comes from the CUMS-Amy group when comparing the locomotor activity parameter in the elevated plus maze and in the open field test. The CUMS-Amy group showed hyper locomotion only in the latter. This discrepancy with the elevated plus maze is likely due to the fact that the open field is more useful for locomotor measurements than it is to anxiety-like behaviors and elevated plus maze is more useful for anxiety-like measurements than it is to locomotor behavior[26,27]. Thereby, intrinsic differences of the apparatus make the open field test more sensitive to changes in locomotor activity than elevated plus maze. Accordingly, other discrepancies between the open field and the elevated plus maze have been previously reported[64–67]. Finally, we found that mice with deletion in the medial prefrontal cortex and hippocampus showed decreased preference for sweet water in the first trials of the sucrose preference test, but they finally became unaffected in the trial number 3. One possible reason is that the two regions seem to contribute together to the short-term memory[68]. Indeed, we already showed in a previous paper that Pyk2 is involved in the regulation of memories mediated by the hippocampus[18]. Therefore, we hypothesize that deletion of Pyk2 in the hippocampus or the medial prefrontal cortex could induce mnemonic alterations that would lead to a faster habituation/acceptation of the sweet solution.

In conclusion, recent large-scale human genetic studies have identified *PTK2B* as a gene associated with neuroticism[22] which in turn is a risk factor to develop MDD[23]. Here we propose for the first time a potential mechanism that could explain the human association of *PTK2B* to the risk to develop depression after chronic stress. Our results reveal a new role of Pyk2 in neuronal dysfunction. We show that it is necessary for several components of the depressive-like phenotype, which appears to require Pyk2-dependent spine alterations in the amygdala. Thus, Pyk2 could be included in the list of molecules known as negative modulators of resilience-like phenotypes against chronic stress and depression, such as BDNF and ΔFOSB[30]. Our findings indicate that targeting Pyk2 in patients suffering from multiple and chronic stressful psychological insults could help to prevent the associated depressive symptoms. Since the activation state of Pyk2 in the amygdala is not clearly altered in response to stress, it could be particularly attractive to modulate the structural role of Pyk2 without affecting its activity. Such structural mechanism was already evoked in our previous paper[18] and is reminiscent of that reported for the closely related focal adhesion kinase (FAK) in non-neuronal cells[69,70].

This alternative signaling may be linked to scaffolding properties of Pyk2 and/or its interaction with specific partners. For instance, in our last paper, we showed that although dendritic spines density was altered in Pyk2-deficient neurons, it could be rescued by transfecting either a mutant form of Pyk2 with a point mutation of the autophosphorylation site or a kinase-dead Pyk2 with a K457A mutation. However, transfection of a mutant form of Pyk2 unable to bind to PSD-95 ($Pyk2_{1-840}$) could not rescue the phenotype showing the importance of this interaction in this particular pathway, which does not involve the autophosphorylation of Pyk2. To sum up, Pyk2 may function as a scaffold which gather some proteins, independently of its kinase activity.

Acknowledgements
A.G. is a Ramón y Cajal fellow (RYC-2016-19466). This work was supported by the NARSAD foundation (young investigator grant 2016 (Ref. 24803) to A.G.) and Ministerio de Ciencia e Innovación (SAF2015-67474-R; MINECO/FEDER to S.G.). J.-A.G. lab was supported in part by Inserm, the *Université Pierre et Marie Curie* (UPMC, Sorbonne Université), the *Fondation pour la Recherche Médicale*, and the Bio-Psy (Biology for Psychiatry) laboratory of excellence. O.A.-M. was funded by the ISCIII/SERGAS thought a research contract "Sara Borrell" (CD14/00091). JA lab was supported by the Spanish Ministry of Economy and Competitiveness (MINECO) (SAF-2014-57160R, SAF-2017-88076-R), Fundació Marató TV3 to J.A. and Instituto Carlos III: Centro de Investigación Biomédica en Red sobre enfermedades neurodegenerativas (CIBERNED), and RETICS RD12/0019/0002 to J.A.).

Author details
[1]Inserm UMR-S 839, 75005 Paris, France. [2]Sorbonne Université, Faculté des Sciences et d'Ingénierie, 75005 Paris, France. [3]Institut du Fer a Moulin, 75005 Paris, France. [4]Department of Physiology, CIMUS, University of Santiago de Compostela-Instituto de Investigación Sanitaria, 15782 Santiago de Compostela, Spain. [5]CIBER Fisiopatología de la Obesidad y Nutrición (CIBERobn), 15706 Santiago de Compostela, Spain. [6]Departament de Biomedicina, Facultat de Medicina, Institut de Neurociencies, Universitat de Barcelona, 08036 Barcelona, Spain. [7]Institut d'Investigacions Biomèdiques August Pi i Sunyer (IDIBAPS), 08036 Barcelona, Spain. [8]Centro de Investigacion Biomedica en Red Sobre Enfermedades Neurodegenerativas (CIBERNED), 28031 Madrid, Spain

Conflict of interest
The authors declare that they have no conflict of interest.

Supplementary Information accompanies this paper at (https://doi.org/10.1038/s41398-018-0352-y).

Received: 26 April 2018 Revised: 27 November 2018 Accepted: 10 December 2018
Published online: 15 January 2019

References

1. Otte, C. et al. Major depressive disorder. *Nat. Rev. Dis. Prim.* **2**, 16065 (2016).
2. Bromet, E. et al. Cross-national epidemiology of DSM-IV major depressive episode. *BMC Med.* **9**, 90 (2011).
3. Paykel, E. S. Stress and affective disorders in humans. *Semin. Clin. Neuropsychiatry* **6**, 4–11 (2001).
4. Griffiths, J., Ravindran, A. V., Merali, Z. & Anisman, H. Dysthymia: a review of pharmacological and behavioral factors. *Mol. Psychiatry* **5**, 242–261 (2000).
5. Anisman, H. & Merali, Z. Understanding stress: characteristics and caveats. *Alcohol. Res. Health* **23**, 241–249 (1999).
6. Kendler, K. S., Thornton, L. M. & Gardner, C. O. Stressful life events and previous episodes in the etiology of major depression in women: an evaluation of the "kindling" hypothesis. *Am. J. Psychiatry* **157**, 1243–1251 (2000).
7. Roy, A. Early parental separation and adult depression. *Arch. Gen. Psychiatry* **42**, 987–991 (1985).
8. Qiao, H. et al. Dendritic spines in depression: what we learned from animal models. *Neural Plast.* **2016**, 8056370 (2016).
9. Christoffel, D. J., Golden, S. A. & Russo, S. J. Structural and synaptic plasticity in stress-related disorders. *Rev. Neurosci.* **22**, 535–549 (2011).
10. Padival, M. A., Blume, S. R. & Rosenkranz, J. A. Repeated restraint stress exerts different impact on structure of neurons in the lateral and basal nuclei of the amygdala. *Neuroscience* **246**, 230–242 (2013).
11. Qiao, H., An, S. C., Ren, W. & Ma, X. M. Progressive alterations of hippocampal CA3-CA1 synapses in an animal model of depression. *Behav. Brain. Res.* **275**, 191–200 (2014).
12. Radley, J. J. et al. Reversibility of apical dendritic retraction in the rat medial prefrontal cortex following repeated stress. *Exp. Neurol.* **196**, 199–203 (2005).
13. Giralt, A., Coura, R. & Girault, J. A. Pyk2 is essential for astrocytes mobility following brain lesion. *Glia* **64**, 620–634 (2016).
14. Girault, J. A., Costa, A., Derkinderen, P., Studler, J. M. & Toutant, M. FAK and PYK2/CAKbeta in the nervous system: a link between neuronal activity, plasticity and survival? *Trends Neurosci.* **22**, 257–263 (1999).
15. Bartos, J. A. et al. Postsynaptic clustering and activation of Pyk2 by PSD-95. *J. Neurosci.* **30**, 449–463 (2010).
16. Hsin, H., Kim, M. J., Wang, C. F. & Sheng, M. Proline-rich tyrosine kinase 2 regulates hippocampal long-term depression. *J. Neurosci.* **30**, 11983–11993 (2010).
17. Huang, Y. et al. CAKbeta/Pyk2 kinase is a signaling link for induction of long-term potentiation in CA1 hippocampus. *Neuron* **29**, 485–496 (2001).
18. Giralt, A. et al. Pyk2 modulates hippocampal excitatory synapses and contributes to cognitive deficits in a Huntington's disease model. *Nat. Commun.* **8**, 15592 (2017).
19. Kinoshita, Y. et al. Role for NUP62 depletion and PYK2 redistribution in dendritic retraction resulting from chronic stress. *Proc. Natl Acad. Sci. USA* **111**, 16130–16135 (2014).
20. Sheehan, T. P., Neve, R. L., Duman, R. S. & Russell, D. S. Antidepressant effect of the calcium-activated tyrosine kinase Pyk2 in the lateral septum. *Biol. Psychiatry* **54**, 540–551 (2003).
21. Porsolt, R. D., Bertin, A. & Jalfre, M. "Behavioural despair" in rats and mice: strain differences and the effects of imipramine. *Eur. J. Pharmacol.* **51**, 291–294 (1978).
22. Okbay, A. et al. Genetic variants associated with subjective well-being, depressive symptoms, and neuroticism identified through genome-wide analyses. *Nat. Genet.* **48**, 624–633 (2016).
23. Kendler, K. S., Gatz, M., Gardner, C. O. & Pedersen, N. L. Personality and major depression: a Swedish longitudinal, population-based twin study. *Arch. Gen. Psychiatry* **63**, 1113–1120 (2006).
24. Nollet, M., Le Guisquet, A. M. & Belzung, C. Models of depression: unpredictable chronic mild stress in mice. *Curr. Protoc. Pharmacol.* 2013; Chapter 5: Unit. 5.65. https://doi.org/10.1002/0471141755.ph0565s61.
25. Strekalova, T., Spanagel, R., Bartsch, D., Henn, F. A. & Gass, P. Stress-induced anhedonia in mice is associated with deficits in forced swimming and exploration. *Neuropsychopharmacology* **29**, 2007–2017 (2004).
26. Crawley, J. N. et al. Behavioral phenotypes of inbred mouse strains: implications and recommendations for molecular studies. *Psychopharmacology* **132**, 107–124 (1997).
27. Crawley, J. N. Behavioral phenotyping of transgenic and knockout mice: experimental design and evaluation of general health, sensory functions, motor abilities, and specific behavioral tests. *Brain Res.* **835**, 18–26 (1999).
28. Li, X., Dy, R. C., Cance, W. G., Graves, L. M. & Earp, H. S. Interactions between two cytoskeleton-associated tyrosine kinases: calcium-dependent tyrosine kinase and focal adhesion tyrosine kinase. *J. Biol. Chem.* **274**, 8917–8924 (1999).
29. Bewernick, B. H., Kayser, S., Sturm, V. & Schlaepfer, T. E. Long-term effects of nucleus accumbens deep brain stimulation in treatment-resistant depression: evidence for sustained efficacy. *Neuropsychopharmacology* **37**, 1975–1985 (2012).

30. Krishnan, V. & Nestler, E. J. The molecular neurobiology of depression. *Nature* **455**, 894–902 (2008).
31. McEwen, B. S. Mood disorders and allostatic load. *Biol. Psychiatry* **54**, 200–207 (2003).
32. Bogdan, R., Williamson, D. E. & Hariri, A. R. Mineralocorticoid receptor Iso/Val (rs5522) genotype moderates the association between previous childhood emotional neglect and amygdala reactivity. *Am. J. Psychiatry* **169**, 515–522 (2012).
33. Dannlowski, U. et al. Limbic scars: long-term consequences of childhood maltreatment revealed by functional and structural magnetic resonance imaging. *Biol. Psychiatry* **71**, 286–293 (2012).
34. Protopopescu, X. et al. Differential time courses and specificity of amygdala activity in posttraumatic stress disorder subjects and normal control subjects. *Biol. Psychiatry* **57**, 464–473 (2005).
35. Davidson, R. J., Irwin, W., Anderle, M. J. & Kalin, N. H. The neural substrates of affective processing in depressed patients treated with venlafaxine. *Am. J. Psychiatry* **160**, 64–75 (2003).
36. Sheline, Y. I. et al. Increased amygdala response to masked emotional faces in depressed subjects resolves with antidepressant treatment: an fMRI study. *Biol. Psychiatry* **50**, 651–658 (2001).
37. Siegle, G. J., Steinhauer, S. R., Thase, M. E., Stenger, V. A. & Carter, C. S. Can't shake that feeling: event-related fMRI assessment of sustained amygdala activity in response to emotional information in depressed individuals. *Biol. Psychiatry* **51**, 693–707 (2002).
38. Thomas, K. M. et al. Amygdala response to fearful faces in anxious and depressed children. *Arch. Gen. Psychiatry* **58**, 1057–1063 (2001).
39. Adamec, R., Blundell, J. & Burton, P. Role of NMDA receptors in the lateralized potentiation of amygdala afferent and efferent neural transmission produced by predator stress. *Physiol. Behav.* **86**, 75–91 (2005).
40. Correll, C. M., Rosenkranz, J. A. & Grace, A. A. Chronic cold stress alters prefrontal cortical modulation of amygdala neuronal activity in rats. *Biol. Psychiatry* **58**, 382–391 (2005).
41. Hubert, G. W., Li, C., Rainnie, D. G. & Muly, E. C. Effects of stress on AMPA receptor distribution and function in the basolateral amygdala. *Brain. Struct. Funct.* **219**, 1169–1179 (2014).
42. Mozhui, K. et al. Strain differences in stress responsivity are associated with divergent amygdala gene expression and glutamate-mediated neuronal excitability. *J. Neurosci.* **30**, 5357–5367 (2010).
43. Rosenkranz, J. A., Venheim, E. R. & Padival, M. Chronic stress causes amygdala hyperexcitability in rodents. *Biol. Psychiatry* **67**, 1128–1136 (2010).
44. Adamec, R., Hebert, M., Blundell, J. & Mervis, R. F. Dendritic morphology of amygdala and hippocampal neurons in more and less predator stress responsive rats and more and less spontaneously anxious handled controls. *Behav. Brain. Res.* **226**, 133–146 (2012).
45. Hill, M. N. et al. Disruption of fatty acid amide hydrolase activity prevents the effects of chronic stress on anxiety and amygdalar microstructure. *Mol. Psychiatry* **18**, 1125–1135 (2013).
46. Mitra, R., Jadhav, S., McEwen, B. S., Vyas, A. & Chattarji, S. Stress duration modulates the spatiotemporal patterns of spine formation in the basolateral amygdala. *Proc. Natl Acad. Sci. USA* **102**, 9371–9376 (2005).
47. Faure, C. et al. Calcineurin is essential for depolarization-induced nuclear translocation and tyrosine phosphorylation of PYK2 in neurons. *J. Cell. Sci.* **120**, 3034–3044 (2007).
48. Ubersax, J. A. & Ferrell, J. E. Jr. Mechanisms of specificity in protein phosphorylation. *Nat. Rev. Mol. Cell Biol.* **8**, 530–541 (2007).
49. Seabold, G. K., Burette, A., Lim, I. A., Weinberg, R. J. & Hell, J. W. Interaction of the tyrosine kinase Pyk2 with the N-methyl-D-aspartate receptor complex via the Src homology 3 domains of PSD-95 and SAP102. *J. Biol. Chem.* **278**, 15040–15048 (2003).
50. Chen, X. et al. PSD-95 family MAGUKs are essential for anchoring AMPA and NMDA receptor complexes at the postsynaptic density. *Proc. Natl Acad. Sci. USA* **112**, E6983–E6992 (2015).
51. Prange, O., Wong, T. P., Gerrow, K., Wang, Y. T. & El-Husseini, A. A balance between excitatory and inhibitory synapses is controlled by PSD-95 and neuroligin. *Proc. Natl Acad. Sci. USA* **101**, 13915–13920 (2004).
52. Fitzgerald, P. J. et al. Durable fear memories require PSD-95. *Mol. Psychiatry* **20**, 913 (2015).
53. Karolewicz, B. et al. Elevated levels of NR2A and PSD-95 in the lateral amygdala in depression. *Int. J. Neuropsychopharmacol.* **12**, 143–153 (2009).
54. Chen, B. S. & Roche, K. W. Regulation of NMDA receptors by phosphorylation. *Neuropharmacology* **53**, 362–368 (2007).
55. Rainnie, D. G. et al. Corticotrophin releasing factor-induced synaptic plasticity in the amygdala translates stress into emotional disorders. *J. Neurosci.* **24**, 3471–3479 (2004).
56. Yasmin, F., Saxena, K., McEwen, B. S. & Chattarji, S. The delayed strengthening of synaptic connectivity in the amygdala depends on NMDA receptor activation during acute stress. *Physiol. Rep.* **4**, pii: e13002 (2016).
57. Calder, A. J., Lawrence, A. D. & Young, A. W. Neuropsychology of fear and loathing. *Nat. Rev. Neurosci.* **2**, 352–363 (2001).
58. Medina, J. F., Repa, J. C., Mauk, M. D. & LeDoux, J. E. Parallels between cerebellum- and amygdala-dependent conditioning. *Nat. Rev. Neurosci.* **3**, 122–131 (2002).
59. Davis, M. & Whalen, P. J. The amygdala: vigilance and emotion. *Mol. Psychiatry* **6**, 13–34 (2001).
60. Johnsrude, I. S., Owen, A. M., White, N. M., Zhao, W. V. & Bohbot, V. Impaired preference conditioning after anterior temporal lobe resection in humans. *J. Neurosci.* **20**, 2649–2656 (2000).
61. Hatfield, T., Han, J. S., Conley, M., Gallagher, M. & Holland, P. Neurotoxic lesions of basolateral, but not central, amygdala interfere with Pavlovian second-order conditioning and reinforcer devaluation effects. *J. Neurosci.* **16**, 5256–5265 (1996).
62. Holland, P. C. Event representation in Pavlovian conditioning: image and action. *Cognition* **37**, 105–131 (1990).
63. Kirby, L. G., Allen, A. R. & Lucki, I. Regional differences in the effects of forced swimming on extracellular levels of 5-hydroxytryptamine and 5-hydroxyindoleacetic acid. *Brain Res.* **682**, 189–196 (1995).
64. Anchan, D., Clark, S., Pollard, K. & Vasudevan, N. GPR30 activation decreases anxiety in the open field test but not in the elevated plus maze test in female mice. *Brain Behav.* **4**, 51–59 (2014).
65. Ramos, A., Mellerin, Y., Mormede, P. & Chaouloff, F. A genetic and multifactorial analysis of anxiety-related behaviours in Lewis and SHR intercrosses. *Behav. Brain Res.* **96**, 195–205 (1998).
66. Sudakov, S. K., Nazarova, G. A., Alekseeva, E. V. & Bashkatova, V. G. Estimation of the level of anxiety in rats: differences in results of open-field test, elevated plus-maze test, and Vogel's conflict test. *Bull. Exp. Biol. Med.* **155**, 295–297 (2013).
67. Trullas, R. & Skolnick, P. Differences in fear motivated behaviors among inbred mouse strains. *Psychopharmacology* **111**, 323–331 (1993).
68. Lee, I. & Kesner, R. P. Time-dependent relationship between the dorsal hippocampus and the prefrontal cortex in spatial memory. *J. Neurosci.* **23**, 1517–1523 (2003).
69. Corsi, J. M. et al. Autophosphorylation-independent and -dependent functions of focal adhesion kinase during development. *J. Biol. Chem.* **284**, 34769–34776 (2009).
70. Zhao, X., Peng, X., Sun, S., Park, A. Y. & Guan, J. L. Role of kinase-independent and -dependent functions of FAK in endothelial cell survival and barrier function during embryonic development. *J. Cell. Biol.* **189**, 955–965 (2010).

4. Summary of the findings and conclusions

In this paper, we showed that Pyk2 deficient mice were less affected to anxiety-like and anhedonia-like phenotypes induced by the CUMS paradigm. This phenotype was fully recapitulated by selective deletion of Pyk2 in the amygdala, a brain structure associated with the processing of emotional responses including fear, anxiety, and aggression.

Deletion of Pyk2 in the amygdala prevented the synaptic markers and spine structure alterations induced by the CUMS paradigm.

These results thus suggest a possible involvement of Pyk2 in the molecular responses, through PSD-95 clustering and NMDA receptors changes, to chronic stress in the amygdala.

III. **PTK2B/Pyk2 overexpression improves a mouse model of Alzheimer's disease**

Albert Giralt, Benoit de Pins, Carmen Cifuentes-Díaz, Laura López-Molina, Amel Thamila Farah, Marion Tible, Vincent Deramecourt, Stefan T Arold, Silvia Ginés, Jacques Hugon and Jean-Antoine Girault

Experimental Neurology
September 2018, 307:62-73

1. Context and objectives

Starting from the previous study showing the importance of Pyk2 in hippocampal function, and from the observation that *PTK2B* is a locus strongly associated with AD, we intended here to explore the potential role of Pyk2 in AD.

AD is a progressive neurodegenerative disorder characterized by the deposit of plaques composed of Aβ peptide and by the intracellular accumulation of tau proteins forming neurofibrillary tangles. This process is associated with neuronal loss and cerebral atrophy notably.

In this paper, we investigated the role of Pyk2 in the 5xFAD mouse model. This model is an amyloid model of AD as it is characterized by a strong Aβ production, due to expression of mutated forms of human APP and presenilin-1. We therefore crossed these AD model mice with Pyk2 knockout mice or injected their hippocampus with a Pyk2-expressing AAV to observe the effect of Pyk2 deletion/overexpression in the development of molecular and behavioral alterations.

2. Contribution to the work

In this work, I personally contributed to the management of mice lines, to the biochemistry experiments and to tissue imaging.

3. Article

Experimental Neurology 307 (2018) 62–73

Contents lists available at ScienceDirect

Experimental Neurology

journal homepage: www.elsevier.com/locate/yexnr

Research Paper

PTK2B/Pyk2 overexpression improves a mouse model of Alzheimer's disease

Albert Giralt[a,b,c,d,e,f], Benoit de Pins[a,b,c], Carmen Cifuentes-Díaz[a,b,c], Laura López-Molina[d,e,f], Amel Thamila Farah[a,b,c,1], Marion Tible[g,h], Vincent Deramecourt[i], Stefan T Arold[j], Silvia Ginés[d,e,f], Jacques Hugon[g,h], Jean-Antoine Girault[a,b,c,*]

[a] Inserm UMR-S 839, Paris, France
[b] Sorbonne Université, Science and Engineering Faculty, Paris, France
[c] Institut du Fer a Moulin, Paris, France
[d] Departament de Biomedicina, Facultat de Medicina, Institut de Neurociències, Universitat de Barcelona, 08036 Barcelona, Spain
[e] Institut d'Investigacions Biomèdiques August Pi i Sunyer (IDIBAPS), 08036 Barcelona, Spain
[f] Centro de Investigacion Biomedica en Red Sobre Enfermedades Neurodegenerativas (CIBERNED), 28031 Madrid, Spain
[g] Inserm UMR-S 942, Paris, France
[h] Research Memory Center, Paris-Nord Ile-de-France, Saint-Louis-Lariboisière-Fernand Widal Hospital, Paris, France
[i] Univ Lille, CHU Lille, INSERM U1172 "Alzheimer et Tauopathies", LabEx DISTALZ, 59000 Lille, France
[j] King Abdullah University of Science and Technology (KAUST), Center for Computational Bioscience Research (CBRC), Division of Biological and Environmental Sciences and Engineering (BESE), Thuwal 23955-6900, Saudi Arabia

ARTICLE INFO

Keywords:
Alzheimer's disease
Mouse model
Non-receptor tyrosine protein kinase
Pyk2
Src

ABSTRACT

Pyk2 is a Ca^{2+}-activated non-receptor tyrosine kinase enriched in forebrain neurons and involved in synaptic regulation. Human genetic studies associated *PTK2B*, the gene coding Pyk2, with risk for Alzheimer's disease (AD). We previously showed that Pyk2 is important for hippocampal function, plasticity, and spine structure. However, its potential role in AD is unknown. To address this question we used human brain samples and 5XFAD mice, an amyloid mouse model of AD expressing mutated human amyloid precursor protein and presenilin1. In the hippocampus of 5XFAD mice and in human AD patients' cortex and hippocampus, Pyk2 total levels were normal. However, Pyk2 Tyr-402 phosphorylation levels, reflecting its autophosphorylation-dependent activity, were reduced in 5XFAD mice at 8 months of age but not 3 months. We crossed these mice with $Pyk2^{-/-}$ mice to generate 5XFAD animals devoid of Pyk2. At 8 months the phenotype of 5XFAD x $Pyk2^{-/-}$ double mutant mice was not different from that of 5XFAD. In contrast, overexpression of Pyk2 in the hippocampus of 5XFAD mice, using adeno-associated virus, rescued autophosphorylated Pyk2 levels and improved synaptic markers and performance in several behavioral tasks. Both $Pyk2^{-/-}$ and 5XFAD mice showed an increase of potentially neurotoxic Src cleavage product, which was rescued by Pyk2 overexpression. Manipulating Pyk2 levels had only minor effects on Aβ plaques, which were slightly decreased in hippocampus CA3 region of double mutant mice and increased following overexpression. Our results show that Pyk2 is not essential for the pathogenic effects of human amyloidogenic mutations in the 5XFAD mouse model. However, the slight decrease in plaque number observed in these mice in the absence of Pyk2 and their increase following Pyk2 overexpression suggest a contribution of this kinase in plaque formation. Importantly, a decreased function of Pyk2 was observed in 5XFAD mice, indicated by its decreased autophosphorylation and associated Src alterations. Overcoming this deficit by Pyk2 overexpression improved the behavioral and molecular phenotype of 5XFAD mice. Thus, our results in a mouse model of AD suggest that Pyk2 impairment may play a role in the symptoms of the disease.

Abbreviations: 5XFAD, mice transgenic for human APP and presenilin1 with 5 mutations found in familial Alzheimer's disease; AAV, adeno-associated virus; Aβ, amyloid β; AD, Alzheimer's disease; ANOVA, analysis of variance; APP, amyloid precursor protein; CA1/3, *cornu Ammoni* 1/3; DAPI 4′, 6-diamidine-2′-phenylindole; DG, dentate gyrus; FAK, focal adhesion kinase; GFAP, glial fibrillary acidic protein; GFP, green fluorescent protein; IB, immunoblotting; IF, immunofluorescence; Inserm, Institut national de la santé et de la recherche médicale; LTM, long term memory; LTP, long term potentiation; mGluR5, metabotropic glutamate receptor 5; NIH, National Institute of Health; NMDA, *N*-methyl-D-aspartate; PLA, proximity ligation assay; PrPc, cellular prion protein; PSD-95, post-synaptic density protein, 95 kDa; PTK2B, protein tyrosine kinase 2B; Pyk2, proline-rich tyrosine kinase 2; SDS, sodium dodecyl sulfate; SEM, standard error of the mean; SFK, Src-family kinase; STEP, striatal enriched phosphatase; STM, short term memory; WT, wild type

* Corresponding author at: Institut du Fer a Moulin, Inserm and Sorbonne Université UMR-S839, France.
E-mail addresses: albertgiralt@ub.edu (A. Giralt), benoit.de-pins@inserm.fr (B. de Pins), carmen.diaz@inserm.fr (C. Cifuentes-Díaz), laura.lopezmo12@ub.edu (L. López-Molina), vincent.deramecourt@chru-lille.fr (V. Deramecourt), stefan.arold@kaust.edu.sa (S.T. Arold), silviagines@ub.edu (S. Ginés), jacques.hugon@inserm.fr (J. Hugon), jean-antoine.girault@inserm.fr (J.-A. Girault).
[1] Current address, Centre de Neurosciences et Psychiatrie, UMR-S894, Inserm and Université Paris Descartes, Paris, France.

https://doi.org/10.1016/j.expneurol.2018.05.020
Received 23 January 2018; Received in revised form 14 May 2018; Accepted 23 May 2018
Available online 24 May 2018

1. Introduction

Late onset Alzheimer's disease (AD) is the most common form of dementia in the aging population accounting for 60–80% of all cases (Alzheimer's Association Report, 2012). AD is a progressive neurodegenerative disorder characterized by plaques composed of β-amyloid protein (Aβ) surrounded by dystrophic neurites and neurofibrillary tangles (Alzheimer's Association Report, 2012). These histopathological hallmarks are accompanied by synaptic and neuronal loss, cerebral atrophy, cerebral amyloid angiopathy (Vinters, 2015), and inflammatory processes (Heneka et al., 2015). The progression of neurodegeneration in AD patients results in memory impairment and decline in other cognitive abilities often combined with non-cognitive symptoms including mood and personality changes (Alzheimer's Association Report, 2012).

A meta-analysis of genome-wide association studies identified 11 new loci associated with AD, among which *PTK2B* was one of the most significant (Lambert et al., 2013). This finding was replicated in other studies (Jiao et al., 2015), which suggested that *PTK2B* was associated with hippocampal sclerosis (Beecham et al., 2014), disease progression (Wang et al., 2015), and cognitive decline (Nettiksimmons et al., 2016). *PTK2B* encodes Pyk2, a Ca^{2+}-activated non-receptor tyrosine kinase closely related to focal adhesion kinase (FAK) (Lev et al., 1995; Sasaki et al., 1995; Avraham et al., 1995). The sensitivity of Pyk2 to increases in intracellular free Ca^{2+} distinguishes it from other tyrosine kinases. In response to Ca^{2+} Pyk2 is autophosphorylated on Tyr-402, which recruits and activates Src-family kinases (SFKs), (Dikic et al., 1996; Walkiewicz et al., 2015). In turn, SFKs phosphorylate other residues in Pyk2 and associated proteins, and initiate multiple signaling pathways. The striatal-enriched protein tyrosine phosphatase (STEP), which is enriched in forebrain regions, dephosphorylates Pyk2 (Xu et al., 2012). Pyk2 plays a role in several cancers and specific inhibitors are under development (Lipinski & Loftus, 2010). Although many cell types express Pyk2, it is highly enriched in forebrain neurons (Menegon et al., 1999) where it is activated by neuronal activity and excitatory neurotransmission (Corvol et al., 2005; Huang et al., 2001; Siciliano et al., 1996). Pyk2 regulates NMDA receptor function and is involved in synaptic plasticity (Huang et al., 2001; Bartos et al., 2010; Hsin et al., 2010). Our recent work with Pyk2 knockout mice shows that Pyk2 in the hippocampus is essential for spatial memory and long-term potentiation (Giralt et al., 2017). It also modulates the density and morphology of spines and the organization of post-synaptic regions (Giralt et al., 2017). Interestingly, heterozygous Pyk2 knockout mice have memory and hippocampal long term potentiation (LTP) deficits similar to homozygous mice and decreased Pyk2 levels contribute to the hippocampal phenotype of a Huntington's disease mouse model (Giralt et al., 2017). Thus, partial loss of Pyk2 function in the hippocampus has clear functional consequences.

The production of Aβ, a particular proteolytic fragment of amyloid precursor protein (APP), is a hallmark of AD (Benilova et al., 2012). It can form plaques and neurotoxic oligomers of various conformation and complexity (Mucke & Selkoe, 2012). Aβ oligomers can bind to cellular prion protein (PrPc) (Lauren et al., 2009) and signaling by PrPc and metabotropic glutamate receptor 5 (mGluR5), which includes Pyk2 activation, is disrupted by Aβ oligomers (Haas & Strittmatter, 2016). Another key molecular abnormality in AD is aberrant phosphorylation of Tau (Mandelkow & Mandelkow, 2012). In *Drosophila* the single orthologue of Pyk2 and FAK interacts with Tau and appears to suppress its toxicity (Dourlen et al., 2016). Moreover, in human AD brain hyperphosphorylated Tau and Pyk2 are colocalized (Dourlen et al., 2016). Finally, inhibitors of STEP enhance Pyk2 phosphorylation in vivo and improve some cognitive deficits in 3xTg-AD mouse model of AD (Xu et al., 2014). Thus, the *PTK2B* locus is reliably associated with AD risk and experimental evidence suggests that Pyk2 has the potential to play a role in the course of the disease, which remains to be characterized.

Here we investigated the role of Pyk2 in the 5XFAD mouse model in which Aβ production is strongly increased, due to expression of mutated forms of human APP and presenilin-1 (Oakley et al., 2006). These mice display age-dependent plaque development with features of AD including hippocampal-related cognitive deficits, neuroinflammation, neuronal loss, and synaptic degeneration (Oakley et al., 2006). We tested the potential role of Pyk2 in this model by genetic deletion and adeno-associated virus (AAV) mediated overexpression. Although Pyk2 levels were not changed in samples from AD or 5XFAD mice, Pyk2 autophosphorylation was reduced in 5XFAD mice indicating a decreased function. Deletion of the Pyk2 gene did not markedly alter the phenotype of 5XFAD mice, whereas overexpression of Pyk2 in the hippocampus rescued some behavioral alterations with correction of deficit in synaptic proteins and Src.

2. Materials and methods

2.1. Mouse lines

5XFAD mice expressing human amyloid precursor protein 695 (APP695) with Swedish, London, and Florida mutations, and M146L/L286V presenilin-1, under the control of the murine Thy-1 promoter (Oakley et al., 2006), were crossed with $Pyk2^{-/-}$ mice (Giralt et al., 2016). Genotyping (Oakley et al., 2006; Giralt et al., 2016) was carried out from tail biopsy (Charles River services, France). Mice were housed at 19–22 °C and 40–60% humidity with ad libitum access to food and water, under a 12:12 h light/dark cycle and used at 8 months, in accordance with ethical guidelines (Declaration of Helsinki and National Institute of Health, publication no. 85-23, revised 1985, European Community Guidelines, and French Agriculture and Forestry Ministry guidelines for handling animals, decree 87,849, license A 75-05-22), approved by the *Charles Darwin* ethical committee. Male and female mice were used.

2.2. Human samples

Prefrontal tissue was from patients with AD Braak grades V-VI (3 females, 2 males, age, 87.6 ± 2.8 years; post-mortem intervals, 8.0 ± 2.4 h, means ± SEM) and control cases (4 females, 1 male, age, 87.2 ± 3.3 years; post-mortem intervals, 7.2 ± 0.9 h) were obtained from the Center of Cognitive Neurology, Lariboisière Hospital (Paris France) with approval by the Ethical Committee of Paris Diderot University Hospitals (CEERB Bichat University Hospital, Paris, France). Hippocampal samples were obtained from two different sources: i) The Lille Neurobank (fulfilling criteria of the French law on biological resources and declared to competent authority under the number DC-2008-642) with donor consent, data protection and ethical committee review, samples managed by the CRB/CIC1403 Biobank, BB-0033-00030, patients with AD Braak stage VI (3 females, 2 males, age, 75.4 ± 3.8 years, post-mortem interval 17.4 ± 3.8 h, means ± SEM) and controls (2 females, 3 males, age, 50.8 ± 9.7 years, post-mortem interval 16.6 ± 4.0 h); ii) the Banc de Teixits Neurològics (Biobanc-HC-IDIBAPS) with the approval of the ethical committee of the University of Barcelona with the reference: IRB00003099, patients with AD Braak grades V-VI (11 females, 4 males, age, 84.7 ± 1.8 years; post-mortem intervals, 9 ± 3.4 h, means ± SEM) and control cases (6 females, 4 males, age, 84.2 ± 3.4 years; post-mortem intervals, 12 ± 1 h). The 2 sets of samples were analyzed separately, results expressed as a % of the control mean in the series and data being similar they were pooled for final comparison (1 aberrant point was discarded). All the patients had an history of progressive dementia and satisfied National Institute of Neurological and Communicative Disorders and Stroke–Alzheimer's Disease and Related Disorders (NINCDS-ADRDA) criteria for probable AD (McKhann et al., 1984) and satisfied neuropathological criteria for AD (Paquet et al., 2012). This research project was.

2.3. Tissue preparation and immunoblotting

Brains were quickly removed from mice deeply anesthetized in a CO_2 chamber, hippocampus dissected out, frozen in dry ice, and stored at −80 °C until use. Briefly, tissue was sonicated in 250 μL of lysis buffer (phosphate buffered saline [PBS, NaCl, 137 mM, KCl, 2.7 mM, Na_2HPO4, 10 mM, $KH2PO_4$, 1.8 mM, pH 7.5] with 1% Nonidet P40 [vol/vol], 1 g/L sodium dodecylsulfate (SDS), 5 g/L sodium deoxycholate, protease inhibitors 1:1, 000 [Sigma], and 2 g/L sodium orthovanadate), centrifuged at 15, 000 ×*g* for 20 min and 15 mg protein from the supernatant were analyzed by SDS-polyacrylamide gel electrophoresis (7.5 g/L acrylamide) and transferred to nitrocellulose membranes (Millipore, Bedford, MA). Human tissue was analyzed similarly. Membranes were blocked in TBS-T (150 mM NaCl, 20 mM Tris-HCl, pH 7.5, 0.5 mL/L Tween 20) with 50 g/L non-fat dry milk and 50 g/L BSA, and incubated overnight at 4 °C with shaking, in the presence of primary antibodies in PBS with 0.2 g/L NaN_3 (Supplementary Table 1). After several washes in TBS-T, blots were incubated with anti-rabbit IgG IRdye800CW-coupled or antimouse IgG IRdye700DXcoupled antibodies (1/2, 000, Rockland Immunochemicals, USA) and signal detected by the Odyssey Li-Cor and analyzed using ImageJ.

2.4. Immunofluorescence

For immunofluorescence (IF), deeply anesthetized mice (pentobarbital 60 mg/kg) were intracardially perfused with a paraformaldehyde solution (40 g/L paraformaldehyde in 0.12 M sodium phosphate, pH 7.2). Brains were removed and post-fixed overnight in the same solution, cryoprotected with 300 g/L sucrose in PBS with 0.2 g/L NaN_3 and frozen in dry ice-cooled isopentane. Serial coronal 30-μm cryostat sections were free-floating incubated as described (Giralt et al., 2017). They were washed three times in PBS, permeabilized 15 min at RT in PBS containing 3 mL/L Triton X-100 and 30 mL/L goat serum (Pierce Biotechnology, Rockford, IL). After these washes, brain sections were incubated overnight at 4 °C with primary antibodies (antibodies sources and dilutions in Supplementary Table 1) in PBS with 0.2 g/L NaN_3. After three washes sections were incubated 2 h at RT with fluorescent secondary 488 anti-rabbit or 555 anti-mouse antibodies (1:250, Molecular Probes, Sunnyvale, CA). No signal was detected in control sections incubated in the absence of primary antibody. Confocal images were acquired with a Leica Confocal SP5-II (63× numerical aperture lens, 5× digital zoom, 1-Airy unit pinhole, 4-frame averaging per *z*-step, *z*-stacks every 2 μm, 1, 024 × 1, 024 pixel resolution). PSD-95- and synaptophysin-1-positive clusters (Prange et al., 2004) were analyzed with NIH ImageJ, in at least 3 slices per mouse and up to 3 CA1 *stratum radiatum* images per slice. Stained β-amyloid plaques were photographed from the entire hippocampus (three slices per mouse) with a DM6000–2 microscope (Leica), analyzed with ImageJ and counted manually in CA1, CA3, and DG.

2.5. Proximity ligation assay

Proximity ligation assay (PLA) was carried out using Duolink® detection kit (Sigma) according to manufacturer's protocol. Floating-sections were incubated with primary Pyk2 and β-amyloid antibodies overnight at 4 °C. PLA probes anti-mouse PLUS and anti-rabbit MINUS were added overnight at 4 °C. Sections were washed in TBS + 0.1% Tween 20 and incubated in Duolink® ligation solutions and ligase for 1 h at 37 °C. Next, the signal was amplified by the addition of Duolink® amplification and polymerase for 2.5 h at 37 °C. The detection of the red fluorophore (excitation 594 nm, emission 624 nm) was used. Nuclei were stained with DAPI using mounting media provided in the kit. As a negative control, one of the two primary antibodies was omitted.

2.6. Behavioral tests

Mouse anxiety was analyzed in a plastic elevated plus-maze made with two opposing 30 × 8 cm open arms, and two opposing 30 × 8 cm arms enclosed by 15 cm-high walls placed 50 cm above the floor and dimly lit (60 lx). Each mouse was placed in the central square, facing an open arm and the time spent in the open arms, which normally correlates with low levels of anxiety, measured for 5 min.

Spontaneous locomotor activity was measured in dim lit (60 lx) open field white square arena (40 × 40 × 40 cm in length, width, and height respectively). Animals were placed at the center and allowed to explore freely for 30 min. Spontaneous locomotor activity was measured.

Novel object recognition was tested in a dimly lit (60 lx) 40 × 40 × 40 cm white square arena. Mice were first habituated to the arena in the absence of objects (3 days, 15 min/day). On the fourth day, two similar objects were presented to each mouse during 10 min (A'A″ condition) after which they were returned to their home cage for 15 min. After that, the animals were placed in the arena where they were tested during 5 min with a familiar and a new object (A′ B condition; short-term memory, STM), and then returned to their home cage. Twenty-four hours later, the same animals were re-tested for 5 min in the arena with a familiar and a new object (BC condition; long-term memory, LTM). The object preference was measured as the time spent exploring each object × 100/time exploring both objects.

The passive avoidance (light-dark) paradigm was conducted in a 2-compartment box, where 1 compartment was dimly lit (20 lx) and the other brightly lit (200 lx). Both chambers were connected by a door (5 cm × 5 cm). During training, mice were placed into the aversive brightly lit compartment, and upon the entry into the preferred dimly lit compartment (with all 4 paws inside the dark chamber), they received a mild foot shock (2-s foot shock, 1 mA intensity). The latency of mice to enter into the dark chamber was recorded. Twenty seconds after receiving the foot shock, mice were returned to the home cage until testing 24 h later (long-term memory). For this retention test, mice were returned to the brightly lit compartment and the latency to enter the shock-paired compartment (dark chamber) was measured (10-min time cutoff).

For all tests at the end of each trial, any defecation was removed and the apparatus was wiped with 30% ethanol. Animals were tracked and recorded with SMART junior software (Panlab, Spain).

2.7. Viral constructs and stereotactic injection

For Pyk2 overexpression we used adeno-associated viruses (AAV) expressing Pyk2 (Giralt et al., 2017) (AAV1-CamKIIα (0.4)-GFP-2A-mPTK2B; Vector Biolabs Malvern, PA, USA) or, as control, AAVs expressing GFP (AV-9-PV1917, AAV9·CamKIIα (0.4).eGFP·WPRE.rBG (AAV-GFP) from Perelman School of Medicine, University of Pennsylvania). Mice were anesthetized with pentobarbital (30 mg/kg) and bilaterally injected with AAV-GFP or AAV-Pyk2 (2.06×10^9 GS) in the dorsal hippocampus at the following coordinates from the bregma (millimeters); anteroposterior, −2.0; lateral, ± 1.5; and dorsoventral, −1.4 and − 2.0. AAVs were injected over 2 min, leaving the cannula in place for 5 additional minutes to ensure complete diffusion of the viruses, and then slowly retracted from the brain. The animals were monitored for 2 h after administration and then returned to the housing facility for 21 days before behavioral assessment and brain analysis.

2.8. Statistical analysis

Analysis was done using GraphPad Prism version 6.00 for Windows, GraphPad Software, La Jolla California USA. Data are expressed as mean + SEM. Normal distribution was tested with d'Agostino and Pearson omnibus, Shapiro-Wilk, and Kolmogorov-Smirnov normality tests. If at least one of them was passed, statistical analysis was

performed using two-tailed Student's *t*-test or ANOVA and Holm-Sidak's post hoc test. Otherwise non-parametric Mann and Whitney or Kruskal-Wallis' and Dunn's tests were used. $p < 0.05$ was considered as statistically significant.

3. Results

3.1. Pyk2 expression and phosphorylation in patients and 5XFAD mice

We first examined Pyk2 protein levels in post-mortem prefrontal and hippocampal human tissue. In the two regions Pyk2 levels did not differ between AD patients and controls (Fig. 1A–B). The detection of the autophosphorylated form of Pyk2 in the human brain samples, either in patients or in controls, was variable from one batch to the other, presumably due to post-mortem endogenous dephosphorylation (not shown) making this measurement unreliable. We then analyzed the hippocampus of 8-month-old 5XFAD mice, at an age at which they have a clear phenotype (Oakley et al., 2006; Schneider et al., 2014) to be comparable to the human samples. Total Pyk2 levels were similar in wild type (WT) and 5XFAD mice, whereas pTyr402-Pyk2 levels were lower in 5XFAD than in WT mice (Fig. 1C-D). Since autophosphorylation at Tyr402 is a key step in the activation of Pyk2 (Dikic et al., 1996; Girault et al., 1999; Park et al., 2004) this result indicated a functional alteration of this kinase. In contrast, in 3-month-old 5XFAD mice, both total Pyk2 and pTyr402-Pyk2 levels were similar to WT (Fig. 1C, E). Our results show that Pyk2 levels were normal in AD patients and 5XFAD mice but that its autophosphorylation was decreased in 8-month 5XFAD mice.

3.2. Pyk2 is co-localized with Aβ in 5XFAD mice

We compared Pyk2 localization in the hippocampus of 5XFAD mice with Aβ immunoreactivity and plaques. Aβ-positive plaques were negative for Pyk2 (Fig. 2A-C). In contrast, Pyk2 and Aβ-like immunofluorescence displayed a significant degree of colocalization in neuropil zones devoid of amyloid plaques (Fig. 2D), as supported by the calculation of the Manders' colocalization coefficient (Manders et al., 1992) in the 3 hippocampal regions studied (Fig. 2E). To corroborate this apparent colocalization, we used an in situ proximity ligation assay (PLA). Hippocampal sections of 5XFAD mice were probed with Pyk2 and β-amyloid antibodies followed by hybridization with secondary antibodies coupled to oligonucleotides that hybridize together if the distance between the two target proteins is < 40 nm. The interaction between Pyk2 and β-amyloid was detected as red dots in all hippocampal regions (Fig. 2F, right panels). As a negative control, only one primary antibody was added and amplification of the signal was not detected (Fig. 2F, left panels). These results provide evidence for some degree of colocalization of Pyk2 and Aβ immunoreactivity in the neuropil of 5XFAD mice.

3.3. Pyk2 genetic deletion does not change the behavioral phenotype of 5XFAD mice

We reasoned that if Pyk2 played a role in the pathogenesis of the 5XFAD model, its deletion should delay or modify their phenotype. We crossed 5XFAD mice with Pyk2$^{-/-}$ mice and studied their phenotype at 8-month, an age at which these mice have a clear but not severe behavioral phenotype (Grinan-Ferre et al., 2016). We focused on a single time point, since the relatively mild phenotype was appropriate to detect either improvement or worsening of the disease. We compared WT and 5XFAD mice, expressing or not Pyk2 (Fig. 3A). All mice displayed similar spontaneous locomotor activity (Fig. 3B). To study memory capabilities, since Pyk2 deletion by itself impairs hippocampus-dependent spatial memory (Giralt et al., 2017), we used the novel object recognition test, which was not impaired in Pyk2$^{-/-}$ mice (Fig. 3C-D). Twenty min after training, mice of all genotypes preferentially explored the novel object (short-term memory, Fig. 3C). One day after object displacement, WT and Pyk2$^{-/-}$ mice still explored more the new object than the familiar one (Fig. 3D). In contrast this preference was completely absent in both 5XFAD and 5XFAD x Pyk2$^{-/-}$ mice, revealing a specific long-term memory deficit in 5XFAD, which was not modified in the absence of Pyk2 (Fig. 3D). We next examined associative memory in the passive avoidance task (Fig. 3E). Latency to step-through during the training session was similar in the 4 genotypes. In the testing session, 24 h later, although all mice showed a pronounced increase in the latency to enter the dark compartment, this latency was lower in 5XFAD, Pyk2$^{-/-}$, and 5XFAD x Pyk2$^{-/-}$ mice than in WT littermates (Fig. 3E). These results showed that Pyk2 deletion induced by itself a deficit in the passive avoidance performance, and that this deficit was not additive with the alterations observed in 5XFAD mice. Finally, we used the elevated plus-maze to evaluate anxiety, which is decreased in 5XFAD mice (Schneider et al., 2014; Grinan-Ferre et al., 2016). As expected,

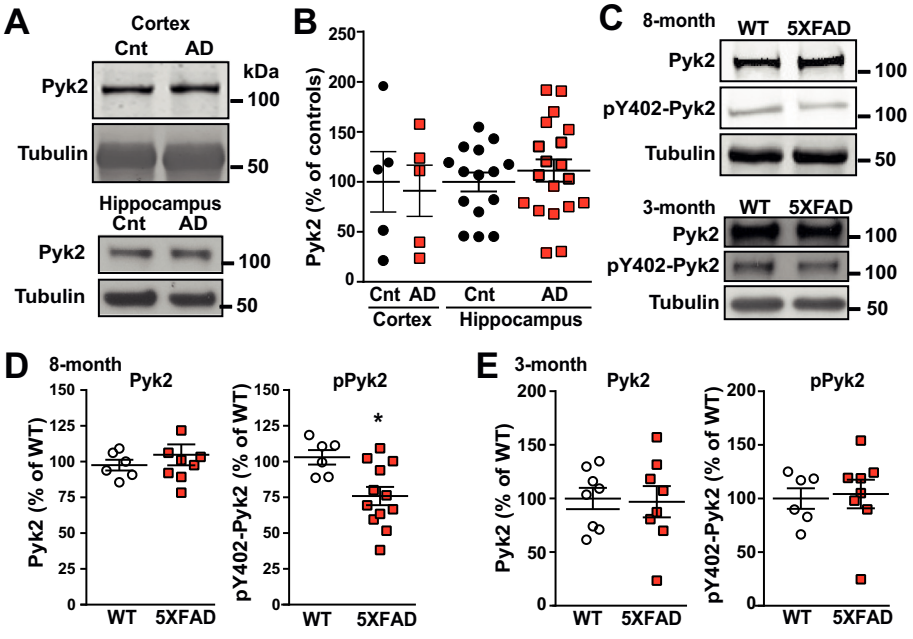

Fig. 1. Pyk2 in Alzheimer disease patients and 5XFAD mice. (A) Immunoblotting for Pyk2 and tubulin as a loading control, in human post-mortem prefrontal cortex (top panel) and hippocampus (bottom panel) samples from controls (Cnt) and AD patients. (B) Densitometric quantification of results as in (A) for prefrontal cortex, unpaired *t*-test $t_8 = 0.22$, ns ($n = 5$ per group), and hippocampus unpaired t-test $t_{32} = 0.76$, ns ($n = 15$ and 19 per group). (C) Immunoblotting for Pyk2, phosphoTyr402-Pyk2 (pY402-Pyk2) and tubulin as a loading control in 8-month (top panel) and 3-month (bottom panel) WT and 5XFAD mice. In A and C molecular weight markers position is indicated in kDa. (D-E) Densitometric quantification of results as in (C) for Pyk2 and pY402-Pyk2 in 8-month (D) and 3-month (E) old mice. In B, D, E, data were normalized to tubulin for each sample and expressed percentage of the mean of WT/controls and means and SEM are indicated. Unpaired t-test: (D) Pyk2, $t_{13} = 0.73$, ns; pY402-Pyk2, $t_{16} = 2.78$, $p = .013$ ($n = 6$ WT, 12 5XFAD), (E) Pyk2, $t_{13} = 0.17$, ns; pY402-Pyk2, $t_{12} = 0.24$, ns ($n = 6$–8 WT, 8 5XFAD).

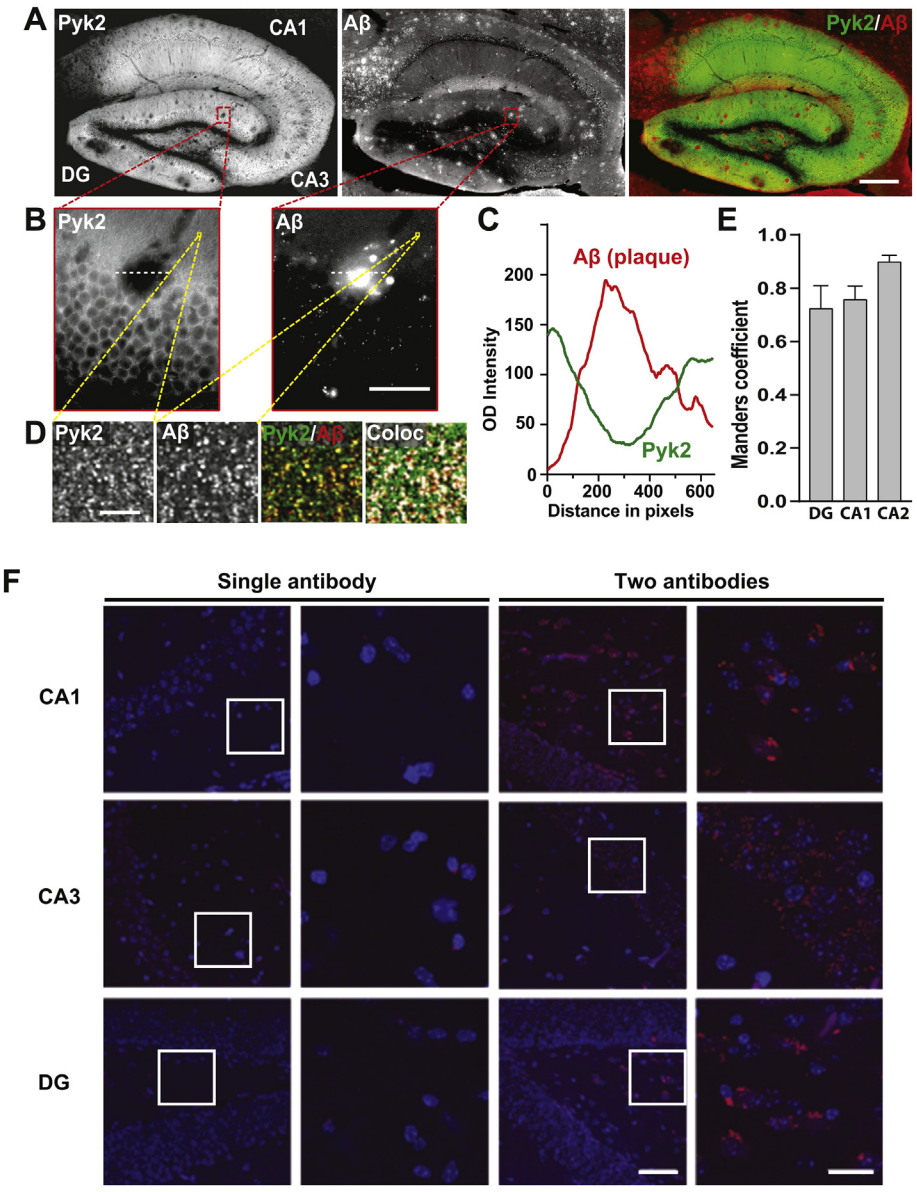

Fig. 2. Pyk2 is colocalized with Aβ in hippocampal neuropil of 5XFAD mice. (A) Stitched confocal images of Pyk2 and Aβ immunoreactivity in the hippocampus of 5XFAD mice. Scale bar 450 μm. (B) Higher magnification of Pyk2 and Aβ immunostaining in the rectangle in (A). Scale bar, 50 μm. (C) Optical density quantification of Pyk2 and Aβ staining in an Aβ-plaque indicated by a dashed line in (B). The intensity of the two immunoreactivities varies in an opposite manner. (D) High magnification of the area indicated (yellow box) in (B). From left to right, panels correspond to Pyk2, Aβ, double immunostaining, and colocalization index (Coloc, indicated in white). Scale bar, 5 μm. (E) Quantification of Pyk2 and Aβ colocalization using the Manders coefficient in 3 hippocampal regions, as in (I). Data are means ± SEM, $n = 3$ photos per mouse, 3 mice. (F) Pyk2/β-amyloid interaction revealed by in situ PLA in the hippocampus of 5XFAD mice. Control is provided by incubation with a single antibody, which did not generate specific signal, whereas with the two antibodies an amplification appears as red dots indicating a close proximity of the two proteins. Nuclei are stained in blue with DAPI. *Left panels*, low magnification confocal images. Scale bar 50 μm. *Right panels*, higher magnification of Pyk2/β-amyloid interaction in boxed areas in the left panels. Scale bar 20 μm.

5XFAD mice spent more time in the open arms than their WT littermates (Fig. 3F). Pyk2$^{-/-}$ mice did not differ from WT mice, nor 5XFAD x Pyk2$^{-/-}$ from 5XFAD (Fig. 3F). Taken together these results confirm the existence of behavioral alterations in 5XFAD mutant mice, which were not modified in the absence of Pyk2.

3.4. *Pyk2 knockout induces only minor changes in 5XFAD mice neuropathology*

The number of synapses decreases in 5XFAD mice in correlation with cognitive decline (Grinan-Ferre et al., 2016; Hongpaisan et al., 2011; Shao et al., 2011). To examine whether this alteration was modified in the absence of Pyk2, we measured immunoreactive puncta for PSD-95 and synaptophysin, which are post- and pre- synaptic markers, respectively, and which have been previously used in AD mouse models as an indication of the number of synapses (Grinan-Ferre et al., 2016; Hongpaisan et al., 2011; Shao et al., 2011). We analyzed these two markers in CA1 *stratum radiatum* of 8-month mice (Fig. 4A-D). PSD-95-positive puncta were decreased in CA1of Pyk2$^{-/-}$ mice, as previously described (Giralt et al., 2017), and in 5XFAD mice (Grinan-Ferre et al., 2016; Hongpaisan et al., 2011; Shao et al., 2011), as well as in the double mutants (Fig. 4A–B). The lack of additivity of the defect on the double mutants suggested that the post-synaptic alteration of PSD-95 might depend on common molecular dysfunction in the two mutant mice. In contrast, synaptophysin-positive puncta were decreased in 5XFAD but not Pyk2$^{-/-}$ hippocampus (Fig. 4C–D), consistent with the predominantly post-synaptic phenotype in Pyk2 KO mice (Giralt et al., 2017).

To test whether the lack of Pyk2 can exacerbate or ameliorate β-amyloidosis in 8-month 5XFAD mice we then counted the number of Aβ-immunoreactive plaques in three regions of dorsal hippocampus (CA1, CA3, and dentate gyrus, DG) in 5XFAD and 5XFAD x Pyk2$^{-/-}$ mice (Fig. 4E–F). Although hippocampal plaque load was similar in the two genotypes in CA1 and DG, the number of plaques was decreased in CA3 of 5XFAD x Pyk2$^{-/-}$ mice as compared to 5XFAD littermates. Hippocampal levels of glial fibrillary acidic protein (GFAP), an index of astrogliosis, were similar in WT and Pyk2$^{-/-}$ mice and were increased in both 5XFAD and 5XFAD x Pyk2$^{-/-}$ mice (Fig. 4G–H). In summary, the absence of Pyk2 did not further modify the synaptic markers, the amyloid plaques or astrogliosis in 5XFAD mice, except for a decrease in the number of plaques in CA3.

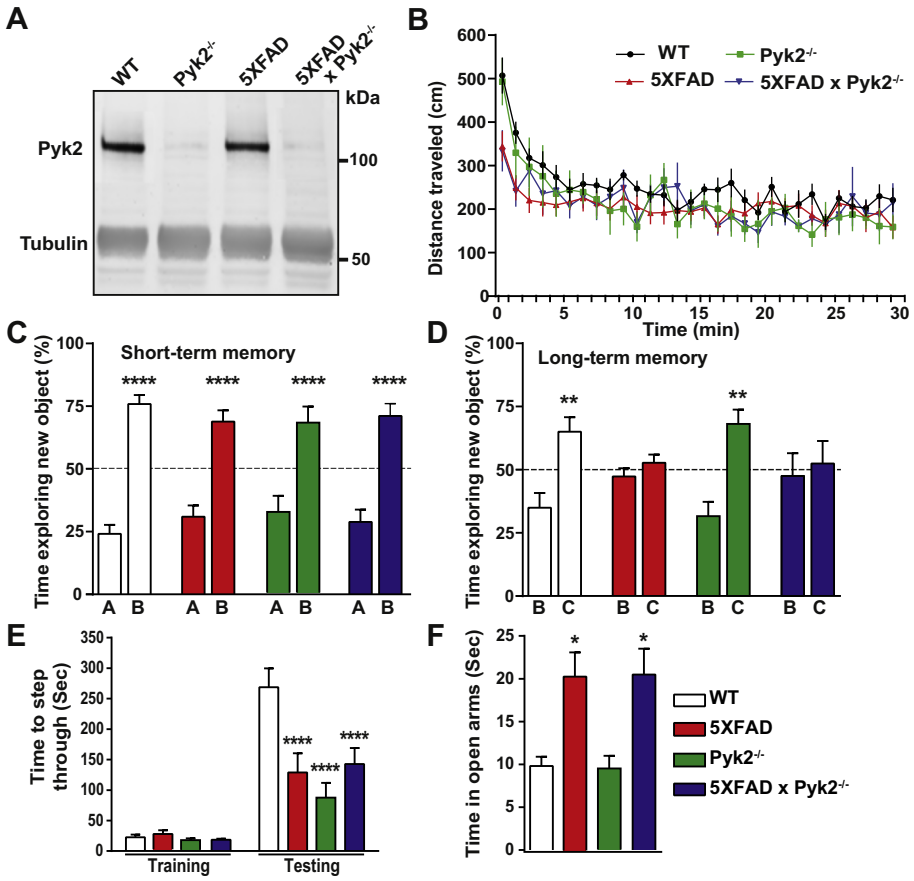

Fig. 3. Behavioral phenotype of 5XFAD x Pyk2$^{-/-}$ mice. (A) Immunoblotting for Pyk2 and tubulin as a loading control in 8-month WT, Pyk2$^{-/-}$, 5XFAD, and 5XFAD x Pyk2$^{-/-}$ (double mutant, DM) mice. (B) Spontaneous locomotor activity in the open field of these mice monitored during 30 min (wt, $n = 12$, Pyk2 −/−, n = 6, 5XFAD, $n = 14$, DM, n = 14). (C-D) Novel object recognition test. (C) Short-term memory was evaluated as the percentage of total time exploring the new object (object B) and old object (object A) 20 min after the training session. (D) Long-term memory was evaluated as the percentage of total time exploring the new object (object C) and old object (object B) 24 h after training. Statistical analysis, 1-way ANOVA, (C), $F_{(7, 86)} = 20.85$, $p < 10^{-4}$, (D) $F_{(7, 84)} = 3.69$, $p = 0.0016$. Post-hoc Holm-Sidak's test within each genotype, **p < 0.01, ****p < 10^{-4}. In (C-D), wt, $n = 11$, Pyk2$^{-/-}$, n = 11, 5XFAD, $n = 13$, DM, $n = 12$. (E) Passive avoidance test. The latency to step-through was measured before (Training) and 24 h after (Testing) receiving an electric shock. Two-way ANOVA: interaction, $F_{(3, 47)} = 6.83$, $p = 0.0007$, time, $F_{(1, 47)} = 92.15$, p < 10^{-4}, genotype, $F_{(3, 47)} = 7.302$, $p = 0.0004$, Holm-Sidak's test vs WT, **** p < 10^{-4}. Wt, n = 11, Pyk2$^{-/-}$, n = 13, 5XFAD, n = 11, DM, $n = 16$. (E) Elevated plus-maze. The time spent in the open arms was monitored for 5 min. One-way ANOVA, $F_{(3, 43)} = 5.49$, $p = 0.003$, Holm-Sidak's test vs WT, * $p < 0.05$. Wt, n = 11, Pyk2$^{-/-}$, $n = 8$, 5XFAD, n = 13, DM, $n = 15$.

3.5. Pyk2 overexpression in dorsal hippocampus partially improves the behavioral phenotype of 5XFAD mice

Since the absence of Pyk2 did not markedly modify the phenotype of 5XFAD mice, it was unlikely that it played a necessary role in the pathogenesis in this model. We therefore hypothesized that, on the contrary, the functional Pyk2 deficit observed in 5XFAD mice might be involved in their phenotype. To test this hypothesis, since there is no means to stimulate Pyk2 directly, we decided to increase its expression levels. Eight-month-old WT and 5XFAD mice received in the dorsal hippocampus a bilateral stereotactic injection of AAV expressing Pyk2 (5XFAD/Pyk2 mice) or GFP (WT/GFP and 5XFAD/GFP), as a control (Fig. 5A). Three weeks later, Pyk2 protein levels increased in 5XFAD/Pyk2 mice as compared to WT/GFP and 5XFAD/GFP mice (Fig. 5B–C). The overall increase in total hippocampal Pyk2 levels was 73% and the increase in pTyr402-Pyk2 levels was 51%, sufficient to restore its levels slightly above those in WT/GFP controls (Fig. 3B–D). We thus, expected to rescue autophosphorylation-dependent functions of Pyk2. We then carried out the same set of behavioral tests in these mice as in Pyk2 KO mice (see Fig. 3). In the elevated plus-maze (Fig. 5E) the increased time spent in the open arms by 5XFAD/GFP mice, compared with WT/GFP mice, was corrected in 5XFAD/Pyk2 mice. Locomotor activity in the open field was similar in all groups of AAV-injected mice (Fig. 5F). In the passive avoidance test no difference was observed between 5XFAD/GFP and 5XFAD/Pyk2 mice (Fig. 5G), showing that, as expected, overexpression of Pyk2 in the hippocampus was not sufficient to restore the associative memory evaluated in this paradigm that also involves other brain regions. As observed above (Fig. 3C), the three groups of mice did not display any deficit in short-term memory in the novel object recognition test (Fig. 5H). However, the deficit in long-term memory observed in 5XFAD/GFP mice, as compared to WT/GFP, was restored in 5XFAD/Pyk2 mice (Fig. 5I). Thus, behavioral evaluation showed that overexpression of Pyk2 in the dorsal hippocampus of 5XFAD mice rescued some deficits including impairment in long-term memory in the novel object recognition test and aberrant performance in the elevated plus-maze.

3.6. Pyk2 overexpression in dorsal hippocampus increases the number of plaques but rescues the loss of synaptic markers in CA1 of 5XFAD mice

To test whether Pyk2 overexpression in the hippocampus modified β-amyloidosis we counted the number of Aβ-immunofluorescent plaques in the hippocampus in 8-month 5XFAD/GFP and 5XFAD/Pyk2 mice (Fig. 6A, B). The plaque number in all three regions studied was higher in 5XFAD/Pyk2 than in 5XFAD/GFP mice by 50–60%. In contrast, GFAP levels were increased to similar levels in 5XFAD/GFP and 5XFAD/Pyk2 mice as compared to WT/GFP (Fig. 6C-D), indicating that astrogliosis was similar in the three groups of mice.

Since the moderate increase in Aβ-plaque load in Pyk2 overexpressing mice contrasted with the partial behavioral improvement, we studied possible improvements of other parameters, focusing on synaptic markers. We examined the PSD-95-immunoreactive and synaptophysin-immunoreactive puncta (post- and pre- synaptic markers, respectively), which are an indication of the number of synapses and are decreased in 5XFAD mice in correlation with cognitive decline (Grinan-Ferre et al., 2016; Hongpaisan et al., 2011; Shao et al., 2011). We analyzed these two markers in CA1 *stratum radiatum* of 8-month mice. As expected and as observed above for mice from the same genotypes (see Fig. 4A–D), the number of PSD-95-positive and synaptophysin-positive puncta was decreased in 5XFAD/GFP as compared to WT/GFP mice (Fig. 6E–H). The PSD-95 decrease was rescued in 5XFAD/Pyk2 mice and the synaptophysin alteration was partly corrected (Fig. 6F, H). These results suggest that the behavioral improvement observed in 5XFAD mice following hippocampal overexpression

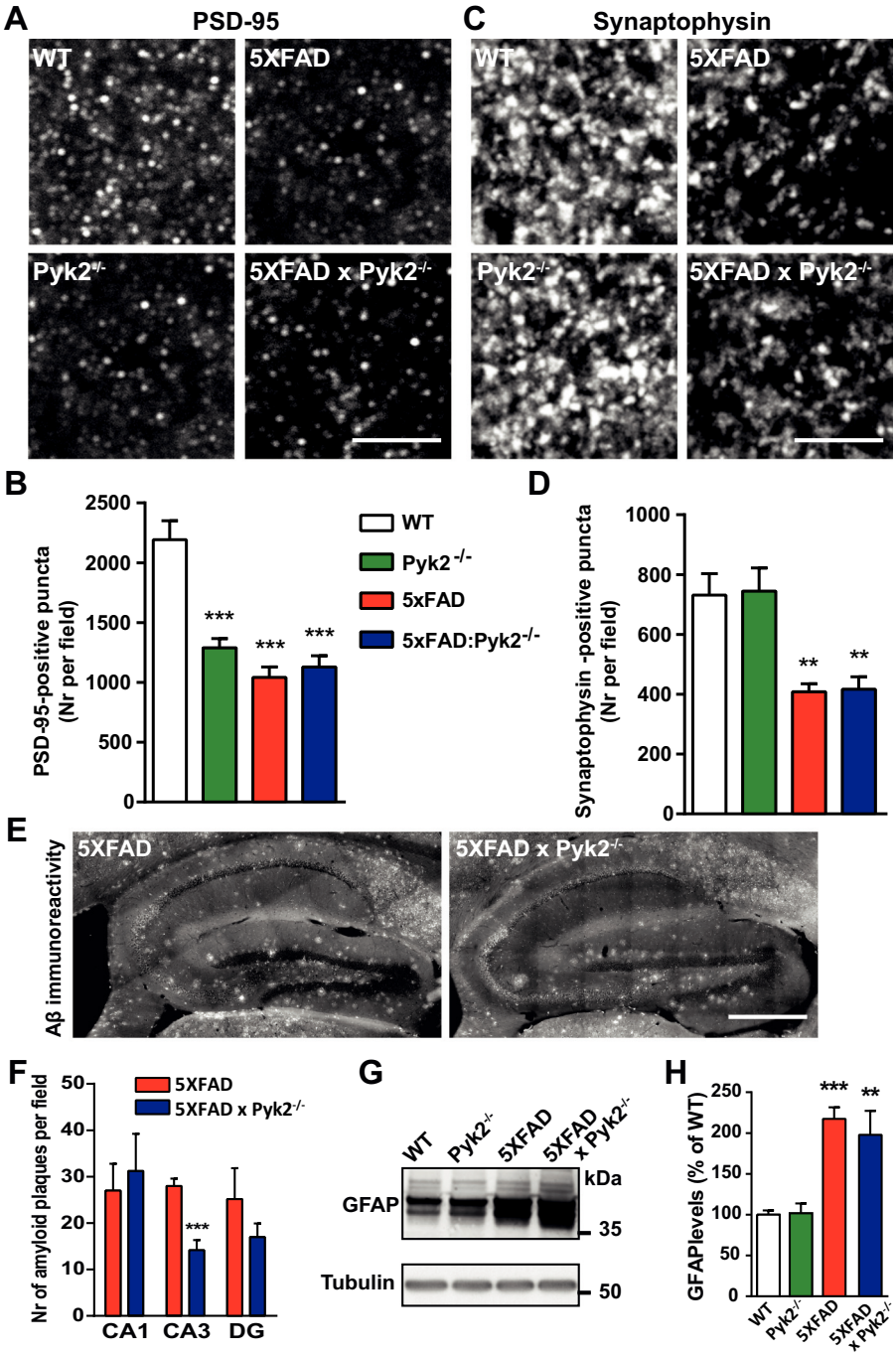

Fig. 4. Histological phenotype of 5XFAD x Pyk2$^{-/-}$ mice. (A) Confocal image of PSD-95 immunofluorescence in CA1 *stratum radiatum* of 8-month WT, Pyk2$^{-/-}$, 5XFAD and 5XFAD x Pyk2$^{-/-}$ double mutant mice, as indicated. Scale bar 10 µm. (B) Quantification of the number of PSD-95-positive puncta per field as in (A), $n = 7–9$ mice per group. One-way ANOVA, $F_{(3,\ 29)} = 23.09$, $p < 10^{-4}$, post-hoc Holm-Sidak's test, *** $p < 0.001$. (C) Synaptophysin immunofluorescence, as in (A). Scale bar 5 µm. (D) Quantification of the number of synaptophysin-positive puncta per field as in (C),), n = 7–9 mice per group. One-way ANOVA, $F_{(3,\ 29)} = 10.92$, $p < 10^{-4}$, post-hoc Holm-Sidak's test, *** $p < 0.001$. (E) Aβ immunofluorescence in the hippocampus of 8-month 5XFAD and 5XFAD x Pyk2$^{-/-}$ mice. Scale bar 500 µm. (F) Quantification of Aβ-positive plaques in CA1, CA3 and DG of 5XFAD and 5XFAD x Pyk2$^{-/-}$ mice. Genotype comparison for each region with Mann-Whitney test. ** $p < 0.01$ (n = 3–6 mice per genotype). (G) Immunoblotting for GFAP and tubulin as a loading control in the hippocampus of the 4 genotypes. (H) Densitometric quantification of results as in (I). Data are means ± SEM. One-way ANOVA, $F_{(3,\ 18)} = 14.19$, $p < 10^{-4}$, Holm-Sidak's test vs WT, ** $p < 0.01$, *** $p < 0.001$, n = 5–6 mice per group.

of Pyk2 was accompanied by an improvement in the number of synapses revealed by both pre- and post-synaptic markers.

3.7. Role of Pyk2 in Src cleavage in 5XFAD mice

Since Pyk2 phosphorylation on Tyr-402 was decreased in 5XFAD mice, we examined Src-family kinases (SFKs), which are recruited and activated when Pyk2 is autophosphorylated at this residue (Dikic et al., 1996). We have previously shown that SFKs autophosphorylation is decreased in Pyk2$^{-/-}$ mice (Giralt et al., 2017). Here we measured the total amount of Src in the hippocampus of Pyk2$^{-/-}$ mice by immunoblotting. Src full-length form (66 kDa) was decreased, whereas a 52-kDa fragment, detected by an antibody that recognizes a C-terminal epitope, was increased in Pyk2$^{+/-}$ and Pyk2$^{-/-}$ mice (Fig. 7A-B). Both changes were gene-dosage-dependent (Fig. 7B). These results on Src contrasted with our previous observations on Fyn, which did not appear to be altered in Pyk2 mutant mice (Giralt et al., 2017) and indicated the existence of a proteolytic cleavage of Src in the absence of Pyk2. Interestingly, a similar 52-kDa cleaved Src with potential neurotoxic properties has been reported following excitotoxic stimuli and ischemia (Hossain et al., 2013), suggesting a possible pathogenic role. We therefore studied Src in 5XFAD mice as compared to WT and found that the 52-kDa form of Src was also increased (Fig. 7C-D). We then measured the two forms of Src in WT, Pyk2$^{-/-}$, 5XFAD, and double mutant mice (Fig. 7E-F). In this experiment the decrease in 66-kDa Src was not observed in Pyk2$^{-/-}$ mice, indicating variability of this parameter. In contrast, the 52-kDa form was reproducibly increased in Pyk2$^{-/-}$, 5XFAD, and double mutant mice (Fig. 7E-F). We repeated this

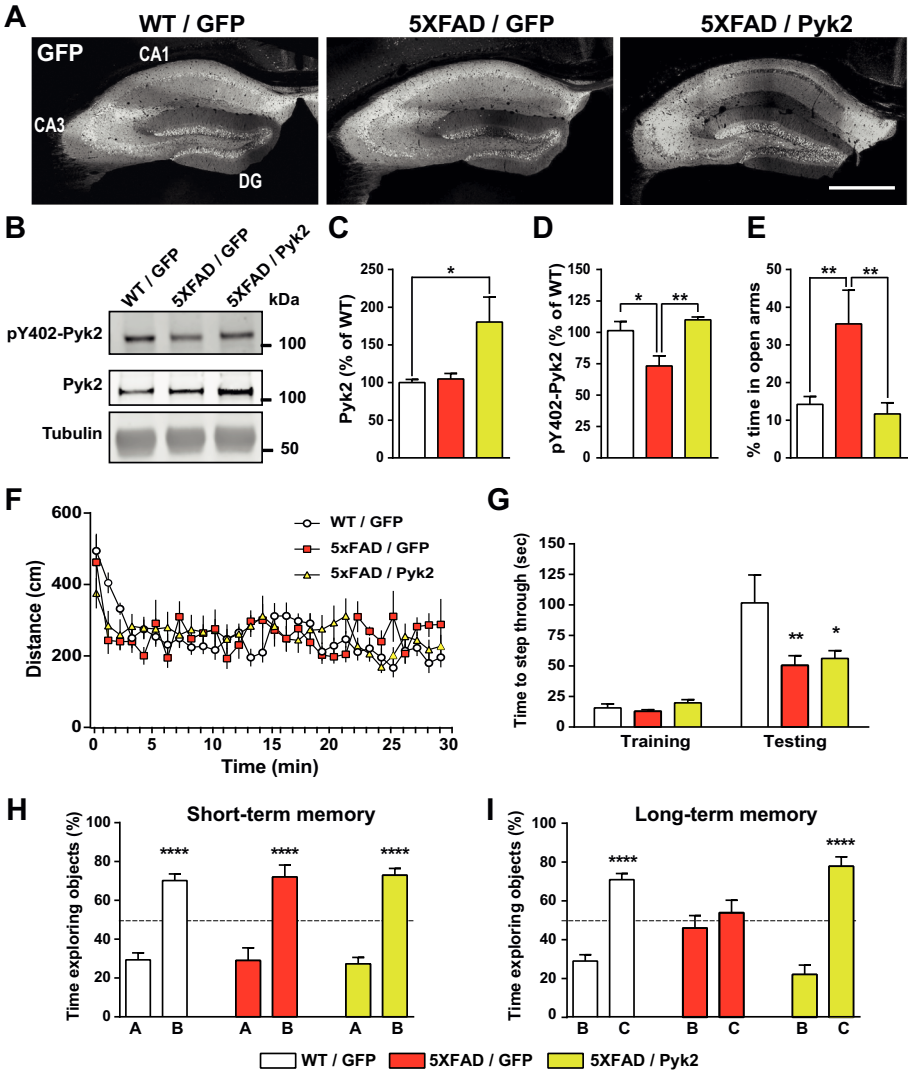

Fig. 5. Pyk2 overexpression in the hippocampus of 5XFAD mice improves some behavioral alterations. (A) GFP fluorescence in the dorsal hippocampus of 8-month WT and 5XFAD mice bilaterally injected in the dorsal hippocampus, 3 weeks before, with AAV expressing GFP (WT/GFP and 5XFAD/GFP) or Pyk2 and GFP (5XFAD/Pyk2) under the control of CaMKIIα promoter (stitched pictures). Scale bar 500 µm. (B) Immunoblotting for Pyk2, phosphoTyr402-Pyk2 (pY402-Pyk2) and tubulin as a loading control in the 3 groups of mice. (C-D) Densitometric quantification of Pyk2 (C) and pY402-Pyk2 (D) as in (B). One-way ANOVA, Pyk2, $F_{(2, 22)} = 5.49$, $p = 0.012$, pY402-Pyk2, $F_{(2, 19)} = 7.91$, $p = 0.003$, $n = 6–9$ mice per group. (E) Elevated plus-maze. The time spent in the open arms was monitored for 5 min in WT/GFP (n = 13), 5XFAD-GFP ($n = 9$) and 5XFAD-Pyk2 ($n = 12$) mice. One-way ANOVA, $F_{(2, 31)} = 6.94$, $p = 0.003$. (F) Spontaneous locomotor activity in the open field monitored in all groups during 30 min (10–13 mice per group). (G) Passive avoidance test. The latency to step-through was measured before (Training) and 24 h after (Testing) receiving an electric shock (10–12 mice per group). Two-way ANOVA, interaction, $F_{(2, 29)} = 4.28$, $p = 0.02$, time, $F_{(1, 29)} = 42.9$, $p < .0001$, groups, $F_{(2, 29)} = 2.58$, $p = 0.09$. (H–I) Novel object recognition test. (H) Short-term memory was evaluated as the percentage of time exploring the new object (object B) and the old object (object A) 20 min after the training session. (I) Long-term memory was evaluated as the percentage of time exploring the new object (object C) and the old object (object B) 24 h after training (9–11 mice per group). Statistical analysis, 1-way ANOVA, (H), $F_{(5, 62)} = 31.5$, $p < 10^{-4}$, (I), $F_{(5, 58)} = 23.2$, $p < 10^{-4}$. In C-E and G-I post-hoc test was Holms-Sidak, * $p < 0.05$, ** $p < 0.01$, **** $p < 10^{-4}$.

experiment in AAV-injected mice and observed again an increase in 52-kDA Src, which was corrected by AAV-mediated Pyk2 expression (Fig. 7D, E). Taken together these results indicate that a decrease in Pyk2 levels and/or autophosphorylation can trigger the appearance of a shorter form of Src, presumably corresponding to a cleaved form missing the N-terminal fragment, with potentially cytotoxic properties. This fragment may contribute to the consequences of Pyk2 decreased function (autophosphorylation) in the 5XFAD model.

4. Discussion

Although *PTK2B* is genetically associated with late onset AD (Lambert et al., 2013; Jiao et al., 2015; Beecham et al., 2014), we do not know whether and how Pyk2, the tyrosine kinase coded by this gene, is involved in the disease. By crossing 5XFAD mice, a transgenic mouse model that mimics human amyloidogenic pathway alterations (Oakley et al., 2006), with Pyk2 *knockout* mice we observed that the absence of Pyk2 did not dramatically alter the neurological phenotype of 5XFAD mice. This showed that Pyk2 is not essential for the deleterious consequences of increased Aβ production. The only difference we detected in comparison to simple 5XFAD mice was a decrease in the number of plaques in CA3, indicating a possible contribution of Pyk2 in their appearance. We did not find any major change in Pyk2 protein levels in cortical or hippocampal samples from human AD patients or in 5XFAD mouse hippocampus. However, in 8-month 5XFAD mice Pyk2 autophosphorylation site, Tyr402, was less phosphorylated than in WT littermates, indicating an alteration of Pyk2 activation. In younger animals (3-month) basal levels of pTyr402-Pyk2 were normal, indicating that Pyk2 autophosphorylation deficit is not a very early alteration. Although the cause of Pyk2 functional deficit in 5XFAD mice is not known, it has been shown that Pyk2 is activated downstream of a complex associating PrPc and mGluR5 glutamate receptors, and that this activation is disrupted by Aβ oligomers (Haas & Strittmatter, 2016). Such disruption might contribute to Pyk2 functional deficit.

To test whether decreased Pyk2 activity in these mice could contribute to their memory deficit we overexpressed Pyk2 in the dorsal hippocampus and thus corrected the levels of autophosphorylated Pyk2. This strategy improved some aspects of the behavioral phenotype, including performance in the elevated plus-maze and novel object recognition long-term memory. Pyk2 overexpression also improved synaptic alterations which are known to be a major source of AD symptomatology (Pozueta et al., 2013; Sheng et al., 2012; Tu et al., 2014). Recent evidence shows that Pyk2 plays an important role at hippocampal synapses (Giralt et al., 2017). Pyk2 is involved in PSD-95 post-synaptic recruitment and clustering (Giralt et al., 2017), regulates NMDA receptors subunits (Huang et al., 2001; Giralt et al., 2017) and even the 50% Pyk2 decrease observed in heterozygous Pyk2 +/− mice is sufficient to markedly alter synaptic properties (Giralt et al., 2017). The behavioral improvement induced by Pyk2 overexpression in 5XFAD mice was associated with a pronounced reduction of previously

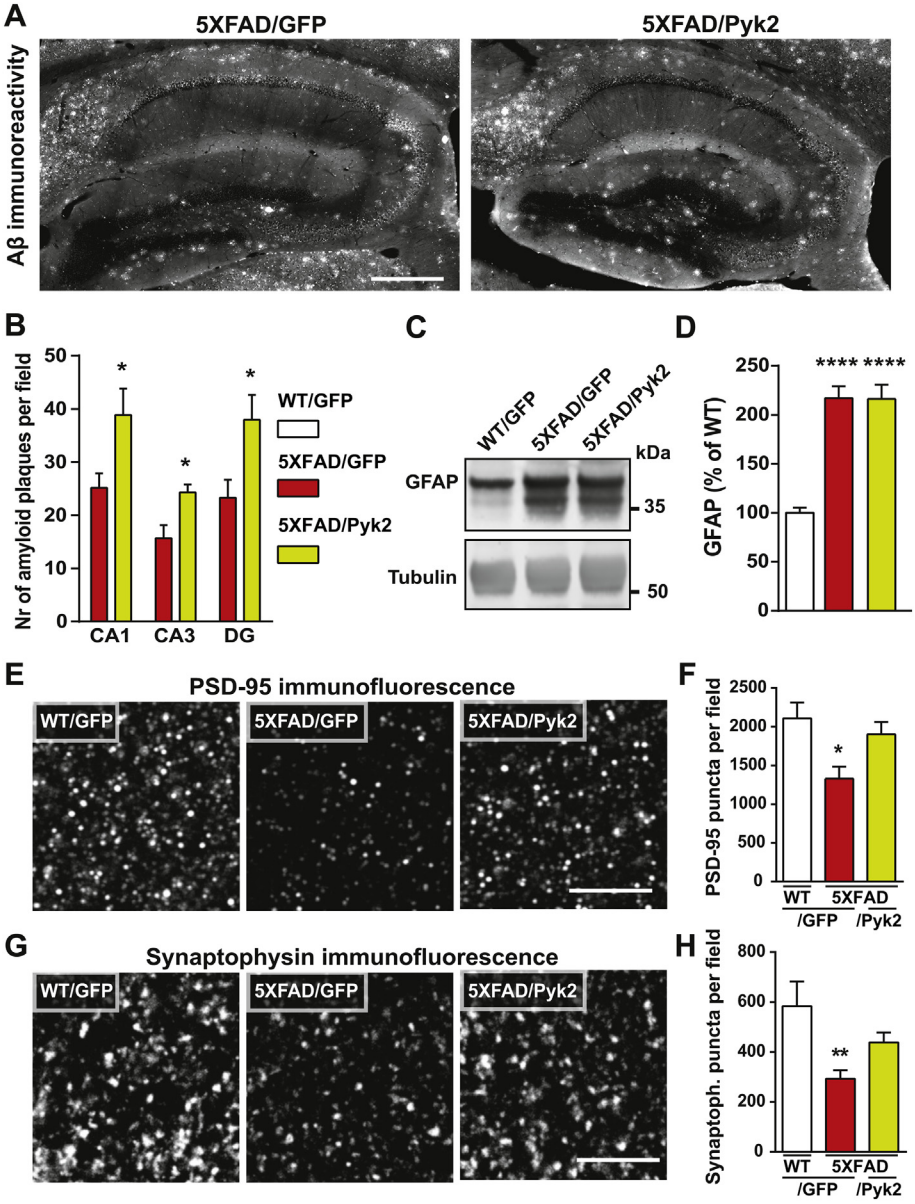

Fig. 6. Neuropathology in 5XFAD mice overexpressing Pyk2 in the hippocampus. (A) Aβ immunofluorescence microscopy imaging in the dorsal hippocampus of 8-month WT and 5XFAD mice injected with AAV expressing GFP without or with Pyk2, as indicted, as in Fig. 3 (stitched pictures). Scale bar 500 μm. (B) Quantification of Aβ-positive plaques in CA1, CA3 and DG of 5XFAD/GFP and 5XFAD/Pyk2 mice (n = 8–11 mice per group). Unpaired *t*-test, CA1 $t_{17} = 2.6$, $p = 0.02$, CA3 $t_{17} = 2.73$, $p = 0.014$, DG $t_{17} = 2.6$, $p = 0.02$. (C) Immunoblotting for GFAP and tubulin as a loading control in the hippocampus of WT/GFP, 5XFAD/GFP and 5XFAD/Pyk2 mice. (D) Densitometric quantification of results as in (C). One-way ANOVA $F_{(2, 18)} = 28.8$, $p < 10^{-4}$. Holm-Sidak's test vs WT/GFP, **** $p < 10^{-4}$. Data are means + SEM (6–9 mice per group). (E) Confocal image of PSD-95 immunofluorescence in CA1 *stratum radiatum* of 8-month WT or 5XFAD mice injected in the hippocampus with AAV expressing GFP without or with Pyk2, as indicted, as in Fig. 3. Scale bar 10 μm. (F) Quantification of the number of PSD-95-positive puncta per field as in (E), $n = 4–8$ mice per group. Kruskal-Wallis test, $p = 0.025$, post-hoc Dunn's test, * $p < 0.05$. (G) Synaptophysin immunofluorescence, as in (E). Scale bar 5 μm. (H) Quantification of the number of synaptophysin-positive puncta per field as in (G), n = 4–8 mice per group. Kruskal-Wallis test, $p = 0.036$, post-hoc Dunn's test, * $p < 0.05$.

reported synaptic alterations (Grinan-Ferre et al., 2016; Hongpaisan et al., 2011), evidenced by the recovery of PSD-95 and synaptophysin clustering. We therefore suggest that Pyk2 functional deficit in 5XFAD mice contributes to the synaptic alterations and that its rescue is an important contribution to Pyk2-induced behavioral improvement.

One of the mechanisms possibly linking Pyk2 deficiency with synaptic dysfunction is a deficit in SFK activation. We previously reported a decreased SFK basal autophosphorylation in the hippocampus of Pyk2 knockout mice with no change in total levels of Fyn (Giralt et al., 2017). We show here that Pyk2 mutant mice display increased levels of a smaller 52-kDa form of Src. This observation is reminiscent of the reported cleavage of Src by calpain, a Ca^{2+}-activated protease, which generates a ~52 kDa protein lacking the N-terminal myristoylation site (Hossain et al., 2013). This truncated Src is generated in vivo following ischemia and has neurotoxic properties (Hossain et al., 2013). In 5XFAD mice although modifications of full-length Src were not detected, the 52-kDa fragment was increased, and Pyk2 overexpression corrected this alteration, possibly alleviating a toxic effect. It can be therefore hypothesized that this Src fragment could contribute to the impairments in 5XFAD mice. The mechanisms leading to the putative cleavage of Src in Pyk2 mutant and 5XFAD mice are not known and will require further exploration.

Our work reveals the multiple roles that SFKs appear to have in AD models. On the one hand, several studies showed that Fyn inhibition either genetically (Lambert et al., 1998; Pena et al., 2010) (but see (Minami et al., 2012)) or using pharmacological inhibition of Fyn (Kaufman et al., 2015; Smith et al., 2018) improves their phenotype, possibly in relation with a contribution of Fyn to Tau pathology at the somatodendritic level (Kaufman et al., 2015; Li & Gotz, 2017; Ittner et al., 2010). On the other hand, our results indicate that a deficit in SFK activation, possibly at the synaptic level, may also contribute to functional deficits in Pyk2 mutant mice and in 5XFAD mice. A toxic Src breakdown product may have an additional negative role. Thus Pyk2 through its capacity to recruit and activate SFKs in response to neuronal activity is strategically located to modulate the balance between their various implications. Importantly, this role of Pyk2 deficit in 5XFAD mice phenotype fully agrees with the observation that inhibition of STEP, a phosphatase active on Pyk2 (Xu et al., 2012), increases Pyk2 phosphorylation and improves the behavior of 3xTg-AD mice (Xu et al., 2014).

The complexity of the role of Pyk2 and SFKs in the context of AD is also illustrated by their possible contribution to amyloidogenesis. SFKs have been reported to contribute to Aβ increase production (Dunning

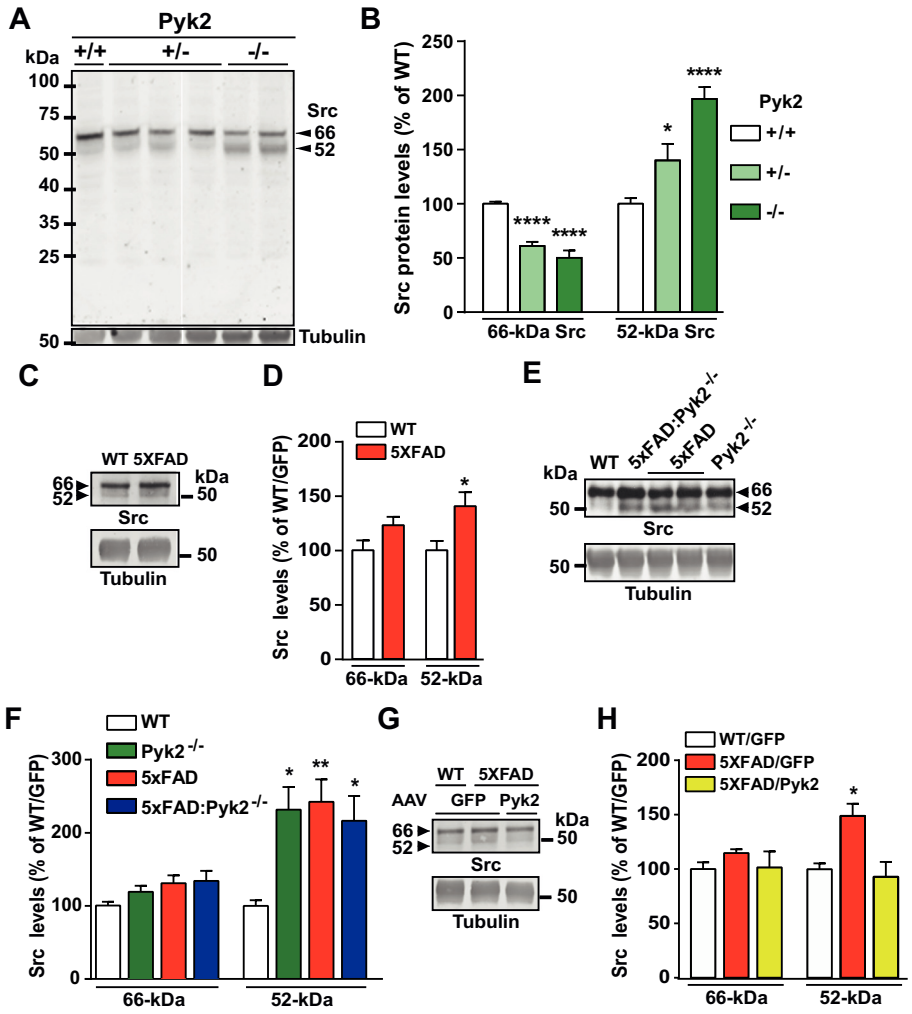

Fig. 7. Src alterations in hippocampus of Pyk2−/− and 5XFAD mice. (A) Immunoblotting for Src (antibody reacting with the C-terminus) and tubulin as a loading control in the hippocampus of $Pyk2^{+/+}$, $Pyk2^{+/-}$ and $Pyk2^{-/-}$ mice. The position of full-length (66 kDa) and cleaved (52 kDa) Src is indicated. (B) Densitometric quantification of results as in (A), n = 6–11 mice per group. One-way ANOVA 66-kDa Src $F_{(2,\ 25)} = 35.6$, $p < 10^{-4}$, 52-kDa Src $F_{(2,\ 25)} = 12.2$, $p = 0.0002$, post-hoc Holm-Sidak's test vs $Pyk2^{+/+}$, * $p < 0.05$, **** $p < 10^{-4}$. (C) Immunoblotting for Src and tubulin in WT and 5XFAD mice. (D) Densitometric quantification of Src in WT (n = 12) and 5XFAD ($n = 21$) mice. 66-kDa-Src, $t_{31} = 1.86$, 52-kDa-Src, $t_{31} = 2.21$, * $p < 0.05$. (E) Immunoblotting for Src and tubulin in $Pyk2^{-/-}$, 5XFAD and 5XFAD x $Pyk2^{-/-}$ double mutant mice, as indicated. (F) Densitometric quantification of results as in (E), n = 6–11 mice per group. One-way ANOVA 66-kDa Src, $F_{(3,\ 31)} = 1.89$, ns, 52-kDa Src, $F_{(3,\ 31)} = 4.685$, $p = 0.008$, post-hoc Holm-Sidak's test vs WT, * $p < 0.05$, ** $p < 0.01$. (G) Immunoblotting for Src and tubulin as a loading control in the hippocampus of WT/GFP, 5XFAD/GFP and 5XFAD/Pyk2 mice, as in Fig. 5. (H) Densitometric quantification of results as in (D), n = 6–15 mice per group. One-way ANOVA 66-kDa Src, $F_{(2,\ 22)} = 0.89$, $p = 0.42$, 52-kDa Src, $F_{(2,\ 20)} = 7.6$, $p = 0.0035$. Holm-Sidak's test vs WT/GFP, * $p < 0.05$. (B, C, E) data are means + SEM. (A, D) Molecular weight markers positions are indicated in kDa.

et al., 2016; Gianni et al., 2003). In our study manipulating Pyk2 levels in vivo had only moderate effects on the number plaques, which were opposite to the functional and synaptic improvements. In the absence of Pyk2, we found a decrease in amyloid plaques in CA3, whereas Pyk2 overexpression in 5XFAD mice slightly increased plaque number throughout the hippocampus. These results suggest that Pyk2 might contribute to plaque formation, possibly through a modulation of Aβ production. In this respect it is interesting to note that Pyk2- and Aβ-like immunoreactivities colocalized in the neuropil but not in plaques, indicating a proximity of Pyk2 with sites of Aβ production. In our experimental conditions, however, the changes in plaque numbers were in opposite direction to the observed behavioral improvement, suggesting they did not play a major role in the overall effect of Pyk2 in the 5XFAD model. It should be noted that although a decrease in plaque number is usually correlated with behavioral improvement in 5XFAD mice (Antonios et al., 2015; Bhattacharya et al., 2014; MacPherson et al., 2017; Aytan et al., 2013), the role of plaques by themselves in the disease is disputed (Castellani et al., 2009; Cohen et al., 2009). It is also possible that the strong effect of mutations responsible for Aβ production in 5XFAD mice partly occluded the contribution of Pyk2 to amyloid production and revealed the prominent impact of Pyk2 deficit in synaptic dysfunction.

In summary, we have explored the potential role of Pyk2 in a transgenic amyloid mouse model of AD. Our results do not support a strong positive or negative role of Pyk2 in this model of the disease. In contrast, they indicate a functional deficit of Pyk2 that is likely to contribute to synaptic alterations and to generation of a potentially toxic Src fragment. In 5XFAD mice, enhancing Pyk2 function by overexpression corrects these various alterations and has an overall beneficial effect on behavior, suggesting that restoring Pyk2 might be a useful target in AD.

Ethics approval

The use of human samples was approved by the Ethical Committee of Paris Diderot University Hospitals (CEERB Bichat University Hospital, Paris, France). Mouse experiments were approved by the Charles Darwin ethical committee.

Competing interests

The authors have no competing financial interest to declare.

Funding

This work was supported in part by Inserm, *Sorbonne-Université* (formerly *Université Pierre et Marie Curie,* UPMC, Paris-6), and grants from ANR MALZ-2013 to JH and JAG, the King Abdullah University of Science and Technology (KAUST) Office of Sponsored Research award (#OSR-2015-CRG4-2602) to SA and JAG, and Ministerio de Ciencia e Innovación (SAF2015-67474-R); MINECO/FEDER to SG. Equipment at the IFM was also supported by DIM NeRF from *Région Ile-de-France* and by the FRC/Rotary "Espoir en tête". AG is a Ramón y Cajal fellow (RYC-2016-19466).

Authors' contributions

AG designed and carried out experiments, analyzed results and wrote the manuscript, BdP, CCD, LLM, ATF, and MT carried out experiments, VD provided material, SG, SA and JH provided expertise and reagents, and participated in the design of the study and the writing of the manuscript, JAG designed and supervised the study, analyzed results and wrote the manuscript.

Acknowledgements

The Girault's lab is affiliated with the Paris School of Neuroscience (ENP) and the “Biology for Psychiatry” laboratory of excellence “Bio-Psy labex”. Imaging was carried out at the *Institut du Fer à Moulin* “Cell and Tissue Imaging facility”. We are grateful to the Banc de Teixits Neurològics (Biobanc-HC-IDIBAPS) for providing brain samples from control subjects and AD patients.

Appendix A. Supplementary data

Supplementary data to this article can be found online at https://doi.org/10.1016/j.expneurol.2018.05.020.

References

Alzheimer's Association Report, 2012. Alzheimer's disease facts and figures. Alzheimers Dement. 2012 (8), 131–168.
Antonios, G., Borgers, H., Richard, B.C., Brauss, A., Meissner, J., Weggen, S., Pena, V., Pillot, T., Davies, S.L., Bakrania, P., et al., 2015. Alzheimer therapy with an antibody against N-terminal Abeta 4-X and pyroglutamate Abeta 3-X. Sci. Rep. 5, 17338.
Avraham, S., London, R., Fu, Y., Ota, S., Hiregowdara, D., Li, J., Jiang, S., Pasztor, L.M., White, R.A., Groopman, J.E., et al., 1995. Identification and characterization of a novel related adhesion focal tyrosine kinase (RAFTK) from megakaryocytes and brain. J. Biol. Chem. 270, 27742–27751.
Aytan, N., Choi, J.K., Carreras, I., Kowall, N.W., Jenkins, B.G., Dedeoglu, A., 2013. Combination therapy in a transgenic model of Alzheimer's disease. Exp. Neurol. 250, 228–238.
Bartos, J.A., Ulrich, J.D., Li, H., Beazely, M.A., Chen, Y., Macdonald, J.F., Hell, J.W., 2010. Postsynaptic clustering and activation of Pyk2 by PSD-95. J. Neurosci. 30, 449–463.
Beecham, G.W., Hamilton, K., Naj, A.C., Martin, E.R., Huentelman, M., Myers, A.J., Corneveaux, J.J., Hardy, J., Vonsattel, J.P., Younkin, S.G., et al., 2014. Genome-wide association meta-analysis of neuropathologic features of Alzheimer's disease and related dementias. PLoS Genet. 10, e1004606.
Benilova, I., Karran, E., De Strooper, B., 2012. The toxic Abeta oligomer and Alzheimer's disease: an emperor in need of clothes. Nat. Neurosci. 15, 349–357.
Bhattacharya, S., Haertel, C., Maelicke, A., Montag, D., 2014. Galantamine slows down plaque formation and behavioral decline in the 5XFAD mouse model of Alzheimer's disease. PLoS One 9, e89454.
Castellani, R.J., Lee, H.G., Siedlak, S.L., Nunomura, A., Hayashi, T., Nakamura, M., Zhu, X., Perry, G., Smith, M.A., 2009. Reexamining Alzheimer's disease: evidence for a protective role for amyloid-beta protein precursor and amyloid-beta. J. Alzheimers Dis. 18, 447–452.
Cohen, E., Paulsson, J.F., Blinder, P., Burstyn-Cohen, T., Du, D., Estepa, G., Adame, A., Pham, H.M., Holzenberger, M., Kelly, J.W., et al., 2009. Reduced IGF-1 signaling delays age-associated proteotoxicity in mice. Cell 139, 1157–1169.
Corvol, J.C., Valjent, E., Toutant, M., Enslen, H., Irinopoulou, T., Lev, S., Herve, D., Girault, J.A., 2005. Depolarization activates ERK and proline-rich tyrosine kinase 2 (PYK2) independently in different cellular compartments in hippocampal slices. J. Biol. Chem. 280, 660–668.
Dikic, I., Tokiwa, G., Lev, S., Courtneidge, S.A., Schlessinger, J., 1996. A role for Pyk2 and Src in linking G-protein-coupled receptors with MAP kinase activation. Nature 383, 547–550.
Dourlen, P., Fernandez-Gomez, F.J., Dupont, C., Grenier-Boley, B., Bellenguez, C., Obriot, H., Caillierez, R., Sottejeau, Y., Chapuis, J., Bretteville, A., et al., 2016. Functional screening of Alzheimer risk loci identifies PTK2B as an in vivo modulator and early marker of Tau pathology. Mol. Psychiatry 22, 874–883.
Dunning, C.J., Black, H.L., Andrews, K.L., Davenport, E.C., Conboy, M., Chawla, S., Dowle, A.A., Ashford, D., Thomas, J.R., Evans, G.J., 2016. Multisite tyrosine phosphorylation of the N-terminus of Mint1/X11alpha by Src kinase regulates the trafficking of amyloid precursor protein. J. Neurochem. 137, 518–527.
Gianni, D., Zambrano, N., Bimonte, M., Minopoli, G., Mercken, L., Talamo, F., Scaloni, A., Russo, T., 2003. Platelet-derived growth factor induces the beta-gamma-secretase-mediated cleavage of Alzheimer's amyloid precursor protein through a Src-Rac-dependent pathway. J. Biol. Chem. 278, 9290–9297.
Giralt, A., Coura, R., Girault, J.A., 2016. Pyk2 is essential for astrocytes mobility following brain lesion. Glia 64, 620–634.
Giralt, A., Brito, V., Chevy, Q., Simonnet, C., Otsu, Y., Cifuentes-Díaz, C., de Pins, B., Coura, R., Alberch, J., Ginés, S., et al., 2017. Pyk2 modulates hippocampal excitatory synapses and contributes to cognitive deficits in a Huntington's disease model. Nat. Commun. 8, 15592.
Girault, J.A., Costa, A., Derkinderen, P., Studler, J.M., Toutant, M., 1999. FAK and PYK2/CAKbeta in the nervous system: a link between neuronal activity, plasticity and survival? Trends Neurosci. 22, 257–263.
Grinan-Ferre, C., Sarroca, S., Ivanova, A., Puigoriol-Illamola, D., Aguado, F., Camins, A., Sanfeliu, C., Pallas, M., 2016. Epigenetic mechanisms underlying cognitive impairment and Alzheimer disease hallmarks in 5XFAD mice. Aging (Albany NY) 8, 664–684.
Haas, L.T., Strittmatter, S.M., 2016. Oligomers of amyloid beta prevent physiological activation of the cellular prion protein-metabotropic glutamate receptor 5 complex by glutamate in Alzheimer disease. J. Biol. Chem. 291, 17112–17121.
Heneka, M.T., Carson, M.J., El Khoury, J., Landreth, G.E., Brosseron, F., Feinstein, D.L., Jacobs, A.H., Wyss-Coray, T., Vitorica, J., Ransohoff, R.M., et al., 2015. Neuroinflammation in Alzheimer's disease. Lancet Neurol. 14, 388–405.
Hongpaisan, J., Sun, M.K., Alkon, D.L., 2011. PKC epsilon activation prevents synaptic loss, Abeta elevation, and cognitive deficits in Alzheimer's disease transgenic mice. J. Neurosci. 31, 630–643.
Hossain, M.I., Roulston, C.L., Kamaruddin, M.A., Chu, P.W., Ng, D.C., Dusting, G.J., Bjorge, J.D., Williamson, N.A., Fujita, D.J., Cheung, S.N., et al., 2013. A truncated fragment of Src protein kinase generated by calpain-mediated cleavage is a mediator of neuronal death in excitotoxicity. J. Biol. Chem. 288, 9696–9709.
Hsin, H., Kim, M.J., Wang, C.F., Sheng, M., 2010. Proline-rich tyrosine kinase 2 regulates hippocampal long-term depression. J. Neurosci. 30, 11983–11993.
Huang, Y., Lu, W., Ali, D.W., Pelkey, K.A., Pitcher, G.M., Lu, Y.M., Aoto, H., Roder, J.C., Sasaki, T., Salter, M.W., MacDonald, J.F., 2001. CAKbeta/Pyk2 kinase is a signaling link for induction of long-term potentiation in CA1 hippocampus. Neuron 29, 485–496.
Ittner, L.M., Ke, Y.D., Delerue, F., Bi, M., Gladbach, A., van Eersel, J., Wolfing, H., Chieng, B.C., Christie, M.J., Napier, I.A., et al., 2010. Dendritic function of tau mediates amyloid-beta toxicity in Alzheimer's disease mouse models. Cell 142, 387–397.
Jiao, B., Liu, X., Zhou, L., Wang, M.H., Zhou, Y., Xiao, T., Zhang, W., Sun, R., Waye, M.M., Tang, B., Shen, L., 2015. Polygenic analysis of late-onset Alzheimer's disease from mainland China. PLoS One 10, e0144898.
Kaufman, A.C., Salazar, S.V., Haas, L.T., Yang, J., Kostylev, M.A., Jeng, A.T., Robinson, S.A., Gunther, E.C., van Dyck, C.H., Nygaard, H.B., Strittmatter, S.M., 2015. Fyn inhibition rescues established memory and synapse loss in Alzheimer mice. Ann. Neurol. 77, 953–971.
Lambert, M.P., Barlow, A.K., Chromy, B.A., Edwards, C., Freed, R., Liosatos, M., Morgan, T.E., Rozovsky, I., Trommer, B., Viola, K.L., et al., 1998. Diffusible, nonfibrillar ligands derived from Abeta1-42 are potent central nervous system neurotoxins. Proc. Natl. Acad. Sci. U. S. A. 95, 6448–6453.
Lambert, J.C., Ibrahim-Verbaas, C.A., Harold, D., Naj, A.C., Sims, R., Bellenguez, C., DeStafano, A.L., Bis, J.C., Beecham, G.W., Grenier-Boley, B., et al., 2013. Meta-analysis of 74, 046 individuals identifies 11 new susceptibility loci for Alzheimer's disease. Nat. Genet. 45, 1452–1458.
Lauren, J., Gimbel, D.A., Nygaard, H.B., Gilbert, J.W., Strittmatter, S.M., 2009. Cellular prion protein mediates impairment of synaptic plasticity by amyloid-beta oligomers. Nature 457, 1128–1132.
Lev, S., Moreno, H., Martinez, R., Canoll, P., Peles, E., Musacchio, J.M., Plowman, G.D., Rudy, B., Schlessinger, J., 1995. Protein tyrosine kinase PYK2 involved in ca(2+)-induced regulation of ion channel and MAP kinase functions. Nature 376, 737–745.
Li, C., Gotz, J., 2017. Somatodendritic accumulation of Tau in Alzheimer's disease is promoted by Fyn-mediated local protein translation. EMBO J. 36, 3120–3138.
Lipinski, C.A., Loftus, J.C., 2010. Targeting Pyk2 for therapeutic intervention. Expert Opin. Ther. Targets 14, 95–108.
MacPherson, K.P., Sompol, P., Kannarkat, G.T., Chang, J., Sniffen, L., Wildner, M.E., Norris, C.M., Tansey, M.G., 2017. Peripheral administration of the soluble TNF inhibitor XPro1595 modifies brain immune cell profiles, decreases beta-amyloid plaque load, and rescues impaired long-term potentiation in 5xFAD mice. Neurobiol. Dis. 102, 81–95.
Mandelkow, E.M., Mandelkow, E., 2012. Biochemistry and cell biology of tau protein in neurofibrillary degeneration. Cold Spring Harb. Perspect. Med. 2, a006247.
Manders, E.M.M., Verbeek, F.J., Aten, J.A., 1992. Measurement of colocalization of objects in dual-color confocal images. J. Microsc. 169, 375–382.
McKhann, G., Drachman, D., Folstein, M., Katzman, R., Price, D., Stadlan, E.M., 1984. Clinical diagnosis of Alzheimer's disease: report of the NINCDS-ADRDA Work Group under the auspices of Department of Health and Human Services Task Force on Alzheimer's Disease. Neurology 34, 939–944.
Menegon, A., Burgaya, F., Baudot, P., Dunlap, D.D., Girault, J.A., Valtorta, F., 1999. FAK + and PYK2/CAKbeta, two related tyrosine kinases highly expressed in the central nervous system: similarities and differences in the expression pattern. Eur. J. Neurosci. 11, 3777–3788.
Minami, S.S., Clifford, T.G., Hoe, H.S., Matsuoka, Y., Rebeck, G.W., 2012. Fyn knockdown increases Abeta, decreases phospho-tau, and worsens spatial learning in 3xTg-AD mice. Neurobiol. Aging 33, 825 e815–824.
Mucke, L., Selkoe, D.J., 2012. Neurotoxicity of amyloid beta-protein: synaptic and network dysfunction. Cold Spring Harb. Perspect. Med. 2, a006338.
Nettiksimmons, J., Tranah, G., Evans, D.S., Yokoyama, J.S., Yaffe, K., 2016. Gene-based aggregate SNP associations between candidate AD genes and cognitive decline. Age (Dordr.) 38, 41.
Oakley, H., Cole, S.L., Logan, S., Maus, E., Shao, P., Craft, J., Guillozet-Bongaarts, A., Ohno, M., Disterhoft, J., Van Eldik, L., et al., 2006. Intraneuronal beta-amyloid aggregates, neurodegeneration, and neuron loss in transgenic mice with five familial Alzheimer's disease mutations: potential factors in amyloid plaque formation. J.

Neurosci. 26, 10129–10140.
Paquet, C., Mouton-Liger, F., Meurs, E.F., Mazot, P., Bouras, C., Pradier, L., Gray, F., Hugon, J., 2012. The PKR activator PACT is induced by Abeta: involvement in Alzheimer's disease. Brain Pathol. 22, 219–229.
Park, S.Y., Avraham, H.K., Avraham, S., 2004. RAFTK/Pyk2 activation is mediated by trans-acting autophosphorylation in a Src-independent manner. J. Biol. Chem. 279, 33315–33322.
Pena, F., Ordaz, B., Balleza-Tapia, H., Bernal-Pedraza, R., Marquez-Ramos, A., Carmona-Aparicio, L., Giordano, M., 2010. Beta-amyloid protein (25-35) disrupts hippocampal network activity: role of Fyn-kinase. Hippocampus 20, 78–96.
Pozueta, J., Lefort, R., Shelanski, M.L., 2013. Synaptic changes in Alzheimer's disease and its models. Neuroscience 251, 51–65.
Prange, O., Wong, T.P., Gerrow, K., Wang, Y.T., El-Husseini, A., 2004. A balance between excitatory and inhibitory synapses is controlled by PSD-95 and neuroligin. Proc. Natl. Acad. Sci. U. S. A. 101, 13915–13920.
Sasaki, H., Nagura, K., Ishino, M., Tobioka, H., Kotani, K., Sasaki, T., 1995. Cloning and characterization of cell adhesion kinase beta, a novel protein-tyrosine kinase of the focal adhesion kinase subfamily. J. Biol. Chem. 270, 21206–21219.
Schneider, F., Baldauf, K., Wetzel, W., Reymann, K.G., 2014. Behavioral and EEG changes in male 5xFAD mice. Physiol. Behav. 135, 25–33.
Shao, C.Y., Mirra, S.S., Sait, H.B., Sacktor, T.C., Sigurdsson, E.M., 2011. Postsynaptic degeneration as revealed by PSD-95 reduction occurs after advanced Abeta and tau pathology in transgenic mouse models of Alzheimer's disease. Acta Neuropathol. 122, 285–292.
Sheng, M., Sabatini, B.L., Sudhof, T.C., 2012. Synapses and Alzheimer's disease. Cold Spring Harb. Perspect. Biol. 4.
Siciliano, J.C., Toutant, M., Derkinderen, P., Sasaki, T., Girault, J.A., 1996. Differential regulation of proline-rich tyrosine kinase 2/cell adhesion kinase beta (PYK2/CAKbeta) and pp125(FAK) by glutamate and depolarization in rat hippocampus. J. Biol. Chem. 271, 28942–28946.
Smith, L.M., Zhu, R., Strittmatter, S.M., 2018. Disease-modifying benefit of Fyn blockade persists after washout in mouse Alzheimer's model. Neuropharmacology 130, 54–61.
Tu, S., Okamoto, S., Lipton, S.A., Xu, H., 2014. Oligomeric Abeta-induced synaptic dysfunction in Alzheimer's disease. Mol. Neurodegener. 9, 48.
Vinters, H.V., 2015. Emerging concepts in Alzheimer's disease. Annu. Rev. Pathol. 10, 291–319.
Walkiewicz, K.W., Girault, J.A., Arold, S.T., 2015. How to awaken your nanomachines: site-specific activation of focal adhesion kinases through ligand interactions. Prog. Biophys. Mol. Biol. 119, 60–71.
Wang, X., Lopez, O.L., Sweet, R.A., Becker, J.T., DeKosky, S.T., Barmada, M.M., Demirci, F.Y., Kamboh, M.I., 2015. Genetic determinants of disease progression in Alzheimer's disease. J. Alzheimers Dis. 43, 649–655.
Xu, J., Kurup, P., Bartos, J.A., Patriarchi, T., Hell, J.W., Lombroso, P.J., 2012. Striatal-enriched protein-tyrosine phosphatase (STEP) regulates Pyk2 kinase activity. J. Biol. Chem. 287, 20942–20956.
Xu, J., Chatterjee, M., Baguley, T.D., Brouillette, J., Kurup, P., Ghosh, D., Kanyo, J., Zhang, Y., Seyb, K., Ononenyi, C., et al., 2014. Inhibitor of the tyrosine phosphatase STEP reverses cognitive deficits in a mouse model of Alzheimer's disease. PLoS Biol. 12, e1001923.

4. Summary of the findings and conclusions

We demonstrated here that, although Pyk2 total levels were normal, Tyr-402 phosphorylation levels reflecting its activity were reduced in the hippocampus of 5xFAD mice at 8 months of age. Accordingly, the overexpression of Pyk2 in the hippocampus of these mice which rescued autophosphorylated Pyk2 levels, improved both synaptic markers and performance in several behavioral tasks.

Pyk2 functional deficiency was associated with an increase of potentially neurotoxic Src cleavage product, which was rescued by Pyk2 overexpression. This may constitute a clue for future investigations on the molecular causes of neurodegeneration associated with AD.

Paradoxically, Pyk2 appeared to contribute to plaque formation in a still unknown mechanism. This opens again the question about the still disputed role of plaques by themselves in the pathogenicity of the disease (Castellani et al., 2009; Cohen et al., 2009).

The results of this paper however suggest that Pyk2 impairment possibly play a role in the symptoms of AD.

IV. Conditional BDNF Delivery from Astrocytes Rescues Memory Deficits, Spine Density, and Synaptic Properties in the 5xFAD Mouse Model of Alzheimer Disease.

Benoit de Pins, Carmen Cifuentes-Díaz, Amel Thamila Farah, Laura López-Molina, Enrica Montalban, Anna Sancho-Balsells, Ana López, Silvia Ginés, José María Delgado-García, Jordi Alberch, Agnès Gruart, Jean-Antoine Girault and Albert Giralt

Journal of Neuroscience
27 March 2019, 39(13):2441-2458

1. Context and objectives

Although not being directly related to Pyk2, I present here the result of a study that was led in parallel with the previous one. We used the same mouse model of AD to explore the potential benefit of astrocyte-targeted delivery of BDNF in this disease.

BDNF is critical for neuron survival and synaptic plasticity (Lynch et al., 2008) and has been shown to be reduced early in the course of the disease in transgenic mouse models of AD (Kaminari et al., 2017). Strategies have been proposed to deliver BDNF to counteract neurodegeneration but BDNF administration has important challenges, such as the lack of control of its release, which does not allow specific targeting to the sick tissue nor releasing the proper amount of levels, mainly considering high doses can be neurotoxic.

Here we used genetically modified mice that overexpress BDNF under the control of the GFAP promoter (pGFAP-BDNF) (Giralt et al., 2010). In these mice, BDNF production and delivery are increased in neuropathological conditions accompanied by astrogliosis, an increase in the number of astrocytes due to the destruction of nearby neurons. We crossed these mice with the 5xFAD transgenic mouse model of AD and compared, with 5xFAD mice, the development of molecular and behavioral alterations.

2. Contribution to the work

In this work, I greatly contributed to cell and tissue imaging and analysis.

3. Article

Development/Plasticity/Repair

Conditional BDNF Delivery from Astrocytes Rescues Memory Deficits, Spine Density, and Synaptic Properties in the 5xFAD Mouse Model of Alzheimer Disease

Benoit de Pins,[1,2,3] Carmen Cifuentes-Díaz,[1,2,3] Amel Thamila Farah,[1,2,3] Laura López-Molina,[4,5,6] Enrica Montalban,[1,2,3] Anna Sancho-Balsells,[4,5,6] Ana López,[4,5,6] Silvia Ginés,[4,5,6] José María Delgado-García,[7] Jordi Alberch,[4,5,6] Agnès Gruart,[7] Jean-Antoine Girault,[1,2,3] and Albert Giralt[4,5,6]

[1]Institut National de la Santé et de la Recherche Médicale Unité Mixte de Recherche-S 839, Paris, France, [2]Sorbonne Université, Faculty of Sciences and Engineering, Paris 75005, France, [3]Institut du Fer à Moulin, Paris F-75005, France, [4]Departament de Biomedicina, Facultat de Medicina, Institut de Neurociències, Universitat de Barcelona, Barcelona, 08036 Spain, [5]Institut d'Investigacions Biomèdiques August Pi i Sunyer, Barcelona 08036, Spain, [6]Centro de Investigación Biomédica en Red sobre Enfermedades Neurodegenerativas, Madrid 28031, Spain, and [7]Division of Neurosciences, Pablo de Olavide University, Seville 41013, Spain

It has been well documented that neurotrophins, including brain-derived neurotrophic factor (BDNF), are severely affected in Alzheimer's disease (AD), but their administration faces a myriad of technical challenges. Here we took advantage of the early astrogliosis observed in an amyloid mouse model of AD (5xFAD) and used it as an internal sensor to administer BDNF conditionally and locally. We first demonstrate the relevance of BDNF release from astrocytes by evaluating the effects of coculturing WT neurons and BDNF-deficient astrocytes. Next, we crossed 5xFAD mice with pGFAP:BDNF mice (only males were used) to create 5xFAD mice that overexpress BDNF when and where astrogliosis is initiated (5xF:pGB mice). We evaluated the behavioral phenotype of these mice. We first found that BDNF from astrocytes is crucial for dendrite outgrowth and spine number in cultured WT neurons. Double-mutant 5xF:pGB mice displayed improvements in cognitive tasks compared with 5xFAD littermates. In these mice, there was a rescue of BDNF/TrkB downstream signaling activity associated with an improvement of dendritic spine density and morphology. Clusters of synaptic markers, PSD-95 and synaptophysin, were also recovered in 5xF:pGB compared with 5xFAD mice as well as the number of presynaptic vesicles at excitatory synapses. Additionally, experimentally evoked LTP *in vivo* was increased in 5xF:pGB mice. The beneficial effects of conditional BDNF production and local delivery at the location of active neuropathology highlight the potential to use endogenous biomarkers with early onset, such as astrogliosis, as regulators of neurotrophic therapy in AD.

Key words: Alzheimer's disease; astrocytes; BDNF; long-term potentiation; memory; mice

Significance Statement

Recent evidence places astrocytes as pivotal players during synaptic plasticity and memory processes. In the present work, we first provide evidence that astrocytes are essential for neuronal morphology via BDNF release. We then crossed transgenic mice (5xFAD mice) with the transgenic pGFAP-BDNF mice, which express BDNF under the GFAP promoter. The resultant double-mutant mice 5xF:pGB mice displayed a full rescue of hippocampal BDNF loss and related signaling compared with 5xFAD mice and a significant and specific improvement in all the evaluated cognitive tasks. These improvements did not correlate with amelioration of β amyloid load or hippocampal adult neurogenesis rate but were accompanied by a dramatic recovery of structural and functional synaptic plasticity.

Introduction

Alzheimer disease (AD) is the most common form of dementia in the aging population, accounting for 60%–80% of the cases. The disease is a progressive neurodegenerative disorder characterized by the presence of extracellular amyloid plaques composed of amyloid-β (Aβ) surrounded by dystrophic neurites and neurofi-

Received Aug. 17, 2018; revised Jan. 23, 2019; accepted Jan. 25, 2019.

Author contributions: A. Gruart and A. Giralt edited the paper. S.G., J.M.D.-G., J.A., A. Gruart, J.-A.G., and A. Giralt designed research; B.d.P., C.C.-D., A.T.F., L.L.-M., E.M., A.S.-B., A.L., A. Gruart, and A. Giralt performed research; B.d.P., C.C.-D., J.M.D.-G., A. Gruart, and A. Giralt analyzed data; J.M.D.-G., J.A., A. Gruart, J.-A.G., and A. Giralt wrote the paper.

A. Giralt is a Ramón y Cajal fellow (RYC-2016-19466). The J.-A.G. laboratory was supported in part by Institut National de la Santé et de la Recherche Médicale, Sorbonne Université, Fondation pour la Recherche Médicale, and

brillary tangles (NFTs) (Alzheimer's Association, 2012). Further pathological hallmarks of the disease include inflammatory processes, synaptic and neuronal loss, cerebral atrophy, and cerebral amyloid angiopathy (Wirths and Bayer, 2012). The complex progression of neurodegeneration in AD patients results in memory impairment and decline in other cognitive abilities often combined with noncognitive symptoms, such as mood and personality changes (Alzheimer's Association, 2012).

One of the most promising therapies in AD is the use of neurotrophic factors, such as NGF or BDNF (Allen and Dawbarn, 2006). Indeed, BDNF plays important roles in neural survival and synaptic plasticity (Lynch et al., 2008). In line with this, BDNF is reduced early in the course of the disease in transgenic mouse models of AD (Kaminari et al., 2017), and TrkB deletion accelerates and worsens the phenotype of these mice (Devi and Ohno, 2015), whereas TrkB agonists improve it (Devi and Ohno, 2012; Zhang et al., 2014). Alterations in the BDNF-TrkB system could account for memory deficits, neuronal cell death, and synaptic plasticity alterations observed in AD (von Bohlen Und Halbach and von Bohlen Und Halbach, 2018). BDNF-TrkB-associated downstream molecular pathways include PLCγ, ERK, and Akt signaling. Interestingly, dysregulation of these pathways is able to modulate the levels of essential synaptic proteins, such as postsynaptic density-95 (PSD-95) and synaptophysin (Tartaglia et al., 2001; Robinet and Pellerin, 2011; Parsons et al., 2014; Yoshii and Constantine-Paton, 2014; Zhang et al., 2017), which in turn are altered in AD models (Yuki et al., 2014; Dorostkar et al., 2015). Finally, altered BDNF-TrkB pathway could also result in deficient adult neurogenesis in the hippocampus (Waterhouse et al., 2012), which could in turn contribute to the memory loss in AD (Toda and Gage, 2018).

Several strategies have been proposed to produce/deliver BDNF to counteract neurodegeneration. However, all of them are associated with deleterious secondary effects or are not satisfactory enough (Lindvall et al., 2004). Important drawbacks are the risk of tumorigenesis, insufficient cell survival in cell therapy, or invasiveness of some delivery systems, as well as the lack of control on the production and delivery of the neurotrophin because too high levels can be neurotoxic (Martínez-Serrano and Björklund, 1996; Rubio et al., 1999; Pineda et al., 2007; Kells et al., 2008). Furthermore, these strategies do not target specifically the diseased tissue or deliver appropriate levels of the neurotrophin depending on the severity of the symptoms.

Astrocytes in AD are reactive at early stages, have impaired Ca^{2+} signaling, regulate β-amyloid burden, and influence synaptic plasticity alterations also contributing to excitotoxicity (Acosta et al., 2017). Interestingly, astrocytes normally express the BDNF protein, although at lesser levels than neurons (Saha et al., 2006; Giralt et al., 2010; Fulmer et al., 2014; Hong et al., 2016). Therefore, engineered astrocytes could be good candidates to release neurotrophic factors. Indeed, genetically modified astrocytes have been used with positive results in some models of neurodegeneration (Yoshimoto et al., 1995; Carpenter et al., 1997). This strategy could be relevant for AD as the numbers of reactive astrocytes increases gradually as the disease progress (Song et al., 2015). Moreover, astrogliosis has been shown to be one of the specific hallmarks of disease progression in mouse models of AD (Oakley et al., 2006). Because of this increase in astrocytes, and the fact that astrogliosis leads to increased GFAP promoter activation, one would predict that the use of this promoter as a self-regulator would provide neurotrophic support at the time when it is critically needed. Therefore, here we sought to investigate the role of BDNF from astrocytes in normal neuronal dendritic growth and whether this could be exploited to design advanced and conditional therapies in AD models.

Materials and Methods

Astrocyte/neuron cocultures. Primary astrocyte cultures were obtained from P1 to P3 $BDNF^{+/+}$ and $BDNF^{-/-}$ mouse pups (Ernfors et al., 1994) (IMSR catalog #EM:00247, RRID:IMSR_EM:00247) by hippocampal dissections. Extracted tissue was dissociated and placed in 25 cm^2 flasks in a MEM 1× conditioned media NM-15 (20% FBS; Invitrogen; D-glucose 90 mM) with L-glutamine and Earle's salts (Invitrogen) and placed in an incubator at 37°C with 5% CO_2. A tail biopsy was obtained from each pup for genotyping. After two passages, cultures were purified by agitating in a shaker during 10 min at 400 rpm. Medium with undesired floating cells was replaced, and flasks were placed in an incubator for 2 h at 37°C. Next, flasks were agitated again for 16–18 h at 250 rpm. Finally, medium with floating cells was replaced with new medium. Once astrocytes reached confluence, they were seeded in 24-well plaques and allowed to reach confluence. Then, 1 d before the addition of hippocampal neurons, astrocyte cultures were preincubated with neurobasal medium (Invitrogen) containing 1 ml per 50 ml of B27 supplement (Invitrogen) and 50 ml of GlutaMAX (100×; Invitrogen). Hippocampal neurons were prepared from E17 C57BL/6J mouse embryos (pregnant mice from Charles River). The neuronal cell suspension was low density seeded in the 24-well plaques already containing astrocytes (10,000 cells cm^2). Cocultures were fixed at 6 DIV or 20 DIV after neuron seeding to evaluate the number of dendrites and dendritic spines, respectively. Cultures collected at 20 DIV were transfected 48 h before cell fixation with Transfectine (Bio-Rad) following the manufacturer's instructions. Cells were transfected with a previously described construct expressing GFP (Giralt et al., 2017) to allow dendritic spine density counting in isolated hippocampal neurons.

qPCR assay. Total RNA from astrocyte cultures (see above) and HEK293 cells was extracted using the RNeasy Lipid Tissue Mini Kit (QIAGEN). Total RNA (500 ng) was used to synthesize cDNA using random primers with the High Capacity cDNA Reverse Transcription Kit (Applied Biosystems). The cDNA synthesis was performed at 37°C for 120 min in a final volume of 20 μl according to the manufacturer's instructions. The cDNA was then analyzed by qPCR using the following gene expression assays: 18S (NR_003286; Integrated DNA Technologies) and BDNF (NM_001048139; Integrated DNA Technologies). RT-PCR was performed in 12 μl of final volume on 96-well plates using the Premix Ex Taq (Probe qPCR; Takara Biotechnology). Reactions included the following: Segment 1, 1 cycle of 30 s at 95°C; Segment 2, 40 cycles of 5 s at 95°C and 20 s at 60°C. All RT-PCR assays were performed in duplicate and repeated for at least three independent experiments. To provide negative controls and exclude contamination by genomic DNA, the RT was omitted in the cDNA synthesis step, and the samples were subjected to the PCR in the same manner with each TaqMan Gene Expression Assay. The RT-PCR data were analyzed using the MxProTM qPCR analysis software version 3.0 (Stratagene). Quantification was performed with the Comparative Quantitation Analysis program of this software and using the 18S gene expression as internal loading control.

Immunocytochemistry and neuronal morphology assessment. Fixed cells were permeabilized in Triton X-100 0.5% (v/v) for 10 min, and then blocking was performed with 10 g/L BSA in PBS for 1 h. Cells were incubated with a mouse monoclonal antibody for MAP2 (1:800, Sigma-

Bio-Psy (Biology for Psychiatry) laboratory of excellence. The cell and tissue imaging facility at the IFM benefited from support of Espoir en Tête/Fondation pour la Recherche sur le Cerveau, Région Ile-de-France, and Institut National de la Santé et de la Recherche Médicale. A. Gruart and J.M.D.-G. were supported by MINECO Grant BFU2017-82375-R and Tatiana Pérez de Guzman el Bueno Foundation. J.A. was supported by Grants SAF2017-88076 (Ministerio de Ciencia, Innovación y Universidades) and Marató TV3 Foundation. S.G. was supported by Grant SAF2015-67474-R (Ministerio de Ciencia, Innovación y Universidades). We thank María Sánchez Enciso and José M. González Martín for help in animal handling and care during *in vivo* experiments.

The authors declare no competing financial interests.

Correspondence should be addressed to Albert Giralt at albertgiralt@ub.edu.

https://doi.org/10.1523/JNEUROSCI.2121-18.2019

 0270-6474/19/392442-18$15.00/0

Aldrich catalog #M1406, RRID:AB_477171) at 4°C overnight. After three washes with PBS, cells were incubated with the corresponding Cy3-coupled fluorescent secondary antibody (1:200; Jackson ImmunoResearch Laboratories catalog #715-165-150, RRID:AB_2340813). After washing twice with PBS, the coverslips were mounted with Vectashield (Vector Laboratories). Hippocampal neuron staining was observed with a confocal SP5-II (see below).

Mouse lines. For this study, we used the transgenic mouse line 5xFAD (MMRRC catalog #034840-JAX, RRID:MMRRC_034840-JAX). 5xFAD mice overexpress the 695-amino acid isoform of the human amyloid precursor protein (APP695) carrying the Swedish, London, and Florida mutations under the control of the murine Thy-1 promoter. In addition, they express human presenilin-1 (PSEN-1) carrying the M146L/L286V mutation, also under the control of the murine Thy-1 promoter (Oakley et al., 2006). We crossed 5xFAD mice with the previously generated pGFAP-BDNF mice (Giralt et al., 2010) to obtain 5xFAD mice that overexpress BDNF under the GFAP promoter (5xF:pGB mice). For astrocyte cultures, we used P1-P3 $BDNF^{+/+}$ and $BDNF^{-/-}$ mice (Ernfors et al., 1994) (IMSR catalog #EM:00247, RRID:IMSR_EM:00247). Mouse genotyping for pGFAP-BDNF, 5xFAD, and $BDNF^{-/-}$ mice was performed from a tail biopsy, as previously described (Oakley et al., 2006; Giralt et al., 2009, 2010) by Charles River services. The animals were housed with access to food and water *ad libitum* in a colony room kept at 19°C–22°C and 40%–60% humidity, under a 12:12 h light/dark cycle. Experimental animals were all males and used at 8 months of age and in accordance with the ethical guidelines (Declaration of Helsinki and NIH Publication no. 85-23, revised 1985, European Community Guidelines, and French Agriculture and Forestry Ministry guidelines for handling animals, decree 87849, license A 75-05-22) and approved by the local ethical committee.

Western blot. Mice were deeply anesthetized in a CO_2 chamber, the brains quickly removed, hippocampus dissected out, frozen in dry ice, and stored at −80°C until use. Briefly, tissue was sonicated in 250 ml of lysis buffer (PBS, 1% Nonidet P40 [v/v], 1 g/L SDS, 5 g/L sodium deoxycholate, protease inhibitors mixture 1:1000 [Sigma-Aldrich], and 2 g/L sodium orthovanadate) and centrifuged at 12,000 rpm for 20 min, and the pellet was discarded. Proteins (15 mg) from hippocampal or cortical tissue were analyzed by SDS-PAGE (7.5% acrylamide, w/v) and transferred to nitrocellulose membranes (Millipore). Membranes were blocked in TBS-T (150 mM NaCl, 20 mM Tris-HCl, pH 7.5, 0.05% [v/v] Tween 20) with 50 g/L nonfat dry milk and 50 g/L BSA. Immunoblots were probed with anti-GFAP (1:1000, Agilent Technologies catalog #Z0334, RRID:AB_10013382), anti-BDNF (1:1000, Santa Cruz Biotechnology catalog #sc-546, RRID:AB_630940), anti-Akt (1:1000, Cell Signaling Technology catalog #9272, RRID:AB_329827), anti-ERK (1:1000, Cell Signaling Technology catalog #4695, RRID:AB_390779), anti-PLCγ (1:1000, Cell Signaling Technology catalog #2822, RRID:AB_2163702), anti-phosphor-Akt (1:1000, Cell Signaling Technology catalog #4056, RRID:AB_331163), anti-phosphor-ERK (1:1000, Cell Signaling Technology catalog #9101, RRID:AB_331646), anti-phosphor-PLCγ (1:1000, Cell Signaling Technology catalog #2821, RRID:AB_330855), or anti-α-tubulin (1:10,000, Sigma-Aldrich catalog #T9026, RRID:AB_477593). All blots were incubated overnight at 4°C with shaking, in the presence of the primary antibody in PBS with 0.2 g/L sodium azide. After several washes in TBS-T, blots were incubated with anti-rabbit IgG IRdye800CW-coupled or anti-mouse IgG IRdye700DX-coupled antibodies (1/2000, Rockland Immunochemicals) and signal detected by the Odyssey system (Li-Cor) and analyzed using ImageJ.

Golgi staining, spine counting, and morphological analysis. Fresh brain hemispheres were processed following the Golgi-Cox method as described previously (Giralt et al., 2017). Essentially, mouse brain hemispheres were incubated in the dark for 21 d in filtered dye solution (10 g L^{-1} $K_2Cr_2O_7$, 10 g L^{-1} $HgCl_2$, and 8 g L^{-1} K_2CrO_4). The tissue was then washed 3 × 2 min in water and 30 min in 90% ethanol (EtOH) (v/v); 200 μm sections were cut in 70% EtOH on a vibratome (Leica Microsystems) and washed in water for 5 min. Next, they were reduced in 16% (v/v) ammonia solution for 1 h before washing in water for 2 min and fixation in 10 g l^{-1} $Na_2S_2O_3$ for 7 min. After a 2 min final wash in water, sections were mounted on superfrost coverslips, dehydrated for 3 min in 50%, then 70%, 80%, and 100% EtOH, incubated for 2 × 5 min in a 2:1 isopropanol:EtOH mixture, followed by 1 × 5 min in pure isopropanol and 2 × 5 min in xylol. Bright-field images of Golgi-impregnated stratum radiatum dendrites from hippocampal CA1 pyramidal neurons were captured with a Nikon DXM 1200F digital camera attached to a Nikon Eclipse E600 light microscope (100× oil objective). Only fully impregnated pyramidal neurons with their soma found entirely within the thickness of the section were used. Image *z* stacks were taken every 0.2 mm and at 1024 × 1024 pixel resolution, yielding an image with pixel dimensions of 49.25 × 49.25 mm. *Z* stacks were deconvolved using the Huygens software (Scientific Volume Imaging) to improve voxel resolution and to reduce optical aberration along the *z* axis. The total number of spines counting and their morphology categorization were performed by using the NeuronStudio freeware (NeuronStudio, RRID:SCR_013798). At least 60 dendrites per group from at least 5 mice per genotype were counted. For spine morphology analysis, we analyzed between 2000 and 3000 spines (500 spines per mouse from 5 mice per group). Each spine was categorized as having or not having a neck. Spines were defined as stubby if they did not contain a visible neck. Spines with necks were separated into thin and mushroom spines based on head width. Filopodia, defined as protrusions 1.5 μm in length without a head, were excluded from the analysis of spine subtypes. Spines with heads less than the average width were categorized as thin, and those with heads greater than the average width were categorized as mushroom as previously described (Giralt et al., 2017). From these measures, the percentage of the various spine types was obtained. Picture acquisition and subsequent analysis were performed independently by two investigators blind to genotypes and results were then pooled. Overall differences between the results were minor.

Tissue fixation and immunofluorescence. Animals were deeply anesthetized with pentobarbital (60 mg/kg) and intracardially perfused with a 4% (w/v) PFA solution in 0.12 M sodium phosphate, pH 7.2. Brains were removed and postfixed overnight in the same solution, cryoprotected with 300 g/L sucrose in 20 mM sodium phosphate, pH 7.5, 150 mM NaCl (PBS) with 0.2 g/L sodium azide, and frozen in dry ice-cooled isopentane. Serial coronal sections (30 μm) obtained with a cryostat were processed for immunohistochemistry as free-floating sections. They were washed three times in PBS, permeabilized 15 min by shaking at room temperature with PBS containing (v/v) 0.3% Triton X-100 and 3% normal goat serum (Pierce Biotechnology). After three washes, brain sections were incubated overnight by shaking at 4°C with antibodies for anti-PSD-95 (1:500, Millipore catalog #MAB1596, RRID:AB_2092365), anti-synaptophysin (1:500, Synaptic Systems catalog #101 011, RRID:AB_887824), or anti-phosphor-$TrkB^{Y816}$ (1:350, Abcam catalog #ab75173, RRID:AB_1281172) in PBS with 0.2 g/L sodium azide. After incubation with primary antibody, sections were washed three times and then placed 2 h on a shaking incubator at room temperature with the subtype-specific fluorescent secondary AlexaFluor-488 anti-rabbit (1:250, Thermo Fisher Scientific catalog #A32731, RRID:AB_2633280) or anti-mouse 555 (1:250, Thermo Fisher Scientific catalog #A32727, RRID:AB_2633276). No signal was detected in control sections incubated in the absence of the primary antibody.

Confocal imaging and analysis. Dorsal hippocampus in fixed tissue and fixed primary cultures were imaged using a Leica Microsystems Confocal SP5-II at the Institut du Fer à Moulin Cell and Tissue Imaging facility, with a 40× or 63× numerical aperture lens with 5× digital zoom and standard (1 Airy disc) pinhole (1 AU) and frame averaging (3 frames per *z* step) were held constant throughout the study. Confocal *z* stacks were taken every 0.2 μm for *in vitro* experiments and every 2 μm for *in vivo* experiments, and at 1024 × 1024 pixel resolution. The *in vitro* Sholl analysis, the dendritic spine counting, the *in vivo* analysis of PSD95- and synaptophysin-positive clusters, and the colocalization of double-labeled PSD-95/phospho-$TrkB^{Y816}$-positive clusters were analyzed with the freeware ImageJ (ImageJ, RRID:SCR_003070). Briefly, for *in vivo* imaging analysis, for each mouse, at least 3 slices of 30 μm containing dorsal hippocampal tissue were analyzed. Up to 3 representative images, from CA1-stratum radiatum layer, were obtained from each slice. For the *in vitro* analysis, in the Sholl experiment, we evaluated 45–60 neurons, all of them MAP2-positive from 3 different cultures. To estimate the density of

dendritic spines, 31–41 dendrites from MAP2-positive neurons (1 or 2 dendrites/neuron) from 3 different cultures were counted.

Electronic microscopy. Mice were transcardially perfused with a solution containing 4% PFA and 0.1% glutaraldehyde made up of 0.1 M PB, pH 7.4. Brains were then immersed in the same fixative for 12 h at 4°C. Tissue blocks containing the hippocampus were dissected and washed in 0.1 M PB, cryoprotected in 100 and 200 g/L sucrose in 0.1 M PB, and freeze-thawed in isopentane and liquid nitrogen. Samples were postfixed in 2.5% glutaraldehyde made up of 0.1 M phosphate buffer for 20 min, washed and treated with 2% osmium tetroxide in PB for 20 min. They were dehydrated in a series of ethanol and flat embedded in epoxy resin (EPON 812 Polysciences). After polymerization, blocks from the CA1 region were cut at 70 nm thickness using an ultramicrotome (Ultracut E Leica Microsystems). Sections were cut with a diamond knife, picked up on formvar-coated 200 mesh nickel grids. For etching resin and remove osmium, sections were treated with saturated aqueous sodium periodate ($NaIO_4$). They were then observed with a CM-100 electron microscope (Philips) at the Institut du Fer à Moulin Cell and Tissue Imaging facility. Digital images were obtained with a CCD camera (Gatan Orius). To test method specificity of the immunostaining procedure, the primary antibody was omitted. In ultrathin sections, the density of synaptic vesicles was calculated by counting the number of vesicles within a defined presynaptic area. The area of postsynaptic densities was also evaluated. All these calculations were performed by using the ImageJ.

Behavioral tests. To analyze mouse anxiety, we used the elevated plus maze paradigm. Briefly, the plus maze was made of plastic and consisted of two opposing 30 × 8 cm open arms, and two opposing 30 × 8 cm arms enclosed by 15-cm-high walls. The maze was raised 50 cm from the floor and lit by dim light. Each mouse was placed in the central square of the raised plus maze, facing an open arm, and its behavior was scored for 5 min. At the end of each trial, any defecation was removed, and the apparatus was wiped with 30% ethanol. We recorded the time spent in the open arms, which normally correlates with low levels of anxiety. Animals were tracked and recorded with SMART junior software (Panlab).

To check spontaneous locomotor activity, we used the open field. Briefly, the apparatus consisted of a white square arena measuring 40 × 40 × 40 cm in length, width, and height, respectively. Dim light intensity was 60 lux throughout the arena. Animals were placed in the arena center and allowed to explore freely for 30 min. Spontaneous locomotor activity was measured. At the end of each trial, any defecation was removed, and the apparatus was wiped with 30% ethanol. Animals were tracked and recorded with SMART junior software (Panlab).

The novelty-suppressed feeding (NSF) measured the mice aversion to eat in a novel environment. This test assesses stress-induced anxiety by measuring the latency of an animal to approach and eat a familiar food in an aversive environment. For this task, mice were food-restricted for a period of 24 h. After food restriction, the animals were placed in a large, brightly lit, open field. A piece of white filter paper was placed in the center of the arena with a small piece of rodent chow. The time to approach and eat a pellet of food located in the center of the arena was measured and used to evaluate anxiety-like behavior.

The forced swimming test was used to evaluate behavioral despair. Animals were subjected to a 6 min trial during which they were forced to swim in an acrylic glass cylinder (35 cm of height × 20 cm of diameter) filled with water, and from which they could not escape. The time that the test animal spent in the cylinder without making any movements beyond those required to keep its head above water was measured.

The spontaneous alternation performance was tested using a symmetrical Y-maze. Each mouse was placed in the center of the Y-maze and could explore freely through the maze during an 8 min session. The sequence and total number of arms entered were recorded. Arm entry was complete when the hindpaws of the mouse had been completely placed in the arm. Percentage alternation is the number of triads containing entries into all three arms divided by the maximum possible alternations (the total number of arms entered − 2) × 100. As the reentry into the same arm was not counted for analysis, the chance performance level in this task was 50% in the choice between the arm mice visited more recently (nonalternation) and the other arm visited less recently (alternation).

The novel object location memory task evaluates spatial memory and is based on the ability of mice to recognize when a familiar object has been relocated. Exploration took place in an open-top arena with quadrangular form (45 × 45 cm). The light intensity was 40 lux throughout the arena. Mice were first habituated to the arena in the absence of objects (1 d, 30 min). Some distal cues were placed throughout the procedure. On the third day during the acquisition phase, mice could explore two duplicate objects (A1 and A2), which were placed close to the far corners of the arena for 10 min. After a delay of 24 h, one object was placed in the diagonally opposite corner. Thus, both objects in the phase were equally familiar, but one was in a new location. The position of the new object was counterbalanced between mice. Animals were tracked and recorded with SMART Junior software (Panlab).

For the passive avoidance (light-dark) paradigm, we conducted the experiments in a 2-compartment box, where 1 compartment was dimly lit (20 lux) and preferable to a rodent and the other compartment was brightly lit (200 lux); both chambers were connected by a door (5 cm × 5 cm). During training, mice were placed into the aversive brightly lit compartment; and upon the entry into the preferred dimly lit compartment (with all 4 paws inside the dark chamber), mice were exposed to a mild foot shock (2 s foot shock, 1 mA intensity). The latency of mice to enter into the dark chamber was recorded. Twenty seconds after receiving the foot shock, mice were returned to the home cage until testing. After 24 h (long-term memory), animals were tested for retention. In the retention test, mice were returned to the brightly lit compartment again, and the latency to enter the shock paired compartment (dark chamber) was measured (retention or recall latency). Ten minutes was used as a time cutoff in the retention test. The animals that learned the task would avoid the location previously paired with the aversive stimulus and showed a greater latency to enter it.

In vivo *electrophysiological recordings.* Animals were anesthetized with 0.8%–1.5% isoflurane (Astra Zeneca) delivered via a special mask (Cibertec). Once anesthetized, animals were implanted with bipolar stimulating electrodes aimed at the right Schaffer collateral-commissural pathway of the dorsal hippocampus (2 mm lateral and 1.5 mm posterior to bregma; depth from brain surface, 1.0–1.5 mm) (Paxinos and Franklin, 2013) and with a recording electrode aimed at the ipsilateral stratum radiatum underneath the CA1 area (1.2 mm lateral and 2.2 mm posterior to bregma; depth from brain surface, 1.0–1.5 mm) (Paxinos and Franklin, 2013). Stimulating and recording electrodes were made of 50 μm, Teflon-coated tungsten wire (Advent Research Materials). The final location of the recording electrode in the CA1 area was determined following the field potential depth profile evoked by paired (40 ms interval) pulses presented to the ipsilateral Schaffer collateral pathway (Gruart et al., 2006). Two bare silver wires were affixed to the skull as ground. Electrodes were connected to a 6-pin socket (RS-Amidata) that was latterly fixed with dental cement to the cranial bone. After surgery, each animal was kept in an independent cage with free access to food and water for the rest of the experiment.

Recording sessions were started 1 week after surgery. Electrophysiological recordings were performed using Grass P511 differential amplifiers with a bandwidth of 0.1–10 kHz (Grass-Telefactor). Electrical stimulation was provided by a CS-220 stimulator across CS-220 isolation units (Cibertec). For input/output curves, monosynaptic fEPSPs were evoked in the CA1 area by single (100 μs, square, and negative-positive) pulses applied to Schaffer collaterals. These pulses were presented at increasing intensities ranging from 20 to 400 μA, in steps of 20 μA. To avoid interactions with the preceding stimuli, an interval of 30 s was allowed between each pair of pulses (Madroñal et al., 2007).

For the characterization of the paired-pulse facilitation at the CA3-CA1 synapse, we used the same type of pulses indicated above, but presented in pairs at increasing interpulse intervals (10, 20, 40, 100, 200, and 500 ms). For each animal, the stimulus intensity was set at 30%–40% of the intensity necessary for evoking a maximum fEPSP response (Gureviciene et al., 2004; Gruart et al., 2006). Intervals between pairs of pulses were set at ~30 s, to avoid unwanted interactions evoked by presynaptic or postsynaptic mechanisms.

LTP experiments were also performed in alert behaving animals. fEPSPs were evoked at the CA3-CA1 synapse for 15 min before LTP

induction. For this, single pulses were presented at a rate of 3 per min. The stimulus intensity was set at 30%–40% of the intensity necessary for evoking a maximum fEPSP response, namely, well below the threshold for evoking a population spike (Gruart et al., 2006; Madroñal et al., 2007). For LTP induction, each animal was subjected to a high-frequency stimulation (HFS) protocol consisting of five 200 Hz, 100 ms trains of pulses at a rate of 1 per second. This protocol was presented six times, at intervals of 1 min. The HFS protocol used here (combining low intensity values and a total of 600 electric shocks) allowed us to evoke LTP lasting >2–3 d, without the appearance of abnormal spikes in EEG recordings and/or overt epileptic seizures (Madroñal et al., 2009). Following the HFS session, animals were stimulated again with single pulses applied for 60 min at the same rate of 3 per min. Additional 30 min recordings of fEPSPs were repeated for 3 d following the HFS session.

Experimental design and statistical analysis. All data are expressed as mean ± SEM. Statistical analysis was performed using the unpaired two-sided Student's *t* test (95% confidence), one-way ANOVA with the Tukey's as *post hoc* tests, or two-way ANOVA with the Bonferroni's *post hoc* test as appropriate and indicated in the figure legends. Values of $p < 0.05$ were considered statistically significant.

All experiments in this study were blinded and randomized. All mice bred for the experiments were used for preplanned experiments and randomized to experimental groups. Visibly sick animals were excluded before data collection and analysis. Data were collected, processed, and analyzed randomly. The experimental design and handling of mice were identical across experiments. Littermates were used as controls with multiple litters (3–5) examined per experiments. All mice were bred in the Institut du Fer à Moulin Animal Facility.

Results

Astrocytes BDNF production regulates cultured hippocampal neurons morphology and dendritic spine density

Although BDNF is mainly produced in neurons, it is also localized in astrocytes (Saha et al., 2006; Giralt et al., 2010). We verified that this was the case in our experimental conditions using RT-PCR to detect BDNF transcripts (3745 ± 1125% increase, $p = 0.0468$) (Fig. 1*A*). However, the precise role of BDNF from astrocytes in neuronal function is still unclear. We evaluated whether BDNF derived from astrocytes was physiologically relevant for neuronal dendrite morphology. We cultured primary astrocytes from mouse pups lacking the BDNF gene ($BDNF^{-/-}$ pups) or WT littermates as a control ($BDNF^{+/+}$ pups). After astrocyte 100% confluence, we seeded primary WT neurons at E17 on the top of the astrocyte monolayer (Fig. 1*B*). Then, some astrocyte-neuron cocultures were fixed at 6 DIV to evaluate the morphological characteristics of the imaged neurons stained for MAP2 by using the Sholl analysis (Fig. 1*C*). The results indicated that the number of intersections in WT neurons grown on $BDNF^{-/-}$ astrocytes were reduced compared with WT neurons on $BDNF^{+/+}$ astrocytes (Fig. 1*D*). We fixed other astrocyte-neuron cocultures at 20 DIV, transfected 48 h before fixation with a GFP-expressing construct (see Material and Methods). We thus were able to evaluate spine density in isolated MAP2-positive neurons. We observed that the number of spines in WT neurons cocultured with $BDNF^{-/-}$ astrocytes was decreased compared with neurons cocultured with $BDNF^{+/+}$ astrocytes (−0.2555 ± 0.046 decrease, $p < 0.0001$) (Fig. 1*E*). These results reveal a crucial role of BDNF released from astrocytes in the modulation of neurons, particularly in dendrite and spine development, in coculture conditions. They provide a rationale for the use of astrocytes to overexpress BDNF in brain locations with high levels of pathology in AD.

Generation and characterization of the 5xFAD mice overexpressing BDNF under the GFAP promoter

To test the potential role of astrocyte-derived BDNF in an AD mouse model, we then took advantage of mice that overexpress BDNF under the control of the GFAP promoter (pGFAP-BDNF mice) (Giralt et al., 2010). In these mice, BDNF production and delivery are increased in neuropathological conditions accompanied by astrogliosis (Giralt et al., 2010, 2011). We crossed pGFAP-BDNF mice with the 5xFAD transgenic mouse model of AD to create 5xF:pGB mice. The 5xFAD mice develop severe amyloid pathology and associated astrogliosis at 1.5–2 months of age, before the onset of the cognitive deficits (observed at 4 months of age) (Oakley et al., 2006). A significant decrease in BDNF levels is also observed in 5xFAD mice (Hongpaisan et al., 2011). We predicted that this decrease would be prevented in the 5xF:pGB double-transgenic mice. To test this hypothesis, we analyzed BDNF hippocampal levels in WT, pGFAP-BDNF, 5xFAD, and 5xF:pGB mice at 8 months of age, when their phenotype is clear. At this age, astrogliosis was obvious throughout the hippocampus, as evidenced by immunofluorescence (Fig. 2*A*) and Western blot (146 ± 18 increase, $p < 0.001$) (Fig. 2*B*,*C*). As expected, BDNF levels were reduced (−58 ± 17 decrease, $p < 0.05$) in the hippocampus of 5xFAD mice compared with WT mice (Fig. 2*B*,*D*). Interestingly, BDNF levels in the hippocampus of 5xF:pGB mice were undistinguishable from those in WT mice, indicating a full recovery of BDNF protein levels in this group of mice. We next studied whether such recovery correlated with an improvement in the BNDF-TrkB downstream signaling. We performed Western blot analyses to measure total and phosphorylated levels of ERK, Akt and, PLCγ, which are key proteins in the three major signaling pathways downstream of BDNF-TrkB (Gupta et al., 2013). Total levels of ERK, Akt, and PLCγ were similar in all the four groups of mice (Fig. 2*E*). Phosphorylation levels of ERK threonine/tyirosine 202/204 and PLCγ tyrosine 783 were decreased in the hippocampus of 5xFAD mice ($ERK^{T202/Y204}$: −69 ± 8.5 decrease, $p < 0.001$; $PLC\gamma^{Y783}$: −40 ± 17 decrease, $p < 0.05$), whereas Akt serine 308 phosphorylation was not significantly affected (Fig. 2*E*,*F*). In 5xF:pGB mice, phosphorylation of ERK and PLCγ was like that in WT mice. Interestingly, in 5xF:pGB mice, the phosphorylated levels of ERK and PLCγ were similar to those in WT mice. No changes in these phosphoproteins were observed in the WT mice expressing the pGFAP-BDNF transgene (Fig. 2*E*,*F*), supporting the specificity of the astrocyte-dependent BDNF expression. These results indicate that the 5xF:pGB mice develop a significant astrogliosis, which, in turn, induces an overproduction of BDNF from astrocytes preventing the loss of BDNF/TrkB function due to the effects of APP695 and PSEN-1 transgenes. Furthermore, normalization of BDNF levels in the 5xF:pGB mice was accompanied by a complete restoration of BDNF-TrkB downstream signaling.

Rescue of memory alterations in 5xF:pGB mice

The 5xFAD transgenic mice display a strong phenotype with a relatively fast time course compared with other AD mouse models. At 8 months of age, they display decreased locomotor activity, altered performance in the elevated plus maze, and memory deficits in hippocampal-related tasks, such as the Y-maze and the novel object location (Oakley et al., 2006; Devi and Ohno, 2015; Schneider et al., 2015; Grinan-Ferre et al., 2016). The passive avoidance, which is also affected in other mouse models of AD (Webster et al., 2014), has not been reported in 5xFAD, to our knowledge. Furthermore, AD patients exhibit high comorbidity with depressive symptoms (Webster

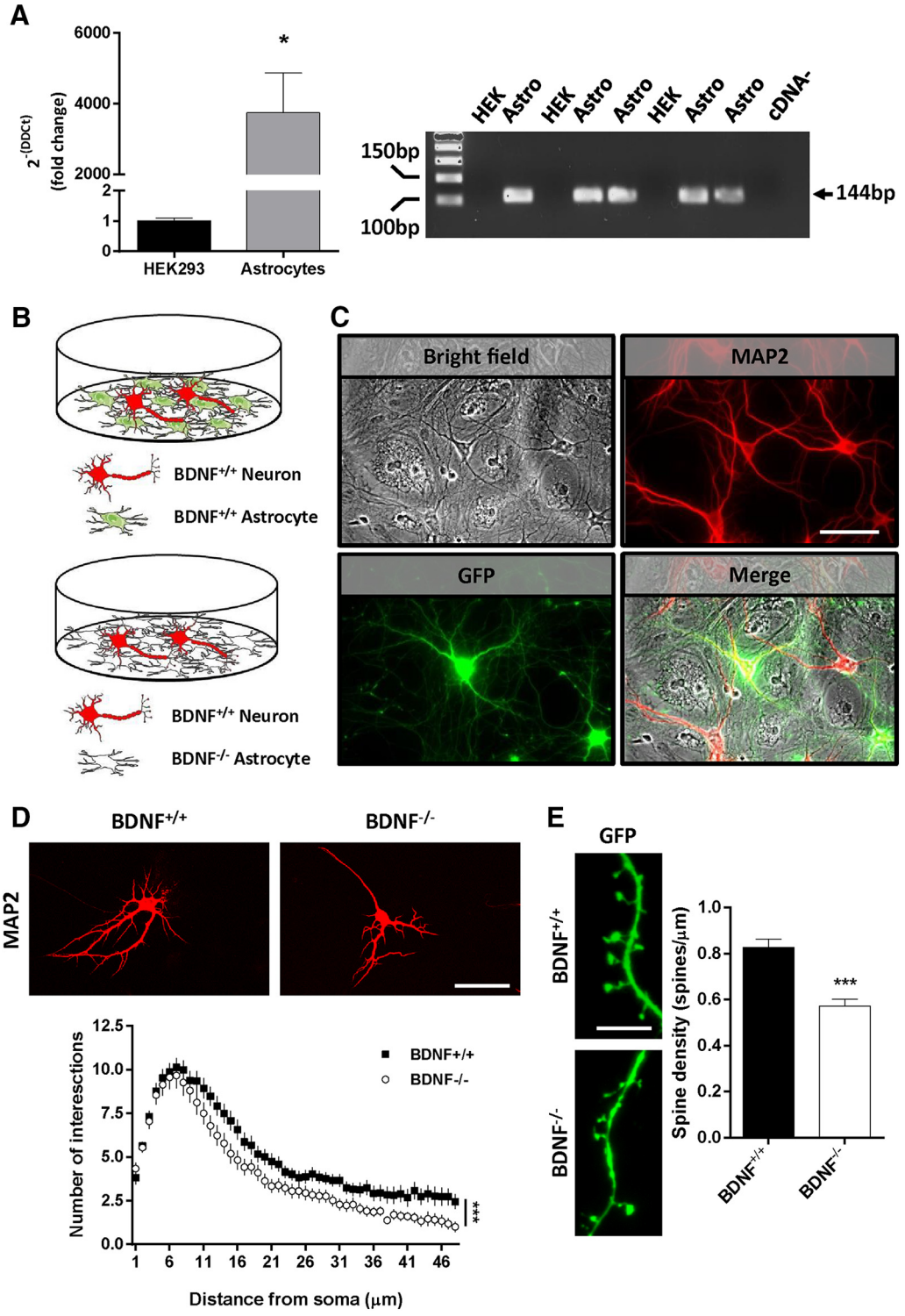

Figure 1. BDNF regulates dendrites and spine number *in vitro*. ***A***, Left, BDNF mRNA levels were determined in WT astrocytes. HEK293 cells were used as negative control (Student's *t* test, $t = 2.496$, df $= 6$; $p < 0.05$; $n = 3$–5). Right, Representative agarose gel. Arrow indicates the molecular weight of the BDNF transcript detected at 114 bp. ***B***, The experimental design is depicted illustrating the two *in vitro* conditions: BDNF $^{+/+}$ astrocyte monolayer cocultured with WT neurons (i.e., BDNF $^{+/+}$) and BDNF $^{-/-}$ astrocyte monolayer cocultured with WT neurons (i.e., BDNF $^{-/-}$). ***C***, Representative images showing the bright-field allowing visualization of the astrocyte monolayer plus some cocultured neurons on the top, hippocampal neurons stained for MAP2 (red), and transfected MAP2-positive neurons transfected with a plasmid coding GFP (green). ***D***, Representative MAP2 images obtained by confocal microscopy from cocultured astrocytes and neurons (top). Scale bar, 40 μm. Bottom, Sholl analysis from MAP2-positive neurons (two-way ANOVA analysis; group effect, $F_{(1,307)} = 81.7$, $p < 0.001$). ***E***, Spine density was studied using GFP fluorescence in transfected MAP2-positive neurons (left). Quantification of spine density (right) is shown (Student's *t* test, $t = 5.462$, df $= 70$; $p < 0.001$). Data are mean ± SEM. ***D***, $n = 45$ and 60 MAP2-positive neurons/group from 3 different experiments. ***E***, $n = 31$ and 41 *dendrites/group from 3 different experiments. ***$p < 0.001$ as compared to BDNF $^{+/+}$ mice.

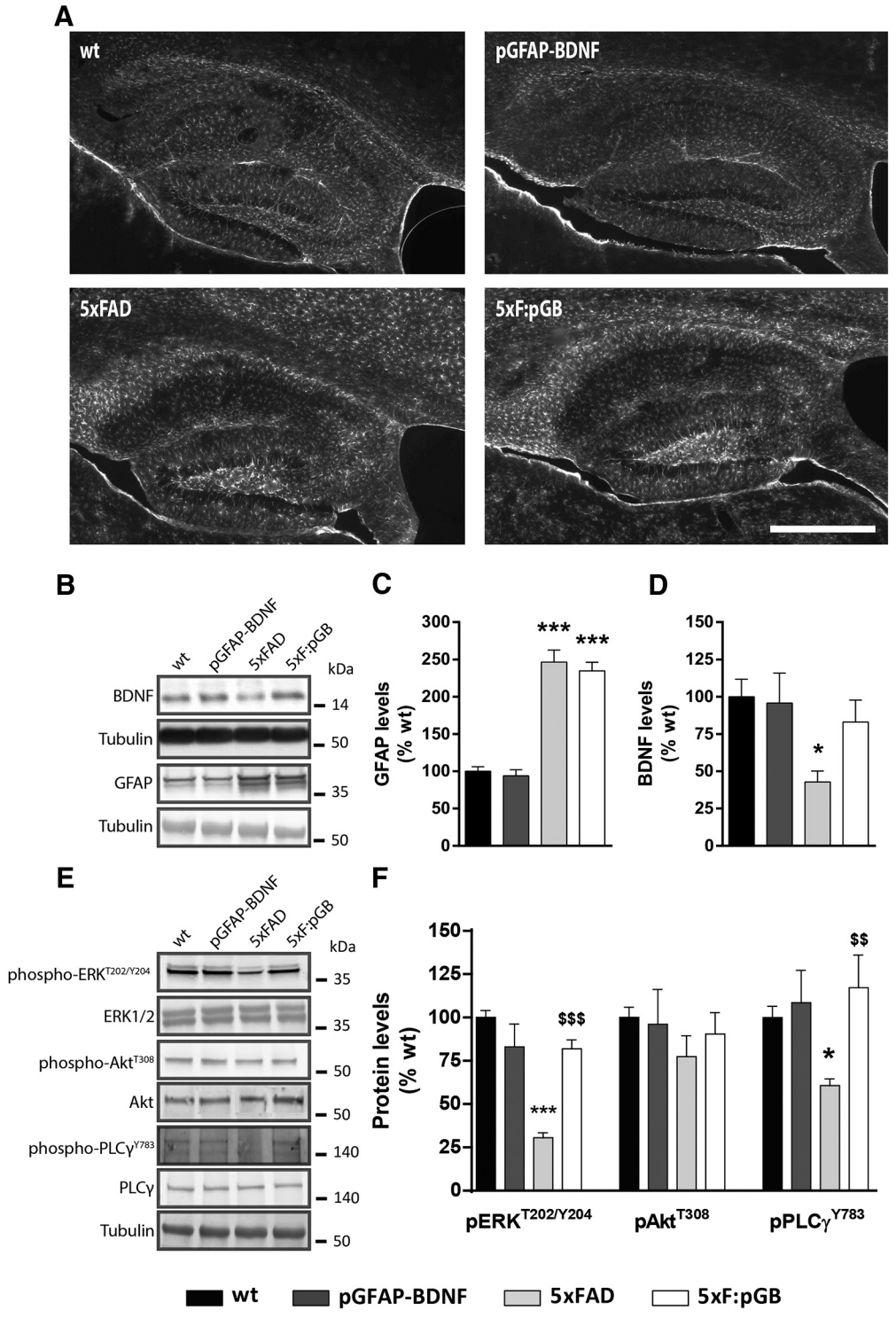

Figure 2. Validation of the 5xF:pGB model. Crossing 5xFAD mice with pGFAP-BDNF mice resulted in four genotypes, namely, WT, pGFAP-BDNF, 5xFAD, and the double-mutant 5xF:pGB mice. We evaluated these mice at 8 months of age. ***A***, GFAP immunofluorescence microscopy imaging in the dorsal hippocampus of 8-month-old WT, pGFAP-BDNF, 5xFAD, and 5xF:pGB mice. Scale bar, 500 μm. ***B***, Immunoblotting for BDNF, GFAP, and tubulin as a loading control in the hippocampus of 8-month-old WT, pGFAP-BDNF, 5xFAD, and 5xF:pGB mice. ***C***, Densitometry quantification of BDNF levels as in ***B***. ***D***, Densitometry quantification of GFAP levels as in ***B***. One-way ANOVA, BDNF genotype effect: $F_{(3,24)} = 4.403$, $p = 0.0103$; GFAP genotype effect: $F_{(3,25)} = 41.18$, $p < 0.001$. Data were normalized to tubulin for each sample and expressed as a percentage of WT. ***E***, Immunoblotting for pAkt^{ser308}, pERK$^{T402/Y404}$, pPLCγ^{Y783}, ERK, Akt, and PLCγ and tubulin as a loading control in the hippocampus of 8-month-old WT, pGFAP-BDNF, 5xFAD, and 5xF:pGB mice. ***F***, Densitometry quantification of pAkt^{ser308}, pERK$^{T402/Y404}$, and pPLCγ^{Y783} levels as in ***E***. One-way ANOVA, pERK$^{T402/Y404}$ genotype effect: $F_{(3,28)} = 29.14$, $p < 0.001$; pAkt^{ser308} genotype effect: $F_{(3,26)} = 0.5666$, $p < 0.646$; pPLCγ^{Y783} genotype effect: $F_{(3,28)} = 5.251$, $p < 0.0053$. Data were normalized to the corresponding total levels of ERK, Akt, and PLCγ for each sample and expressed as a percentage of WT. Data are mean ± SEM. ***C–F***, Tukey's test as a *post hoc* analysis was used. $^{*}p < 0.05$; $^{***}p < 0.001$; compared with WT mice. $^{\$\$}p < 0.01$; $^{\$\$\$}p < 0.001$; compared with 5xFAD mice. ***B***, ***E***, Molecular weight markers positions are indicated in kDa. ***C–F***, $n = 6$–11/group.

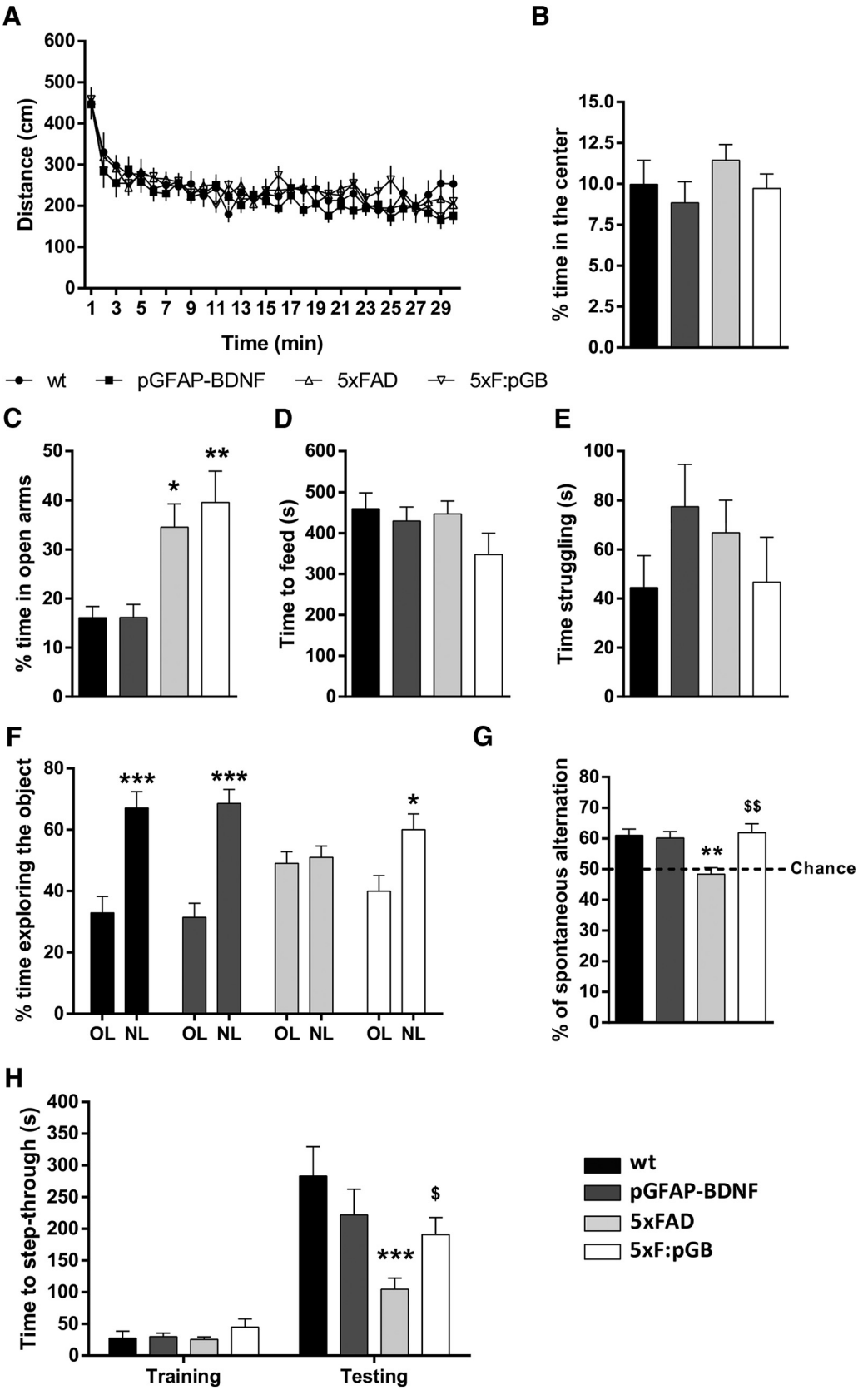

Figure 3. Characterization of 5xF:pGB mice. ***A***, WT, pGFAP-BDNF, 5xFAD, and mice at 8 months of age were subjected to a comprehensive behavioral characterization. In the open field, (***A***) locomotor activity and (***B***) time spent in the center of the arena were monitored for 30 min in WT, pGFAP-BDNF, 5xFAD, and 5xF:pGB mice. Locomotor activity, two-way ANOVA, genotype effect: $F_{(3,116)} = 1.2654, p = 0.2899$; time in center, one-way ANOVA: $F_{(3,80)} = 1.009, p = 0.3934$. ***C***, In the plus maze, the time spent in the open arms was monitored for 5 min in the four groups of mice. One-way ANOVA: $F_{(3,77)} = 6.907, p = 0.005$. ***D***, In the NSF test, the time to reach and eat the pellet in the center of the arena was evaluated in the four genotypes. One-way ANOVA: $F_{(3,76)} = 1.467$, $p = 0.2303$. ***E***, In the forced swimming test, the immobility time was evaluated during the last 4 min of the 6 min trial in all groups. One-way ANOVA: $F_{(3,80)} = 0.9903, p = 0.417$. ***F***, In the novel object location test, spatial long-term memory was evaluated 24 h after a training trial as the percentage of time exploring the object placed in a new location (NL) (*Figure legend continues.*)

et al., 2014) and depressive behaviors have been reported at least in one mouse model of AD (Filali et al., 2009).

To evaluate the potential beneficial effects of reactive astrocytes-targeted BDNF expression in 5XFAD mice, we characterized all these behavioral parameters. We first evaluated the basal locomotor activity and anxiety in the open field in WT, pGFAP-BDNF, 5xFAD, and 5xF:pGB mice. All groups of mice displayed a similar initial habituation and comparable levels of locomotor activity (Fig. 3*A*) and time spent in the center (Fig. 3*B*). Next, we investigated anxiety by performing the elevated plus maze and the NSF tests. In the elevated plus maze, both 5xFAD mice (18.45 ± 6.6 increase, $p < 0.05$) and 5xF:pGB mice (23.50 ± 6.92 increase, $p < 0.01$) spent more time in the open arms than WT and pGFAP-BDNF mice (Fig. 3*C*), but there were no differences between 5xFAD and 5xF:pGB mice. In the NSF, the mice from all four groups showed similar latencies to feed in the aggressive environment (Fig. 3*D*). We also tested the behavioral resignation in the four groups of mice by performing the forced swimming test. The amount of time during which the mice were swimming trying to escape from the water was similar in all mice, independently of their genotype (Fig. 3*E*). These results indicate that 5XFAD mice displayed only minor anxiety or mood-related alterations, with only an apparent decrease in anxiety in the elevated plus maze, which was not modified by BDNF overexpression.

We next studied memory in these mice. First, we evaluated spatial memory in the novel object location test, which is based on the ability of rodents to recognize when a familiar object has been relocated. After habituation to the open field arena, mice were trained in the presence of 2 identical objects (A1 and A2), and spatial memory was assessed 24 h later by displacing one of the two objects. 5xFAD mice exhibited a significantly lower preference for the displaced object compared (1.877 ± 5.64, not significant between old location and new location) with either WT or pGFAP-BDNF mice (Fig. 3*F*). The spatial memory deficit was prevented in the 5xF:pGB mice (Fig. 3*F*). Next, mice were tested in the spontaneous alternation Y-maze paradigm that assesses spatial working memory (Lalonde, 2002). The spontaneous alternation behavior relies on the tendency of mice to enter a less recently visited arm compared with the other one. WT and pGFAP-BDNF mice displayed a spontaneous alternation, whereas the arm choice was decreased to 50% (chance levels) in the 5xFAD mice (−12.70 ± 3.27 decrease, $p < 0.01$) (Fig. 3*G*). The spontaneous alternation was restored to WT control levels in 5xF:pGB mice. Finally, we examined associative memory in the passive avoidance task, based on the association formed between an electrical foot shock and a spontaneously preferred specific environmental context (darkness vs light). Latency to step-through during the training session was similar between genotypes (Fig. 3*H*). However, in the testing session, although all genotypes showed a significant increase in the latency to enter the dark compartment 24 h after receiving an electrical shock (wt: 255 ± 39 increase, $p < 0.001$; pGFAP-BDNF: 192 ± 32 increase, $p < 0.001$; 5xFAD 78.8 ± 28 increase, $p < 0.05$; 5xF:pGB: 145 ± 35 increase $p < 0.001$), this latency was shorter in mutant 5xFAD mice compared with WT (−178 ± 34 decrease, $p < 0.001$) or pGFAP-BDNF mice (−117.70 ± 30 decrease, $p < 0.01$) (Fig. 3*H*). This alteration was absent in double-mutant 5xF:pGB mice (Fig. 3*H*). The results of the novel object location, spontaneous alternation, and passive avoidance tests demonstrate that targeted increased expression of BDNF prevented several memory deficits in 5xFAD mice.

Normalization of BDNF levels in double-mutant 5xF:pGB mice does not prevent plaque formation and neurogenesis deficits

To test whether the restoration of BDNF levels modulated β-amyloidosis in 8-month-old 5xFAD mice, toluidine blue staining was performed to determine the number of plaques in the hippocampus and PFC of 5xFAD and 5xF:pGB mice (Fig. 4*A*). The cortical plaque load in 5xF:pGB mice was indistinguishable from that in age-matched 5xFAD control mice. However, in the hippocampus, we detected an increase in the number of plaques in 5xF:pGB mice compared with 5xFAD mice (0.3507 ± 0.0469 increase, $p = 0.017$) (Fig. 4*B*). We hypothesized that the size of the plaques could be different between genotypes, indicating different dynamics in β-amyloidosis. To test this possibility, we characterized the plaques in the hippocampus of 5xFAD and 5xF:pGB mice by using electron microscopy (Fig. 4*C*). Ultrastructural analysis revealed that hippocampal plaques in 5xF:pGB mice were visually more compact but significantly smaller than the plaques in 5xFAD mice (−131 ± 27 decrease, $p = 0.015$) (Fig. 4*C*,*D*), supporting the hypothesis that β-amyloid accumulation in 5xF:pGB mice is different compared with that in 5xFAD mice. Because findings on hippocampal plaque quantification appeared inconsistent with memory improvements, we then evaluated the rate of newborn cells in the dentate gyrus, whose deficits have been previously reported to be associated with cognitive impairments (Moon et al., 2014). We counted the number of Ki67-positive cells in the dentate gyrus of the four groups of mice. A significant decrease in the number of newborn cells was observed in the dentate gyrus of both 5xFAD (−5 ± 1.69 decrease, $p < 0.05$) and 5xF:pGB (−5.26 ± 1.84 decrease, $p < 0.05$) mice compared with WT or pGFAP-BDNF mice (Fig. 4*E*,*F*). These data indicate that normalizing BDNF levels in 5xF:pGB mice is not enough to prevent the alterations in neurogenesis observed in 5xFAD mice.

Normalization of BDNF levels in double-mutant 5xF:pGB mice restores dendritic spines and synaptic alterations

Because BDNF normalization did not improve neuropathological hallmarks in 5xFAD mice, including astrogliosis (Fig. 2*A*–*C*), plaque number (Fig. 4*A*,*B*), and neurogenesis deficit (Fig. 4*E*,*F*), we assumed that phenotypic improvements observed in 5xF:pGB mice could be related with synaptic changes. To test this hypothesis, we performed Golgi staining in two different brain regions in all 4 genotypes at the age of 8 months to examine dendritic spine density and morphology in pyramidal neurons. We examined the cortical layer V in the PFC and the stratum radiatum of CA1. First, we observed that spine density in secondary dendrites of cortical pyramidal neurons was significantly decreased in 5xFAD mice compared with WT mice (−0.231 ± 0.034 decrease, $p < 0.001$) (Fig. 5*A*,*B*). This decrease was partially rescued in 5xF:

←

(*Figure legend continued.*) versus the time exploring the object placed in an old location (OL). Two-way ANOVA, object in a new location effect: $F_{(3,150)} = 40.80$, $p < 0.001$. Interaction effect: $F_{(3,150)} = 7.14$, $p = 0.002$. ***G***, In the Y-maze, the spontaneous alternation was measured (as triads) in an 8 min trial in all four genotypes. One-way ANOVA: $F_{(3,44)} = 7.717$, $p = 0.003$. ***H***, In the passive avoidance paradigm, the latency (seconds) to step-through was evaluated in the training trial and in the testing trial 24 h after receiving an electric shock (2 s/1 mA). One-way ANOVA: $F_{(3,126)} = 5.384$, $p = 0.0016$. Data are mean ± SEM. ***A***, ***B***, ***H***, $n = 18$–25 mice/genotype. ***G***, $n = 12$–14 mice/genotype. Tukey's *post hoc* test was used for all behavioral tasks. ***C***, ***G***, ***H***, *$p < 0.05$; **$p < 0.01$; ***$p < 0.001$; compared with WT. $^{\$}p < 0.05$; $^{\$\$}p < 0.01$; compared with 5xFAD. ***F***, *$p < 0.05$; ***$p < 0.001$; compared with percentage of time exploring the object in an old location (OL).

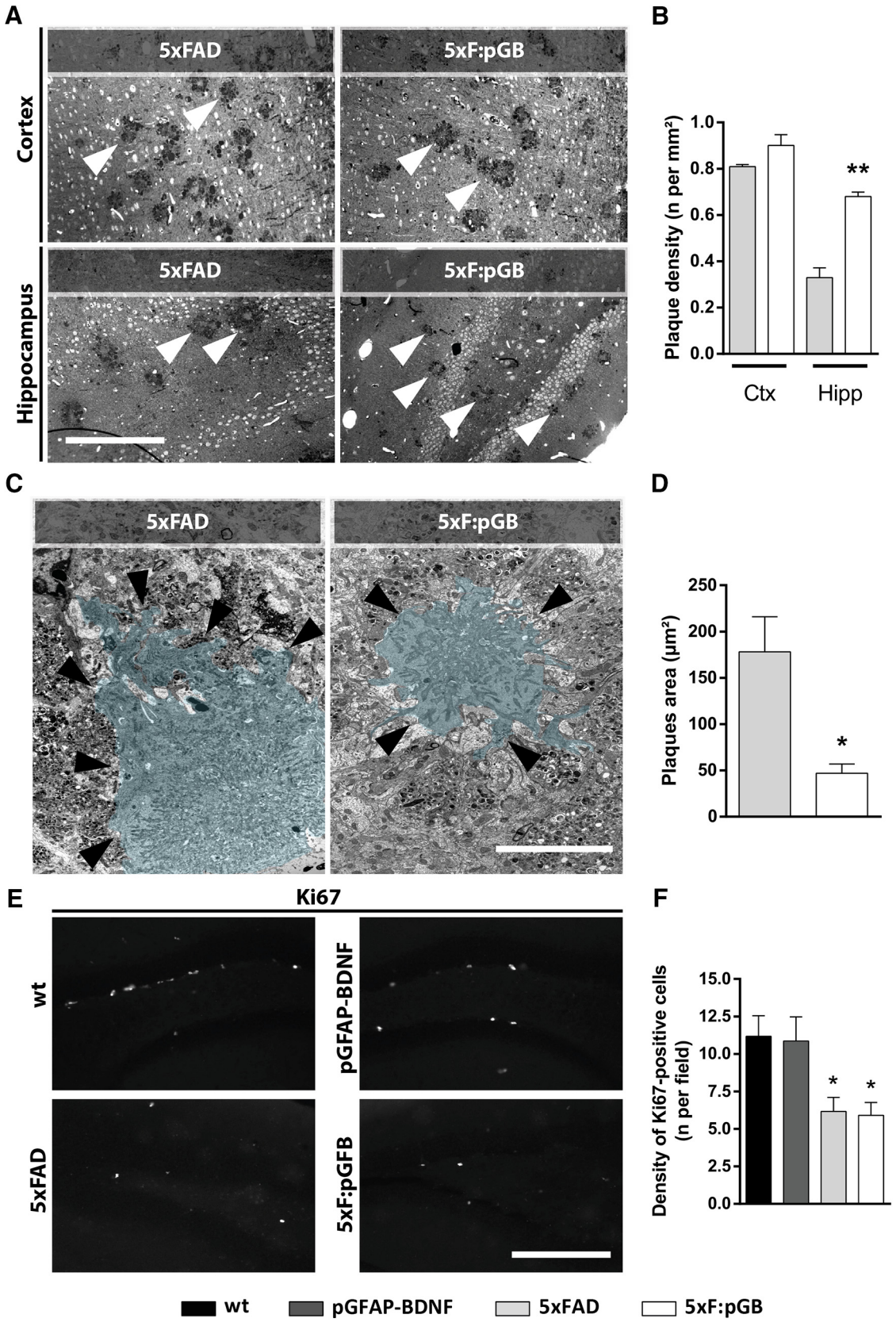

Figure 4. Analysis of gross neuropathology and neurogenesis in WT, pGFAP-BDNF, 5xFAD, and 5xF:pGB mice. ***A***, Amyloid plaques images stained with blue toluidine obtained in a bright-field microscope in the frontal cortex (top left) and in the hippocampus (bottom left) of 5xFAD and 5xF:pGB mice at 8 months of age. Scale bar, 400 μm. ***B***, The plaque density was determined by manual counting in the PFC and in the hippocampus of all four genotypes (right). Student's unpaired *t* test: PFC, $t = 1.923$, df $= 4$, $p = 0.1268$; hippocampus, $t = 7.446$, df $= 4$, $p = 0.0017$. ***C***, Amyloid plaque images obtained with electronic microscopy (left). Plaques have been colorized for easy visualization for the reader. Black arrows indicate the plaque boundary. ***D***, The hippocampal plaque area was determined by using the ImageJ software (right). Scale bar, 10 μm. Student's unpaired *t* test: $t = 4.743$, df $= 8$, $p = 0.0015$. ***E***, Ki67-positive cells obtained by confocal microscopy imaging in the dentate gyrus in 8-month-old WT, pGFAP-BDNF, 5xFAD, and 5xF:pGB mice (left). Scale bar, 300 μm. ***F***, Quantification of the number of the Ki67-positive cells per (*Figure legend continues.*)

pGB mice (−0.089 ± 0.036 decrease, $p < 0.05$) (Fig. 5*A*,*B*). Then, we analyzed spine morphology and the density of the three different spine types (mushroom, thin, and stubby) in the same pyramidal neurons (Fig. 5*C*). No differences were observed in the density of stubby spines, whereas thin spines were markedly decreased in 5xFAD mice (−0.108 ± 0.021 decrease, $p < 0.001$) and completely recovered in 5xF:pGB mice (Fig. 5*C*). In contrast, mushroom spines were decreased equally in 5xFAD (−0.098 ± 0.021 decrease, $p < 0.001$) and in 5xF:pGB (−0.067 ± 0.023 decrease, $p < 0.05$) mice compared with WT and pGFAP-BDNF mice. These results revealed that overexpression of astrocytic BDNF in 5xF:pGB mice specifically rescued thin spines but not mushroom spines in the PFC.

Next, we examined the same parameters in CA1 pyramidal neurons in the four genotypes. Spine density was decreased in 5xFAD mice compared with WT mice (−0.132 ± 0.046 decrease, $p < 0.05$), and this decrease was rescued in 5xF:pGB mice (Fig. 5*D*,*E*). When we analyzed spine morphology, we detected a small decrease in stubby spine density only in 5xF:pGB compared with WT mice (−0.076 ± 0.048 decrease, $p < 0.05$) whose meaning is uncertain (Fig. 5*F*). In contrast, a clear decrease in thin spines density was observed in 5xFAD compared with WT mice (−0.100 ± 0.026 decrease, $p < 0.01$) that was rescued in 5xF:pGB mice (Fig. 5*F*). Finally, no changes in the density of mushroom spines were detected in any group. These results show that the main alteration in both PFC and hippocampal CA1 region was a decrease in thin spines in 5xFAD mice which was rescued in 5xF:pGB mice.

To explore changes in excitatory synapses likely associated with spine alterations, we evaluated presynaptic and postsynaptic markers. We examined the number of positive clusters for PSD-95 and synaptophysin, which are postsynaptic and presynaptic markers, respectively, previously reported to be decreased in 5xFAD mice, correlating with cognitive decline (Yang et al., 2015; Giralt et al., 2018). We analyzed these two markers in CA1 stratum radiatum of 8-month-old mice. As expected, the number of PSD-95-positive puncta was decreased in 5xFAD compared with WT mice (−754 ± 125 decrease, $p < 0.001$) (Fig. 6*A*,*B*). This decrease was rescued in 5xF:pGB mice (Fig. 6*A*,*B*). The number of synaptophysin-positive puncta was also decreased in CA1 stratum radiatum of 5xFAD compared with WT mice (−685 ± 190 decrease, $p < 0.05$) (Fig. 6*C*,*D*). Synaptophysin puncta were recovered in 5xF:pGB mice. Together, these results suggest that the behavioral improvement observed in 5xF:pGB mice compared with 5xFAD mice was accompanied by an improvement in the clusters of presynaptic and postsynaptic markers, indicative of actual synapses. Additionally, we evaluated whether these changes were associated with direct TrkB-mediated signaling in neurons. To do so, we counted the number of double-labeled PSD-95/phospho-TrkB^{Y816}-positive puncta in the CA1 stratum radiatum of 8-month-old mice. We observed that 5xFAD mice displayed a reduction of double-labeled PSD-95/phospho-TrkB^{Y816}-positive puncta in the stratum radiatum (−65 ± 20 decrease, $p < 0.05$), whereas such parameter was fully recovered in 5xF:pGB mice (Fig. 6*E*,*F*), indicating that 5xF:pGB mice improvements were associated with a TrkB-dependent signaling recovery in neurons. Next, to further examine presynaptic and postsynaptic changes, we performed electronic microscopy experiments and analyzed the PSD area and the number of presynaptic vesicles per synapse, in the CA1 stratum radiatum of the four groups of mice at 8 months. We observed no alteration of the PSD area in 5xFAD mice but an unexpected increase in pGFAP-BDNF controls (0.0059 ± 0.00089 increase, $p < 0.001$) (Fig. 6*G*,*H*). Conversely, the number of presynaptic vesicles per synapse was significantly decreased in 5xFAD mice (−5.088 ± 1.046 decrease, $p < 0.001$) but was completely rescued in 5xF:pGB mice (Fig. 6*G*,*I*). These results on spines, synaptic marker clusters, and synaptic vesicles suggest that the cognitive improvements observed in 5xF:pGB mice resulted from synaptic improvements.

In vivo study of electrophysiological properties of the CA3-CA1 synapses in 5xF:pGB mice

To determine whether the rescue of histological alterations following BDNF astrocytic expression was associated with functional improvements, we studied the *in vivo* electrophysiological properties of hippocampal circuits in the four groups of mice. We recorded input/output curves, paired-pulse facilitation, and LTP evoked at the CA3-CA1 synapses (Fig. 7*A*–*C*).

We first analyzed the response of CA1 pyramidal neurons to single pulses of increasing intensity (0.02–0.4 mA) presented to the ipsilateral Schaffer collaterals. As illustrated in Figure 7*D*, the four groups (wt, $n = 13$; pGFAP-BDNF, $n = 15$; 5xFAD, $n = 11$; 5xF:pGB, $n = 13$) presented similar increases ($F_{(57,912)} = 1.460$; $p < 0.017$; two-way repeated-measures ANOVA) in the slope of fEPSP evoked in CA1 by stimuli presented to the ipsilateral Schaffer collaterals. No significant differences ($F_{(3,912)} = 0.718$; $p = 0.546$) between the four collected curves were observed. These two relationships were best fitted by sigmoid curves ($r \geq 0.99$; $p < 0.0001$; not illustrated), suggesting a normal basal function of the CA3-CA1 synapses in the four mouse genotypes.

Changes in synaptic strength evoked by a pair of pulses are a form of presynaptic short-term plasticity, mostly related to variations in neurotransmitter release (Zucker and Regehr, 2002). In this regard, paired-pulse stimulation is commonly used as an indirect measurement of changes in the probability of neurotransmitter release at presynaptic terminals of hippocampal synapses (Zucker and Regehr, 2002). In addition, it has been shown that these synaptic properties can be studied in alert behaving mice (Madroñal et al., 2009). The paired-pulse facilitation evoked in the four groups (wt, $n = 15$; pGFAP-BDNF, $n = 19$; 5xFAD, $n = 13$; 5xF:pGB, $n = 14$) was analyzed presenting a fix stimulus intensity (30%–40% of asymptotic values) with increasing interpulse intervals (see Materials and Methods). As illustrated in Figure 7*E*, the four groups of mice presented a paired-pulse facilitation at short (10, 20, and 40 ms) interpulse intervals ($F_{(5,240)} = 21.290$; $p < 0.001$). However, no significant differences were observed between groups ($F_{(15,240)} = 0.464$; $p = 0.956$).

Finally, we performed an LTP study in the four groups of behaving mice. It is generally accepted that CA3-CA1 synapses are involved in the acquisition of different types of associative (classical eye blink conditioning) and nonassociative (object recognition, spatial orientation) learning tasks, and it is usually selected for evoking LTP in behaving mice (Gruart et al., 2006). For baseline values, animals were stimulated at the implanted Schaffer collaterals 3 times/min for 15 min (Fig. 7*F*). Then, animals (wt, $n = 16$; pGFAP-BDNF, $n = 19$; 5xFAD, $n = 13$; 5xF:pGB, $n = 14$) were presented with the selected HFS protocol (Fig. 7*F*, dashed line). Following HFS, the same single stimulus used to

←

(*Figure legend continued.*) field (right). Genotype effect: $F_{(3,20)} = 5.323$, $p < 0.0073$. Data are mean ± SEM. ***B***, ***D***, Student's unpaired *t* test. ***F***, One-way ANOVA and Tukey's *post hoc* test. ***B***, ***D***, *$p < 0.05$; **$p < 0.01$; compared with 5xFAD mice. ***F***, *$p < 0.01$; compared with WT mice. ***B***, $n = 4$ mice/genotype. ***D***, $n = 4$ mice/genotype. ***F***, $n = 6$ or 7 mice/genotype. Ctx, Frontal cortex; Hipp, hippocampus.

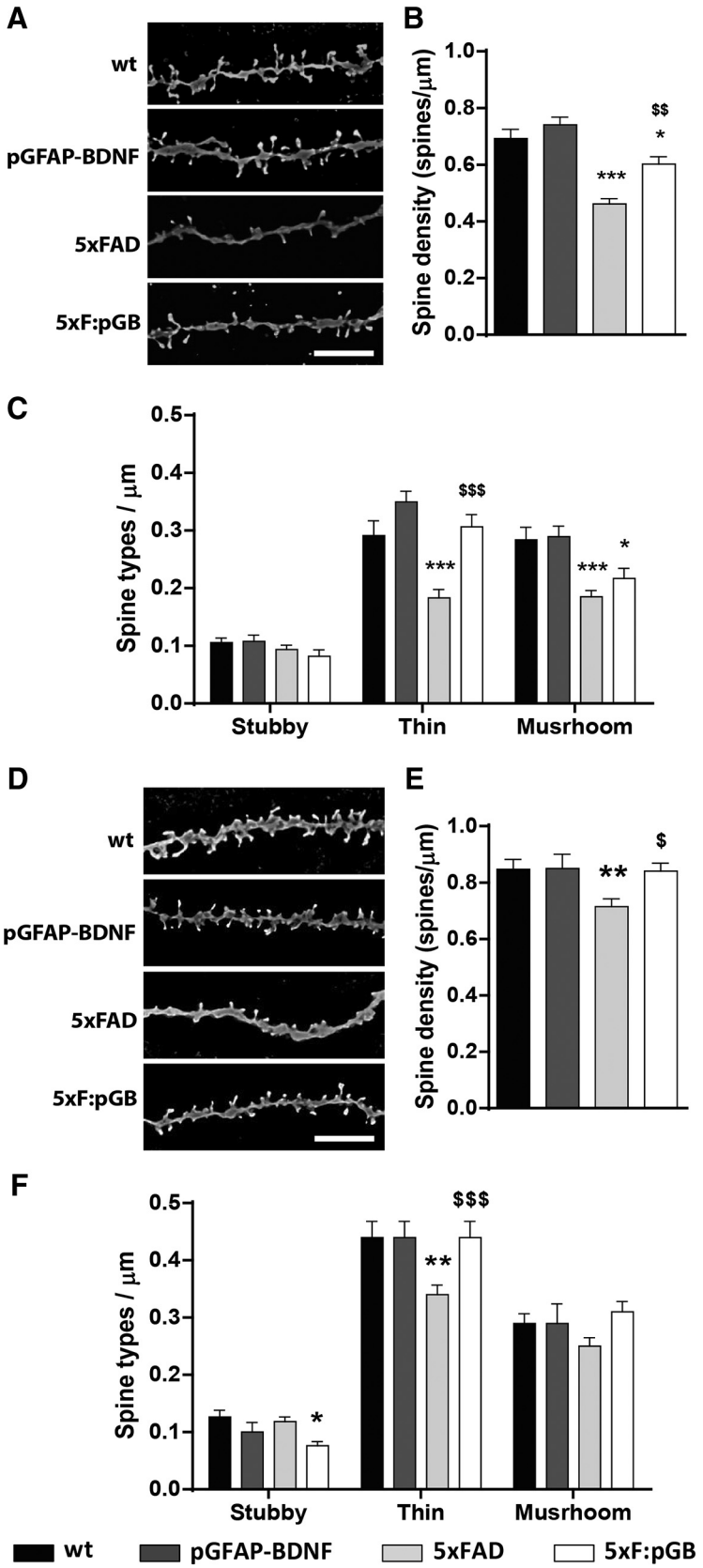

Figure 5. Dendritic spine density and morphology analysis in the PFC and hippocampus of WT, pGFAP-BDNF, 5xFAD, and 5xF:pGB mice. ***A***, Images of apical dendrites from pyramidal neurons of the layer V in PFC stained with Golgi staining obtained in a bright-field microscope in 8-month-old WT, pGFAP-BDNF, 5xFAD, and 5xF:pGB mice. Scale bar, 5 μm. ***B***, The dendritic spine density was determined in all four genotypes by using the ImageJ freeware. One-way ANOVA: $F_{(2,100)} = 23.09$, $p < 0.001$. ***C***, Density of each type of dendritic spine (stubby, thin, and mushroom) in apical dendrites of pyramidal neurons of the layer V of the PFC in 8-month-old WT, pGFAP-BDNF, 5xFAD, and 5xF:pGB mice. Two-way ANOVA, genotype effect: $F_{(3,390)} = 21.83$, $p < 0.001$; interaction effect, $F_{(3,390)} = 6.036$, $p < 0.001$. ***D***, Images of apical dendrites from pyramidal neurons of the hippocampal CA1 stained with Golgi staining obtained in a bright-field microscope in 8-month-old WT, pGFAP-BDNF, 5xFAD, and 5xF:pGB mice. Scale bar, 5 μm. ***E***, The dendritic spine density was determined in all four genotypes by using the ImageJ freeware. One-way ANOVA: $F_{(3,185)} = 4.070$, $p = 0.0079$. ***F***, Density of each type of dendritic spine (stubby, thin, and mushroom) in apical dendrites of pyramidal neurons from the hippocampal CA1 in 8-month-old WT, pGFAP-BDNF, 5xFAD, and 5xF:pGB mice. Two-way ANOVA, genotype effect: $F_{(3,552)} = 3.678$, $p = 0.0121$; interaction effect, $F_{(3,390)} = 2.750$, $p = 0.0122$. Data are mean ± SEM. ***B***, ***E***, One-way ANOVA with Tukey's test as a *post hoc* was used. ***C***, ***F***, Two-way ANOVA and Bonferroni's *post hoc* test. ***B***, ***C***, ***E***, ***F***, $^{*}p < 0.05$; $^{**}p < 0.01$; $^{***}p < 0.001$; compared with WT mice. $^{\$}p < 0.05$; $^{\$\$}p < 0.01$; $^{\$\$\$}p < 0.001$; compared with 5xFAD mice. ***B***, ***C***, $n = 31–41$ dendrites/genotype (from 5 mice/genotype). ***E***, ***F***, $n = 35–56$ dendrites/genotype (from 5 mice/genotype).

generate baseline records was presented at the initial rate (3/min) for another 60 min. Recording sessions were repeated for three additional days (30 min each; Fig. 7*F*). The four groups of mice presented a significant increase in fEPSP slopes following the HFS session ($F_{(114,1976)} = 1.863$; $p < 0.001$). Nevertheless, a point-to-point comparison between fEPSPs evoked in the four groups of mice after the HFS protocol indicated that 5xF:pGB animals presented larger LTP values for the first recording session ($p \leq 0.045$) than the three other groups.

Figure 7*F* (inset) illustrates the evolution of paired-pulse facilitation in the four groups of mice. In accordance with previous descriptions (Madroñal et al., 2009), and as observed here for WT, pGFAP-BDNF, and 5xF:pGB mice, paired-pulse facilitation decreased immediately after HFS and was recovered in the following days. Interestingly, the 5xFAD group did not show any sign of recovery of paired-pulse facilitation for the four recording days after the HFS session, indicating an increase in the response to the first pulse in this stressful situation.

In conclusion, the four groups of mice presented similar basal synaptic properties and short-term plasticity. Interestingly, although the four groups of mice presented a significant LTP with respect to baseline values, LTP was significantly larger in the 5xF:pGB group than in the other three groups during the first recording session following the HFS protocol. The 5xFAD group presented LTP values like those reached by WT and pGFAP-BDNF group; this result could be ascribed to an increase in neurotransmitter release evoked by a first pulse because their paired-pulse facilitation was decreased

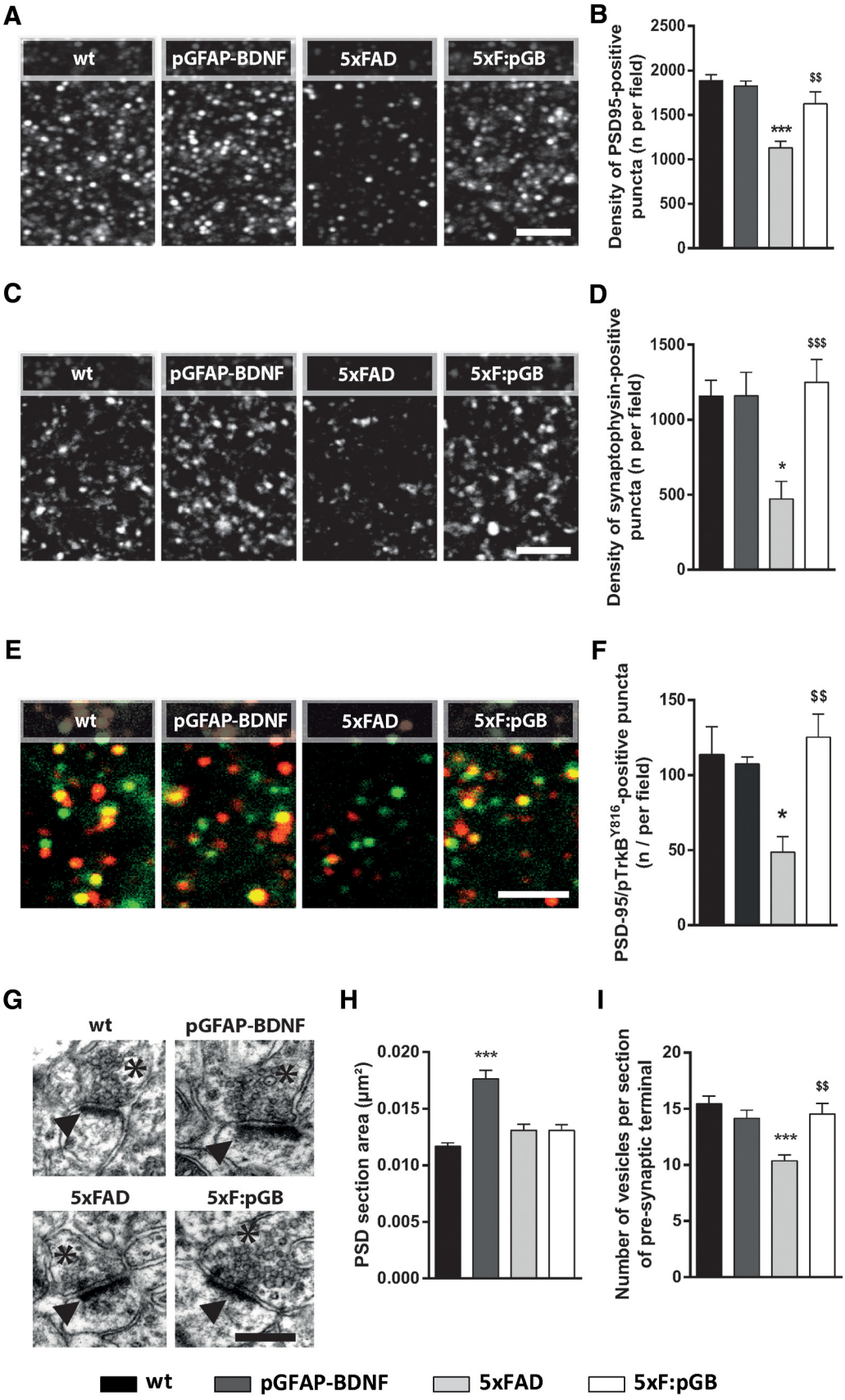

Figure 6. Hippocampal excitatory synapse characterization of WT, pGFAP-BDNF, 5xFAD, and 5xF:pGB mice. ***A***, Confocal image of PSD-95 immunofluorescence in CA1 stratum radiatum of 8-month-old WT, pGFAP-BDNF, 5xFAD, and 5xF:pGB mice. Scale bar, 10 μm. ***B***, Quantification of the number of PSD-95-positive puncta per field. One-way ANOVA: $F_{(3,16)} = 14.90$, $p < 0.001$. ***C***, Synaptophysin immunofluorescence. Scale bar, 10 μm. ***D***, Quantification of the number of synaptophysin-positive puncta per field. One-way ANOVA: $F_{(3,16)} = 7.194$, $p < 0.0028$. ***E***, Confocal image of a double PSD-95 (green) and phosphoTrkB ^{Y816} (red) immunofluorescence in CA1 stratum radiatum of 8-month-old WT, pGFAP-BDNF, 5xFAD, and 5xF:pGB mice. (*Figure legend continues.*)

and remained in this situation across the four recording sessions after HFS.

Discussion

In the present study, we tested an approach to deliver BDNF in a conditional targeted fashion in an AD mouse model. We used a transgenic mouse model recently generated and characterized by our team (Giralt et al., 2010, 2011) to overexpress BDNF under the GFAP promoter. Here we show how this method restores the production and delivery of the neurotrophin in the diseased neural tissue when the pathology starts because of the accompanying astrogliosis. We first observed that endogenous BDNF from astrocytes regulates neurite formation and spine density in neurons *in vitro*. We then used a *pGFAP*:BDNF transgene to rescue the BDNF loss in 5xFAD mice and observed a significant improvement of learning and memory deficits in the hybrid transgenic mice. These improvements were associated with a restoration of dendritic spines density and morphology and a recovery of clusters of presynaptic and postsynaptic markers, synaptophysin and PSD-95. We also observed a stronger LTP in CA1 *in vivo* in behaving 5xF:pGB mice, which could be related with the other changes.

We first demonstrated that BDNF produced by astrocytes can play a relevant role in dendrite maturation. Although the present results do not demonstrate a clear *in vivo* proof that BDNF is produced and released in physiological conditions, they are in line with the idea that astrocytes may play a role in synapse formation and plasticity (Ronzano, 2017) and could play such a role by regulating the BDNF availability to neurons (Vignoli et al., 2016). They also reinforce the idea of astrocytes as potent regulators of neurotrophin availability to neurons. After showing that astrocytes are a potential source of BDNF with morphological effects on neurons delivery, we generated the double-mutant mice 5xF:pGB. We demonstrated that BDNF levels and the activation of TrkB and its downstream pathways (PLCγ and ERK1/2) were fully recovered in these double-mutant 5xF:pGB mice, which are the most important regulating synaptic plasticity pathways upon TrkB activation (Yoshii and Constantine-Paton, 2010). Indeed, PLCγ downstream signaling is essential for hippocampal associative learning and CA3-CA1 LTP (Minichiello et al., 2002; Gruart et al., 2007).

By comparing these double-mutant mice with 5xFAD mice, we observed that the cognitive alterations related to hippocampal dysfunction were rescued. Regarding the neuropathology, genetically recovered BDNF levels did not change astrogliosis in 5xFAD mice. Normalization of BDNF levels increased the number of plaques but reduced their size. These findings contrast with the belief that reduced plaque number associates with an amelioration of the 5xFAD mice phenotype (Murphy and LeVine, 2010). However, the role of plaques is complex, and previous reports have correlated a hyperaggregation of Aβ with an improvement in AD transgenic mice phenotype due to a lower presence of soluble Aβ, which is the most toxic form of the molecule (Castellani et al., 2009; Cohen et al., 2009; Lublin and Gandy, 2010). We also checked for neurogenesis in the dentate gyrus, which has been described to be altered (Moon et al., 2014), as a possible neural correlate of the observed improvements. However, the number of Ki67-positive cells in the dentate gyrus were equally reduced in 5xFAD and 5xF:pGB compared with WT mice. These results revealed that behavioral improvements in 5xF:pGB mice did not result from plaque number reduction or neurogenesis improvement. We therefore hypothesized that the rescued phenotype in 5xF:pGB mice could be rather due to changes in structural and functional synaptic properties. In 5xFAD mice, as well as in AD patients, there is a prominent dendritic spine pathology and loss of synaptic markers, such as synaptophysin and PSD-95 (Hongpaisan et al., 2011; Crowe and Ellis-Davies, 2014; Yuki et al., 2014; Dorostkar et al., 2015; Yang et al., 2015). We found several synaptic changes associated with the cognitive improvements in 5xF:pGB mice. We hypothesize that BDNF delivered from transgenic astrocytes may have induced these changes by reactivating the neuronal TrkB-PLCγ/ERK1/2 pathway. The PLCγ pathway is important for correct PSD-95 location, whereas BDNF-TrkB-ERK is important for PSD-95 expression (Robinet and Pellerin, 2011; Parsons et al., 2014; Yoshii and Constantine-Paton, 2014). BDNF signaling can also regulate synaptophysin levels (Tartaglia et al., 2001; Zhang et al., 2017) and its function/location (Bamji et al., 2006). BDNF could also be directly responsible for the rescue of dendritic spine density and morphology as described previously (Kellner et al., 2014). However, although here we show that BDNF from astrocytes activates TrkB in neurons, we cannot rule out a collateral effect of BDNF on neighboring astrocytes or even microglia as previously described in the literature (Mizoguchi et al., 2011; Sasi et al., 2017), producing a more widespread effect than the one specifically evaluated in the present work. Overall, our results strongly indicate that 5xF:pGB mice improvements could be due to a local and self-regulated delivery of BDNF in the diseased tissue, likely rescuing the ERK1/2 and PLCγ pathways in neurons, which in turn improved dendritic spine pathology.

A significant body of evidence indicates that enhancement of the BDNF delivery or function via activation of its high-affinity receptor TrkB could be a promising therapeutic approach in AD (Allen and Dawbarn, 2006; Devi and Ohno, 2012, 2015; Zhang et al., 2014; Kaminari et al., 2017). Based on our results, we propose that the use of engineered astrocytes could be an interesting means to achieve this objective. Astrocytes are currently considered as very promising potential targets for AD treatment, including through genetic manipulation to regulate neurotrophin production (Bronzuoli et al., 2017; Gorshkov et al., 2018). Indeed, astrocytes are uniquely positioned to promote the regeneration of damaged nerve cells or protect existing cells from degeneration and dysfunction in the CNS (Anderson et al., 2016; Blanco-Suárez et al., 2017). At least three main strategies have been proposed: astrocyte transplantation or pharmacological correction of their dysfunction or by its genetic manipulation (Gorshkov et al., 2018). We propose that targeting astrocytes to produce and deliver BDNF could be a potential therapeutic tool for the treatment of AD. Much previous and present evidence supports this idea. First, astrocytes have been recently shown to be crucial for hippocampal-related cognitive function and syn-

←

(*Figure legend continued.*) Scale bar, 10 μm. ***F***, Quantification of the number of PSD-95/phosphoTrkB^{Y816}-positive puncta per field. One-way ANOVA: $F_{(3,26)} = 5.303$, $p < 0.01$. ***G***, Electronic microscopy imaging of excitatory synapses in the stratum radiatum of the CA1 in 8-month-old WT, pGFAP-BDNF, 5xFAD, and 5xF:pGB mice. Asterisks indicate the presynaptic component. Black arrows indicate the postsynaptic component. Scale bar, 0.3 μm. ***H***, Quantification of the PSD area. One-way ANOVA: $F_{(3,253)} = 17.16$, $p < 0.001$. ***I***, Quantification of the number of presynaptic vesicles per synapse. One-way ANOVA: $F_{(3,201)} = 9.18$, $p < 0.001$. One-way ANOVA with Tukey's test as a *post hoc* was used. Data are mean ± SEM. ***B***, ***D***, ***F***, ***H***, ***I***, $^{*}p < 0.05$; $^{***}p < 0.001$; compared with WT mice. $^{\$\$}p < 0.01$; $^{\$\$\$}p < 0.001$; compared with 5xFAD mice. ***B***, ***D***, ***F***, Two pictures per slice and 3 slices per mouse were taken. ***B***, ***D***, $n = 5$/genotype. ***F***, $n = 7$–9/genotype. ***H***, ***I***, 51 ± 3 excitatory synapses from 3 different mice/genotype were evaluated.

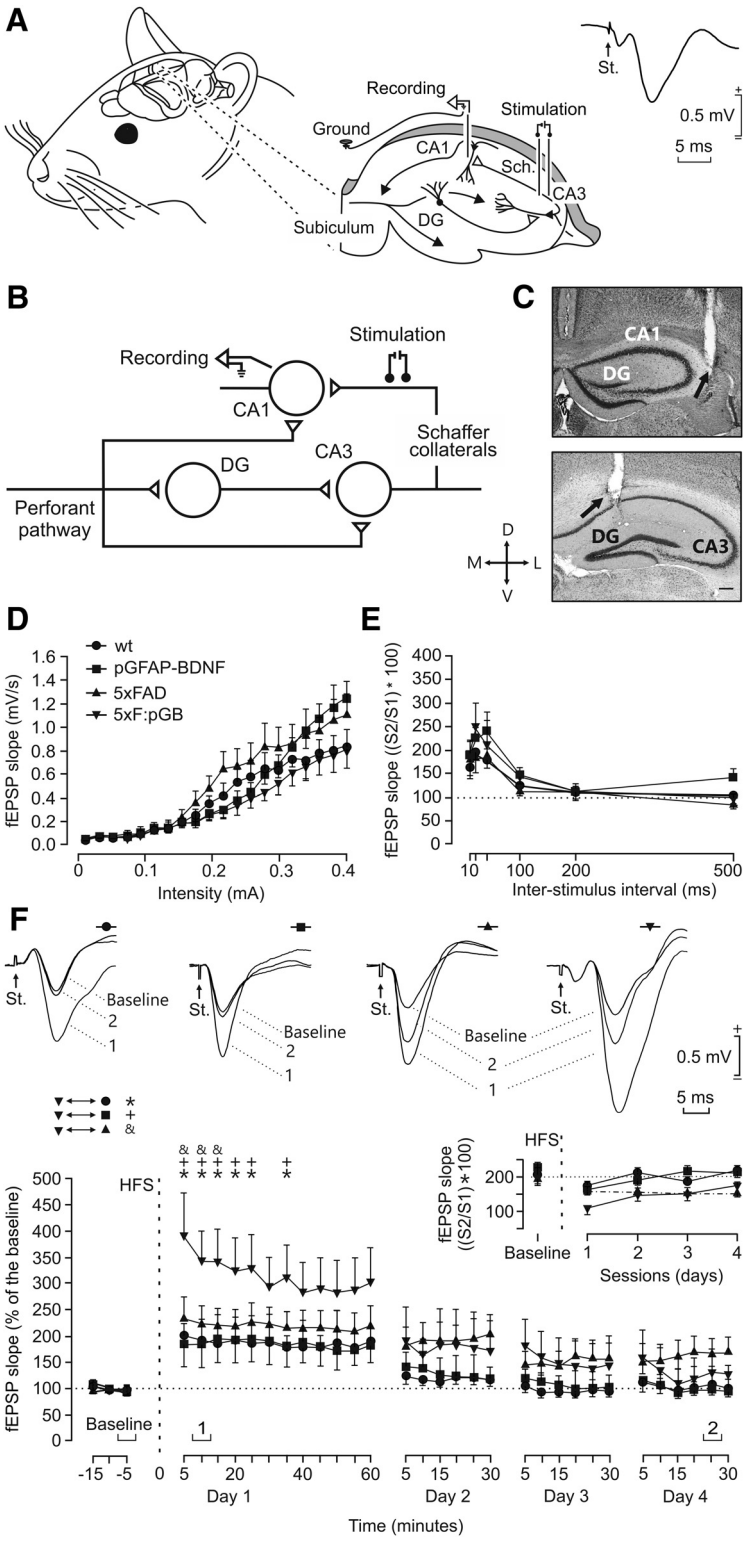

Figure 7. *In vivo* hippocampal synaptic plasticity in WT, pGFAP-BDNF, 5xFAD, and 5xF:pGB mice. ***A***, Animals were chronically implanted with bipolar stimulating electrodes in CA3 Schaffer (Sch.) collaterals and with a recording electrode in the ipsilateral CA1 area. Two extra wires were attached to the bone as ground. DG, Dentate gyrus. Right, Representative example of fEPSP (averaged 5 times) evoked at the CA3-CA1 synapse in a WT animal. ***B***, Diagram illustrating the location of stimulating and recording electrodes in the intrinsic hippocampal circuit. ***C***, Representative micrographs illustrating the final location of stimulating and recording electrodes. D, L, M, and V, dorsal, lateral, medial, and ventral, respectively. Calibration bar: 0.2 mm. ***D***, Input/output curves of fEPSPs evoked at the CA3-CA1 synapse by single pulses of increasing intensities (0.02– 0.4 in mA) in WT ($n = 13$), pGFAP-BDNF ($n = 15$), 5xFAD ($n = 11$), and 5xF:pGB ($n = 13$) mice. Data are mean ± SEM. No significant differences ($F_{(3,912)} = 0.718$; $p = 0.546$) were observed between groups. ***E***, No significant ($F_{(15,240)} = 0.464$; $p = 0.956$) differences in paired-pulse facilitation between the four experimental groups were observed (wt = 15; pGFAP-BDNF = 19; 5xFAD = 13; 5xF:pGB = 14). Data are mean ± SEM slopes of the second fEPSP expressed as the percentage of the first for six (10, 20, 40, 100, 200, and 500) interpulse intervals. ***F***, Graphs represent the time course of LTP evoked in the CA3-CA1 synapse following an HFS session presented to mice included in the four experimental groups (wt, $n = 16$; pGFAP-BDNF, $n = 19$; 5xFAD, $n = 13$; 5xF:pGB, $n = 14$). The HFS was presented after 15 min of baseline recordings, at the time marked by the dashed line. LTP evolution was followed for 3 d. Top, Representative examples of fEPSPs collected at the times indicated in the bottom graphs from a representative animal of each group. fEPSP slopes are given as a percentage of fEPSP values collected during baseline recordings (100%). Although the four groups presented significant ($F_{(114,1976)} = 1.863$; $p < 0.001$) increases (ANOVA, two-tailed) in fEPSP slopes following HFS compared with baseline recordings, the 5xF:pGB group did present a larger LTP than that presented by the other three groups: *5xF:pGB versus WT; $^{+}$5xF:pGB versus pGFAP-BDNF; $^{\&}$5xF:pGB versus 5xFAD; $p \leq 0.045$. Top left, inset, The evolution of paired-pulse facilitation (determined at 40 ms of interpulse interval) for fEPSPs recorded during baseline and following the HFS session is illustrated for the four experimental groups. Dotted/dashed line indicates the 5xFAD group.

aptic plasticity (Adamsky et al., 2018). Second, facilitating BDNF expression from astrocytes has previously been shown to be useful in another neurodegenerative disease, Huntington's disease (Giralt et al., 2011; Corbett et al., 2013; Reick et al., 2016). Furthermore, astrocytes per se not only produce, but also buffer, BDNF in case of necessity (Stary et al., 2015) or recycle it for LTP maintenance and memory retention (Vignoli et al., 2016), thus making them perfect candidates to deliver the neurotrophin in a controlled fashion. Additionally, in the field of cell therapy, astrocytes would be good therapeutic tools because they survive for a long time when grafted (Giralt et al., 2010), and they are specifically reactive where Aβ is accumulated and where neuritic dystrophy is localized (Song et al., 2015). Furthermore, astrocytes are easily manipulated, do not proliferate aberrantly as for example engineered cell lines (Hoffman et al., 1993), and they do not suffer of teratogenic potential, in contrast to stem cells (Martínez-Serrano and Björklund, 1996; Pineda et al., 2007; Rubio et al., 1999). Neural cells may be another candidate source for the overexpression of BDNF. However, as an excessive amount of this neurotrophin is deleterious (Kells et al., 2008), its release must be controlled (Martínez-Serrano and Björklund, 1996; Rubio et al., 1999). Transgenic astrocytes would overcome all these drawbacks. A promising therapeutic strategy could be the use of astrocytes from induced pluripotent stem cells (Gorshkov et al., 2018). Once astrocytes have been obtained and characterized and genetically modified to express BDNF under

the GFAP promoter, they could be transplanted to promote the survival and appropriate functioning of existing neurons, such as synaptic plasticity processes.

Although 5xFAD mice presented noticeable losses in the expression of PSD-95 and synaptophysin, they did not present any significant alteration in input/output curves, paired-pulse facilitation, or in LTP evoked *in vivo*. In this regard, it has been already reported that LTP can be preserved longer than other behavioral functions in aging mice (López-Ramos et al., 2012) and that motor exercise can help to recover some behavioral and associative learning abilities, but not synaptic changes and LTP in 3xTg-AD mice (García-Mesa et al., 2011). In addition, age seems to be a critical factor; for example, in 3-month-old mice, it is almost impossible to distinguish differences in learning abilities and LTP strength and duration between WT versus APP, PS1, and APP-PS1 mice (Gruart et al., 2008). For the present experiments, we can assume that baseline measures of transmission (input/output curves and paired-pulse facilitation) and LTP were sustained in 8-month-old 5xFAD mice by an increase in neurotransmitter release (Fig. 7*F*), as reported by some of us in TgNTRK3 transgenic mice (Sahún et al., 2007). Indeed, the latter study is an excellent example of dissociation between CA3-CA1 synaptic plasticity and associative learning capabilities in genetically manipulated mice.

The present results have some limitations. First, although the 5xFAD mouse model has been shown to recapitulate several hallmarks of AD pathology, they do not show tauopathy or formation of intraneuronal neurofibrillary tangles. From a therapeutic point of view, the interpretation of our results should be taken with caution, and studies evaluating our approach in models of tauopathy are needed. Second, we observed recovered BDNF levels in 5xF:pGB mice with respect to 5xFAD mice at 8 months of age, but we cannot rule out the possibility that earlier beneficial effects could have taken place in our double-mutant mice. It is known that astrocytes synthesize GFAP from the first days of age (Guo et al., 2013). Thereby, putative early increases on BDNF levels in 5xF:pGB mice could also counteract the deleterious effects of the five transgenic mutations at very early stages.

In conclusion, our study supports the idea that the use of engineered astrocytes to deliver BDNF under the control of the GFAP promoter in AD has a strong potential. It may correspond to the increase of a physiological function; and the delivery is conditionally and locally administered, creating then a customized neurotrophin-based treatment.

References

Acosta C, Anderson HD, Anderson CM (2017) Astrocyte dysfunction in Alzheimer disease. J Neurosci Res 95:2430–2447.

Adamsky A, Kol A, Kreisel T, Doron A, Ozeri-Engelhard N, Melcer T, Refaeli R, Horn H, Regev L, Groysman M, London M, Goshen I (2018) Astrocytic activation generates de novo neuronal potentiation and memory enhancement. Cell 174:59–71.e14

Allen SJ, Dawbarn D (2006) Clinical relevance of the neurotrophins and their receptors. Clin Sci (Lond) 110:175–191.

Alzheimer's Association (2012) 2012 Alzheimer's disease facts and figures. Alzheimers Dement 8:131–168.

Anderson MA, Burda JE, Ren Y, Ao Y, O'Shea TM, Kawaguchi R, Coppola G, Khakh BS, Deming TJ, Sofroniew MV (2016) Astrocyte scar formation aids central nervous system axon regeneration. Nature 532:195–200.

Bamji SX, Rico B, Kimes N, Reichardt LF (2006) BDNF mobilizes synaptic vesicles and enhances synapse formation by disrupting cadherin-beta-catenin interactions. J Cell Biol 174:289–299.

Blanco-Suárez E, Caldwell AL, Allen NJ (2017) Role of astrocyte-synapse interactions in CNS disorders. J Physiol 595:1903–1916.

Bronzuoli MR, Facchinetti R, Steardo L, Scuderi C (2017) Astrocyte: an innovative approach for Alzheimer's disease therapy. Curr Pharm Des 23:4979–4989.

Carpenter MK, Winkler C, Fricker R, Emerich DF, Wong SC, Greco C, Chen EY, Chu Y, Kordower JH, Messing A, Björklund A, Hammang JP (1997) Generation and transplantation of EGF-responsive neural stem cells derived from GFAP-hNGF transgenic mice. Exp Neurol 148:187–204.

Castellani RJ, Lee HG, Siedlak SL, Nunomura A, Hayashi T, Nakamura M, Zhu X, Perry G, Smith MA (2009) Reexamining Alzheimer's disease: evidence for a protective role for amyloid-beta protein precursor and amyloid-beta. J Alzheimers Dis 18:447–452.

Cohen E, Paulsson JF, Blinder P, Burstyn-Cohen T, Du D, Estepa G, Adame A, Pham HM, Holzenberger M, Kelly JW, Masliah E, Dillin A (2009) Reduced IGF-1 signaling delays age-associated proteotoxicity in mice. Cell 139:1157–1169.

Corbett GT, Roy A, Pahan K (2013) Sodium phenylbutyrate enhances astrocytic neurotrophin synthesis via protein kinase C (PKC)-mediated activation of cAMP-response element-binding protein (CREB): implications for Alzheimer disease therapy. J Biol Chem 288:8299–8312.

Crowe SE, Ellis-Davies GC (2014) Spine pruning in 5xFAD mice starts on basal dendrites of layer 5 pyramidal neurons. Brain Struct Funct 219:571–580.

Devi L, Ohno M (2012) 7,8-Dihydroxyflavone, a small-molecule TrkB agonist, reverses memory deficits and BACE1 elevation in a mouse model of Alzheimer's disease. Neuropsychopharmacology 37:434–444.

Devi L, Ohno M (2015) TrkB reduction exacerbates Alzheimer's disease-like signaling aberrations and memory deficits without affecting beta-amyloidosis in 5XFAD mice. Transl Psychiatry 5:e562.

Dorostkar MM, Zou C, Blazquez-Llorca L, Herms J (2015) Analyzing dendritic spine pathology in Alzheimer's disease: problems and opportunities. Acta Neuropathol 130:1–19.

Ernfors P, Lee KF, Jaenisch R (1994) Mice lacking brain-derived neurotrophic factor develop with sensory deficits. Nature 368:147–150.

Filali M, Lalonde R, Rivest S (2009) Cognitive and non-cognitive behaviors in an APPswe/PS1 bigenic model of Alzheimer's disease. Genes Brain Behav 8:143–148.

Fulmer CG, VonDran MW, Stillman AA, Huang Y, Hempstead BL, Dreyfus CF (2014) Astrocyte-derived BDNF supports myelin protein synthesis after cuprizone-induced demyelination. J Neurosci 34:8186–8196.

García-Mesa Y, López-Ramos JC, Giménez-Llort L, Revilla S, Guerra R, Gruart A, Laferla FM, Cristòfol R, Delgado-García JM, Sanfeliu C (2011) Physical exercise protects against Alzheimer's disease in 3xTg-AD mice. J Alzheimers Dis 24:421–454.

Giralt A, Rodrigo T, Martín ED, Gonzalez JR, Milà M, Ceña V, Dierssen M, Canals JM, Alberch J (2009) Brain-derived neurotrophic factor modulates the severity of cognitive alterations induced by mutant huntingtin: involvement of phospholipaseCgamma activity and glutamate receptor expression. Neuroscience 158:1234–1250.

Giralt A, Friedman HC, Caneda-Ferrón B, Urbán N, Moreno E, Rubio N, Blanco J, Peterson A, Canals JM, Alberch J (2010) BDNF regulation under GFAP promoter provides engineered astrocytes as a new approach for long-term protection in Huntington's disease. Gene Ther 17:1294–1308.

Giralt A, Carretón O, Lao-Peregrin C, Martín ED, Alberch J (2011) Conditional BDNF release under pathological conditions improves Huntington's disease pathology by delaying neuronal dysfunction. Mol Neurodegener 6:71.

Giralt A, Brito V, Chevy Q, Simonnet C, Otsu Y, Cifuentes-Díaz C, de Pins B, Coura R, Alberch J, Ginés S, Poncer JC, Girault JA (2017) Pyk2 modulates hippocampal excitatory synapses and contributes to cognitive deficits in a Huntington's disease model. Nat Commun 8:15592.

Giralt A, de Pins B, Cifuentes-Díaz C, López-Molina L, Farah AT, Tible M, Deramecourt V, Arold ST, Ginés S, Hugon J, Girault JA (2018) PTK2B/Pyk2 overexpression improves a mouse model of Alzheimer's disease. Exp Neurol 307:62–73.

Gorshkov K, Aguisanda F, Thorne N, Zheng W (2018) Astrocytes as targets for drug discovery. Drug Discov Today 23:673–680.

Grinan-Ferre C, Sarroca S, Ivanova A, Puigoriol-Illamola D, Aguado F, Camins A, Sanfeliu C, Pallas M (2016) Epigenetic mechanisms underlying cognitive impairment and Alzheimer disease hallmarks in 5XFAD mice. Aging (Albany NY) 8:664–684.

Gruart A, Muñoz MD, Delgado-García JM (2006) Involvement of the CA3-CA1 synapse in the acquisition of associative learning in behaving mice. J Neurosci 26:1077–1087.

Gruart A, Sciarretta C, Valenzuela-Harrington M, Delgado-García JM, Minichiello L (2007) Mutation at the TrkB PLCγ-docking site affects hippocampal LTP and associative learning in conscious mice. Learn Mem 14:54–62.

Gruart A, López-Ramos JC, Muñoz MD, Delgado-García JM (2008) Aged wild-type and APP, PS1, and APP + PS1 mice present similar deficits in associative learning and synaptic plasticity independent of amyloid load. Neurobiol Dis 30:439–450.

Guo Z, Wang X, Xiao J, Wang Y, Lu H, Teng J, Wang W (2013) Early postnatal GFAP-expressing cells produce multilineage progeny in cerebrum and astrocytes in cerebellum of adult mice. Brain Res 1532:14–20.

Gupta VK, You Y, Gupta VB, Klistorner A, Graham SL (2013) TrkB receptor signalling: implications in neurodegenerative, psychiatric and proliferative disorders. Int J Mol Sci 14:10122–10142.

Gureviciene I, Ikonen S, Gurevicius K, Sarkaki A, van Groen T, Pussinen R, Ylinen A, Tanila H (2004) Normal induction but accelerated decay of LTP in APP + PS1 transgenic mice. Neurobiol Dis 15:188–195.

Hoffman D, Breakefield XO, Short MP, Aebischer P (1993) Transplantation of a polymer-encapsulated cell line genetically engineered to release NGF. Exp Neurol 122:100–106.

Hong Y, Zhao T, Li XJ, Li S (2016) Mutant huntingtin impairs BDNF release from astrocytes by disrupting conversion of Rab3a-GTP into Rab3a-GDP. J Neurosci 36:8790–8801.

Hongpaisan J, Sun MK, Alkon DL (2011) PKC epsilon activation prevents synaptic loss, Abeta elevation, and cognitive deficits in Alzheimer's disease transgenic mice. J Neurosci 31:630–643.

Kaminari A, Giannakas N, Tzinia A, Tsilibary EC (2017) Overexpression of matrix metalloproteinase-9 (MMP-9) rescues insulin-mediated impairment in the 5XFAD model of Alzheimer's disease. Sci Rep 7:683.

Kellner Y, Gödecke N, Dierkes T, Thieme N, Zagrebelsky M, Korte M (2014) The BDNF effects on dendritic spines of mature hippocampal neurons depend on neuronal activity. Front Synaptic Neurosci 6:5.

Kells AP, Henry RA, Connor B (2008) AAV-BDNF mediated attenuation of quinolinic acid-induced neuropathology and motor function impairment. Gene Ther 15:966–977.

Lalonde R (2002) The neurobiological basis of spontaneous alternation. Neurosci Biobehav Rev 26:91–104.

Lindvall O, Kokaia Z, Martínez-Serrano A (2004) Stem cell therapy for human neurodegenerative disorders: how to make it work. Nat Med 10 [Suppl]:S42–S50.

López-Ramos JC, Jurado-Parras MT, Sanfeliu C, Acuña-Castroviejo D, Delgado-García JM (2012) Learning capabilities and CA1-prefrontal synaptic plasticity in a mice model of accelerated senescence. Neurobiol Aging 33:627–726.

Lublin AL, Gandy S (2010) Amyloid-beta oligomers: possible roles as key neurotoxins in Alzheimer's disease. Mt Sinai J Med 77:43–49.

Lynch G, Rex CS, Chen LY, Gall CM (2008) The substrates of memory: defects, treatments, and enhancement. Eur J Pharmacol 585:2–13.

Madroñal N, Delgado-García JM, Gruart A (2007) Differential effects of long-term potentiation evoked at the CA3 CA1 synapse before, during, and after the acquisition of classical eyeblink conditioning in behaving mice. J Neurosci 27:12139–12146.

Madroñal N, Gruart A, Delgado-García JM (2009) Differing presynaptic contributions to LTP and associative learning in behaving mice. Front Behav Neurosci 3:7.

Martínez-Serrano A, Björklund A (1996) Protection of the neostriatum against excitotoxic damage by neurotrophin-producing, genetically modified neural stem cells. J Neurosci 16:4604–4616.

Minichiello L, Calella AM, Medina DL, Bonhoeffer T, Klein R, Korte M (2002) Mechanism of TrkB-mediated hippocampal long-term potentiation. Neuron 36:121–137.

Mizoguchi Y, Monji A, Kato TA, Horikawa H, Seki Y, Kasai M, Kanba S, Yamada S (2011) Possible role of BDNF-induced microglial intracellular Ca(2+) elevation in the pathophysiology of neuropsychiatric disorders. Mini Rev Med Chem 11:575–581.

Moon M, Cha MY, Mook-Jung I (2014) Impaired hippocampal neurogenesis and its enhancement with ghrelin in 5XFAD mice. J Alzheimers Dis 41:233–241.

Murphy MP, LeVine H 3rd (2010) Alzheimer's disease and the amyloid-beta peptide. J Alzheimers Dis 19:311–323.

Oakley H, Cole SL, Logan S, Maus E, Shao P, Craft J, Guillozet-Bongaarts A, Ohno M, Disterhoft J, Van Eldik L, Berry R, Vassar R (2006) Intraneuronal beta-amyloid aggregates, neurodegeneration, and neuron loss in transgenic mice with five familial Alzheimer's disease mutations: potential factors in amyloid plaque formation. J Neurosci 26:10129–10140.

Parsons MP, Kang R, Buren C, Dau A, Southwell AL, Doty CN, Sanders SS, Hayden MR, Raymond LA (2014) Bidirectional control of postsynaptic density-95 (PSD-95) clustering by huntingtin. J Biol Chem 289: 3518–3528.

Paxinos G, Franklin KB (2013) The mouse brain in stereotaxic coordinates. San Diego: Academic.

Pineda JR, Rubio N, Akerud P, Urbán N, Badimon L, Arenas E, Alberch J, Blanco J, Canals JM (2007) Neuroprotection by GDNF-secreting stem cells in a Huntington's disease model: optical neuroimage tracking of brain-grafted cells. Gene Ther 14:118–128.

Reick C, Ellrichmann G, Tsai T, Lee DH, Wiese S, Gold R, Saft C, Linker RA (2016) Expression of brain-derived neurotrophic factor in astrocytes: beneficial effects of glatiramer acetate in the R6/2 and YAC128 mouse models of Huntington's disease. Exp Neurol 285:12–23.

Robinet C, Pellerin L (2011) Brain-derived neurotrophic factor enhances the hippocampal expression of key postsynaptic proteins in vivo including the monocarboxylate transporter MCT2. Neuroscience 192: 155–163.

Ronzano R (2017) Astrocytes and microglia: active players in synaptic plasticity. Med Sci (Paris) 33:1071–1078.

Rubio FJ, Kokaia Z, del Arco A, García-Simón MI, Snyder EY, Lindvall O, Satrústegui J, Martínez-Serrano A (1999) BDNF gene transfer to the mammalian brain using CNS-derived neural precursors. Gene Ther 6:1851–1866.

Saha RN, Liu X, Pahan K (2006) Up-regulation of BDNF in astrocytes by TNF-alpha: a case for the neuroprotective role of cytokine. J Neuroimmune Pharmacol 1:212–222.

Sahún I, Delgado-García JM, Amador-Arjona A, Giralt A, Alberch J, Dierssen M, Gruart A (2007) Dissociation between CA3-CA1 synaptic plasticity and associative learning in TgNTRK3 transgenic mice. J Neurosci 27: 2253–2260.

Sasi M, Vignoli B, Canossa M, Blum R (2017) Neurobiology of local and intercellular BDNF signaling. Pflugers Arch 469:593–610.

Schneider F, Baldauf K, Wetzel W, Reymann KG (2015) Effects of methylphenidate on the behavior of male 5xFAD mice. Pharmacol Biochem Behav 128:68–77.

Song MS, Learman CR, Ahn KC, Baker GB, Kippe J, Field EM, Dunbar GL (2015) In vitro validation of effects of BDNF-expressing mesenchymal stem cells on neurodegeneration in primary cultured neurons of APP/PS1 mice. Neuroscience 307:37–50.

Stary CM, Sun X, Giffard RG (2015) Astrocytes protect against isoflurane neurotoxicity by buffering pro-brain-derived neurotrophic factor. Anesthesiology 123:810–819.

Tartaglia N, Du J, Tyler WJ, Neale E, Pozzo-Miller L, Lu B (2001) Protein synthesis-dependent and -independent regulation of hippocampal synapses by brain-derived neurotrophic factor. J Biol Chem 276:37585–37593.

Toda T, Gage FH (2018) Review: adult neurogenesis contributes to hippocampal plasticity. Cell Tissue Res 373:693–709.

Vignoli B, Battistini G, Melani R, Blum R, Santi S, Berardi N, Canossa M (2016) Peri-synaptic glia recycles brain-derived neurotrophic factor for LTP stabilization and memory retention. Neuron 92:873–887.

von Bohlen Und Halbach O, von Bohlen Und Halbach V (2018) BDNF effects on dendritic spine morphology and hippocampal function. Cell Tissue Res 373:729–741.

Waterhouse EG, An JJ, Orefice LL, Baydyuk M, Liao GY, Zheng K, Lu B, Xu B (2012) BDNF promotes differentiation and maturation of adult-born neurons through GABAergic transmission. J Neurosci 32:14318–14330.

Webster SJ, Bachstetter AD, Nelson PT, Schmitt FA, Van Eldik LJ (2014) Using mice to model Alzheimer's dementia: an overview of the clinical disease and the preclinical behavioral changes in 10 mouse models. Front Genet 5:88.

Wirths O, Bayer TA (2012) Intraneuronal abeta accumulation and neurodegeneration: lessons from transgenic models. Life Sci 91:1148–1152.

Yang EJ, Ahn S, Ryu J, Choi MS, Choi S, Chong YH, Hyun JW, Chang MJ,

Kim HS (2015) Phloroglucinol attenuates the cognitive deficits of the 5XFAD mouse model of Alzheimer's disease. PLoS One 10:e0135686.
Yoshii A, Constantine-Paton M (2010) Postsynaptic BDNF-TrkB signaling in synapse maturation, plasticity, and disease. Dev Neurobiol 70:304-322.
Yoshii A, Constantine-Paton M (2014) Postsynaptic localization of PSD-95 is regulated by all three pathways downstream of TrkB signaling. Front Synaptic Neurosci 6:6.
Yoshimoto Y, Lin Q, Collier TJ, Frim DM, Breakefield XO, Bohn MC (1995) Astrocytes retrovirally transduced with BDNF elicit behavioral improvement in a rat model of Parkinson's disease. Brain Res 691:25–36.
Yuki D, Sugiura Y, Zaima N, Akatsu H, Takei S, Yao I, Maesako M, Kinoshita A, Yamamoto T, Kon R, Sugiyama K, Setou M (2014) DHA-PC and PSD-95 decrease after loss of synaptophysin and before neuronal loss in patients with Alzheimer's disease. Sci Rep 4:7130.
Zhang Y, Qiu B, Wang J, Yao Y, Wang C, Liu J (2017) Effects of BDNF-transfected BMSCs on neural functional recovery and synaptophysin expression in rats with cerebral infarction. Mol Neurobiol 54:3813–3824.
Zhang Z, Liu X, Schroeder JP, Chan CB, Song M, Yu SP, Weinshenker D, Ye K (2014) 7,8-Dihydroxyflavone prevents synaptic loss and memory deficits in a mouse model of Alzheimer's disease. Neuropsychopharmacology 39:638–650.
Zucker RS, Regehr WG (2002) Short-term synaptic plasticity. Annu Rev Physiol 64:355–405.

4. Summary of the findings and conclusions

We demonstrated here that BDNF produced by astrocytes is crucial for dendrite outgrowth and spine number in neurons *in vitro*.

We discovered that overexpressing BDNF under the control of the GFAP promotor in astrocytes had beneficial effects on molecular and behavioral disorders associated with 5xFAD mutations. 5xF:pGB mice exhibited rescued BDNF/TrkB signaling activity associated with an improvement of dendritic spine density and morphology. Synaptic markers including PSD-95 and synaptophysin were also recovered in these mice and LTP *in vivo* was increased as compared to 5xFAD littermates.

Interestingly, we know that Pyk2 may be involved in the BDNF pathway as BDNF was shown to activate Pyk2 through STEP inhibition (Xu et al., 2016). Recently, BDNF was also shown to induce synaptic synthesis of Pyk2 in hippocampal neurons (Afonso et al., 2019). In light of this, the beneficial effects of overexpressing Pyk2 (Giralt et al., 2018) or BDNF (de Pins et al., 2019) in the hippocampus of 5xFAD mice are absolutely accordant.

Though, both BDNF and Pyk2 impairments may possibly contribute to the symptoms of AD and this particular study revealed the potential to take advantage of astrogliosis to produce and deliver BDNF locally in the damaged hippocampus of this transgenic AD model.

V. Pyk2 in nucleus accumbens D1 receptor-expressing neurons is selectively involved in the acute locomotor response to cocaine

Benoit de Pins, Enrica Montalban, Peter Vanhoutte, Albert Giralt and Jean-Antoine Girault

1. Context and objectives

We present here, in the form of a preliminary manuscript, the study of the role of Pyk2 in striatal function. The aim of this study was to analyze the potential function of Pyk2 in another brain area in which Pyk2 is also highly expressed but poorly studied. Moreover, knowing the aforementioned role of Pyk2 in HD, we wondered if such role could imply the striatum as well.

Being the main input structure of the basal ganglia, the striatum controls motor coordination, action selection and motivation. It is mainly composed of GABAergic striatal projection neurons (SPNs) divided in two populations according to the dopamine receptor (D1 and D2) expressed.

In this paper we aim to understand the role of Pyk2 in striatal associated functions and thereby focused on rotarod locomotor training and psychostimulant drugs responses.

Here we used various genetically modified mice (i.e. Pyk2 total knockout, conditioned to D1 or D2 neurons, or to specific striatal regions) and analyzed their relative performance in striatal-associated tasks (i.e. locomotor learning and drug-responses).

2. Contribution to the work

In this work, I personally contributed to the management of mice lines. I greatly contributed to the biochemistry experiments, behavior studies and tissue imaging and analysis. I also greatly contributed to the redaction of the manuscript.

3. Article

Pyk2 in D1 receptor-expressing neurons of the nucleus accumbens modulates the acute locomotor effects of cocaine

Benoit de Pins, MSc[1,2,3], Enrica Montalban, PhD[a,1,2,3], Peter Vanhoutte, PhD[2,4,5], Albert Giralt, PhD[b,1,2,3,*], and Jean-Antoine Girault, MD, PhD[d,1,2,3,*]

[1]Inserm UMR-S 1270, Paris, France.

[2]Sorbonne Université, Faculty of Sciences and Engineering, Paris, France.

[3]Institut du Fer à Moulin, Paris 75005, France.

[4]Inserm UMR-S 1130, Neurosciences Paris Seine, Paris, France.

[5]CNRS UMR 8246, Paris, France.

*equal contribution

[a] Current address: BFA - Unité de Biologie Fonctionnelle et Adaptative - CNRS UMR 8251, Université de Paris, 75205 Paris, France.

[b] Current address: Departament de Biomedicina, Facultat de Medicina, Institut de Neurociències, Universitat de Barcelona, Institut d'Investigacions Biomèdiques August Pi i Sunyer (IDIBAPS), Barcelona 08036, Spain and Centro de Investigación Biomédica en Red sobre Enfermedades Neurodegenerativas (CIBERNED), Madrid 28031, Spain.

[d] Corresponding author, e-mail: jean-antoine.girault@inserm.fr

Abstract

The striatum is a critical brain region for locomotor response to cocaine. Although the D1 receptor-expressing neurons are centrally involved in mediating the locomotor effects of cocaine, the molecular pathways controlling this response are not fully understood. Here we studied the role of Pyk2, a non-receptor calcium-dependent protein-tyrosine kinase, in striatum-related functions. We discovered that cocaine injection increases Pyk2 phosphorylation in the striatum of mice *in vivo*. Pyk2-deficient mice displayed an altered locomotor response to acute cocaine injection. In contrast, they developed normal locomotor sensitization and cocaine-conditioned place preference. Accordingly, a cocaine-activated signaling pathway essential for these late responses, ERK phosphorylation, was not altered. Specific deletion of Pyk2 in the nucleus accumbens or in D1 neurons reproduced this phenotype, whereas deletion of Pyk2 in the dorsal striatum or in A_{2A} receptor-expressing neurons did not. Mice lacking Pyk2 in D1-neurons also displayed lower locomotor response to the D1 receptor agonist SKF-81297 but not to an anticholinergic drug. Our results identify Pyk2 as a regulator of acute locomotor responses to psychostimulants and suggest that changes in Pyk2 expression or activation may alter specific responses to drugs of abuse, or possibly other behavioral responses linked to dopamine action.

Introduction

The striatum is the main input structure of the basal ganglia, involved in motor coordination, action selection, and motivation. The GABAergic medium-size, spiny striatal projection neurons (SPNs) constitute the vast majority of striatal neurons (~95% in rodents). They integrate cortical and thalamic excitatory inputs and are modulated by dopaminergic inputs and striatal interneurons [1]. Two major populations of SPNs can be distinguished according to their projection targets and their molecular profile [1–3]. SPNs enriched in enkephalin, D2 dopamine (D2R), and A_{2A} adenosine ($A_{2A}R$) receptors project to the external globus pallidus (GPe) thus participating in the indirect striatonigral pathway, while SPNs enriched in substance P, dynorphin, and D1 dopamine receptor (D1R) innervate the internal globus pallidus (GPi) and the substantia nigra pars reticulata (SNr), forming the direct pathway [1,2,4]. Striatal dysfunction is associated with several pathologies ranging from movement disorders in Parkinson's or Huntington's diseases to addiction [5]. The striatum is a major site of action of drugs of abuse which all share the ability to increase extracellular dopamine levels [6]. The signaling pathways involved in the action of glutamate, dopamine, and other neurotransmitters in SPNs have been extensively studied [7]. Although attention mostly focused on pathways involving protein serine/threonine phosphorylation, tyrosine phosphorylation is also likely to be important [8]. The regulation and functional importance of tyrosine kinases in striatal neurons are still poorly characterized.

Pyk2 is a Ca^{2+}-dependent non-receptor tyrosine kinase highly expressed in forebrain neurons [9] where it is activated by neuronal activity and excitatory neurotransmission [10–12]. Pyk2 can associate with the NMDA receptor complex and has a role in synaptic plasticity [11,13–15]. Ca^{2+} triggers Pyk2 autophosphorylation on Tyr-402, which recruits and activates Src-family kinases (SFKs) [16,17]. In turn, SFKs phosphorylate other residues in Pyk2 and associated proteins, and initiate multiple signaling pathways. The striatal-enriched protein tyrosine phosphatase (STEP) dephosphorylates Pyk2 [18]. Activated Pyk2 regulates many cellular functions [19,20] and Pyk2 is associated with several pathologies including cancer [21], inflammatory diseases [20], Huntington's [15] and Alzheimer's diseases [22–25]. Work with Pyk2 knockout mice showed that Pyk2 in the hippocampus is involved in spatial memory and regulates spine density and morphology, as well as long-term potentiation [15] and depression [26]. These studies illustrate the role of Pyk2 in synaptic functions and behavior in physiological and pathological conditions.

Here, we use constitutive and conditional KO mice to explore Pyk2 function in the striatum. We find that Pyk2 is preferentially expressed in D1 receptor-expressing SPNs in the ventral striatum. Pyk2 phosphorylation is increased following cocaine injection. Deletion of Pyk2 reduces the acute locomotor response to cocaine but, surprisingly, neither locomotor sensitization nor conditioned place preference. Use of conditional deletion shows a specific involvement of Pyk2 in D1 receptor-expressing SPNs of the nucleus accumbens (NAc) in this response.

Materials and Methods

Animals

Floxed Pyk2 mice ($Pyk2^{f/f}$) were generated by the insertion of LoxP sequences (Gen-O-way, Lyon, France) surrounding *PTK2B* exons 15b-18 coding for the kinase domain [27]. Homologous recombination was carried out in C57/Bl6 embryonic stem cells and germline transmission of the mutated allele was achieved in the same background. Floxed Pyk2 mice were initially bred to Cre-deleter mice to generate constitutive knockout mice, or to *Drd1::Cre* mice, Tg(Drd1a-cre)EY262Gsat [28], or *Adora2a::Cre* mice, Tg(Adora2a-cre)2MDkde [29], to generate conditional KO mice ($Pyk2^{f/f;D1::Cre}$ and $Pyk2^{f/f;A2A::Cre}$, respectively). Mice were housed at 19–22 °C with 40–60% humidity, under a 12:12 h light/dark cycle, and had ad libitum access to food and water. Animal experiments and handling were in accordance with ethical guidelines of Declaration of Helsinki and NIH, (1985-revised publication no. 85-23, European Community Guidelines), and French Agriculture and Forestry Ministry guidelines for handling animals (decree 87849, licence A 75-05-22) and approval of the Charles Darwin ethical committee project #2016111620082809. Mice used in this study were 3-6-month-old males.

Viral vectors and stereotaxic injection

For deletion of Pyk2 in the NAc or dorsal striatum (DS), 3-month $Pyk2^{f/f}$ mice were stereotaxically injected with AAV expressing Cre recombinase (AV-9-PV2521, AAV9.CamKII.HI.eGFP-Cre.WPRE.SV40, Perelman School of Medicine, University of Pennsylvania, USA), referred to below as AAV-Cre. As control, we injected AAVs expressing GFP (AV-9-PV1917, AAV9.CamKII0.4.eGFP.WPRE.rBG, same source), referred to below as AAV-GFP. Following anesthesia with pentobarbital (30 mg kg^{-1}), we performed

bilateral stereotaxic injections of AAV-GFP, AAV-GFP-Cre or AAV-GFP (2.6×10^9 GS per injection) in the NAc at the following coordinates from the bregma (millimeters), anteroposterior, 1.3, lateral, ±1.3, and dorsoventral, -4.5 or in the DS, anteroposterior, 0.9, lateral, ±1.5, and dorsoventral, -2.75. AAV injection was carried out in 2 min. The cannula was left in place for 5 min for complete virus diffusion before being slowly pulled out of the tissue. Mice were placed on a warm plate for 2 h after surgery, received a subcutaneous injection of a non-steroidal anti-inflammatory drug (meloxicam, 2 mg/kg) during 3 days, and allowed to recover for 3 weeks before starting behavioral experiments.

Behavioral experiments

Rotarod: 4-month mice were trained at accelerating speed (4 - 40 rpm for 5 min), with four sessions per day for three consecutive days and the latency to fall was recorded.

Locomotor activity: Mice were placed either in a open-field chamber (50 cm × 50 cm, L x W) for cocaine response or in a 20-cm diameter cylinder for SKF-81297 [SKF] or trihexyphenidyl [THX] response. After 30 minutes, mice were i.p. injected with cocaine (20 mg/kg), SKF (3 mg/kg), or THX (15 mg/kg) and placed back in the chamber for 1 hour. Locomotion was recorded using an overhead digital camera. The distance traveled was measured in 5-min bins using EthoVision software (Noldus, Wageningen, The Netherlands).

Conditioned place preference (CPP) was performed in two compartments of a Y-shaped maze (Imetronic, Pessac, France) with different wall textures and visual cues as follows. (i) Pretest: day-1, mice were placed in the center of the apparatus and allowed to explore freely both compartments for 20 min. The time spent in each compartment was recorded and the preferred and un-preferred compartments deduced for every mouse. (ii) Conditioning: day-2, mice were injected with saline and placed immediately in the preferred compartment for 15 min. The next day, they were placed in the other closed compartment after cocaine injection (15 mg/kg). This was repeated twice (3 saline-, 3 cocaine-pairings in total). (iii) Test: time spent in each compartment was measured on day-8 during 20 min. The CPP-score was calculated as the time spent in the cocaine-paired compartment during the test minus the time spent in this compartment during the pre-test.

Tissue preparation and immunofluorescence

Mice were euthanized, brains rapidly dissected and divided at the midline; one hemisphere was drop-fixed in 40 g/L paraformaldehyde (PFA) for 24 hours. The other hemisphere was

flash-frozen using CO_2 pellets and stored at -80º C. Following PFA fixation, 30-µm-thick sections were cut with a Vibratome (Leica, Wetzlar, Germany). Sections were incubated overnight at 4 °C with primary antibodies, rinsed several times in TBS, and incubated for 45 min with secondary antibody (all antibodies used are in **Table S1**). Nuclei were labelled with DAPI-containing Vectashield (Vector Laboratories, Burlingame, CA, USA). Pyk2 and GFP overall distribution was imaged with a DM6000–2 microscope (Leica). Calbindin and Pyk2 images were acquired with a Leica Confocal SP5-II (63× numerical aperture lens, 5× digital zoom, 1-Airy unit pinhole, 4-frame averaging per *z*-step, *z*-stacks every 2 µm, 1024 × 1024 pixel resolution). Images were analyzed with Icy open source software (https://icy.bioimageanalysis.org) [30].

Immunobloting

For the analysis of striatal proteins untreated mice were killed by cervical dislocation, striata dissected out, frozen using CO_2 pellets and stored at −80 °C until use. For pharmacological responses mice were i.p. injected with cocaine (20 mg/kg) or saline and placed in a 43 cm x 27 cm cage. After 10 minutes, mice were euthanized and heads were dipped in liquid nitrogen for 12 seconds. The frozen heads were cut into 210-µm-thick slices with a cryostat, and 10 frozen microdisks (1.4 mm diameter) were punched out bilaterally from the striatum and stored at −80°C until use. Tissue samples were sonicated in 10 g/L SDS and 1 mM sodium orthovanadate in water, and placed at 100 °C for 5 min. Extracts (15 µg protein) were separated by SDS–PAGE and transferred to nitrocellulose membranes (GE Healthcare, Chicago, IL, USA). Membranes were blocked in TBS-T (150 mM NaCl, 20 mM Tris-HCl, pH 7.5, 0.5 ml l^{-1} Tween 20) with 30 g/L BSA. Membranes were incubated overnight at 4 °C with primary antibodies (**Table S1**), washed several times in TBS-T, and incubated with secondary antibodies, which were detected by Odyssey infrared imaging (Li-Cor Inc., Lincoln, NE, USA). For loading control a mouse monoclonal β-actin antibody was used.

Immunoprecipitation

Mice were i.p. injected with cocaine (20 mg/kg) and placed in a 43 cm x 27 cm cage. After 10 minutes, mice were euthanized and heads dipped in liquid nitrogen for 5 seconds. The striatum was dissected out, lysed by sonication in 250 µl NP-40 lysis buffer [150 mM NaCl, 50 mM Tris-HCl, pH 8.0, 10 mM NaF, 1% NP40 (v/v) supplemented with 1 mM sodium orthovanadate, phosphatase inhibitor (PhosSTOP, Roche, Basel, Switzerland) and protease inhibitor (Complete, Roche)]. Lysates were centrifuged for 20 min at 20,937 g (4°C). Protein

A-Sepharose beads (GE Healthcare) were pre-cleared by mixing with 14% Sephacryl S-100 (v/v) (GE Healthcare) and saturated with BSA (25 g/L). The beads were then mixed for 1 hour at 4 °C with rabbit polyclonal anti-Pyk2 antibody (1.7% v/v) (#P3902, Sigma-Aldrich, St. Louis, MO, USA) prior incubation overnight at 4°C with supernatant. The beads were washed three times, resuspended in Laemmli loading buffer, heated at 100 °C for 10 min, and subjected to SDS-PAGE.

Statistical analysis

Analyses were done using Prism version 6.00 for Windows (GraphPad Software, La Jolla, CA, USA). Data are expressed as means $\pm$ SEM. Normal distribution was tested with d'Agostino and Pearson omnibus, Shapiro-Wilk, and Kolmogorov-Smirnov tests. If no difference from normality was detected, statistical analysis was performed using two-tailed Student's t-test or ANOVA and Holm-Sidak's post-hoc test. Otherwise non-parametric Mann and Whitney or Kruskal-Wallis' and Dunn's tests were used. $p < 0.05$ was considered as significant.

Results

Pyk2 is enriched in ventral D1 SPNs

We used immunohistochemistry to evaluate the regional distribution of Pyk2 in the striatum. Pyk2 immunoreactivity was enriched in the NAc as opposed to the DS (**Figure 1A**), in agreement with a previous study of mRNA distribution [31]. Since Pyk2 striatal immunoreactivity displayed an irregular pattern, we assessed whether its distribution followed the neurochemically-defined patch/matrix compartmentalization [32–34] defined by calbindin, a matrix-enriched protein (**Figures S1A** and **B**). Pyk2 was slightly more expressed in calbindin-positive neurons indicating an enrichment of Pyk2 in matrix compartments (**Figure S1C**). To evaluate the relative expression of Pyk2 in neurons of the direct and indirect pathways, we compared its decrease following conditional deletion. Pyk2 striatal protein levels were decreased by 67 % in $Pyk2^{f/f;D1::Cre}$ mice and by 36% in $Pyk2^{f/f;A2A::Cre}$ mice as compared to matched $Pyk2^{f/f}$ mice (**Figure 1B**), suggesting a higher expression of Pyk2 in D1R-expressing SPNs. Although the wider expression of D1R during the development of the striatum than in the adult [35,36] could lead to a broader developmental action of D1::Cre and subsequent overestimation of the apparent enrichment of Pyk2 in D1

neurons, the conclusion was strengthened by the parallel lower Pyk2 protein decrease in $Pyk2^{f/f;A2A::Cre}$ mice.

Pyk2 deletion does not alter striatal proteins

In the hippocampus of $Pyk2^{-/-}$ mice, we previously observed decreased levels of several synaptic proteins [15]. In the striatum, neither GluN2A nor PSD-95 levels were altered in $Pyk2^{-/-}$ mice (**Figures 1C** and **D**). GluN2B levels were slightly increased in the striatum of $Pyk2^{-/-}$ mice without change in its phosphorylation. To examine the overall status of SPNs, we measured SPN-enriched proteins, Gαolf [37] and dopamine- and cAMP-regulated neuronal phosphoprotein (DARPP-32) [38]. Their levels were not altered by the mutation (**Figures S2A** and **B**). We finally assessed whether Pyk2 deletion affected a general presynaptic marker synapsin 1 or a dopamine terminals marker tyrosine hydroxylase (TH) in the striatum. We did not observe any change in these protein levels (**Figures S2C** and **D**). These results show that, in contrast to other brain regions, the absence of Pyk2 does not alter basal synaptic or neuronal markers, suggesting regional differences in its function.

Pyk2 knockout does not impair motor coordination

To study the role of Pyk2 in the striatum, we first assessed motor coordination. $Pyk2^{+/+}$ and $Pyk2^{-/-}$ mice were trained on an accelerating rotarod for 3 days and their motor coordination was evaluated by measuring the time they were able to stay on the rod during each trial. Mice of both genotypes displayed similar performance, improving their ability to stay on the rod trial after trial (**Figure S3A**). Similarly, specific deletion of Pyk2 in the NAc or the DS induced by AAV-mediated Cre expression, or in $Pyk2^{f/f;D1::Cre}$ or $Pyk2^{f/f;A2A::Cre}$ mice had no effect on the rotarod performance (**Figures S3B-E**), showing that motor coordination in this test is not altered in the absence of Pyk2.

Pyk2 is activated by cocaine and involved in its acute locomotor effects but not in sensitization

Considering the relative enrichment of Pyk2 in the NAc, a region involved in reward response and addiction, we assessed a possible role of Pyk2 in the effects of cocaine. We immunoprecipitated Pyk2 from striatal extracts of saline- or cocaine-injected mice and measured its tyrosine phosphorylation by immunoblotting (**Figure 2A**). Tyrosine phosphorylation of Pyk2 was increased 10 min after cocaine injection, indicating its activation in response to cocaine injection (**Figure 2B**).

We then explored a possible role of Pyk2 in the acute response to cocaine by comparing locomotor activity of $Pyk2^{+/+}$ and $Pyk2^{-/-}$ mice after cocaine injection. Basal locomotor activity was similar in the two groups of mice, whereas cocaine-induced hyperlocomotion was decreased in $Pyk2^{-/-}$ mice (**Figure 2C**). Repeated cocaine exposure increases behavioral responses due to a sensitization mechanism [39], which is clearly visible following a single cocaine administration [40]. We therefore injected cocaine a second time, thirteen days later, to assess locomotor sensitization (**Figure 2D**). Locomotor response to the second injection of cocaine was increased in both $Pyk2^{+/+}$ and $Pyk2^{-/-}$ mice (**Figure 2E**) and the 2^{nd} injection/ 1^{st} injection response ratio was not different between the two groups (**Figure 2F**). These results show a role of Pyk2 in the acute cocaine-induced locomotor response but not in its sensitization.

Pyk2 deficit in the NAc, but not DS, recapitulates the effects of full KO on acute cocaine effects

To identify the striatal region implicated in the effects of Pyk2 deletion, we studied cocaine responses in $Pyk2^{f/f}$ mice bilaterally injected with AAV-GFP-Cre in the NAc or in the DS (**Figure 3**). The position of the tip of the injection needle and the spread of GFP expression was systematically checked on one side of the brain (**Figures 3A** and **B)**, the other side being used for immunoblotting. Animals in which the injection was not correctly located were not included in the statistical analysis. Pyk2 immunoreactivity was clearly decreased in the GFP-expressing area (**Figures 3A** and **B**). In mice injected with AAV-GFP-Cre in the NAc, basal locomotor activity was unchanged, but acute locomotor response to cocaine was decreased as compared to mice injected with AAV-GFP (**Figure 3C**). Following a second injection of cocaine at day 14, the locomotor response increased in the two groups of mice and the difference between them was blunted (**Figure 3D**). Sensitization was observed in AAV-GFP and AAV-GFP-Cre mice and the response ratio was not significantly different between the two groups (**Figures S4A** and **3E**). Bilateral injection of AAV-GFP or AAV-GFP-Cre in the DS did not alter the locomotor effects of the first (**Figure 3F**) or second injection of cocaine (**Figures 3G**, **S4B**, and **3H**). These results provide evidence that the NAc is the region implicated in Pyk2 regulation of cocaine locomotor response.

Pyk2 deficit in D1, but not A_{2A} SPNs, recapitulates the effects of the full KO on acute cocaine effects

To determine which SPN population was involved in the consequences of Pyk2 deletion, we studied cocaine responses in $Pyk2^{f/f;D1::Cre}$ and $Pyk2^{f/f;A2A::Cre}$ mice (see **Figures 1B** and **4**). Acute locomotor effects of cocaine first injection were decreased in $Pyk2^{f/f;D1::Cre}$ as compared to $Pyk2^{f/f}$ control mice (**Figure 4A**). The response of $Pyk2^{f/f;D1::Cre}$ mice to the second injection of cocaine was still decreased as compared to controls (**Figure 4B**) but a similar sensitization was observed in both genotypes (**Figures S5A** and **4C**). Conversely $Pyk2^{f/f;A2A::Cre}$ mice displayed similar responses as $Pyk2^{f/f}$ mice in response to the first and second injections and comparable sensitization (**Figures 4D-E** and **S5B**). These results indicate that the absence of Pyk2 in D1R-expressing neurons is responsible for the alteration of the locomotor response to cocaine.

Pyk2 knockout has minor effects on cocaine-induced signaling and does not alter conditioned place preference

Cocaine injection was reported to increase GluN2B phosphorylation at Tyr-1472 and to activate SFK, thus contributing to ERK activation [8]. To evaluate the role of Pyk2 in this response we compared the effects of cocaine on Tyr1472-GluN2B phosphorylation in $Pyk2^{f/f;D1::Cre}$ and $Pyk2^{f/f}$ mice. In Pyk2-mutant mice, 10 min after cocaine injection, the increase in pTyr1472-GluN2B was blunted and not significant (**Figures S6A** and **B**). This minor alteration may reflect the direct or indirect role of Pyk2 in the phosphorylation of the NMDA receptor. However, the absence of Pyk2 in D1 SPNs did not prevent the activation of ERK (**Figures S6A** and **C**), a step critical for long-term effects of cocaine [7].

We then evaluated the rewarding properties of cocaine in Pyk2 mutant mice, which involve D1 receptors [41–43]. We measured cocaine-CPP in wild-type and mutant mice (**Figure S7**). The time spent in the cocaine-paired arm after conditioning was similarly increased in $Pyk2^{-/-}$ and $Pyk2^{+/+}$ mice (**Figure S7A**). The CPP score did not differ between $Pyk2^{-/-}$ and $Pyk2^{+/+}$ mice (**Figure S7B**), demonstrating that mice underwent efficient CPP in the absence of Pyk2. We also examined whether specific deletion of Pyk2 in the NAc or DS, or in D1R- or A_{2A}R-expressing SPNs had any effect on CPP (**Figure S7C-F**). CPP scores were not modified in any of the mutant groups as compared to their respective controls, confirming the lack of involvement of Pyk2 in CPP. This result is in agreement with the observation that in the absence of Pyk2, ERK signaling pathway, which plays a critical role in cocaine-CPP [44], was still activated.

Pyk2 is involved in the acute locomotor effects of a D1R agonist but not a cholinergic antagonist

Since the consequences of the absence of Pyk2 on acute locomotor effects of cocaine appeared to result from Pyk2 deficit in D1 neurons, we examined whether effects of D1R stimulation were altered. We used SKF-81297, a D1R selective agonist, known to increase locomotor activity [45–47]. The acute locomotor response to SKF-81297 was slightly reduced in $Pyk2^{f/f;D1::Cre}$ mice as compared to $Pyk2^{f/f}$ mice (**Figure 5A**). As reported in previous studies [48–50], a sensitization of the response was observed following the second injection in wild-type and mutant mice (**Figure 5B**). Interestingly, the first and second injection of SKF-81297 both had a biphasic effect on locomotor activity, not previously reported to our knowledge. We analyzed separately the sensitization during the first 10 minutes following injection (**Figures 5C** and **D**) and from 10 to 40 minutes (**Figures 5E** and **F**). Sensitization was significant for these two different phases without difference between $Pyk2^{f/f;D1::Cre}$ and $Pyk2^{f/f}$ mice (**Figures 5-F**). To determine whether Pyk2 could decrease any kind of drug-induced locomotor activity, we tested the effects of trihexyphenidine (THX), an anticholinergic substance that increases locomotor activity [51]. We found no difference in locomotor activity between $Pyk2^{f/f;D1::Cre}$ and $Pyk2^{f/f}$ mice following the first or second injection of THX (**Figure S8A** and **B**). The responses to the two injections of THX were similar without locomotor sensitization in either genotype (**Figure S8C**). These results indicate that Pyk2 is selectively involved in the locomotor activity induced by stimulation of D1 receptors.

Discussion

In this study, we show the involvement of the non-receptor tyrosine kinase Pyk2 in the acute locomotor response to cocaine. We demonstrate that complete knockout of Pyk2 or its specific deletion in the NAc or in D1R-expressing neurons decreases acute cocaine-induced hyperlocomotion. Acute locomotor response to a selective D1 agonist but not to a cholinergic antagonist was also decreased. These results indicate a role of Pyk2 located in D1R-expressing neurons of the NAc in the D1-induced acute locomotor response. In contrast no alteration was observed in locomotor sensitization or cocaine-CPP.

Our study of the expression pattern of Pyk2 in the striatum confirmed its enrichment of Pyk2 in the ventral part of the striatum, previously reported [31]. We also provide evidence for a relative enrichment in D1R- expressing SPNs which form the 'direct pathway' [52] and in the matrix compartment of the striatum which plays a specific yet incompletely characterized role in striatal function [53]. The dorsal striatum is implicated in the control of movement and the learning process of skilled task [54,55]. We assessed motor coordination of mice with accelerating rotarod training [56], which can be impaired by alteration of various brain areas, including basal ganglia, motor cortex, and cerebellum [57]. We did not observe any difference between control and Pyk2 mutant mice, suggesting that Pyk2 is not necessary for the function of the dorsal striatum where it is relatively less expressed. Pyk2 is more expressed in the NAc, which is a key component in brain circuitry underlying drug-evoked behaviors [58,59]. We demonstrated that tyrosine phosphorylation of Pyk2 in the striatum was increased following a single injection of cocaine. Pyk2 is activated by Ca^{2+}-induced autophosphorylation of Tyr-402, followed by recruitment of SFKs which in turn phosphorylate Pyk2 on other tyrosine residues, although in some cells activation of SFKs can be the triggering mechanism (see ref. [17] for a review). Cocaine injection in naïve mice increases the concentration of calcium in D1 SPNs [60] providing a possible basis for Pyk2 activation. In addition, cocaine-induced activation of Fyn has been reported in the striatum and proposed to be involved in NMDA receptors regulation and their synergism with D1R to activate the ERK pathway [8]. Although this could suggest a role of Pyk2 in ERK activation, ERK phosphorylation was still observed in Pyk2-deficient mice, underlining the redundancy in the mechanisms controlling ERK activation.

Concerning the functional consequences of Pyk2 knock-out, we found that the acute cocaine locomotor response was decreased, whereas locomotor sensitization and CPP, which are known to involve synaptic plasticity and ERK activation [7], were not altered. The impaired acute locomotor response was also observed in mice specifically lacking Pyk2 in the NAc or in D1R-expressing neurons, but not in those devoid of Pyk2 in the DS or in A_{2A}R-expressing neurons. This combination of results implicates an alteration induced by the absence of Pyk2 in the D1R-expressing neurons of the NAc. This conclusion is supported by the role of these neurons in the acute locomotor effects of psychostimulants [61–63]. A decreased locomotor response without alteration in locomotor sensitization or CPP was also observed in Gαolf heterozygous (*Gnal*$^{+/-}$) mutant mice in which cAMP production is decreased [64]. These similarities could indicate a role for Pyk2 in D1R/Gαolf/cAMP

pathway modulation, a hypothesis supported by slightly lower locomotor response to the D1 agonist SKF-81297 in $Pyk2^{f/f;D1::Cre}$ mice. However we did not find any change in Gαolf levels in the mutant mice. The only effect we observed was a blunting of GluN2B receptor phosphorylation at Tyr1472, in good agreement with the role of Pyk2 in the phosphorylation of the NMDAR [11], but unlikely to explain by itself the effects on locomotor activity. Therefore we hypothesize that Pyk2 is also implicated in the regulation of other signaling mechanisms important for D1-mediated regulation of locomotor activity. Further work will be necessary to explore this hypothesis and in particular whether Pyk2 modulates the production of cAMP in response to D1R stimulation. Our study clearly identifies the significant but circumscribed contribution of Pyk2 in NAC D1 neurons to the acute locomotor effects of cocaine. It raises the question of its role in other dopamine-mediated actions and opens novel avenues for investigating signaling mechanisms in striatal neurons.

Funding and Disclosure

BdP was supported in part by the *Fondation pour la Recherche Médicale* (FRM). AG is now a Ramón y Cajal fellow (RYC-2016-19466). JAG lab was supported in part by Inserm, *Sorbonne Université*, the FRM, ERC AdG-2009, a KAUST collaborative grant to JAG and S Arold, and the Bio-Psy (Biology for Psychiatry) laboratory of excellence. Relevant experiments were carried out at the IFM *Rodent breeding and phenotyping* and *Cell and Tissue Imaging* facilities. The *Cell and tissue imaging* facility at the IFM benefited from supports of *Espoir en Tête/Fondation pour la Recherche sur le Cerveau, Région Ile-de-France*, and Inserm.

The authors declare no competing financial interests

Acknowledgements

The authors thank the late Paul Greengard (The Rockefeller University) for the gift of antibodies for synapsin 1, DARPP-32 and phosphoT75-DARPP-32, and Alban de Kerchove d'Exaerde (*Université libre de Bruxelles*) for providing Adora2a::Cre mice, Manuel Mameli (University of Lausanne) and Kristina Valentinova (University of Bern) for their help when they were at the IFM and for critical reading of the manuscript. We thank Denis Hervé for expert advice.

References

1. Gerfen CR, Surmeier DJ. Modulation of striatal projection systems by dopamine. Annu Rev Neurosci. 2011;34:441–466.

2. Gerfen CR, Engber TM, Mahan LC, Susel Z, Chase TN, Monsma FJ, et al. D1 and D2 dopamine receptor-regulated gene expression of striatonigral and striatopallidal neurons. Science. 1990;250:1429–1432.

3. Valjent E, Bertran-Gonzalez J, Hervé D, Fisone G, Girault J-A. Looking BAC at striatal signaling: cell-specific analysis in new transgenic mice. Trends Neurosci. 2009;32:538–547.

4. Gerfen CR, Young WS. Distribution of striatonigral and striatopallidal peptidergic neurons in both patch and matrix compartments: an in situ hybridization histochemistry and fluorescent retrograde tracing study. Brain Res. 1988;460:161–167.

5. Gardoni F, Bellone C. Modulation of the glutamatergic transmission by Dopamine: a focus on Parkinson, Huntington and Addiction diseases. Front Cell Neurosci. 2015;9:25.

6. Lüscher C, Malenka RC. Drug-evoked synaptic plasticity in addiction: from molecular changes to circuit remodeling. Neuron. 2011;69:650–663.

7. Girault J-A. Signaling in striatal neurons: the phosphoproteins of reward, addiction, and dyskinesia. Prog Mol Biol Transl Sci. 2012;106:33–62.

8. Pascoli V, Besnard A, Hervé D, Pagès C, Heck N, Girault J-A, et al. Cyclic adenosine monophosphate-independent tyrosine phosphorylation of NR2B mediates cocaine-induced extracellular signal-regulated kinase activation. Biol Psychiatry. 2011;69:218–227.

9. Menegon A, Burgaya F, Baudot P, Dunlap DD, Girault JA, Valtorta F. FAK+ and PYK2/CAKbeta, two related tyrosine kinases highly expressed in the central nervous system: similarities and differences in the expression pattern. Eur J Neurosci. 1999;11:3777–3788.

10. Corvol J-C, Valjent E, Toutant M, Enslen H, Irinopoulou T, Lev S, et al. Depolarization activates ERK and proline-rich tyrosine kinase 2 (PYK2) independently

in different cellular compartments in hippocampal slices. J Biol Chem. 2005;280:660–668.

11. Huang Y, Lu W, Ali DW, Pelkey KA, Pitcher GM, Lu YM, et al. CAKbeta/Pyk2 kinase is a signaling link for induction of long-term potentiation in CA1 hippocampus. Neuron. 2001;29:485–496.

12. Siciliano JC, Toutant M, Derkinderen P, Sasaki T, Girault JA. Differential regulation of proline-rich tyrosine kinase 2/cell adhesion kinase beta (PYK2/CAKbeta) and pp125(FAK) by glutamate and depolarization in rat hippocampus. J Biol Chem. 1996;271:28942–28946.

13. Hsin H, Kim MJ, Wang C-F, Sheng M. Proline-Rich Tyrosine Kinase 2 Regulates Hippocampal Long-Term Depression. J Neurosci. 2010;30:11983–11993.

14. Bartos JA, Ulrich JD, Li H, Beazely MA, Chen Y, Macdonald JF, et al. Postsynaptic clustering and activation of Pyk2 by PSD-95. J Neurosci. 2010;30:449–463.

15. Giralt A, Brito V, Chevy Q, Simonnet C, Otsu Y, Cifuentes-Díaz C, et al. Pyk2 modulates hippocampal excitatory synapses and contributes to cognitive deficits in a Huntington's disease model. Nat Commun. 2017;8:15592.

16. Dikic I, Tokiwa G, Lev S, Courtneidge SA, Schlessinger J. A role for Pyk2 and Src in linking G-protein-coupled receptors with MAP kinase activation. Nature. 1996;383:547–550.

17. Walkiewicz KW, Girault J-A, Arold ST. How to awaken your nanomachines: Site-specific activation of focal adhesion kinases through ligand interactions. Prog Biophys Mol Biol. 2015;119:60–71.

18. Xu J, Kurup P, Bartos JA, Patriarchi T, Hell JW, Lombroso PJ. Striatal-enriched Protein-tyrosine Phosphatase (STEP) Regulates Pyk2 Kinase Activity. J Biol Chem. 2012;287:20942–20956.

19. Schaller MD. Cellular functions of FAK kinases: insight into molecular mechanisms and novel functions. J Cell Sci. 2010;123:1007–1013.

20. Zhu X, Bao Y, Guo Y, Yang W. Proline-Rich Protein Tyrosine Kinase 2 in Inflammation and Cancer. Cancers (Basel). 2018;10:139.

21. Shen T, Guo Q. Role of Pyk2 in Human Cancers. Med Sci Monit. 2018;24:8172–8182.

22. Lambert JC, Ibrahim-Verbaas CA, Harold D, Naj AC, Sims R, Bellenguez C, et al. Meta-analysis of 74,046 individuals identifies 11 new susceptibility loci for Alzheimer's disease. Nat Genet. 2013;45:1452–1458.

23. Salazar S V., Cox TO, Lee S, Brody AH, Chyung AS, Haas LT, et al. Alzheimer's Disease Risk Factor Pyk2 Mediates Amyloid-β-Induced Synaptic Dysfunction and Loss. J Neurosci. 2019;39:758–772.

24. Lee S, Salazar S V., Cox TO, Strittmatter SM. Pyk2 Signaling through Graf1 and RhoA GTPase Is Required for Amyloid-β Oligomer-Triggered Synapse Loss. J Neurosci. 2019;39:1910–1929.

25. Giralt A, de Pins B, Cifuentes-Díaz C, López-Molina L, Farah AT, Tible M, et al. PTK2B/Pyk2 overexpression improves a mouse model of Alzheimer's disease. Exp Neurol. 2018;307:62–73.

26. Montalban E, Al-Massadi O, Sancho-Balsells A, Brito V, de Pins B, Alberch J, et al. Pyk2 in the amygdala modulates chronic stress sequelae via PSD-95-related micro-structural changes. Transl Psychiatry. 2019;9:3.

27. Giralt A, Coura R, Girault J-A. Pyk2 is essential for astrocytes mobility following brain lesion. Glia. 2016;64:620–634.

28. Gong S, Doughty M, Harbaugh CR, Cummins A, Hatten ME, Heintz N, et al. Targeting Cre recombinase to specific neuron populations with bacterial artificial chromosome constructs. J Neurosci. 2007;27:9817–9823.

29. Durieux PF, Bearzatto B, Guiducci S, Buch T, Waisman A, Zoli M, et al. D2R striatopallidal neurons inhibit both locomotor and drug reward processes. Nat Neurosci. 2009;12:393–395.

30. de Chaumont F, Dallongeville S, Chenouard N, Hervé N, Pop S, Provoost T, et al. Icy: an open bioimage informatics platform for extended reproducible research. Nat Methods. 2012;9:690–696.

31. Sheehan TP, Neve RL, Duman RS, Russell DS. Antidepressant effect of the calcium-activated tyrosine kinase Pyk2 in the lateral septum. Biol Psychiatry. 2003;54:540–551.

32. Gerfen CR. The neostriatal mosaic: compartmentalization of corticostriatal input and striatonigral output systems. Nature;311:461–464.

33. Pert CB, Kuhar MJ, Snyder SH. Opiate receptor: autoradiographic localization in rat brain. Proc Natl Acad Sci. 1976;73:3729–3733.

34. Herkenham M, Pert CB. Mosaic distribution of opiate receptors, parafascicular projections and acetylcholinesterase in rat striatum. Nature. 1981;291:415–418.

35. Shearman LP, Zeitzer J, Weaver DR. Widespread expression of functional D1-dopamine receptors in fetal rat brain. Brain Res Dev Brain Res. 1997;102:105–115.

36. Araki KY, Sims JR, Bhide PG. Dopamine receptor mRNA and protein expression in the mouse corpus striatum and cerebral cortex during pre- and postnatal development. Brain Res. 2007;1156:31–45.

37. Hervé D, Lévi-Strauss M, Marey-Semper I, Verney C, Tassin JP, Glowinski J, et al. G(olf) and Gs in rat basal ganglia: possible involvement of G(olf) in the coupling of dopamine D1 receptor with adenylyl cyclase. J Neurosci. 1993;13:2237–2248.

38. Ouimet CC, Miller PE, Hemmings HC, Walaas SI, Greengard P. DARPP-32, a dopamine- and adenosine 3':5'-monophosphate-regulated phosphoprotein enriched in dopamine-innervated brain regions. III. Immunocytochemical localization. J Neurosci. 1984;4:111–124.

39. Steketee JD, Kalivas PW. Drug wanting: behavioral sensitization and relapse to drug-seeking behavior. Pharmacol Rev. 2011;63:348–365.

40. Valjent E, Bertran-Gonzalez J, Aubier B, Greengard P, Hervé D, Girault J-A. Mechanisms of locomotor sensitization to drugs of abuse in a two-injection protocol. Neuropsychopharmacology. 2010;35:401–415.

41. Marion-Poll L, Besnard A, Longueville S, Valjent E, Engmann O, Caboche J, et al. Cocaine conditioned place preference: unexpected suppression of preference due to testing combined with strong conditioning. Addict Biol. 2019;24:364–375.

42. Galaj E, Manuszak M, Arastehmanesh D, Ranaldi R. Microinjections of a dopamine D1 receptor antagonist into the ventral tegmental area block the expression of cocaine conditioned place preference in rats. Behav Brain Res. 2014;272:279–285.

43. Zhang L, Huang L, Lu K, Liu Y, Tu G, Zhu M, et al. Cocaine-induced synaptic structural modification is differentially regulated by dopamine D1 and D3 receptors-mediated signaling pathways. Addict Biol. 2017;22:1842–1855.

44. Girault J-A, Valjent E, Caboche J, Hervé D. ERK2: a logical AND gate critical for drug-induced plasticity? Curr Opin Pharmacol. 2007;7:77–85.

45. Chartoff EH, Marck BT, Matsumoto AM, Dorsa DM, Palmiter RD. Induction of stereotypy in dopamine-deficient mice requires striatal D1 receptor activation. Proc Natl Acad Sci U S A. 2001;98:10451–10456.

46. Medvedev IO, Ramsey AJ, Masoud ST, Bermejo MK, Urs N, Sotnikova TD, et al. D1 Dopamine Receptor Coupling to PLC Regulates Forward Locomotion in Mice. J Neurosci. 2013;33:18125–18133.

47. Yano H, Cai N-S, Xu M, Verma RK, Rea W, Hoffman AF, et al. Gs- versus Golf-dependent functional selectivity mediated by the dopamine D1 receptor. Nat Commun. 2018;9:486.

48. Chen J-F, Moratalla R, Yu L, Martín AB, Xu K, Bastia E, et al. Inactivation of adenosine A2A receptors selectively attenuates amphetamine-induced behavioral sensitization. Neuropsychopharmacology. 2003;28:1086–1095.

49. Edwards S, Whisler KN, Fuller DC, Orsulak PJ, Self DW. Addiction-related alterations in D1 and D2 dopamine receptor behavioral responses following chronic cocaine self-administration. Neuropsychopharmacology. 2007;32:354–366.

50. Doly S, Quentin E, Eddine R, Tolu S, Fernandez SP, Bertran-Gonzalez J, et al. Serotonin 2B Receptors in Mesoaccumbens Dopamine Pathway Regulate Cocaine Responses. J Neurosci. 2017;37:10372–10388.

51. Sipos ML, Burchnell V, Galbicka G. Dose-response curves and time-course effects of selected anticholinergics on locomotor activity in rats. Psychopharmacology (Berl). 1999;147:250–256.

52. Grillner S, Robertson B. The Basal Ganglia Over 500 Million Years. Curr Biol. 2016;26:R1088–R1100.

53. Brimblecombe KR, Cragg SJ. The Striosome and Matrix Compartments of the Striatum: A Path through the Labyrinth from Neurochemistry toward Function. ACS

Chem Neurosci. 2017;8:235–242.

54. Costa RM, Cohen D, Nicolelis MAL. Differential Corticostriatal Plasticity during Fast and Slow Motor Skill Learning in Mice. Curr Biol. 2004;14:1124–1134.

55. Luft AR, Buitrago MM, Ringer T, Dichgans J, Schulz JB. Motor Skill Learning Depends on Protein Synthesis in Motor Cortex after Training. J Neurosci. 2004;24:6515–6520.

56. Jones BJ, Roberts DJ. A rotarod suitable for quantitative measurements of motor incoordination in naive mice. Naunyn Schmiedebergs Arch Exp Pathol Pharmakol. 1968;259:211.

57. Doyon J, Bellec P, Amsel R, Penhune V, Monchi O, Carrier J, et al. Contributions of the basal ganglia and functionally related brain structures to motor learning. Behav Brain Res. 2009;199:61–75.

58. Quintero GC. Role of nucleus accumbens glutamatergic plasticity in drug addiction. Neuropsychiatr Dis Treat. 2013;9:1499–1512.

59. Hikida T, Morita M, Macpherson T. Neural mechanisms of the nucleus accumbens circuit in reward and aversive learning. Neurosci Res. 2016;108:1–5.

60. Luo Z, Volkow ND, Heintz N, Pan Y, Du C. Acute cocaine induces fast activation of D1 receptor and progressive deactivation of D2 receptor striatal neurons: in vivo optical microprobe [Ca2+]i imaging. J Neurosci. 2011;31:13180–13190.

61. Kelly PH, Iversen SD. Selective 6OHDA-induced destruction of mesolimbic dopamine neurons: abolition of psychostimulant-induced locomotor activity in rats. Eur J Pharmacol. 1976;40:45–56.

62. Kaddis FG, Wallace LJ, Uretsky NJ. AMPA/kainate antagonists in the nucleus accumbens inhibit locomotor stimulatory response to cocaine and dopamine agonists. Pharmacol Biochem Behav. 1993;46:703–708.

63. Xu M, Hu XT, Cooper DC, Moratalla R, Graybiel AM, White FJ, et al. Elimination of cocaine-induced hyperactivity and dopamine-mediated neurophysiological effects in dopamine D1 receptor mutant mice. Cell. 1994;79:945–955.

64. Faure C, Corvol J-C, Toutant M, Valjent E, Hvalby O, Jensen V, et al. Calcineurin is

essential for depolarization-induced nuclear translocation and tyrosine phosphorylation of PYK2 in neurons. J Cell Sci. 2007;120:3034–3044.

Figure legends

Figure 1: Characterization of Pyk2 expression in the striatum. a Left panel, dorsoventral distribution of Pyk2 immunoreactivity in the striatum of wild type mice. Right panel, Pyk2 labelling intensity in the dorsal and ventral striatum was measured in 8 sections from -0.2 to 1.2 mm to bregma, averaged and plotted (3 mice). Scale bar: 300 µm. Unpaired t test, ** p<0.01. **b** Immunoblotting analysis of Pyk2 protein in the striatum of $Pyk2^{f/f;D1::Cre}$ and $Pyk2^{f/f;A2A::Cre}$, and matched $Pyk2^{f/f}$ control mice. Unpaired t-test, ****$p < 0.0001$, **$p < 0.01$. **c** Immunoblotting analysis of Pyk2, NMDA receptors subunits, PSD-95 and actin as loading control, in 4-month $Pyk2^{+/+}$ and $Pyk2^{-/-}$ mice. **d** Densitometry quantification of results as in **c**. Data were normalized to actin for each sample and expressed as percentage of wild type mean density. Unpaired t-test, *$p < 0.05$ and ****$p < 0.0001$. For number of replicates and detailed statistical analysis, see **Supplementary Table 2**.

Figure 2: Pyk2 is implicated in acute cocaine responses. a, Phospho-Tyr immunoblotting of Pyk2 immunoprecipitated (IP) from striatal extracts of wild-type mice killed 10 min after i.p. injection of saline (Sal) or cocaine (20 mg/kg, Coc). **b**, Densitometry quantification of results as in **a**. Data are ratios of phospho/total Pyk2 for each sample and expressed as percentage of the mean ratios in saline-treated samples. Unpaired t-test, *p < 0.05. **c-d**, Locomotor activity of $Pyk2^{+/+}$ and $Pyk2^{-/-}$ mice after the first (**c**) and the second injection (**d**, 13 days later) of cocaine. Cocaine (20 mg/kg, Coc, arrow) was injected 30 min after mice were placed in the open field. Two-way ANOVA, Sidak's multiple comparisons post hoc tests, **p < 0.01, *p < 0.05. Values are means ± SEM indicated by a shaded area. **e-f**, Locomotor sensitization. **e** Comparison of the distance traveled 0-15 minutes following the first and the second injection of $Pyk2^{+/+}$ and $Pyk2^{-/-}$ mice (from data in **c** and **d**). Two-way ANOVA, Sidak's multiple comparisons post hoc tests, **p < 0.01, *p < 0.05. **f**, Ratio of the distances traveled 0-15 min after the second (day 14) / first (day 1) cocaine injections, (from data in **e**), in $Pyk2^{+/+}$ and $Pyk2^{-/-}$ mice. Means ± SEM are indicated. Unpaired t-test, ns, not significant. For number of replicates and detailed statistical analysis, see **Supplementary Table 2**.

Figure 3: Specific deletion of Pyk2 in the NAc but not in the DS alters the acute locomotor response to cocaine. a-b $Pyk2^{f/f}$ mice were bilaterally injected in the NAc (**a**) or the DS (**b**) with AAV expressing GFP ($Pyk2^{f/f;NAc,GFP}$) or Cre and GFP ($Pyk2^{f/f;NAc,GFP-Cre}$). **a**,

Anatomical verification of the stereotaxic injections of AAV-GFP-Cre in the NAc: representative Pyk2 immunoreactivity (left panel) and GFP (green) and Pyk2 (red) immunoreactivity colabeling (middle panel). The location of the tips of injecting cannula in all mice used for further analysis is summarized (right panel). **b**, Same as in **a** but for mice receiving injections in the DS. **c-d**, locomotor activity of the mice injected in the NAc (**a**) after the first (**c**) and the second (**d**, 13 days later) injection of cocaine (20 mg/kg, Coc, arrow), as in **Fig. 2c-d**. Two-way ANOVA, AAV effect $p<0.001$ (**c**), not significant (**d**), Sidak's multiple comparisons post hoc tests, ***$p < 0.001$, **$p < 0.01$, *$p < 0.05$. **e**, Ratio of the distances traveled 0-15 min after the second (day 14, **d**) / first (day 1, **c**) cocaine injections. Unpaired t-test, not significant, ns. **f-g**, Locomotor activity of the mice injected in the DS (**b**). **f**, Locomotor activity of $Pyk2^{f/f;DS,GFP}$ and $Pyk2^{f/f;DS,GFP\text{-}Cre}$ mice after the first (**f**) and the second (**g**, 13 days later) injection of 20 mg/kg cocaine. Two-way ANOVA, no significant AAV effect. **h**, Ratio of the distances traveled 0-15 min after the second (day 14, **g**) / first (day 1, **f**) cocaine injections in $Pyk2^{f/f;DS,GFP}$ and $Pyk2^{f/f;DS,GPF\text{-}Cre}$ mice. Unpaired t-test, not significant, ns. All values are means ± SEM, indicated by a shaded area in **c**, **d**, **f**, and **g**. For number of animals and detailed statistical analysis, see **Supplementary Table 2**.

Figure 4: Specific deletion of Pyk2 in D1 but not in A_{2A} neurons alters the locomotor response to cocaine. a-b, Locomotor activity of $Pyk2^{f/f}$ and $Pyk2^{f/f;D1::Cre}$ mice after a first (**a**) and, 13 days later, a second (**b**) injection of cocaine (20 mg/kg, Coc, arrow) as described in the legend to **Fig. 2c-d**. Two-way ANOVA, genotype effect $p < 0.0001$ (**a**), $p < 0.0001$ (**b**), Sidak's multiple comparisons post hoc tests, **$p < 0.01$, *$p < 0.05$. **c**, Ratio of the distances traveled 0-15 min after the second (day 14, **b**) / first (day 1, **a**) cocaine injections in $Pyk2^{f/f}$ and $Pyk2^{f/f;D1::Cre}$ mice. Unpaired t-test, not significant, ns. **d-e** Same as in **a-b** but in $Pyk2^{f/f}$ and $Pyk2^{f/f;A2A::Cre}$ mice. Two-way ANOVA, no genotype effect. **f** Ratio of the distances traveled 0-15 min after the second (day 14, **e**) / first (day 1, **d**) cocaine injections in $Pyk2^{f/f}$ and $Pyk2^{f/f;A2A::Cre}$ mice. Unpaired t-test, ns, not significant. All values are means ± SEM, indicated by a shaded area in **a**, **b**, **d**, and **e**. For number of animals and detailed statistical analysis, see **Supplementary Table 2**.

Figure 5: Specific deletion of Pyk2 in D1 neurons alters the acute locomotor response to a D1R agonist, SKF-81297. a-b, Locomotor activity of $Pyk2^{f/f}$ and $Pyk2^{f/f;D1::Cre}$ mice after a first (**a**) and a second (**b**, 13 days later) injection of SKF-81297 (SKF). SKF (3 mg/kg, arrow) was injected 30 min after mice were placed in the open field. Two-way ANOVA, genotype

effect, p = 0.016 (**a**), not significant (**b**). **c**-**d**, Sensitization of the response during the first 10 min after SKF injection (data from **a** and **b**). **c**, Distance traveled during the first 10 minutes following the first and the second SKF injections in $Pyk2^{f/f}$ and $Pyk2^{f/f;D1::Cre}$ mice. Two-way ANOVA, Sidak's multiple comparisons post hoc test, ****p<0.0001, ***p < 0.001. **d**, Ratios of the distances traveled 0-15 min after the second (day 14, **b**) / first (day 1, **a**) and SKF injections in $Pyk2^{f/f}$ and $Pyk2^{f/f;D1::Cre}$ mice. Unpaired t-test, ns, not significant. **e**-**f**, Same analyses as in **c** and **d**, but for the distance traveled 15 to 40 minutes after SKF injection (data from **a** and **b**). **a-f**, Values are means ± SEM, indicated by a shaded area in **a** and **b**. For number of animals and detailed statistical analysis, see **Supplementary Table 2**.

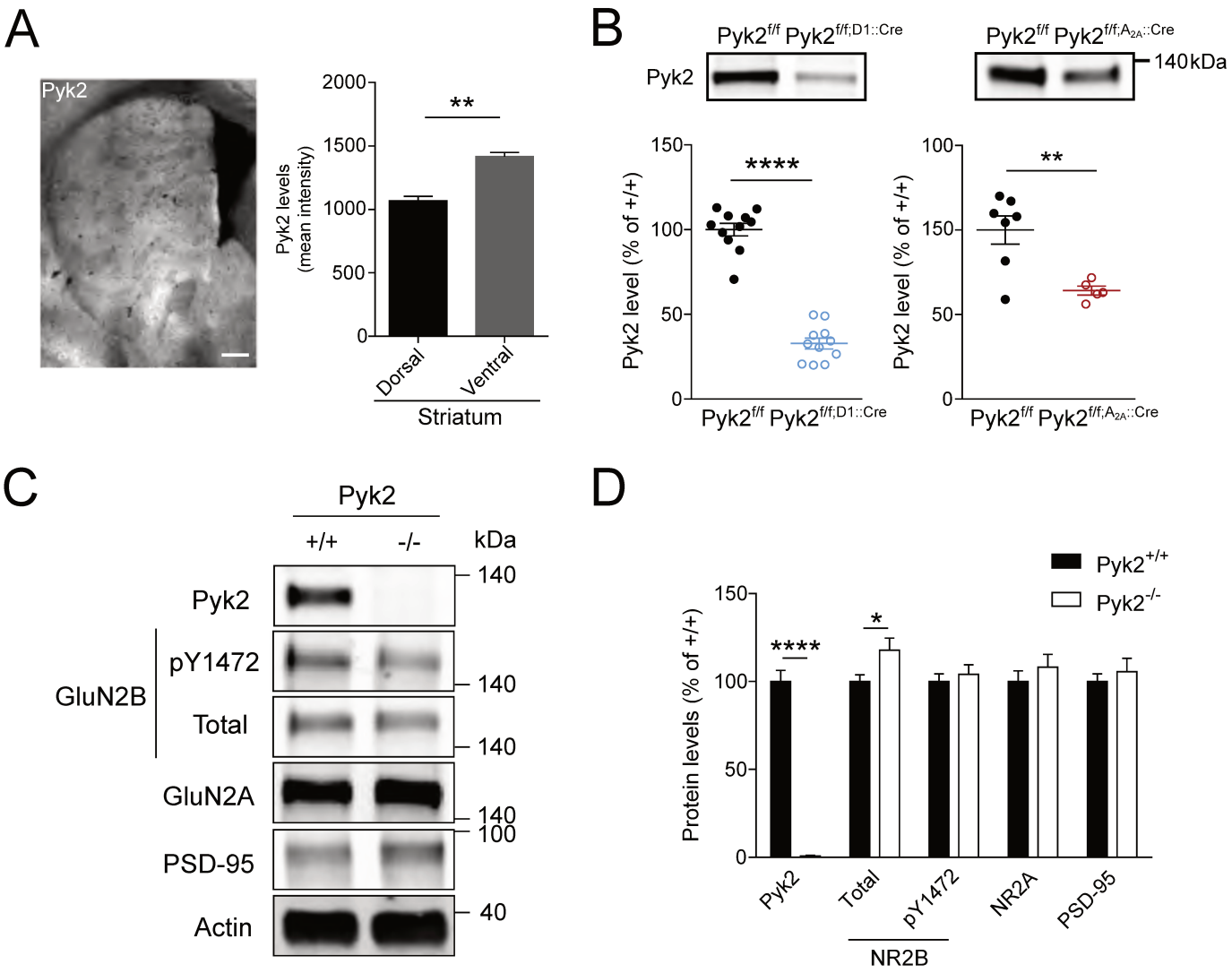
A
Pyk2
Pyk2 levels (mean intensity)
2000
1500
1000
500
0
**
Dorsal
Ventral
Striatum
B
Pyk2f/f Pyk2f/f;D1::Cre
Pyk2f/f Pyk2f/f;A2A::Cre
Pyk2
140kDa
Pyk2 level (% of +/+)
150
100
50
0
****
**
Pyk2f/f Pyk2f/f;D1::Cre
Pyk2f/f Pyk2f/f;A2A::Cre
C
Pyk2
+/+
-/-
kDa
Pyk2
GluN2B
pY1472
Total
GluN2A
PSD-95
Actin
140
140
140
140
100
40
D
Pyk2+/+
Pyk2-/-
Protein levels (% of +/+)
150
100
50
0
****
*
Pyk2
Total
pY1472
NR2A
PSD-95
NR2B

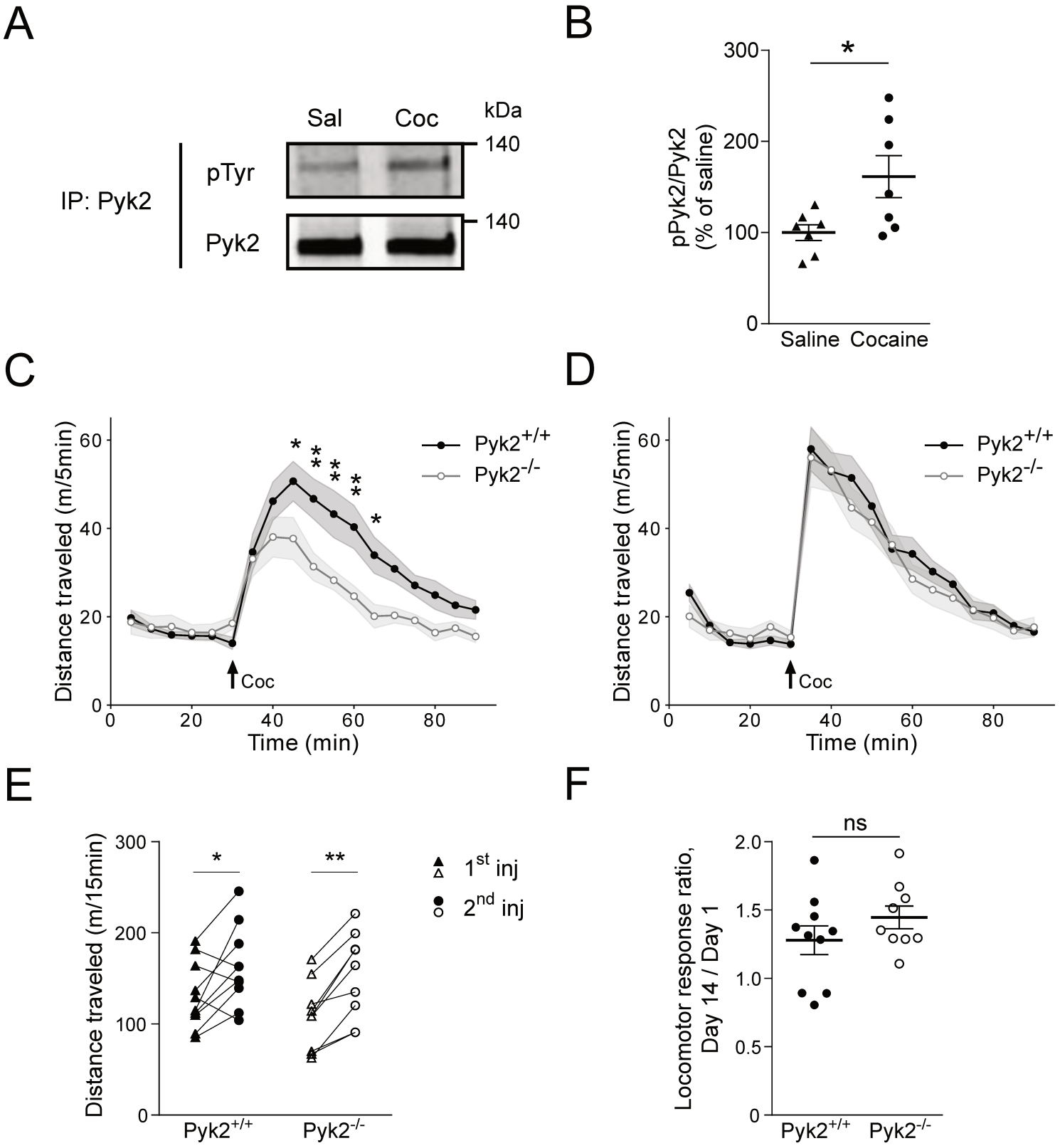
A
Sal
Coc
kDa
IP: Pyk2
pTyr
Pyk2
140
140
B
pPyk2/Pyk2
(% of saline)
300
200
100
0
*
Saline
Cocaine
C
Distance traveled (m/5min)
60
40
20
0
Pyk2+/+
Pyk2-/-
Coc
0
20
40
60
80
Time (min)
D
Distance traveled (m/5min)
Pyk2+/+
Pyk2-/-
Coc
Time (min)
E
Distance traveled (m/15min)
300
200
100
0
*
**
1st inj
2nd inj
Pyk2+/+
Pyk2-/-
F
Locomotor response ratio,
Day 14 / Day 1
2.0
1.5
1.0
0.5
0
ns
Pyk2+/+
Pyk2-/-

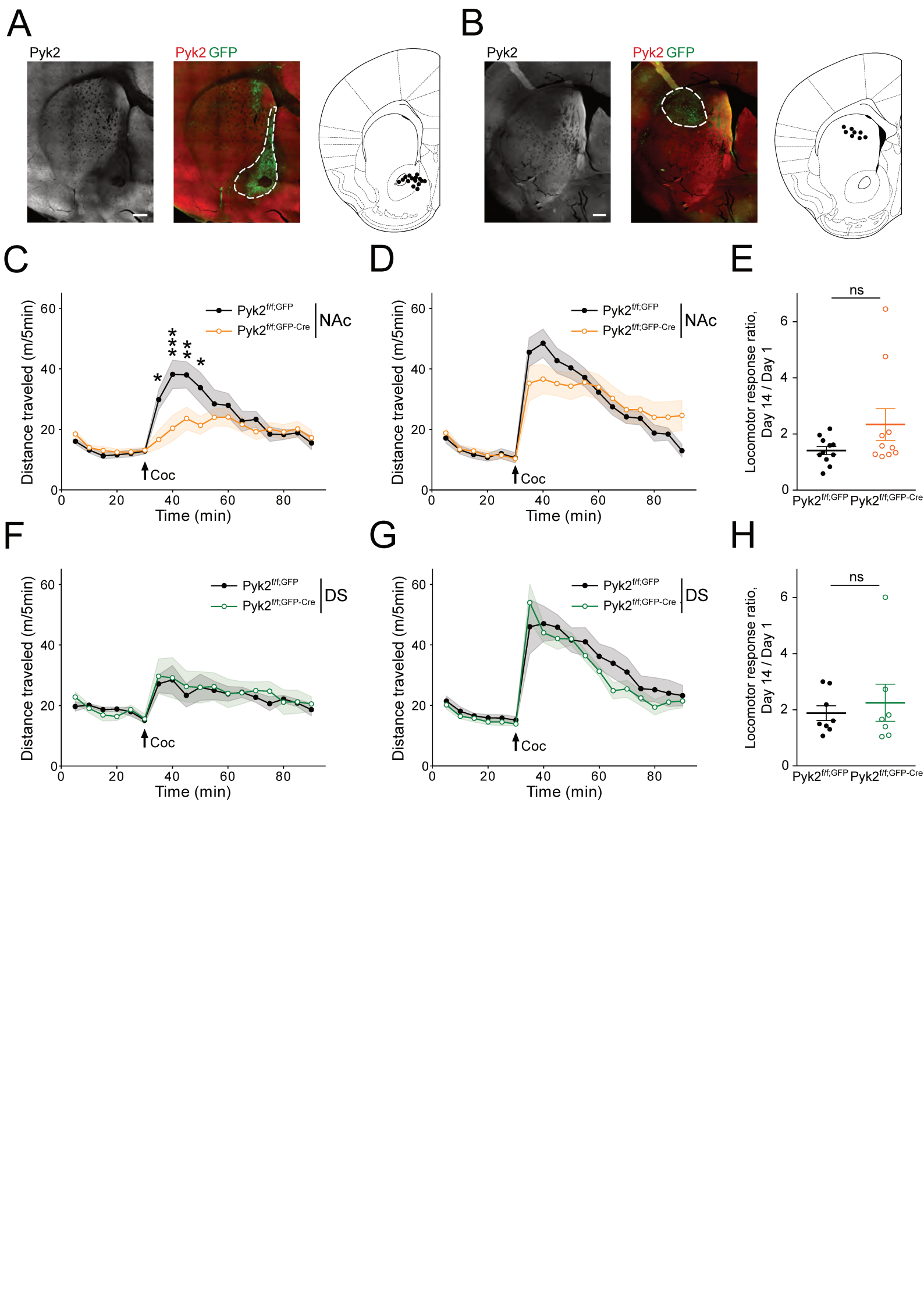
A
Pyk2
Pyk2 GFP
B
Pyk2
Pyk2 GFP
C
Distance traveled (m/5min)
Pyk2f/f;GFP
Pyk2f/f;GFP-Cre
NAc
Coc
Time (min)
D
Distance traveled (m/5min)
Pyk2f/f;GFP
Pyk2f/f;GFP-Cre
NAc
Coc
Time (min)
E
ns
Locomotor response ratio, Day 14 / Day 1
Pyk2f/f;GFP
Pyk2f/f;GFP-Cre
F
Distance traveled (m/5min)
Pyk2f/f;GFP
Pyk2f/f;GFP-Cre
DS
Coc
Time (min)
G
Distance traveled (m/5min)
Pyk2f/f;GFP
Pyk2f/f;GFP-Cre
DS
Coc
Time (min)
H
ns
Locomotor response ratio, Day 14 / Day 1
Pyk2f/f;GFP
Pyk2f/f;GFP-Cre

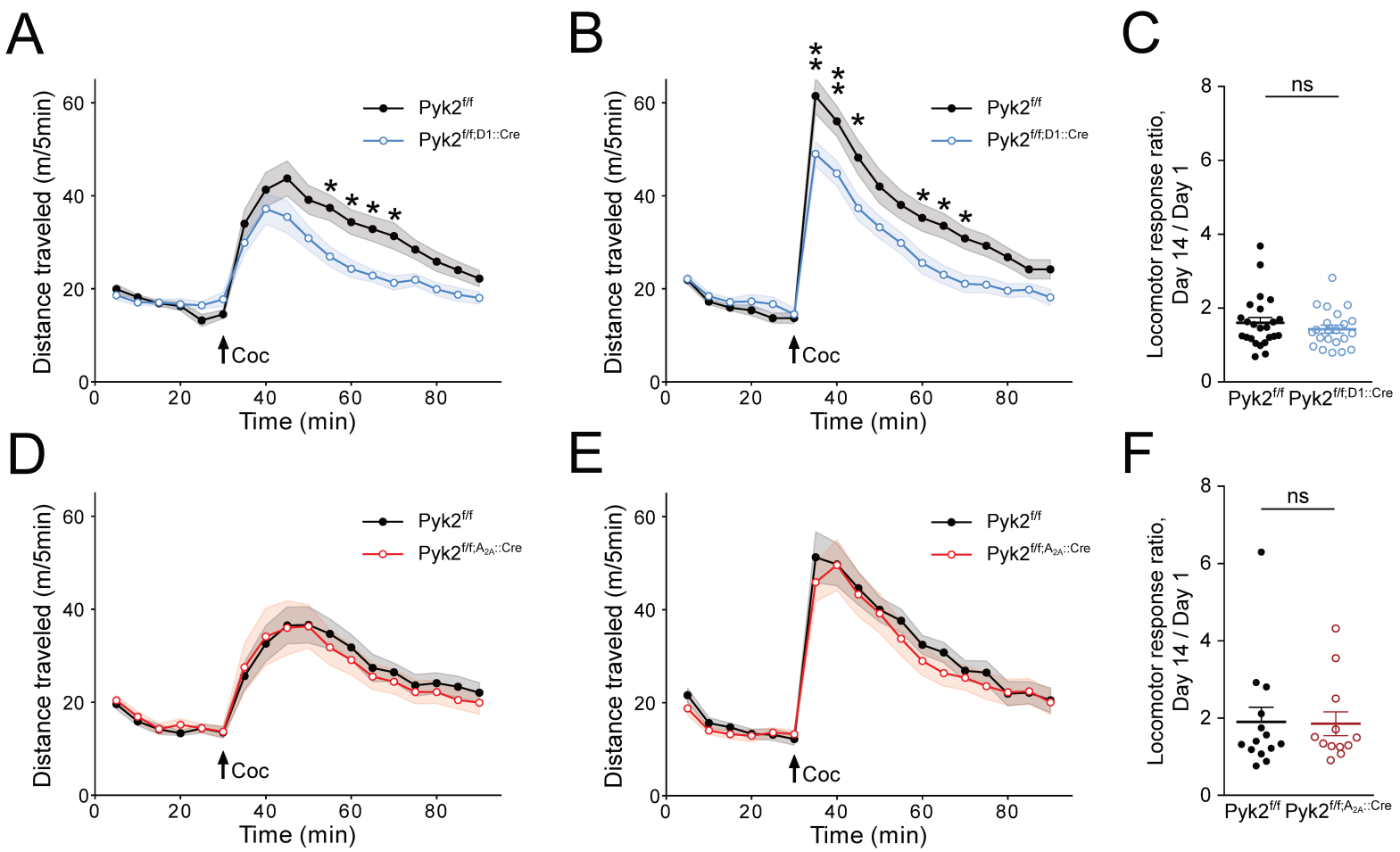
A
B
C
Distance traveled (m/5min)
Time (min)
Coc
Pyk2f/f
Pyk2f/f;D1::Cre
Locomotor response ratio, Day 14 / Day 1
ns
Pyk2f/f Pyk2f/f;D1::Cre

D
E
F
Distance traveled (m/5min)
Time (min)
Coc
Pyk2f/f
Pyk2f/f;A2A::Cre
Locomotor response ratio, Day 14 / Day 1
ns
Pyk2f/f Pyk2f/f;A2A::Cre

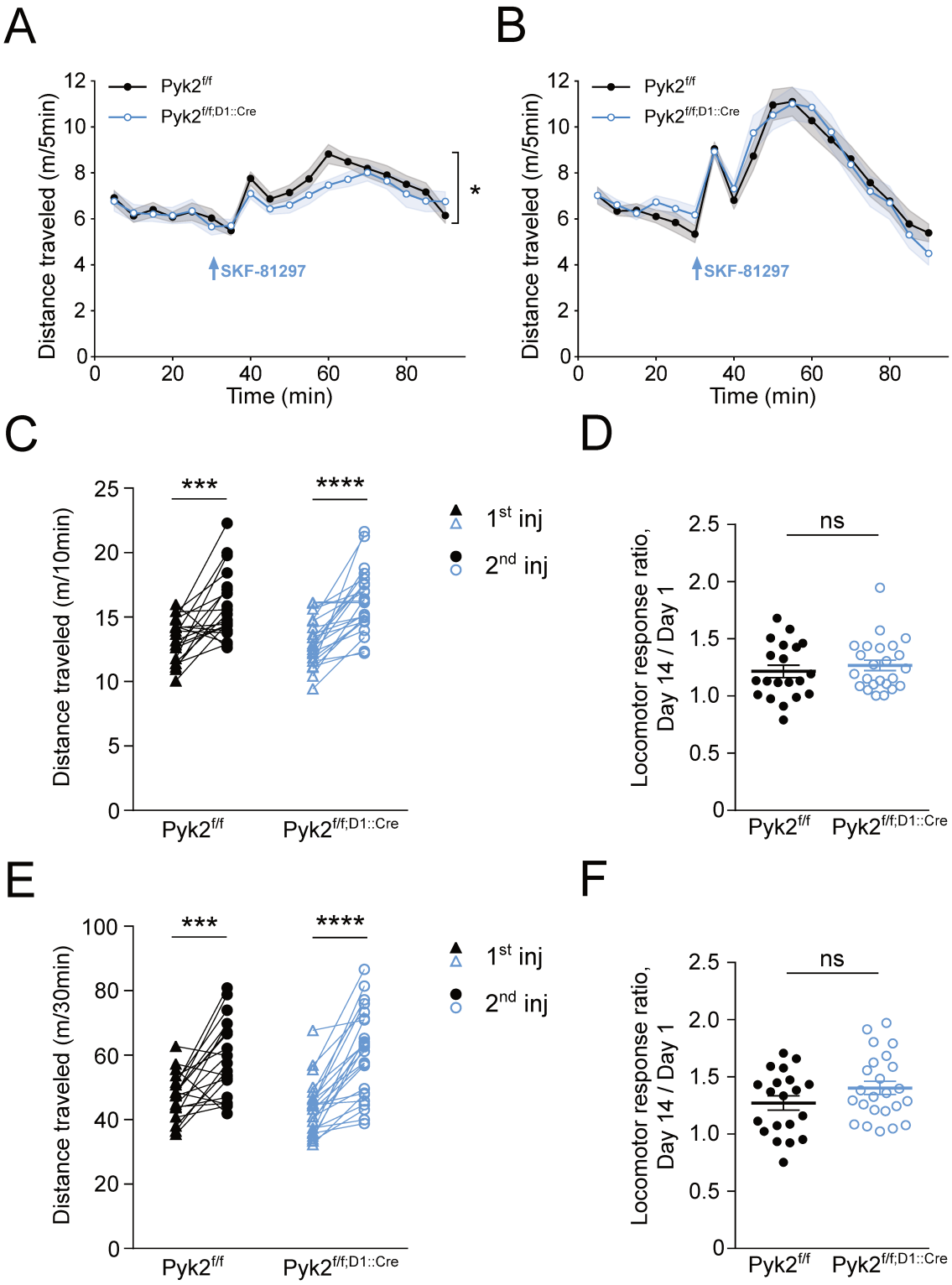
A
B
C
D
E
F
Pyk2f/f
Pyk2f/f;D1::Cre
Distance traveled (m/5min)
Time (min)
SKF-81297
*
Distance traveled (m/10min)
Distance traveled (m/30min)
***
****
1st inj
2nd inj
Locomotor response ratio, Day 14 / Day 1
ns

Antibody table				
Antibody	**Species**	**Dilution for WB**	**Dilution for IF**	**Company (reference number)**
Pyk2	Rabbit	1:1000	1:500	Sigma-Aldrich (#P3902)
PSD-95	Rabbit	1:1000	-	Cell Signaling Technology (#3450)
phosphoY1472-GluN2B	Rabbit	1:1000	-	Cayman chemical (#10009761)
GluN2B	Rabbit	1:1000	-	Merck KGaA (#06-600)
GluN2A	Rabbit	1:1000	-	Merck KGaA (#05-901R)
Gαolf	Rabbit	1:1000	-	produced as described [30]
synapsin 1	Rabbit	1:500	-	gift from Pr. Greengard (G-486)
tyrosine hydroxylase	Rabbit	1:1000	-	Merck KGaA (#AB1541)
STEP	Rabbit	1:1000	-	Cell Signaling Technology (#9069)
phosphoS845-GluA1	Rabbit	1:1000	-	Abcam (#ab3901)
phosphoT202/Y204-Erk1/2	Rabbit	1:1000	-	Cell Signaling Technology (#9101)
Erk1/2	Rabbit	1:1000	-	Cell Signaling Technology (#9102)
Calbindin D28k	Mouse	-	1:1000	Swant (#300)
Pyk2	Mouse	1:1000	-	Cell Signaling Technology (#3480)
DARPP-32	Mouse	1:5000	-	gift from Pr. Greengard (m6Ab)
phosphoT75-DARPP-32	Mouse	1:1000	-	gift from Pr. Greengard (RU911)
phosphotyrosine	Mouse	1:1000	-	Cell Signaling Technology (#05-947)
β-actin	Mouse	1:5000	-	Sigma-Aldrich (#A5441)
tyrosine hydroxylase	Chicken	1:1000	-	Aves Labs (#TH)
GFP	Chicken	-	1:500	Thermo Fisher (#A10262)
anti-rabbit IgG DyLight™ 680	Goat	1:10000	-	Rockland Immunochemicals (#611-144-002)
anti-rabbit IgG DyLight™ 800	Goat	1:10000	-	Rockland Immunochemicals (#611-145-002)
anti-mouse IgG DyLight™ 680	Goat	1:10000	-	Rockland Immunochemicals (#610-144-002)
anti-mouse IgG DyLight™ 800	Goat	1:10000	-	Rockland Immunochemicals (#610-145-002)
anti-chicken IgG DyLight™ 800	Goat	1:10000	-	Rockland Immunochemicals (#603-145-002)
anti-Rabbit IgG Alexa Fluor 555	Donkey	-	1:400	Thermo Fisher (#A-31572)
anti-Mouse IgG Alexa Fluor 488	Goat	-	1:400	Thermo Fisher (#A-11001)
anti-Chicken IgG Alexa Fluor 488	Goat	-	1:400	Thermo Fisher (#A-11039)

Figure	Group	Mean	SEM	Comparison	Statistical analysis	DF	Test value	*P* value	n
1A	Dorsal	1069	33.22						3 mice
	Ventral	1416	33.36						3 mice
				Dorsal vs Ventral	Two-tailed unpaired t-test	4	t = 7.37	**0.0018**	
1B left panel	$Pyk2^{f/f}$	100	3.70						11 mice
	$Pyk2^{f/f;D1::Cre}$	32.76	3.20						11 mice
				$Pyk2^{f/f}$ vs $Pyk2^{f/f;D1::Cre}$	Two-tailed unpaired t-test	20	t = 13.75	**< 0.0001**	
1B right panel	$Pyk2^{f/f}$	100	8.31						7 mice
	$Pyk2^{f/f;A2A::Cre}$	64.13	2.63						5 mice
				$Pyk2^{f/f}$ vs $Pyk2^{f/f;A2A::Cre}$	Two-tailed unpaired t-test	10	t = 3.515	**0.0056**	
1D	Pyk2 - $Pyk2^{+/+}$	100	6.36						6 mice
	Pyk2 - $Pyk2^{-/-}$	0.72	0.45						6 mice
				Pyk2 - $Pyk2^{+/+}$ vs $Pyk2^{-/-}$	Two-tailed unpaired t-test	10	t = 15.57	**< 0.0001**	
	NR2B - $Pyk2^{+/+}$	100	3.76						15 mice
	NR2B - $Pyk2^{-/-}$	117.79	6.92						16 mice
				NR2B - $Pyk2^{+/+}$ vs $Pyk2^{-/-}$	Two-tailed unpaired t-test	29	t = 2.22	**0.0346**	
	pY1472NR2B - $Pyk2^{+/+}$	100	4.35						15 mice
	pY1472NR2B - $Pyk2^{-/-}$	104.04	5.5						16 mice
				pY1472NR2B - $Pyk2^{+/+}$ vs $Pyk2^{-/-}$	Two-tailed unpaired t-test	29	t = 0.57	0.5721	
	NR2A - $Pyk2^{+/+}$	100	6.12						6 mice
	NR2A - $Pyk2^{-/-}$	108.23	7.24						6 mice
				NR2A - $Pyk2^{+/+}$ vs $Pyk2^{-/-}$	Two-tailed unpaired t-test	10	t = 0.87	0.4058	
	PSD-95 - $Pyk2^{+/+}$	100	4.37						6 mice
	PSD-95 - $Pyk2^{-/-}$	105.61	7.53						8 mice
				PSD-95 - $Pyk2^{+/+}$ vs $Pyk2^{-/-}$	Two-tailed unpaired Mann Whitney test		U = 24	> 0.9999	
2B	Saline	100	8.74						7 mice
	Cocaine	161.3	23.05						7 mice
				Saline vs Cocaine	Two-tailed unpaired t-test	12	t = 2.49	**0.0286**	
2C	$Pyk2^{+/+}$								10 mice
	$Pyk2^{-/-}$								9 mice
					Two-way ANOVA:				
					Interaction	17	F = 2.44	**0.0014**	
					Time	17	F = 20.43	**< 0.0001**	
					Genotype	1	F = 39.05	**< 0.0001**	
2D	$Pyk2^{+/+}$								10 mice
	$Pyk2^{-/-}$								9 mice
					Two-way ANOVA:				
					Interaction	17	F = 0.43	0.9769	
					Time	17	F = 40.18	**< 0.0001**	
					Genotype	1	F = 1.59	0.208	

2E	1st injection - $Pyk2^{+/+}$	13147	1163.53						10 mice
	2nd injection - $Pyk2^{+/+}$	16230	1383.59						9 mice
	1st injection - $Pyk2^{-/-}$	10885	1264.40						10 mice
	2nd injection - $Pyk2^{-/-}$	15390	1567.73						9 mice
					Two-way ANOVA:				
					Interaction	1	F = 0.90	0.3572	
					Genotype	1	F = 0.78	0.3886	
					Injection	1	F = 25.49	**< 0.0001**	
					Subjects (matching)	17	F = 5.44	**0.0005**	
				$Pyk2^{+/+}$: 1st inj vs 2nd inj	Sidak's multiple comparisons test	17	t = 2.98	**0.0167**	
				$Pyk2^{-/-}$: 1st inj vs 2nd inj	Sidak's multiple comparisons test	17	t = 4.13	**0.0014**	
2F	$Pyk2^{+/+}$	1.28	0.1						10 mice
	$Pyk2^{-/-}$	1.45	0.08						9 mice
				$Pyk2^{+/+}$ vs $Pyk2^{-/-}$	Two-tailed unpaired t-test	17	t = 1.24	0.2315	
3C	$Pyk2^{f/f;NAc,GFP}$								11 mice
	$Pyk2^{f/f;NAc,GFP-Cre}$								10 mice
					Two-way ANOVA:				
					Interaction	17	F = 2.85	**0.0002**	
					Time	17	F = 10.15	**< 0.0001**	
					AAV type	1	F = 12.94	**0.0004**	
3D	$Pyk2^{f/f;NAc,GFP}$								11 mice
	$Pyk2^{f/f;NAc,GFP-Cre}$								10 mice
					Two-way ANOVA:				
					Interaction	17	F = 1.49	0.0942	
					Time	17	F = 22.16	**< 0.0001**	
					AAV type	1	F = 0.02	0.9015	
3E	$Pyk2^{f/f;NAc,GFP}$	1.41	0.14						11 mice
	$Pyk2^{f/f;NAc,GFP-Cre}$	2.34	0.57						10 mice
				$Pyk2^{f/f;NAc,GFP}$ vs $Pyk2^{f/f;NAc,GFP-Cre}$	Two-tailed unpaired Mann-Whitney test		U = 39	0.2785	
3F	$Pyk2^{f/f;DS,GFP}$								8 mice
	$Pyk2^{f/f;DS,GFP-Cre}$								7 mice
					Two-way ANOVA:				
					Interaction	17	F = 0.16	> 0.9999	
					Time	17	F = 3.00	**< 0.0001**	
					AAV type	1	F = 0.55	0.4586	
3G	$Pyk2^{f/f;DS,GFP}$								8 mice
	$Pyk2^{f/f;DS,GFP-Cre}$								7 mice
					Two-way ANOVA:				
					Interaction	17	F = 0.78	0.7197	
					Time	17	F = 22.93	**< 0.0001**	
					AAV type	1	F = 7.93	**0.0053**	
3H	$Pyk2^{f/f;DS,GFP}$	1.88	0.26						8 mice
	$Pyk2^{f/f;DS,GFP-Cre}$	2.25	0.66						7 mice
				$Pyk2^{f/f;DS,GFP}$ vs $Pyk2^{f/f;DS,GFP-Cre}$	Two-tailed unpaired Mann-Whitney test		U = 27	0.9203	

4A	$Pyk2^{f/f}$ $Pyk2^{f/f;D1::Cre}$								24 mice 22 mice
					Two-way ANOVA: Interaction Time Genotype	 17 17 1	 F = 1.73 F = 24.04 F = 35.32	 **0.0329** **< 0.0001** **< 0.0001**	
4B	$Pyk2^{f/f}$ $Pyk2^{f/f;D1::Cre}$								24 mice 22 mice
					Two-way ANOVA: Interaction Time Genotype	 17 17 1	 F = 2.38 F = 52.38 F = 47.46	 **0.0014** **< 0.0001** **< 0.0001**	
4C	$Pyk2^{f/f}$ $Pyk2^{f/f;D1::Cre}$	1.60 1.43	0.14 0.11						24 mice 22 mice
				$Pyk2^{+/+}$ vs $Pyk2^{f/f;D1::Cre}$	Two-tailed unpaired t-test	44	t = 0.95	0.3471	
4D	$Pyk2^{f/f}$ $Pyk2^{f/f;A2A::Cre}$								14 mice 12 mice
					Two-way ANOVA: Interaction Time Genotype	 17 17 1	 F = 0.17 F = 14.73 F = 0.44	 > 0.9999 **< 0.0001** 0.5077	
4E	$Pyk2^{f/f}$ $Pyk2^{f/f;A2A::Cre}$								14 mice 12 mice
					Two-way ANOVA: Interaction Time Genotype	 17 17 1	 F = 0.22 F = 38.01 F = 2.85	 0.9997 **< 0.0001** 0.0924	
4F	$Pyk2^{f/f}$ $Pyk2^{f/f;A2A::Cre}$	1.90 1.85	0.38 0.31						14 mice 12 mice
				$Pyk2^{+/+}$ vs $Pyk2^{f/f;A2A::Cre}$	Two-tailed unpaired Mann-Whitney test		U = 79	0.8101	
5A	$Pyk2^{f/f}$ $Pyk2^{f/f;D1::Cre}$								20 mice 27 mice
					Two-way ANOVA: Interaction Time Genotype	 17 17 1	 F = 0.71 F = 9.14 F = 5.80	 0.7985 **< 0.0001** **0.0163**	
5B	$Pyk2^{f/f}$ $Pyk2^{f/f;D1::Cre}$								20 mice 24 mice
					Two-way ANOVA: Interaction Time Genotype	 17 17 1	 F = 0.47 F = 26.32 F = 0.36	 0.9648 **< 0.0001** 0.5485	

5C	1st injection - $Pyk2^{f/f}$	13.25	0.38						20 mice
	2nd injection - $Pyk2^{f/f}$	15.86	0.59						24 mice
	1st injection - $Pyk2^{f/f;D1::Cre}$	12.97	0.38						20 mice
	2nd injection - $Pyk2^{f/f;D1::Cre}$	16.24	0.49						24 mice
					Two-way ANOVA:				
					Interaction	1	F = 0.60	0.4416	
					Genotype	1	F = 0.01	0.9188	
					Injection	1	F = 48.70	**< 0.0001**	
					Subjects (matching)	42	F = 1.44	0.1197	
				$Pyk2^{f/f}$: 1st inj vs 2nd inj	Sidak's multiple comparisons test	42	t = 4.20	**0.0003**	
				$Pyk2^{f/f;D1::Cre}$: 1st inj vs 2nd inj	Sidak's multiple comparisons test	42	t = 5.75	**< 0.0001**	
5D	$Pyk2^{f/f}$	1.22	0.05						20 mice
	$Pyk2^{f/f;D1::Cre}$	1.27	0.05						24 mice
				$Pyk2^{+/+}$ vs $Pyk2^{f/f;D1::Cre}$	Two-tailed unpaired t-test	42	t = 0.75	0.4589	
5E	1st injection - $Pyk2^{f/f}$	47.24	1.58						20 mice
	2nd injection - $Pyk2^{f/f}$	59.13	2.64						24 mice
	1st injection - $Pyk2^{f/f;D1::Cre}$	43.38	1.72						20 mice
	2nd injection - $Pyk2^{f/f;D1::Cre}$	60.27	2.76						24 mice
					Two-way ANOVA:				
					Interaction	1	F = 1.91	0.1745	
					Genotype	1	F = 0.26	0.6103	
					Injection	1	F = 63.19	**< 0.0001**	
					Subjects (matching)	42	F = 2.14	**0.0077**	
				$Pyk2^{f/f}$: 1st inj vs 2nd inj	Sidak's multiple comparisons test	42	t = 2.98	**0.0167**	
				$Pyk2^{f/f;D1::Cre}$: 1st inj vs 2nd inj	Sidak's multiple comparisons test	42	t = 4.13	**0.0014**	
5F	$Pyk2^{f/f}$	1.27	0.06						20 mice
	$Pyk2^{f/f;D1::Cre}$	1.40	0.06						24 mice
				$Pyk2^{+/+}$ vs $Pyk2^{f/f;D1::Cre}$	Two-tailed unpaired t-test	42	t = 1.56	0.1268	
S1C	Matrix	2910	40.9						20 regions (from 3 mice)
	Patch	2396	58.53						20 regions (from 3 mice)
				Matrix vs Patch	Two-tailed unpaired t-test	38	t = 7.21	**< 0.0001**	
S2B	Gαolf - $Pyk2^{+/+}$	100	5.23						6 mice
	Gαolf - $Pyk2^{-/-}$	100.63	3.18						6 mice
				Gαolf - $Pyk2^{+/+}$ vs $Pyk2^{-/-}$	Two-tailed unpaired t-test	10	t = 0.10	0.9206	
	DARPP-32 - $Pyk2^{+/+}$	100	5.19						6 mice
	DARPP-32 - $Pyk2^{-/-}$	106.28	3.52						6 mice
				DARPP-32 - $Pyk2^{+/+}$ vs $Pyk2^{-/-}$	Two-tailed unpaired t-test	10	t = 1.00	0.3405	

S2D	Synapsin - $Pyk2^{+/+}$	100	2.79						6 mice
	Synapsin - $Pyk2^{-/-}$	94.57	3.99						8 mice
				Synapsin - $Pyk2^{+/+}$ vs $Pyk2^{-/-}$	Two-tailed unpaired t-test	12	t = 1.04	0.3193	
	TH - $Pyk2^{+/+}$	100	6.00						6 mice
	TH - $Pyk2^{-/-}$	92.00	5.39						8 mice
				TH - $Pyk2^{+/+}$ vs $Pyk2^{-/-}$	Two-tailed unpaired t-test	10	t = 0.99	0.3449	
S3A	$Pyk2^{+/+}$								9 mice
	$Pyk2^{-/-}$								9 mice
					Two-way ANOVA:				
					Interaction	11	F = 0.39	0.9576	
					Trial	11	F = 14.03	**< 0.0001**	
					Genotype	1	F = 2.57	0.1108	
S3B	$Pyk2^{f/f;NAc,GFP}$								17 mice
	$Pyk2^{f/f;NAc,GFP-Cre}$								14 mice
					Two-way ANOVA:				
					Interaction	11	F = 0.44	0.9377	
					Trial	11	F = 12.20	**< 0.0001**	
					Genotype	1	F = 1.83	0.1775	
S3C	$Pyk2^{f/f;DS,GFP}$								8 mice
	$Pyk2^{f/f;DS,GFP-Cre}$								7 mice
					Two-way ANOVA:				
					Interaction	11	F = 0.70	0.7394	
					Trial	11	F = 4.99	**< 0.0001**	
					Genotype	1	F = 1.07	0.3034	
S3D	$Pyk2^{f/f}$								14 mice
	$Pyk2^{f/f;D1::Cre}$								13 mice
					Two-way ANOVA:				
					Interaction	11	F = 0.59	0.836	
					Trial	11	F = 22.46	**< 0.0001**	
					Genotype	1	F = 0.02	0.8827	
S3E	$Pyk2^{f/f}$								14 mice
	$Pyk2^{f/f;A2A::Cre}$								12 mice
					Two-way ANOVA:				
					Interaction	11	F = 0.27	0.991	
					Trial	11	F = 14.47	**< 0.0001**	
					Genotype	1	F = 0.84	0.3605	

S4A	1st injection - $Pyk2^{f/f;NAc,GFP}$	106.02	11.90						11 mice
	2nd injection - $Pyk2^{f/f;NAc,GFP}$	136.72	11.76						10 mice
	1st injection - $Pyk2^{f/f;NAc,GFP-Cre}$	60.59	10.64						11 mice
	2nd injection - $Pyk2^{f/f;NAc,GFP-Cre}$	107.09	12.42						10 mice
					Two-way ANOVA:				
					Interaction	1	F = 0.84	0.3712	
					AAV type	1	F = 6.99	**0.016**	
					Injection	1	F = 20.05	**0.0003**	
					Subjects (matching)	19	F = 2.71	**0.0177**	
				$Pyk2^{f/f;NAc,GFP}$: 1st inj vs 2nd inj	Sidak's multiple comparisons test	19	t = 2.58	**0.0363**	
				$Pyk2^{f/f;NAc,GFP-Cre}$: 1st inj vs 2nd inj	Sidak's multiple comparisons test	19	t = 3.73	**0.0029**	
S4B	1st injection - $Pyk2^{f/f;DS,GFP}$	78.99	10.00						8 mice
	2nd injection - $Pyk2^{f/f;DS,GFP}$	136.62	13.62						7 mice
	1st injection - $Pyk2^{f/f;DS,GFP-Cre}$	85.11	17.02						8 mice
	2nd injection - $Pyk2^{f/f;DS,GFP-Cre}$	140.06	9.79						7 mice
					Two-way ANOVA:				
					Interaction	1	F = 0.01	0.9044	
					AAV type	1	F = 0.11	0.7478	
					Injection	1	F = 26.55	**0.0002**	
					Subjects (matching)	13	F = 1.78	0.1562	
				$Pyk2^{f/f;DS,GFP}$: 1st inj vs 2nd inj	Sidak's multiple comparisons test	13	t = 3.86	**0.0039**	
				$Pyk2^{f/f;DS,GFP-Cre}$: 1st inj vs 2nd inj	Sidak's multiple comparisons test	13	t = 3.44	**0.0087**	
S5A	1st injection - $Pyk2^{f/f}$	117.36	9.77						25 mice
	2nd injection - $Pyk2^{f/f}$	168.15	9.16						23 mice
	1st injection - $Pyk2^{f/f;D1::Cre}$	101.92	8.24						25 mice
	2nd injection - $Pyk2^{f/f;D1::Cre}$	132.43	6.76						23 mice
					Two-way ANOVA:				
					Interaction	1	F = 2.65	0.1103	
					Genotype	1	F = 5.89	**0.0191**	
					Injection	1	F = 42.60	**< 0.0001**	
					Subjects (matching)	46	F = 2.86	**0.0003**	
				$Pyk2^{f/f}$: 1st inj vs 2nd inj	Sidak's multiple comparisons test	46	t = 5.89	**< 0.0001**	
				$Pyk2^{f/f;D1::Cre}$: 1st inj vs 2nd inj	Sidak's multiple comparisons test	46	t = 3.39	**0.0029**	
S5B	1st injection - $Pyk2^{f/f}$	94.73	10.02						14 mice
	2nd injection - $Pyk2^{f/f}$	145.63	11.84						12 mice
	1st injection - $Pyk2^{f/f;A2A::Cre}$	97.61	16.40						14 mice
	2nd injection - $Pyk2^{f/f;A2A::Cre}$	138.78	13.16						12 mice
					Two-way ANOVA:				
					Interaction	1	F = 0.43	0.5172	
					Genotype	1	F = 0.01	0.9057	
					Injection	1	F = 38.68	**< 0.0001**	
					Subjects (matching)	24	F = 5.01	**< 0.0001**	
				$Pyk2^{+/+}$: 1st inj vs 2nd inj	Sidak's multiple comparisons test	24	t = 5.06	**< 0.0001**	
				$Pyk2^{f/f;A2A::Cre}$: 1st inj vs 2nd inj	Sidak's multiple comparisons test	24	t = 3.79	**0.0018**	

S6B left	sal - Pyk2$^{f/f}$	100.00	7.23						10 mice
	coc - Pyk2$^{f/f}$	123.55	3.85						11 mice
	sal - Pyk2$^{f/f;D1::Cre}$	103.95	2.78						13 mice
	coc - Pyk2$^{f/f;D1::Cre}$	115.20	6.61						12 mice
					Two-way ANOVA:				
					Interaction	1	F = 1.36	0.2498	
					Genotype	1	F = 0.17	0.6789	
					Drug	1	F = 10.89	**0.0020**	
				Pyk2$^{f/f}$: sal vs coc	Sidak's multiple comparisons test	42	t = 3.03	**0.0084**	
				Pyk2$^{f/f;D1::Cre}$: sal vs coc	Sidak's multiple comparisons test	42	t = 1.58	0.2291	
S6B right	sal - Pyk2$^{f/f}$	100.00	6.12						10 mice
	coc - Pyk2$^{f/f}$	105.97	4.89						11 mice
	sal - Pyk2$^{f/f;D1::Cre}$	99.63	3.42						12 mice
	coc - Pyk2$^{f/f;D1::Cre}$	100.99	6.36						12 mice
					Two-way ANOVA:				
					Interaction	1	F = 0.19	0.6662	
					Genotype	1	F = 0.25	0.6165	
					Drug	1	F = 0.48	0.4933	
				Pyk2$^{f/f}$: sal vs coc	Sidak's multiple comparisons test	41	t = 0.77	0.6925	
				Pyk2$^{f/f;D1::Cre}$: sal vs coc	Sidak's multiple comparisons test	41	t = 0.19	0.978	
S6C left	sal - Pyk2$^{f/f}$	100.00	3.82						5 mice
	coc - Pyk2$^{f/f}$	131.15	9.70						6 mice
	sal - Pyk2$^{f/f;D1::Cre}$	108.69	7.61						6 mice
	coc - Pyk2$^{f/f;D1::Cre}$	135.62	7.83						6 mice
					Two-way ANOVA:				
					Interaction	1	F = 0.07	0.7905	
					Genotype	1	F = 0.70	0.4124	
					Drug	1	F = 13.69	**0.0015**	
				Pyk2$^{f/f}$: sal vs coc	Sidak's multiple comparisons test	19	t = 2.74	**0.0257**	
				Pyk2$^{f/f;D1::Cre}$: sal vs coc	Sidak's multiple comparisons test	19	t = 2.49	**0.0443**	
S6C right	sal - Pyk2$^{f/f}$	100.00	4.02						5 mice
	coc - Pyk2$^{f/f}$	102.00	4.58						6 mice
	sal - Pyk2$^{f/f;D1::Cre}$	100.37	5.43						6 mice
	coc - Pyk2$^{f/f;D1::Cre}$	99.56	7.15						6 mice
					Two-way ANOVA:				
					Interaction	1	F = 0.06	0.8034	
					Genotype	1	F = 0.03	0.8541	
					Drug	1	F = 0.01	0.9161	
				Pyk2$^{f/f}$: sal vs coc	Sidak's multiple comparisons test	19	t = 0.25	0.9626	
				Pyk2$^{f/f;D1::Cre}$: sal vs coc	Sidak's multiple comparisons test	19	t = 0.11	0.9931	

S7A	Day 0 - $Pyk2^{+/+}$	402.42	26.47						10 mice
	Day 7 - $Pyk2^{+/+}$	556.80	28.46						9 mice
	Day 0 - $Pyk2^{-/-}$	374.17	30.01						10 mice
	Day 7 - $Pyk2^{-/-}$	515.37	36.99						9 mice
					Two-way ANOVA:				
					Interaction	1	F = 0.04	0.8526	
					Genotype	1	F = 1.90	0.1859	
					Injection	1	F = 17.90	**0.0006**	
					Subjects (matching)	17	F = 0.52	0.9038	
				$Pyk2^{+/+}$: Day 0 vs Day 7	Sidak's multiple comparisons test	17	t = 3.21	**0.0102**	
				$Pyk2^{-/-}$: Day 0 vs Day 7	Sidak's multiple comparisons test	17	t = 2.79	**0.0252**	
S7B	$Pyk2^{+/+}$	154.4	46.39						10 mice
	$Pyk2^{-/-}$	141.2	52.61						9 mice
				$Pyk2^{+/+}$ vs $Pyk2^{-/-}$	Two-tailed unpaired t-test	17	t = 0.19	0.8526	
S7C	$Pyk2^{f/f;NAc,GFP}$	114.4	30.14						18 mice
	$Pyk2^{f/f;NAc,GFP-Cre}$	83.26	32.02						15 mice
				$Pyk2^{f/f;NAc,GFP}$ vs $Pyk2^{f/f;NAc,GFP-Cre}$	Two-tailed unpaired t-test	31	t = 0.71	0.4855	
S7D	$Pyk2^{f/f;DS,GFP}$	142.4	46.55						8 mice
	$Pyk2^{f/f;DS,GFP-Cre}$	145.8	41.61						7 mice
				$Pyk2^{f/f;DS,GFP}$ vs $Pyk2^{f/f;DS,GFP-Cre}$	Two-tailed unpaired t-test	13	t = 0.05	0.958	
S7E	$Pyk2^{f/f}$	135.4	39.96						13 mice
	$Pyk2^{f/f;D1::Cre}$	160.4	21.3						12 mice
				$Pyk2^{+/+}$ vs $Pyk2^{f/f;D1::Cre}$	Two-tailed unpaired t-test	23	t = 0.54	0.5948	
S7F	$Pyk2^{f/f}$	170	26.14						14 mice
	$Pyk2^{f/f;A2A::Cre}$	136.5	34.62						12 mice
				$Pyk2^{+/+}$ vs $Pyk2^{f/f;A2A::Cre}$	Two-tailed unpaired t-test	24	t = 0.78	0.4405	
S8A	$Pyk2^{f/f}$								13 mice
	$Pyk2^{f/f;D1::Cre}$								12 mice
					Two-way ANOVA:				
					Interaction	17	F = 0.95	0.51	
					Time	17	F = 19.11	**< 0.0001**	
					Genotype	1	F = 0.00	0.9499	
S8B	$Pyk2^{f/f}$								12 mice
	$Pyk2^{f/f;D1::Cre}$								12 mice
					Two-way ANOVA:				
					Interaction	17	F = 0.60	0.8922	
					Time	17	F = 20.46	**< 0.0001**	
					Genotype	1	F = 0.44	0.5052	
S8C	$Pyk2^{f/f}$	1.11	0.04						12 mice
	$Pyk2^{f/f;D1::Cre}$	1.16	0.05						12 mice
				$Pyk2^{+/+}$ vs $Pyk2^{f/f;D1::Cre}$	Two-tailed unpaired t-test	22	t = 0.83	0.413	

Pyk2 in D1 receptor-expressing neurons of the nucleus accumbens modulates the acute locomotor effects of cocaine

Supplementary Figures
S1-S8

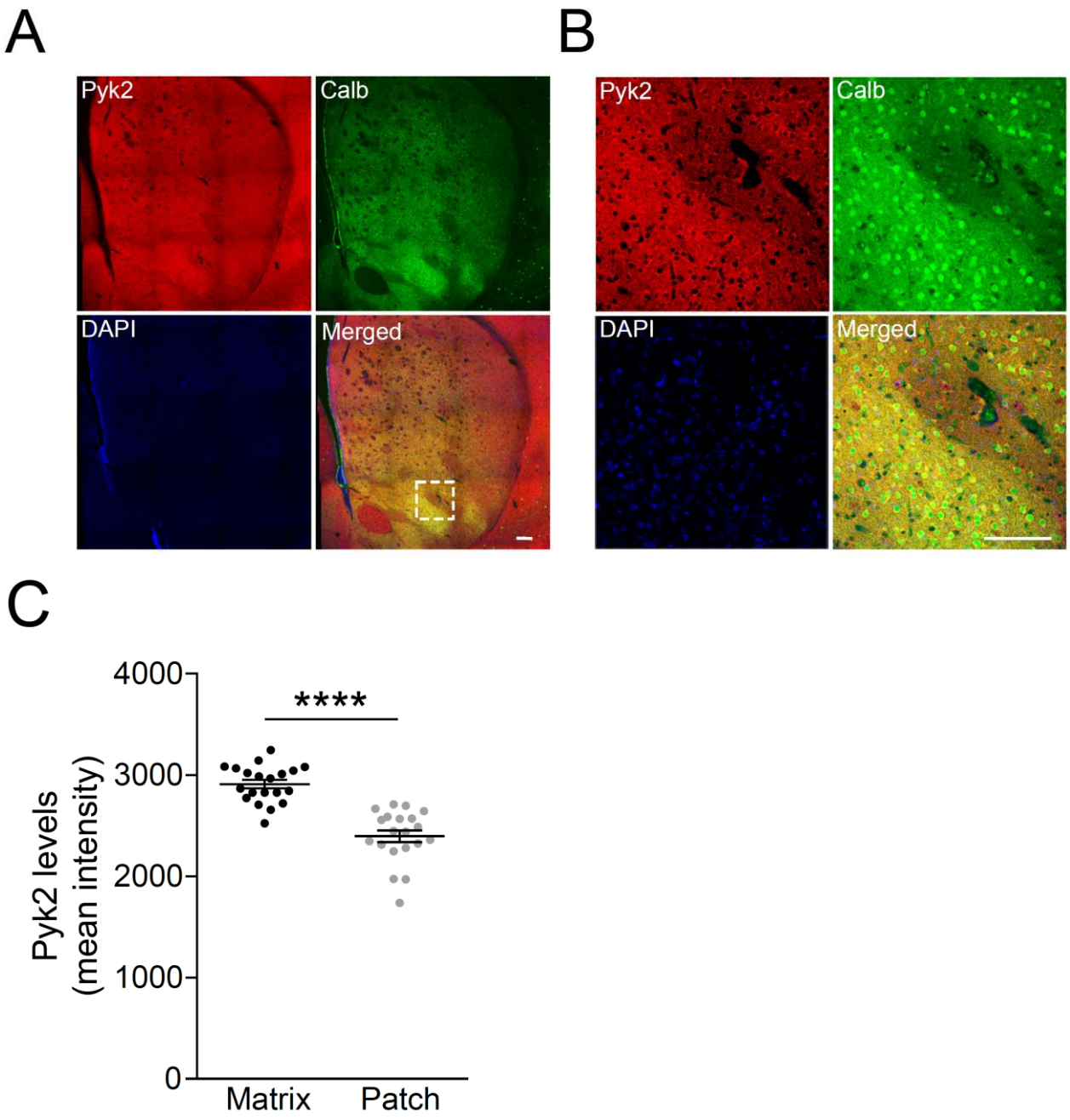

Figure S1: Enrichment of Pyk2 in the striatal matrix. a, Distribution of Pyk2 (red) and calbindin (green) immunoreactivity, and DAPI (blue) in the striatum of wild-type mice. Scale bar: 150 µm. **b**, Zoom in the white square indicated in **a. c**, Pyk2 labelling intensity in striatal matrix as defined as calbindin-enriched areas. Values are means ± SEM. Unpaired t-test, ****p<0.0001. For number of replicates and statistical analysis, see **Supplementary Table 2**.

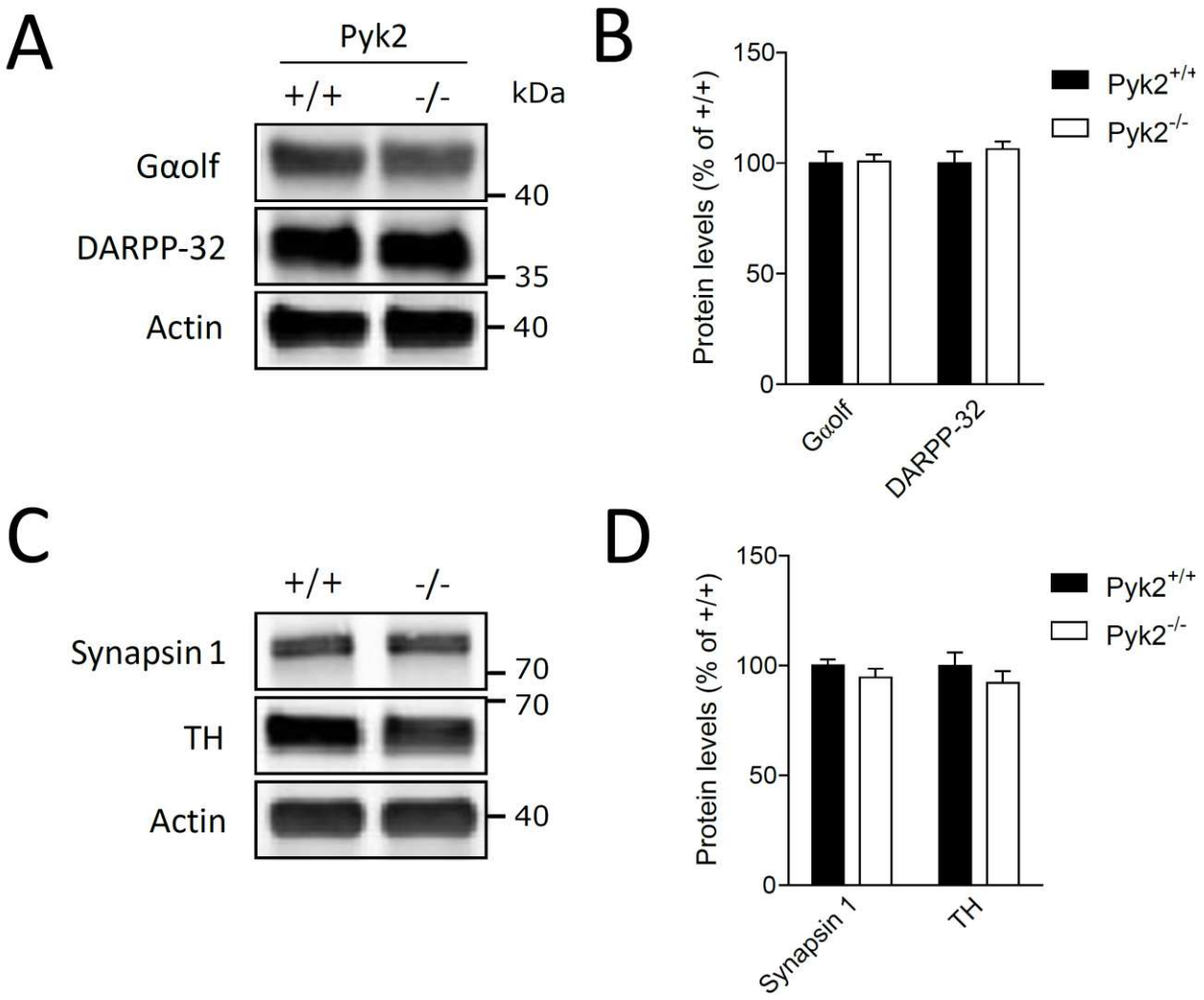

Figure S2: Striatal proteins levels in Pyk2-deficient mice. a, Immunoblotting analysis of Gαolf, DARPP-32, and actin as loading control in 4-month-old $Pyk2^{+/+}$ and $Pyk2^{-/-}$ mice. **b**, Densitometry quantification of results as in **a**. Data were normalized to actin for each sample and expressed as percentage of wild type averge. **c**, Synapsin 1, tyrosine hydroxylase, and actin were analyzed by immunoblotting. **d**, Results as in **c** were quantified and analyzed as indicated in **b.** In **d** and **d**, statistical analysis was done with unpaired t-test. No significant difference. In all graphs, values are means + SEM. For number of mice and detailed statistical analysis, see **Supplementary Table 2**.

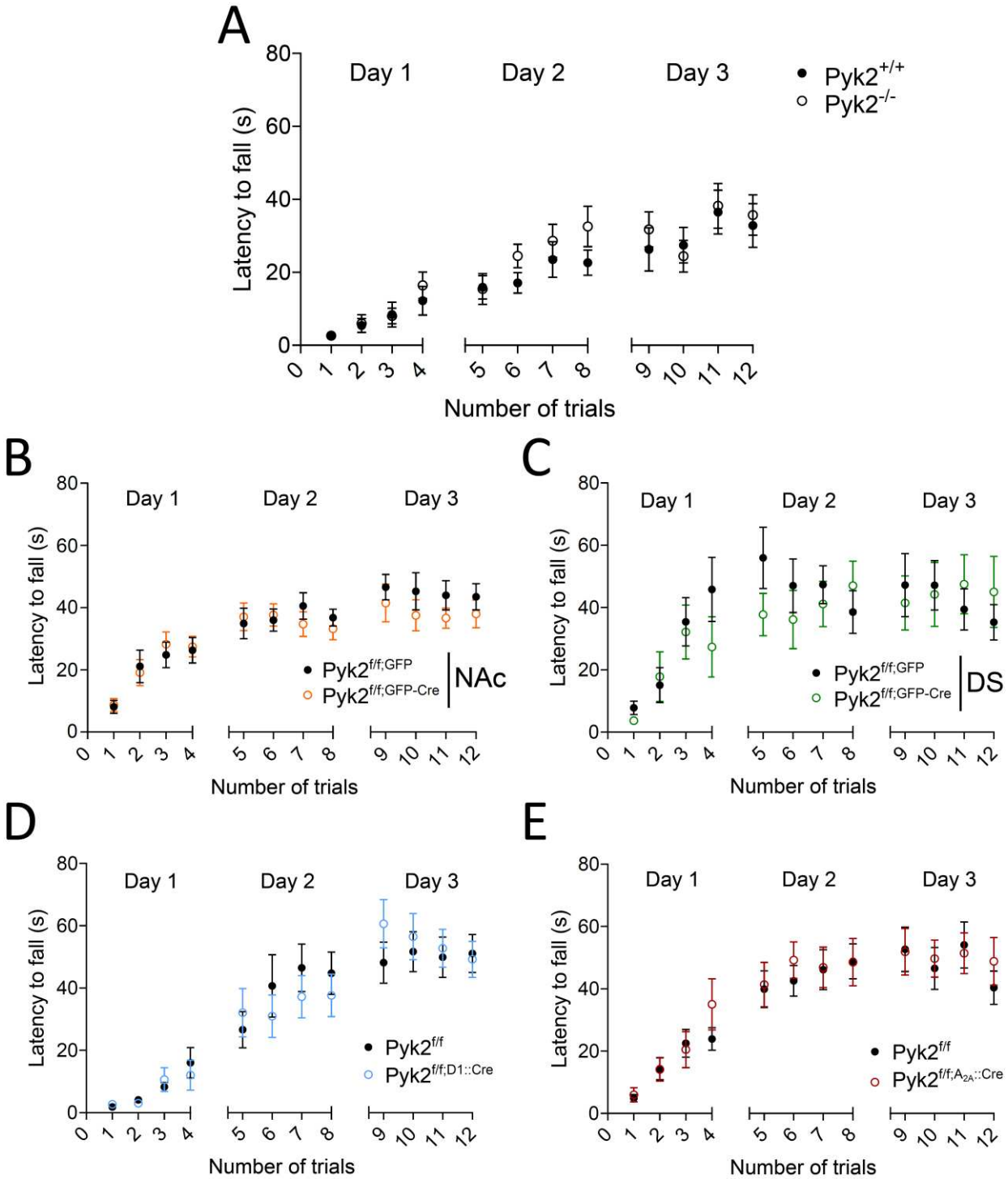

Figure S3: Motor skill learning on the accelerated rotarod is not altered in Pyk2 mutant mice. Latency to fall on the accelerating rotarod for each trial at days 1, 2, and 3 for the various Pyk2 mutant mice and their respective matched controls. **a**, $Pyk2^{+/+}$ and $Pyk2^{-/-}$. **b**, $Pyk2^{f/f;NAc,GFP}$ and $Pyk2^{f/f;NAc,GFP\text{-}Cre}$. **c**, $Pyk2^{f/f;DS,GFP}$ and $Pyk2^{f/f;DS,GPF\text{-}Cre}$. **d**, $Pyk2^{f/f}$ and $Pyk2^{f/f;D1::Cre}$. **e**, $Pyk2^{f/f}$ and $Pyk2^{f/f;A2A::Cre}$ mice. Values are means ± SEM. Two-way ANOVA, genotype or AAV effect, no difference. For number of mice and detailed statistical analysis, see **Supplementary Table 1**.

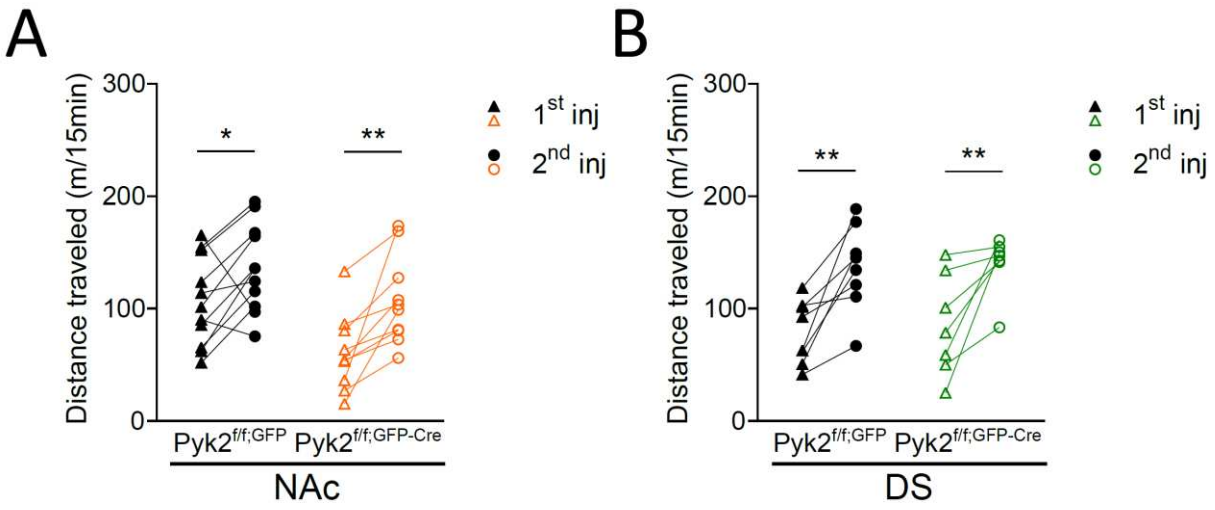

Figure S4: Pyk2 deletion in the NAc or in the DS does not alter locomotor sensitization. Thirty minutes after being placed in a circular open space, mice received an intraperitoneal injection of 20 mg/kg cocaine on Day 1 (1st injection) and Day 14 (2nd injection), as described in the Materials and Methods. The distances traveled during the 15 first minutes following the injection is plotted for each mouse (see average locomotor activity in **Fig. 3**). **a**, $Pyk2^{f/f;NAc,GFP}$ and $Pyk2^{f/f;NAc,GFP\text{-}Cre}$ mice. **b**, $Pyk2^{f/f;DS,GFP}$ and $Pyk2^{f/f;DS,GPF\text{-}Cre}$ mice. In **a** and **b**, statistical analysis with two-way ANOVA and Sidak's multiple comparisons post hoc test, $^{**}p < 0.01$, $^{*}p < 0.05$. For number of mice and detailed statistical analysis, see **Supplementary Table 1**.

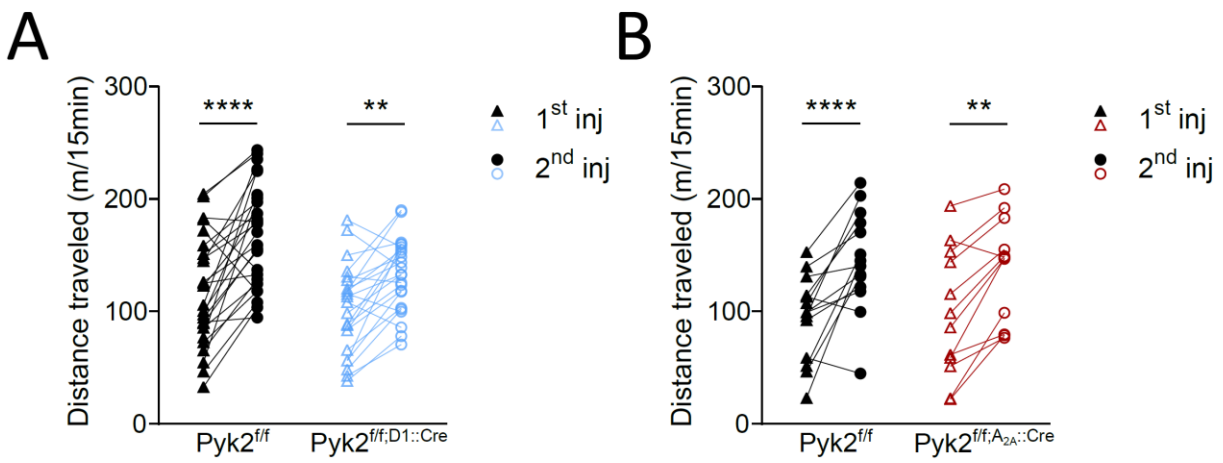

Figure S5: Pyk2 deletion in D1 or in A_{2A} neurons does not alter locomotor sensitization. Thirty minutes after being placed in a circular open space, mice received an intraperitoneal injection of 20 mg/kg cocaine on Day 1 (1st injection) and Day 14 (2nd injection), as described in the Materials and Methods. The distances traveled during the 15 first minutes following the injection is plotted for each mouse (see average locomotor activity in **Fig. 4**). **a**, $Pyk2^{f/f}$ and $Pyk2^{f/f;D1::Cre}$ mice. **b**, $Pyk2^{f/f}$ and $Pyk2^{f/f;A2A::Cre}$ mice. In **a** and **b**, statistical analysis with two-way ANOVA and Sidak's multiple comparisons post hoc test, ****$p < 0.0001$, **$p < 0.01$, *$p < 0.05$. For number of mice and detailed statistical analysis, see **Supplementary Table 1**.

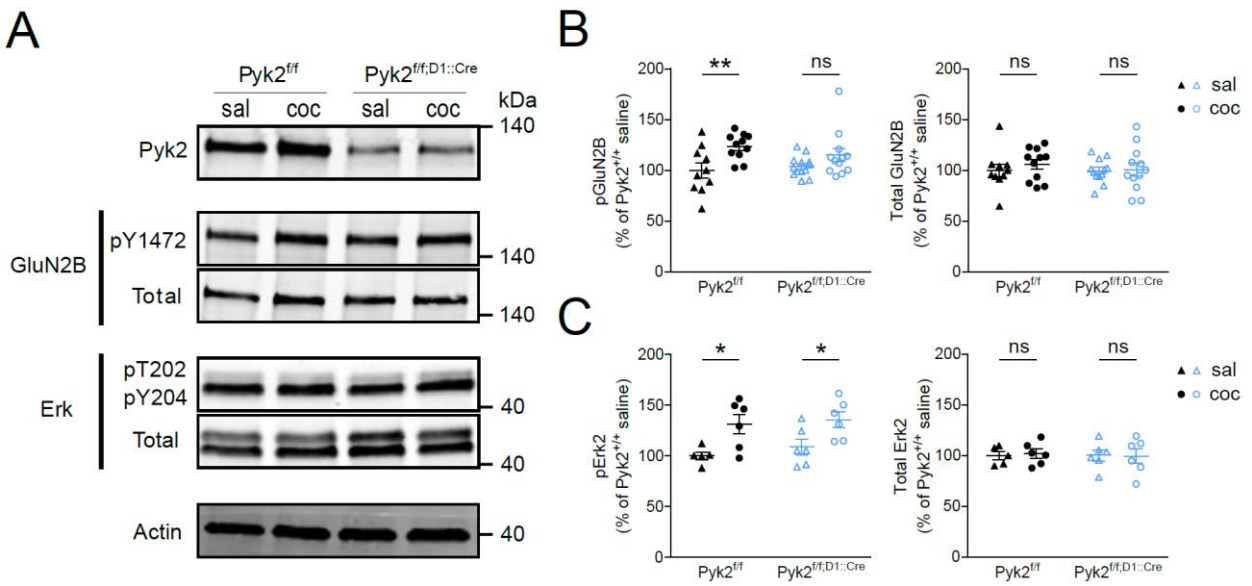

Figure S6: Specific deletion of Pyk2 in D1 neurons decreases cocaine effects on GluN2B phosphorylation but not ERK. a Immunoblotting analysis of Pyk2, GluN2B phosphorylated an Tyr-1472 (**pY1472**) and total levels (**Total**), ERK phosphorylated at Thr-202 and Tyr-204 (**pT202/pY204**) and total levels (**Total**), and actin as loading control in 3-month $Pyk2^{f/f}$ and $Pyk2^{f/f;D1::Cre}$ mice, 10 min after saline (**sal**) or cocaine (20 mg/kg, **coc**) i.p. injection . **b** Densitometry quantification of phospho (**left**) and total (**right**) GluN2B levels. **c** Densitometry quantification of phosphorylated (**left**) and total (**right**) ERK levels. In **b** and **c**, data were normalized to actin for each sample and expressed as percentages of the average in saline-injected $Pyk2^{f/f}$ mice. Statistical analysis was done with two-way ANOVA and Sidak's multiple comparisons post hoc test, *$p < 0.05$, *$p < 0.05$, not significant, ns. In all graphs, means +/- SEM are indicated. For number of mice and detailed statistical analysis, see **Supplementary Table 2**.

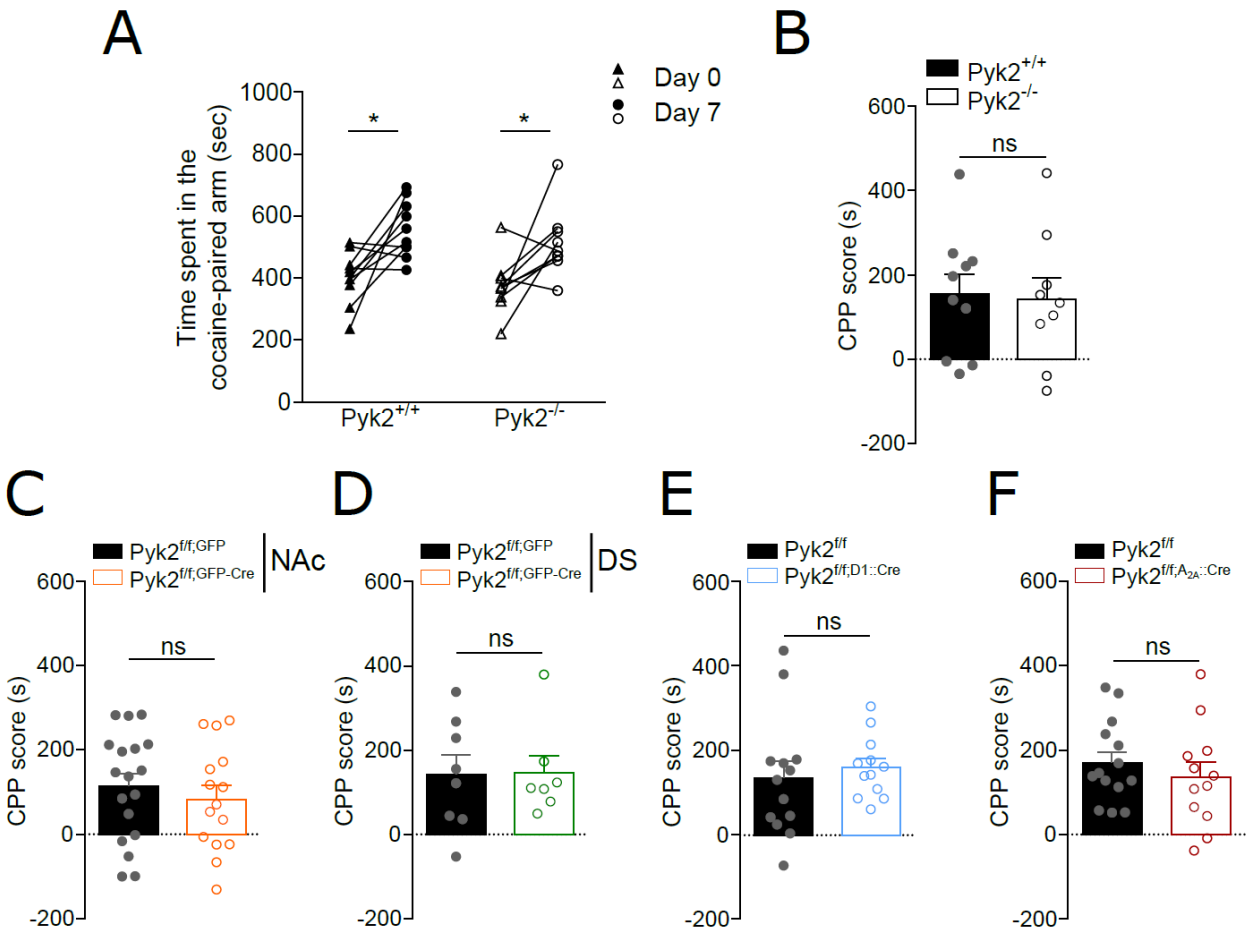

Figure S7: Pyk2 deletion does not alter cocaine-conditioned place preference. For each group of Pyk2 mutant mice and their respective matched controls, the time spent in the cocaine-paired arm before (Day 0) and after (Day 7) cocaine (15 mg/kg) conditioning was measured (see **Materials and Methods**). **a**, Time spent in the cocaine-paired arm in $Pyk2^{+/+}$ and $Pyk2^{-/-}$ mice. Two-way ANOVA and Sidak's multiple comparisons post hoc tests, *$p < 0.05$. **b**, The CPP score was calculated for each $Pyk2^{+/+}$ and $Pyk2^{-/-}$ mouse in **a** as the excess time spent in the cocaine-paired arm. **c-f**, Same CPP score as in B for $Pyk2^{f/f;NAc,GFP}$ and $Pyk2^{f/f;NAc,GFP\text{-}Cre}$ mice (**c**), $Pyk2^{f/f;DS,GFP}$ and $Pyk2^{f/f;DS,GPF\text{-}Cre}$, mice (**d**), $Pyk2^{f/f}$ and $Pyk2^{f/f;D1::Cre}$ (**e**), and $Pyk2^{f/f}$ and $Pyk2^{f/f;A2A::Cre}$ mice (**f**). **b-f**, Bars indicate means + SEM, unpaired t-test, ns, not significant. For number of mice and detailed statistical analysis, see **Supplementary Table 2**.

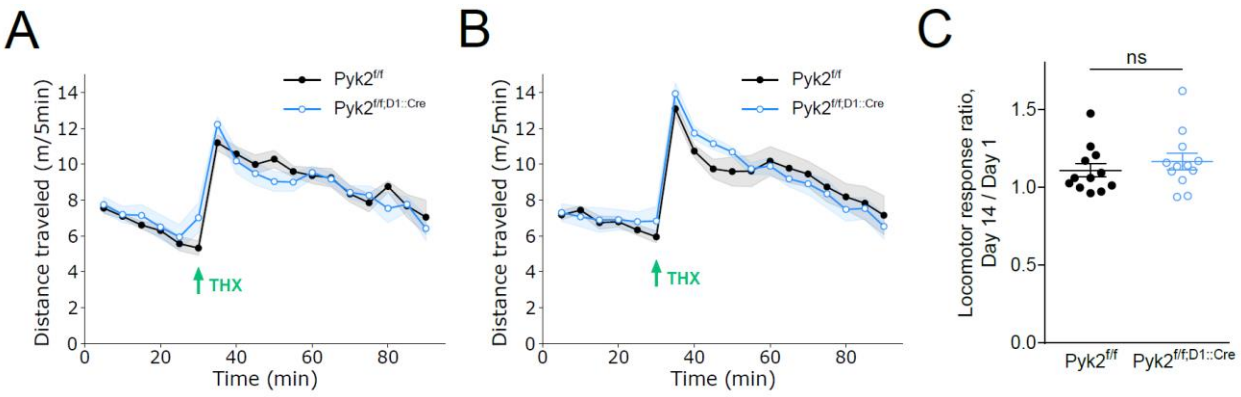

Figure S8: Specific deletion of Pyk2 in D1 neurons does not alter the locomotor responses to trihexyphenidine. a-b, Locomotor activity of Pyk2$^{f/f}$ and Pyk2$^{f/f;D1::Cre}$ mice after a first (**a**) and, 13 days later, a second (**b**) injection of trihexyphenidine (THX). THX (15 mg/kg i.p., arrow) was injected 30 min after mice were placed in the open field. Two-way ANOVA, no genotype effect. **c**, Sensitization during the first 10 min after SKF injection (data from **a** and **b**). **c**, Ratio of the distances traveled 0-15 min after the second (Day 14) / the first (Day 1) THX injections. Unpaired t-test, not significant, ns. In all graphs, means ± SEM, are indicated (shaded area in **a** and **b**). For detailed statistical analysis, see **Supplementary Table 2**.

4. Summary of the findings and conclusions

We observed here that cocaine injection increases Pyk2 phosphorylation in the striatum of mice in vivo suggesting a role for Pyk2 in cocaine response.

According to this hypothesis, Pyk2 knock-out reduced locomotor response to acute cocaine injection without affecting locomotor sensitization and cocaine-conditioned place preference. Specific deletion of Pyk2 in the NAc or in D1 neurons recapitulated this phenotype whereas deletion of Pyk2 in the dorsal striatum or in A_{2A} receptor-expressing neurons did not. Mice lacking Pyk2 in D1-neurons also displayed lower locomotor response to the D1 receptor agonist SKF-81297.

This study identifies a potential role for Pyk2 in acute responses to psychostimulants. It also reveals differences between the striatum and the hippocampus in the biochemical and synaptic changes caused by Pyk2 deletion.

VI. Supplementary data: spine density and morphology in the NAc of Pyk2$^{-/-}$ mice

As Pyk2 deletion was associated with fewer and shorter spines in the hippocampus (Giralt et al., 2017) and the amygdala (Montalban et al., 2019), we decided to explore spine density and morphology in the NAc of Pyk2$^{-/-}$ mice to see if these features were observed as well in this region of the brain.

1. Materials and methods

Fresh brain hemispheres were processed following the Golgi-Cox method. Mouse brain hemispheres were incubated in the dark for 14–17 days in filtered dye solution (10 g l^{-1} $K_2Cr_2O_7$, 10 g l^{-1} $HgCl_2$ and 8 g l^{-1} K_2CrO_4). The tissue was then washed 3 × 2 min in water and 30 min in 90% EtOH (v/v). Two hundred-µm sections were cut in 70% EtOH on a Vibratome (Leica) and washed in water for 5 min. Next, they were reduced in 160 g l^{-1} ammonia for 1 h before washing in water for 2 min and fixation in 10 g l^{-1} $Na_2S_2O_3$ for 7 min. After a 2-min final wash in water, sections were mounted on Superfrost coverslips, dehydrated for 3 min in 50%, then 70, 80 and 100% EtOH, incubated for 2 × 5 min in a 2:1 isopropanol:EtOH mixture, followed by 1 × 5 min in pure isopropanol and 2 × 5 min in xylol. Bright-field images of Golgi-impregnated SPN dendrites from the NAc were acquired with a Nikon DXM 1200F digital camera attached to a Nikon Eclipse E600 light microscope (× 100 oil objective). Fifty-four (Pyk2$^{+/+}$) and 48 (Pyk2$^{-/-}$) dendrites from three mice per genotype were analyzed. Spines were counted manually using ImageJ software (National Institute of Health, Bethesda, MD, USA). Spine density was calculated by quantifying the number of spines per dendritic segment divided by its length. For morphological analysis, *Z*-stacks were deconvolved using the Huygens software (Scientific volume imaging, Hilversum, the Netherlands) to improve voxel resolution and to reduce optical aberration along the *z* axis, followed by Neuronstudio freeware (CNIC, Mount Sinai School of Medicine) processing in order to measure spine length and head diameter and perform a distribution analysis of these two parameters.

2. Results

We performed Golgi staining in the NAc of Pyk2$^{+/+}$ and Pyk2$^{-/-}$ mice (**Figure 16A**). Unexpectedly, we observed an increased spine density associated with longer spines in Pyk2$^{-/-}$ mice possibly suggesting different roles of Pyk2 in the striatum as compared to hippocampus or amygdala (**Figure 16B-D**).

This dissimilarity will be discussed further in detail.

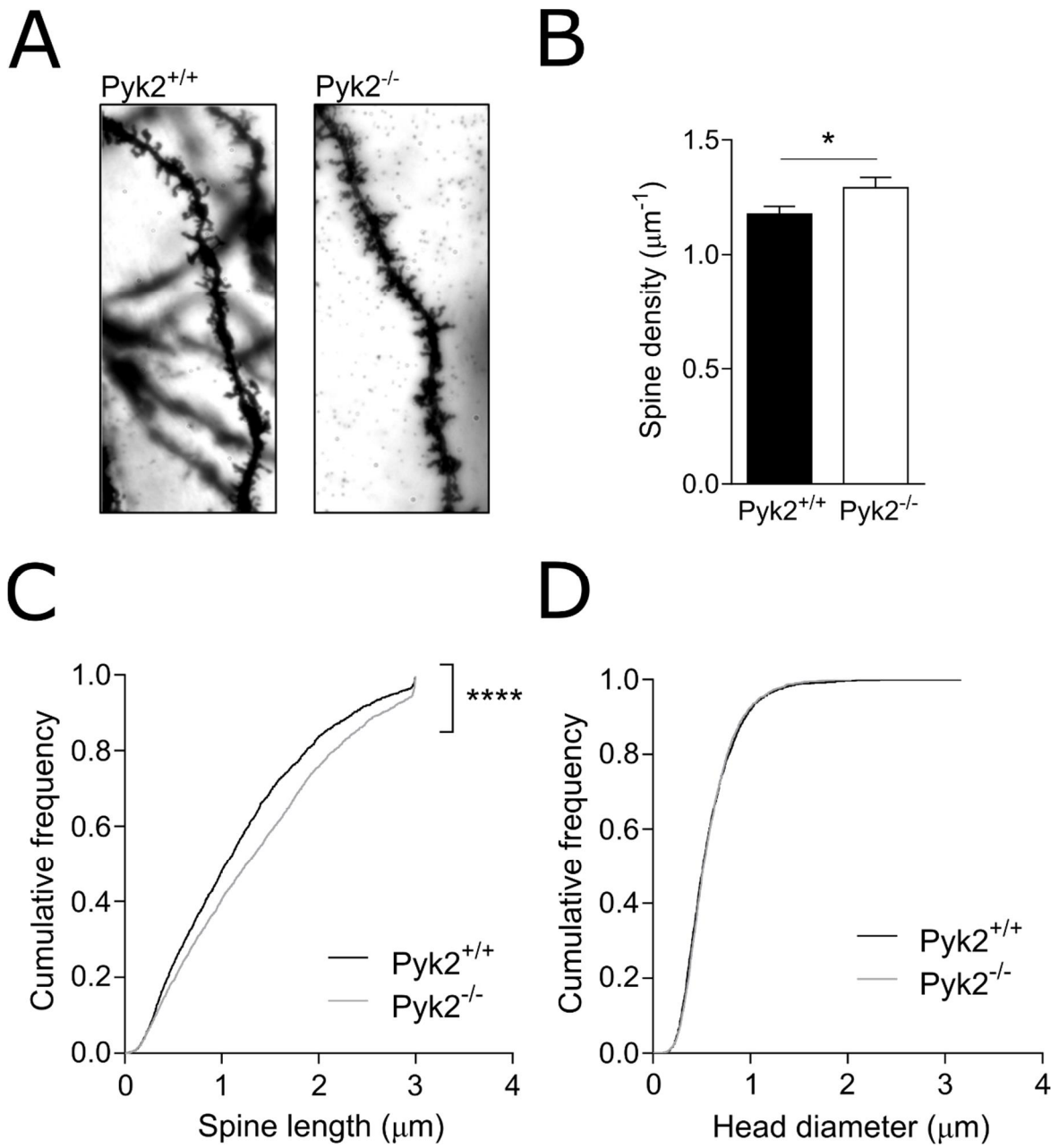

Figure 16. Spines are more dense and longer in the NAc of Pyk2$^{-/-}$ mice. a Confocal acquisition of dendrites of NAc SPNs from Pyk2$^{+/+}$ and Pyk2$^{-/-}$ mice colored by Golgi stained. **b** Spine density of NAc SPNs in Pyk2$^{+/+}$ and Pyk2$^{-/-}$ mice. Unpaired t-test, *$p < 0.05$. **c** Cumulative distribution of spine length in Pyk2$^{+/+}$ and Pyk2$^{-/-}$ mice. Log-rank (Mantel-Cox) test, ****$p < 0.0001$. **d** Cumulative distribution of spine head diameter in Pyk2$^{+/+}$ and Pyk2$^{-/-}$ mice. Log-rank (Mantel-Cox) test.

DISCUSSION

The work presented in this thesis addresses the pathophysiological role of Pyk2 in the central nervous system. It provides evidence for the implication of Pyk2 in several cellular and physiological processes in the central nervous system.

Pyk2 is particularly involved in synaptic organization and plasticity in the hippocampus and the amygdala whereas it appears to play a more limited role within the striatum. We also demonstrated its contribution to three neuropsychiatric conditions, HD, AD, and the chronic stress-induced behavioral alterations. Besides, genetic manipulation of Pyk2 expression in mice models of these pathologies allowed improvement of the phenotype indicating that Pyk2 might be a useful target for neuropsychiatric diseases.

In the first part of this chapter, we will discuss the role of Pyk2 in the establishment of memory, a feature that appears to result from its biochemical function at synapses.

Afterwards, we will summarize the different functions of Pyk2 revealed in this thesis work and we will discuss their dependence on Pyk2 kinase function. This will reveal that beyond being a tyrosine kinase Pyk2 has also other functions, presumably as molecular scaffold at synapses.

We will then comment on the apparently contradictory effects of Pyk2 deletion on spine density and morphology revealed in this study.

Finally, we will focus on the controverted role of Pyk2 in AD. We will discuss about the apparent discrepancy between our results and recent papers coming from another group. Such discussion will let us appreciate the complexity of this tyrosine kinase in the central nervous system and in neurological diseases.

I. Role of Pyk2 in memory

Our results confirm the previous findings of a role of Pyk2 in synaptic plasticity and in the establishment of memory.

The Ca^{2+} ion is a fundamental player in the formation and consolidation of memory. Neurons developed Ca^{2+} signaling systems based on the release and sensing of intracellular calcium leading to the activation of many biochemical pathways (Berridge, 2012). In the light of our results, Pyk2 appears as a crucial calcium sensor at the crossroad of signaling events leading to the formation of synaptic plasticity and to the establishment of memory.

In previous studies, Pyk2 was established as an important modulator of synaptic plasticity and particularly of LTP (Huang et al., 2001; Bartos et al., 2010). We confirmed this hypothesis by the use of Pyk2 deficient mice: CA1 LTP was severely impaired in $Pyk2^{-/-}$ mice resulting in spatial learning and memory defects (Giralt et al., 2017). This was associated with biochemical alterations at synapses. Among them, the decreased total and tyrosine phosphorylated GluN2A and the decreased tyrosine phosphorylation of GluN2B are likely to contribute to synaptic defects in Pyk2 knockout mice.

The decreased function of Pyk2 observed in a mouse model of AD substantiated the hypothesis of a role for Pyk2 in the establishment of memory (Giralt et al., 2018). Overcoming this deficit by Pyk2 overexpression improved the molecular (PSD-95 and synaptophysin expression rescue) and behavioral (restored responses to elevated plus-maze and novel object recognition tests) phenotype of these mice (Giralt et al., 2018). It should be noted that the restored response to elevated plus-maze following Pyk2 overexpression in the hippocampus could appear surprising as this test is measuring anxiety-like behavior which is usually associated to limbic circuits. But hippocampus has been shown to

contribute to anxiety and to behavior in the elevated plus-maze (Barkus et al., 2010; Xiang et al., 2011; Jimenez et al., 2018) thus explaining the observed phenotype of 5XFAD-Pyk2 mice.

Additionally, Pyk2 deletion in the amygdala was also shown to impair the synaptic markers and structural changes induced by chronic stress (Montalban et al., 2019). Such alterations were accompanied with a reduction of anxiety-like and anhedonia-like phenotypes induced by chronic stress (Montalban et al., 2019). Moreover, the Pyk2 interactor PSD-95 was already demonstrated to be essential for the maintenance of long-lasting fear memories via remodeling excitatory synapses (Fitzgerald et al., 2015). It this thus likely that Pyk2 deletion impairs the establishment of a cellular memory (through, *inter alia*, PSD-95 and NMDAR levels in PSDs, NMDAR phosphorylation, and increased spine density) thereby partially preventing the development of stress-induced phenotype.

Seeing Pyk2 as critical for the establishment of plasticity and memory thus provide a better understanding of the apparent complex and ambivalent role of Pyk2 in neurologic diseases. In the light of this idea, Pyk2 can be considered at the same time as an aggravating factor of stress-induced pathologies (in which Pyk2 appears necessary for some ill-defined synaptic changes), and as a possible rescue factor in neurodegenerative diseases such as HD or AD (in which, in constrat, the diseases are notably characterized by a loss of plasticity). The controversy about the exact role of Pyk2 in AD will be discussed further.

II. Kinase-dependent and independent functions of Pyk2

Along this study, it clearly appeared that Pyk2 may embody different functions which can be either kinase or kinase-independent.

Spine density, which is decreased in the hippocampus of $Pyk2^{-/-}$ mice, was rescued by transfection of a form of Pyk2 mutated on the autophosphorylation site or on the kinase domain but not by transfection of a mutant form of Pyk2 unable to bind PSD-95 (Giralt et al., 2017). This result reveals a kinase-independent Pyk2 function on spine density. Such function could be linked to scaffolding properties of Pyk2 (i.e. its ability to bind several proteins such as PSD-95 for instance). Paradoxically, none of this transfected mutants allowed recovery of PSD-95 recruitment to synapses indicating 1; that the entire sequence of Pyk2 is needed for PSD-95 recruitment and 2; that this kinase-independent function of Pyk2 does not rely on PSD-95 recruitment but maybe involves other proteins which remain to be identified (Giralt et al., 2017).

In the amygdala, while Pyk2 deletion resulted in reduced anxiety-like and anhedonia-like phenotypes induced by chronic stress, we did not observe any increased phosphorylation of Pyk2 following stress. Here, it is very likely that the conditions tested (24 hours following CUMS or 0 or 3 hours following acute restraint stress) were possibly not appropriate which means that Pyk2 could have been transiently activated and already returned to basal state when mice were sacrificed. Another interpretation of this result is that Pyk2 function in response to stress is also kinase-independent and may rely as well on its scaffolding properties. Accordingly, we observed that chronic stress induced an increased Pyk2/PSD-95 colocalization concomitant with an increase in GluN2B and pSer896-GluN1 which were prevented in the absence of Pyk2. Being a tyrosine kinase, Pyk2 cannot be directly responsible for Ser896-GluN1 phosphorylation. Thus, these results may not reflect Pyk2 kinase activity but rather its interaction with molecular partners including, at least, PSD-95.

In contrast, in the hippocampus of 5xFAD mice, Pyk2 total levels were not changed as compared to wild type mice, but its phosphorylation was decreased indicating a reduced activity of Pyk2 in this mouse model of AD (Giralt et al., 2018). In the striatum, we observed a phosphorylation of Pyk2 following cocaine injection showing that the role of Pyk2 in such contexts may be related to its autophosphorylation and, by extent, to its kinase activity.

If both kinase-dependent and independent functions of Pyk2 should not be opposed as inherently exclusive (the so-called kinase-independent function of Pyk2, which essentially refers to its scaffolding properties, must probably be important as well in the two last conditions, i.e. AD and cocaine response), the interest of such discussion is to underlie the wide functionality of protein kinases which shall not be seen as simple catalyst but as complex proteins with different features.

This question could be addressed in the future by performing a comparative proteomic study of the proteins interacting with phosphorylated and non-phosphorylated Pyk2. Such approach could be assessed in different conditions (e.g. after saline or cocaine injection) and/or different brain regions (e.g. NAc versus dorsal striatum or striatum versus hippocampus). This would give a comprehensive idea of the relative contribution of the kinase-dependent and independent functions of Pyk2 in every situation and could be relevant for a better understanding of its role in neurologic disorders.

III. **Antagonistic effect of Pyk2 on spine density and morphology**

Our results revealed antagonistic effects of Pyk2 on spine density and morphology.

In CA1 pyramidal neurons of the hippocampus, spine density was decreased in $Pyk2^{+/-}$ (−8%) and $Pyk2^{-/-}$ (−16%) mice as compared to wild type (Giralt et al., 2017). This was also associated with a decreased spine neck length (Giralt et al., 2017). In neurons in culture spine density but not spine neck length was rescued by transfection of a mutant form of Pyk2 with a point mutation of the autophosphorylation site or o the ATP-binding lysine in the kinase domain (kinase-dead, KD mutant) suggesting that scaffolding properties of Pyk2 may be involved in the control of spine density in the hippocampus. However, one cannot exclude here a pre-synaptic role of Pyk2 as electron microscopy experiments showed the presence of Pyk2 in nerve terminals as well (Giralt et al., 2017).

In the amygdala, Pyk2 deletion prevented the CUMS-induced spine density increase (Montalban et al., 2019). Here again, the same hypothesis as for the hippocampus could explain this effect. Pyk2 would play a role of scaffold at synapses promoting interactions between partners (PSD-95, NDMAR, etc.) leading to structural plasticity (Montalban et al., 2019). The role of Pyk2-dependent phosphorylation in this response remains to be investigated more thoroughly.

In contrast, in the NAc, the lack of Pyk2 is associated with increased SPNs spine density and neck length. This is the exact opposite of the effect of Pyk2 deletion in hippocampal neurons and it reveals an antipodal role for Pyk2 on spine density and morphology.

One could explain such discrepancy by the diversity of the neurons studied here, hippocampal neurons being glutamatergic as opposed to SPNs of the striatum being GABAergic for instance. Hence, it could be hypothesized that Pyk2 has distinct roles depending on the neuronal type. However, such opposite role of Pyk2 within the hippocampus was already mentioned in the literature showing that, in a same neuronal

population, Pyk2 can have different effects on spine density and morphology. In 2007, Bourgin et al. demonstrated that EphA4 activation by ephrin-A3 in hippocampal slices led to decreased tyrosine phosphorylation of pCas, FAK and Pyk2, associated with a decreased spine density and neck length (Bourgin et al., 2007). Such result ties up with the hypothesis of a *positive* role for Pyk2 on spine density and neck length. On the contrary, in 2012, Suo et al showed that overexpression of Pyk2 induced the inhibition of Rac1 thereby leading to dendritic simplification and spine loss in CA1 (Suo et al., 2012). In this instance, Pyk2 displays a *negative* role on spine density, just as what we observed in the NAc.

Such divergence reveals the complexity of the role of Pyk2 in neurons. It looks like, depending on the situation, Pyk2 alterations can have opposite effects on structural plasticity. Further studies will be needed to understand the molecular basis at the origin of this apparent discrepancy.

IV. **BDNF and Pyk2 merging functions**

Interestingly, over the presented results we obtained, it appears that Pyk2 and BDNF share, in some extent, common role in maintaining synaptic structure, biochemical markers and functions as well as in preventing AD-associated defects.

BDNF was shown to induce LTP in hippocampal neurons (Kang et al., 1997; Kuipers et al., 2016). Pyk2 was also shown to be involved in hippocampal LTP (Girault et al., 1999a; Huang et al., 2001; Bartos et al., 2010). Notably, LTP of CA1 synapses is prevented by a kinase-dead Pyk2 (Huang et al., 2001) or by competition of Pyk2:PSD95 interaction (Bartos et al., 2010). Here, we showed that Pyk2 is critical for recruiting PSD-95 at synapses (Giralt et al., 2017). Besides, BDNF was also shown to promote PSD-95 expression and targeting to synapses (Yoshii and Constantine-Paton, 2007, 2014; Robinet and Pellerin, 2011; Parsons et al., 2014). In the same vein, both BDNF and Pyk2 were shown to enhance spine density in the hippocampus (Giralt et al., 2017; von Bohlen und Halbach and von Bohlen und Halbach, 2018). Both Pyk2 and BDNF thus contribute to PSD-95 recruitment at synapses, spines maintenance and LTP expression.

These features are all altered in AD models (Walsh et al., 2002; Shankar et al., 2008; Yuki et al., 2014; Dorostkar et al., 2015). However and interestingly, if we observed a decreased activation of Pyk2 in the hippocampus of 5xFAD mice at 8 months of age (Giralt et al., 2018), it is still debated whether BDNF levels are affected or not in the course of the disease (Song et al., 2015). Nevertheless, overexpression of BDNF (de Pins et al., 2019) and Pyk2 (Giralt et al., 2018) were both shown to rescue memory deficits, spine density, and synaptic properties in 5xFAD mice.

It is also noteworthy that BDNF was shown to activate Pyk2 through STEP inhibition (Xu et al., 2016) and to induce its synaptic synthesis in hippocampal neurons (Afonso et al., 2019). It is thus likely that these two pathways, contributing to the same evoked functions, are at least partially interdependent.

V. **Pyk2 and AD: risk or rescue factor?**

Our results published in 2018 on the role of Pyk2 in a mouse model of Alzheimer's disease were unexpected since our hypothesis before carrying out the experiments was that the loss of Pyk2 could have a protective role. In the light of previously published results, we first

hypothesized a role of Pyk2 in the development of AD. Several GWAS identified *PTK2B* as a susceptibility locus of LOAD, suggesting a role for Pyk2 in AD (Kamboh et al., 2012; Lambert et al., 2013; Beecham et al., 2014; De Jager et al., 2014; Wang et al., 2014; Chan et al., 2015; Jiao et al., 2015; Li et al., 2016; Nettiksimmons et al., 2016; Lin et al., 2017). These association data do not provide indication on the positive or negative effect. However, rs28834970C, one of the SNPs associated with increased AD risk was associated with increased Pyk2 mRNA expression in peripheral blood monocytes suggesting that *PTK2B* expression increases AD risk (Chan et al., 2015). Previous studies from the group of Strittmatter also indicated a possible role for Pyk2 in the development of AD implicating its Aβo-dependent activation through the PrPc-mGluR5 complex receptor (Kaufman et al., 2015; Haas and Strittmatter, 2016; Haas et al., 2016, 2017; Brody and Strittmatter, 2018). Finally, Pyk2 was also linked with tauopathy since it colocalizes with hyperphosphorylated tau in the brain of AD patients and in Tau transgenic pR5 mouse model (Köhler et al., 2013; Dourlen et al., 2017) and as it was recently reported to phosphorylate tau directly (Li and Götz, 2018).

Our first expectation was that Pyk2 deletion could rescue the behavioral and biochemical phenotype of a mouse model of AD, the 5xFAD mouse. Thus, the absence of effect, except from the slight decrease in amyloid plaque number, was a surprise. The observation of a decreased Pyk2 Tyr-402 phosphorylation in 5xFAD mice at 8 months of age led us to the idea to rescue this deficiency by overexpressing Pyk2 instead of suppressing it. Remarkably, such strategy improved synaptic markers and performance in several behavioral tasks but slight increased amyloid plaque number. Because both Pyk2$^{-/-}$ and 5xFAD mice showed an increase of potentially toxic Src fragment, we hypothesized that the neuroprotective role of Pyk2 highlighted in this study could be related to the prevention of Src cleavage. However, several questions remains open such as the precise role of Pyk2 in amyloid plaque formation.

Afterwards, a comment of our article from Polis and Gil-Henn gave new explanation lines on the apparent discrepancies between the previous bibliography and our results (Polis and Gil-Henn, 2019). First, one should note that, for leading to the development of a relatively fast and aggressive pathology, the 5xFAD mouse may represent a model for early onset AD (EOAD) instead of the LOAD examined in the aforementioned GWAS studies. Pyk2 may display different role along the development of the disease thereby explaining the contrasted results in the different studies. Moreover, the lack of Tau pathology in the 5xFAD mouse model (which is an amyloid model of AD) might at least partially explain the lack of phenotype in 5xFAD/Pyk2$^{-/-}$ mice. Polis and Gil-Henn thus suggest the use of an AD mouse model which would more closely mimic LOAD such as the 3xTg-AD model that harbors mutations in PS1, APP and Tau (Oddo et al., 2003). They also develop an interesting hypothesis concerning the putative role of Pyk2 in amyloid plaque formation. We observed a decreased plaque number in 5xFAD/Pyk2$^{-/-}$ mice and an increased plaque number in 5xFAD mice overexpressing Pyk2. We also noted colocalization of Pyk2 and Aβ in the neuropil zone but not in plaques, suggesting a putative role of Pyk2 in Aβ production. Such role could be due to a Pyk2-induced calcium release from endoplasmic reticulum (Grossi et al., 2017) and the subsequent calcium-induced activation of γ-secretase, an APP processing enzyme (Small et al., 2010). This model would explain our observations and would need to be tested in further studies.

However, two recent studies from the Strittmatter group reported again evidences for Pyk2 being an AD risk factor (Lee et al., 2019; Salazar et al., 2019). In the first study,

Salazar et al. reported, in 2- to 6-month-old mice, that Pyk2 contributed to synaptic LTD, but was not required for basal synaptic function or LTP (Salazar et al., 2019). In the hippocampus from 6-8 and in 12 month-old mice, they did not observe any synaptic defect as observed in our previous study. Finally, they also observed in APPswe/PS1ΔE9 mice, another mouse model of AD, that Pyk2 was necessary for LTP suppression in slices by Aβo and for memory impairment plus synapse loss (Salazar et al., 2019).

Following this study, Lee et al. tried to explore the molecular mechanisms underlying the role of Pyk2 in the development of cognitive decline in APPswe/PS1ΔE9 mice (Lee et al., 2019). In vitro, Pyk2 overexpression results in a decreased spine density in a kinase activity-dependent mechanism: Pyk2 phosphorylates and inhibits Graf1, a RhoA GAP protein. Such inhibition of Graf1 results in the activation of RhoA and subsequent ROCK2-dependent actin contractility, thereby leading to dendritic spines retraction and synapse loss (Lee et al., 2019).

These findings are clearly different from ours. Nonetheless, some parameters may explain the observed discrepancies. About the synaptic markers and plasticity defects observed in Giralt et al. 2017, we led our experiments on male mice only whereas the two aforementioned studies of the Strittmatter group were done with no preference for male or female mice (Giralt et al., 2017; Lee et al., 2019; Salazar et al., 2019). Hormonal cycles in female may create variability preventing the observation of LTP and synaptic markers defects previously revealed in our Pyk2 knockout mice. Additionally, differences in the Pyk2-null strains cannot be excluded: our Pyk2 knockout mice were produced by deleting exons 15 to 18 of *Ptk2b* whereas the Strittmatter group used $Pyk2^{-/-}$ mice from Schlessinger group, in which a neo-expressing cassette was inserted into the 5' portion of Pyk2 sequence encoding for the kinase domain (Okigaki et al., 2003; Giralt et al., 2016). In principle the resulting deletion should be the same and neither group detected Pyk2 immunoreactive forms with either N- or C-terminus specific antibodies (Giralt et al 2017 and unpublished results mentioned in Okigaki et al. 2003). However the existence of PRNK, which should be unaffected, but is not expected to be expressed in the CNS, has not been extensively investigated. One cannot exclude a possible change in the chromatin structure leading to different regulation of additional genes in one of the aforementioned genetic constructs. Schlessinger's lab knockout mice were generated by deletion in R1 ES cells which are derived from 129S1/SvImJ and 129X1/SvJ blastocyst and chimeric mice brought to be homozygous in a 129Sv/Ev background (Okigaki et al., 2003) and later transferred onto a C57BL/6J background after 10 backcrosses (Salazar et al., 2019). Our mice were generated by homologous recombination of C57/Bl6 ES cells and then transferred to the same background. Finally, the line used by Salazar et al. had been generated about 15 years before the experiments, and the appearance and selection of additional mutations moderating the phenotype cannot be excluded. Moreover, while our observations were made in 3-4 month-old mice, the biochemistry studies reported in Salazar et al. were carried out in 6-8 and in 12 month-old mice, and the synaptic plasticity tests in 2-6 month-old mice (Giralt et al., 2017; Salazar et al., 2019). Thus, another hypothesis is that Pyk2 deletion induces synaptic defects which are reverted with age. Further studies will be needed to unravel this conundrum.

About the role of Pyk2 in the development of AD, some other parameters can explain the discrepancies observed between these results. Again, the mouse model of AD used in these studies are different. In 5xFAD mice, the onset of the phenotype is at juvenile or early adult stages whereas it develops at late adult stages in APPswe/PS1ΔE9 mice. As

mentioned before in this discussion, 5xFAD mice are thereby more related to EOAD, whereas APPswe/PS1ΔE9 mice would better represent LOAD. Besides, the correction of Pyk2$^{-/-}$ synaptic phenotypes from early (Giralt et al., 2017) to late adult stages (Salazar et al., 2019) must also be taken into account, as the ages of the mice differ between the studies.

Finally, it is noteworthy that none of these studies deal with Tau pathology. Neither 5xFAD, nor APPswe/PS1ΔE9 mice develop clear Tau pathology as they are do not harbor mutations in the gene coding for Tau and a clear effect of APP alterations on Tau is not observed in mice. As discussed above, Pyk2 is a very probable modulator of Tau pathology as it was shown to colocalize and phosphorylate Tau (Köhler et al., 2013; Dourlen et al., 2017; Li and Götz, 2018). The comment of Polis and Gil-Henn thus remains accurate for the future: a study on 3xTg-AD, which not only harbors mutations in PS1 and APP but also in Tau, would be highly beneficial for a better understanding of the role of Pyk2 in the development of AD (Polis and Gil-Henn, 2019).

VI. Contrasted function of Pyk2 in the striatum

The study of the role of Pyk2 in the striatum gave unexpected results.

In contrast to the hippocampus where it seems important for learning and memory, in the striatum Pyk2 is not necessary for cocaine locomotor sensitization or conditioned place preference, underlining regional specificity in its actions.

As evoked above, this dissimilarity could be explained by the differences between the neuronal populations of these two areas of the brain. Hippocampal neurons are glutamatergic whereas the main neuronal population of the striatum, the SPNs, are GABAergic. Moreover, these neurons do not receive the same afferences and thus may differ in their signaling pathways. The slightly lower locomotor response to the D1 agonist SKF-81297 in Pyk2$^{f/f;D1::Cre}$ mice support the hypothesis of a role for Pyk2 in D1R/G*a*olf/cAMP pathway modulation. Accordingly, the decreased locomotor response to psychostimulants without alteration in locomotor sensitization or CPP is reminiscent of the phenotype of G*a*olf heterozygous (*Gnal*$^{+/-}$) mutant mice in which cAMP production is decreased (Corvol et al., 2007). It is thus likely that this particular and unexpected role of Pyk2 in the striatum may account on a newly identified function of Pyk2 as a modulator of the D1R/G*a*olf/cAMP pathway.

It is noteworthy that we did not study more procedural memory, which are known to involve the sensorimotor striatum (dorso-lateral part of the striatum) (Willuhn and Steiner, 2009). This memory could be tested, in the future, by operant behavior experiment in mice, involving longer-term protocols of cocaine (or food) delivery in response to a specific behavior. Such experiment would complete our overview of Pyk2 function in the striatum.

Additional work will thus be needed to unravel the precise molecular mechanism underlying the specific function of Pyk2 in the striatum and its difference with other brain regions such as the hippocampus.

The results obtained in this thesis shed a new light on the putative role of Pyk2 in synaptic function and in neuropsychiatric conditions. Pyk2 appears to be, at least in the hippocampus and the amygdala, a critical player in synaptic plasticity. Because of that, it contributes in three neuropsychiatric conditions, HD, AD, and chronic stress-induced behavioral alterations. Genetic manipulation of Pyk2 expression in mice models of these

conditions improved the phenotype of these mice indicating that Pyk2 might be a useful target for neuropsychiatric diseases. Conversely, deletion of Pyk2 in the striatum was associated with fewer molecular defects but altered acute effects of cocaine or D1 dopamine receptors stimulation. This contrast reveals the complexity of Pyk2 function, in agreement with findings in non-neuronal cell types. Pyk2 cannot be assigned to one single simple biological function but its role can vary depending on the cell type and the conditions. A deeper understanding of this complexity will require further works in the coming years.

BIBLIOGRAPHY

Adams JP, Sweatt JD (2002) M OLECULAR P SYCHOLOGY□ : Roles for the ERK MAP Kinase Cascade in Memory. Annu Rev Pharmacol Toxicol 42:135–163.

Afonso P, De Luca P, Carvalho RS, Cortes L, Pinheiro P, Oliveiros B, Almeida RD, Mele M, Duarte CB (2019) BDNF increases synaptic NMDA receptor abundance by enhancing the local translation of Pyk2 in cultured hippocampal neurons. Sci Signal 12:eaav3577.

Alawieyah Syed Mortadza S, Sim JA, Neubrand VE, Jiang L-H (2018) A critical role of TRPM2 channel in Aβ $_{42}$ -induced microglial activation and generation of tumor necrosis factor-α. Glia 66:562–575.

Alier KA, Morris BJ (2005) Divergent regulation of Pyk2/CAKbeta phosphorylation by Ca2+ and cAMP in the hippocampus. Biochim Biophys Acta 1745:342–349.

Allen JG, Lee MR, Han C-YE, Scherrer J, Flynn S, Boucher C, Zhao H, O'Connor AB, Roveto P, Bauer D, Graceffa R, Richards WG, Babij P (2009) Identification of small molecule inhibitors of proline-rich tyrosine kinase 2 (Pyk2) with osteogenic activity in osteoblast cells. Bioorg Med Chem Lett 19:4924–4928.

Allingham MJ, van Buul JD, Burridge K (2007) ICAM-1-mediated, Src- and Pyk2-dependent vascular endothelial cadherin tyrosine phosphorylation is required for leukocyte transendothelial migration. J Immunol 179:4053–4064.

André E, Becker-André M (1993) Expression of an N-terminally truncated form of human focal adhesion kinase in brain. Biochem Biophys Res Commun 190:140–147.

Andreev J, Simon JP, Sabatini DD, Kam J, Plowman G, Randazzo PA, Schlessinger J (1999) Identification of a new Pyk2 target protein with Arf-GAP activity. Mol Cell Biol 19:2338–2350.

Aoto H, Sasaki H, Ishino M, Sasaki T (2002) Nuclear translocation of cell adhesion kinase beta/proline-rich tyrosine kinase 2. Cell Struct Funct 27:47–61.

Arcucci A, Montagnani S, Gionti E (2006) Expression and intracellular localization of Pyk2 in normal and v-src transformed chicken epiphyseal chondrocytes. Biochimie 88:77–84.

Arold ST, Ulmer TS, Mulhern TD, Werner JM, Ladbury JE, Campbell ID, Noble ME (2001) The role of the Src homology 3-Src homology 2 interface in the regulation of Src kinases. J Biol Chem 276:17199–17205.

Astier A, Manié SN, Avraham H, Hirai H, Law SF, Zhang Y, Golemis EA, Fu Y, Druker BJ, Haghayeghi N, Freedman AS, Avraham S (1997) The related adhesion focal tyrosine kinase differentially phosphorylates p130Cas and the Cas-like protein, p105HEF1. J Biol Chem 272:19719–19724.

Avraham H, Park SY, Schinkmann K, Avraham S (2000) RAFTK/Pyk2-mediated cellular signalling. Cell Signal 12:123–133.

Avraham S, London R, Fu Y, Ota S, Hiregowdara D, Li J, Jiang S, Pasztor LM, White RA, Groopman JE (1995) Identification and characterization of a novel related adhesion focal tyrosine kinase (RAFTK) from megakaryocytes and brain. J Biol Chem 270:27742–27751.

Bagi CM, Christensen J, Cohen DP, Roberts WG, Wilkie D, Swanson T, Tuthill T, Andresen CJ (2009) Sunitinib and PF-562,271 (FAK/Pyk2 inhibitor) effectively block growth and recovery of human hepatocellular carcinoma in a rat xenograft model. Cancer Biol Ther 8:856–865.

Banno Y, Nemoto S, Murakami M, Kimura M, Ueno Y, Ohguchi K, Hara A, Okano Y, Kitade Y, Onozuka M, Murate T, Nozawa Y (2008) Depolarization-induced differentiation of PC12 cells is mediated by phospholipase D2 through the transcription factor CREB pathway. J Neurochem 104:1372–1386.

Banno Y, Ohguchi K, Matsumoto N, Koda M, Ueda M, Hara A, Dikic I, Nozawa Y (2005) Implication of Phospholipase D2 in Oxidant-induced Phosphoinositide 3-Kinase Signaling via Pyk2 Activation in PC12 Cells. J Biol Chem 280:16319–16324.

Barkus C, McHugh SB, Sprengel R, Seeburg PH, Rawlins JNP, Bannerman DM (2010) Hippocampal NMDA receptors and anxiety: at the interface between cognition and emotion. Eur J Pharmacol 626:49–56.

Barry ST, Critchley DR (1994) The RhoA-dependent assembly of focal adhesions in Swiss 3T3 cells is associated with increased tyrosine phosphorylation and the recruitment of both pp125FAK and protein kinase C-delta to focal adhesions. J Cell Sci 107 (Pt 7):2033–2045.

Bartos JA, Ulrich JD, Li H, Beazely MA, Chen Y, Macdonald JF, Hell JW (2010) Postsynaptic clustering and activation of Pyk2 by PSD-95. J Neurosci 30:449–463.

Battistone MA, Alvau A, Salicioni AM, Visconti PE, Da Ros VG, Cuasnicu PS (2014) Evidence for the involvement of proline-rich tyrosine kinase 2 in tyrosine phosphorylation downstream of protein kinase A activation during human sperm capacitation. Mol Hum Reprod 20:1054–1066.

Beauséjour M, Noël D, Thibodeau S, Bouchard V, Harnois C, Beaulieu J-F, Demers M-J, Vachon PH (2012) Integrin/Fak/Src-mediated regulation of cell survival and anoikis in human intestinal epithelial crypt cells: selective engagement and roles of PI3-K isoform complexes. Apoptosis 17:566–578.

Bechara A, Nawabi H, Moret F, Yaron A, Weaver E, Bozon M, Abouzid K, Guan J-L, Tessier-Lavigne M, Lemmon V, Castellani V (2008) FAK-MAPK-dependent adhesion disassembly downstream of L1 contributes to semaphorin3A-induced collapse. EMBO J 27:1549–1562.

Beecham GW et al. (2014) Genome-wide association meta-analysis of neuropathologic features of Alzheimer's disease and related dementias. Gibson G, ed. PLoS Genet 10:e1004606.

Beggs HE, Schahin-Reed D, Zang K, Goebbels S, Nave KA, Gorski J, Jones KR, Sretavan D, Reichardt LF (2003) FAK deficiency in cells contributing to the basal lamina results in cortical abnormalities resembling congenital muscular dystrophies. Neuron 40:501–514.

Behmoaram E, Bijian K, Jie S, Xu Y, Darnel A, Bismar TA, Alaoui-Jamali MA (2008) Focal adhesion kinase-related proline-rich tyrosine kinase 2 and focal adhesion kinase are co-overexpressed in early-stage and invasive ErbB-2-positive breast cancer and cooperate for breast cancer cell tumorigenesis and invasiveness. Am J Pathol 173:1540–1550.

Beierle EA, Trujillo A, Nagaram A, Kurenova E V, Finch R, Ma X, Vella J, Cance WG, Golubovskaya VM (2007) N-MYC regulates focal adhesion kinase expression in human neuroblastoma. J Biol Chem 282:12503–12516.

Belrose JC, Jackson MF (2018) TRPM2: a candidate therapeutic target for treating neurological diseases. Acta Pharmacol Sin 39:722–732.

Benbernou N, Muegge K, Durum SK (2000) Interleukin (IL)-7 induces rapid activation of Pyk2, which is bound to Janus kinase 1 and IL-7Ralpha. J Biol Chem 275:7060–7065.

Benilova I, Karran E, De Strooper B (2012) The toxic Aβ oligomer and Alzheimer's disease: an emperor in need of clothes. Nat Neurosci 15:349–357.

Benzing T, Gerke P, Höpker K, Hildebrandt F, Kim E, Walz G (2001) Nephrocystin interacts with Pyk2, p130(Cas), and tensin and triggers phosphorylation of Pyk2. Proc Natl Acad Sci U S A 98:9784–9789.

Bermudez Y, Yang H, Cheng JQ, Kruk PA (2008) Pyk2/ERK 1/2 mediate Sp1- and c-Myc-dependent induction of telomerase activity by epidermal growth factor. Growth Factors 26:1–11.

Berridge MJ (2012) Calcium signalling remodelling and disease. Biochem Soc Trans 40:297–309.

Bhaskar K, Hobbs GA, Yen S-H, Lee G (2010) Tyrosine phosphorylation of tau accompanies disease progression in transgenic mouse models of tauopathy. Neuropathol Appl Neurobiol 36:462–477.

Bhaskar K, Yen S-H, Lee G (2005) Disease-related modifications in tau affect the interaction between Fyn and Tau. J Biol Chem 280:35119–35125.

Bibli S-I, Szabo C, Chatzianastasiou A, Luck B, Zukunft S, Fleming I, Papapetropoulos A (2017) Hydrogen Sulfide Preserves Endothelial Nitric Oxide Synthase Function by Inhibiting Proline-Rich Kinase 2: Implications for Cardiomyocyte Survival and Cardioprotection. Mol Pharmacol 92:718–730.

Bikis C, Moris D, Vasileiou I, Patsouris E, Theocharis S (2015) FAK/Src family of kinases:

protective or aggravating factor for ischemia reperfusion injury in nervous system? Expert Opin Ther Targets 19:539–549.
Bjarnadottir M, Misner DL, Haverfield-Gross S, Bruun S, Helgason VG, Stefansson H, Sigmundsson A, Firth DR, Nielsen B, Stefansdottir R, Novak TJ, Stefansson K, Gurney ME, Andresson T (2007) Neuregulin1 (NRG1) Signaling through Fyn Modulates NMDA Receptor Phosphorylation: Differential Synaptic Function in NRG1+/- Knock-Outs Compared with Wild-Type Mice. J Neurosci 27:4519–4529.
Blaukat A, Ivankovic-Dikic I, Grönroos E, Dolfi F, Tokiwa G, Vuori K, Dikic I (1999) Adaptor proteins Grb2 and Crk couple Pyk2 with activation of specific mitogen-activated protein kinase cascades. J Biol Chem 274:14893–14901.
Bond M, Sala-Newby GB, Newby AC (2004) Focal adhesion kinase (FAK)-dependent regulation of S-phase kinase-associated protein-2 (Skp-2) stability. A novel mechanism regulating smooth muscle cell proliferation. J Biol Chem 279:37304–37310.
Bonnette PC, Robinson BS, Silva JC, Stokes MP, Brosius AD, Baumann A, Buckbinder L (2010) Phosphoproteomic characterization of PYK2 signaling pathways involved in osteogenesis. J Proteomics 73:1306–1320.
Bouallegue A, Pandey NR, Srivastava AK (2009) CaMKII knockdown attenuates H2O2-induced phosphorylation of ERK1/2, PKB/Akt, and IGF-1R in vascular smooth muscle cells. Free Radic Biol Med 47:858–866.
Bourgin C, Murai KK, Richter M, Pasquale EB (2007) The EphA4 receptor regulates dendritic spine remodeling by affecting beta1-integrin signaling pathways. J Cell Biol 178:1295–1307.
Brami-Cherrier K, Gervasi N, Arsenieva D, Walkiewicz K, Boutterin M-C, Ortega A, Leonard PG, Seantier B, Gasmi L, Bouceba T, Kadare G, Girault J-A, Arold ST (2014) FAK dimerization controls its kinase-dependent functions at focal adhesions. EMBO J 33:356–370.
Brinson AE, Harding T, Diliberto PA, He Y, Li X, Hunter D, Herman B, Earp HS, Graves LM (1998) Regulation of a calcium-dependent tyrosine kinase in vascular smooth muscle cells by angiotensin II and platelet-derived growth factor. Dependence on calcium and the actin cytoskeleton. J Biol Chem 273:1711–1718.
Brody AH, Strittmatter SM (2018) Synaptotoxic Signaling by Amyloid Beta Oligomers in Alzheimer's Disease Through Prion Protein and mGluR5. In: Advances in pharmacology (San Diego, Calif.), pp 293–323.
Brown MC, Perrotta JA, Turner CE (1996) Identification of LIM3 as the principal determinant of paxillin focal adhesion localization and characterization of a novel motif on paxillin directing vinculin and focal adhesion kinase binding. J Cell Biol 135:1109–1123.
Bruce-Staskal PJ, Weidow CL, Gibson JJ, Bouton AH (2002) Cas, Fak and Pyk2 function in diverse signaling cascades to promote Yersinia uptake. J Cell Sci 115:2689–2700.
Brukman NG, Nuñez SY, Puga Molina LDC, Buffone MG, Darszon A, Cuasnicu PS, Da Ros VG (2019) Tyrosine phosphorylation signaling regulates Ca2+ entry by affecting intracellular pH during human sperm capacitation. J Cell Physiol 234:5276–5288.
Buckbinder L et al. (2007) Proline-rich tyrosine kinase 2 regulates osteoprogenitor cells and bone formation, and offers an anabolic treatment approach for osteoporosis. Proc Natl Acad Sci U S A 104:10619–10624.
Burdick AD, Ivnitski-Steele ID, Lauer FT, Burchiel SW (2006) PYK2 mediates anti-apoptotic AKT signaling in response to benzo[a]pyrene diol epoxide in mammary epithelial cells. Carcinogenesis 27:2331–2340.
Burgaya F, Menegon A, Menegoz M, Valtorta F, Girault JA (1995) Focal adhesion kinase in rat central nervous system. Eur J Neurosci 7:1810–1821.
Burgaya F, Toutant M, Studler JM, Costa A, Le Bert M, Gelman M, Girault JA (1997) Alternatively spliced focal adhesion kinase in rat brain with increased autophosphorylation activity. J Biol Chem 272:28720–28725.
Cao J, Chen Y, Fu J, Qian Y-W, Ren Y-B, Su B, Luo T, Dai R-Y, Huang L, Yan J-J, Wu M-C, Yan

Y-Q, Wang H-Y (2013) High expression of proline-rich tyrosine kinase 2 is associated with poor survival of hepatocellular carcinoma via regulating phosphatidylinositol 3-kinase/AKT pathway. Ann Surg Oncol 20 Suppl 3:S312-23.

Cao Z, George J, Baden DG, Murray TF (2007) Brevetoxin-induced phosphorylation of Pyk2 and Src in murine neocortical neurons involves distinct signaling pathways. Brain Res 1184:17–27.

Carragher NO, Frame MC (2004) Focal adhesion and actin dynamics: a place where kinases and proteases meet to promote invasion. Trends Cell Biol 14:241–249.

Castellani RJ, Lee H, Siedlak SL, Nunomura A, Hayashi T, Nakamura M, Zhu X, Perry G, Smith MA (2009) Reexamining Alzheimer's disease: evidence for a protective role for amyloid-beta protein precursor and amyloid-beta. Bissette G, ed. J Alzheimers Dis 18:447–452.

Cazaubon S, Chaverot N, Romero IA, Girault JA, Adamson P, Strosberg AD, Couraud PO (1997) Growth factor activity of endothelin-1 in primary astrocytes mediated by adhesion-dependent and -independent pathways. J Neurosci 17:6203–6212.

Ceccarelli DFJ, Song HK, Poy F, Schaller MD, Eck MJ (2006) Crystal Structure of the FERM Domain of Focal Adhesion Kinase. J Biol Chem 281:252–259.

Chacón MR, Navarro AI, Cuesto G, del Pino I, Scott R, Morales M, Rico B (2012) Focal adhesion kinase regulates actin nucleation and neuronal filopodia formation during axonal growth. Development 139:3200–3210.

Chan G, White CC, Winn PA, Cimpean M, Replogle JM, Glick LR, Cuerdon NE, Ryan KJ, Johnson KA, Schneider JA, Bennett DA, Chibnik LB, Sperling RA, Bradshaw EM, De Jager PL (2015) CD33 modulates TREM2: convergence of Alzheimer loci. Nat Neurosci 18:1556–1558.

Chan MWC, Arora PD, Bozavikov P, McCulloch CA (2009) FAK, PIP5KI and gelsolin cooperatively mediate force-induced expression of -smooth muscle actin. J Cell Sci 122:2769–2781.

Chauhan D, Pandey P, Hideshima T, Treon S, Raje N, Davies FE, Shima Y, Tai YT, Rosen S, Avraham S, Kharbanda S, Anderson KC (2000) SHP2 mediates the protective effect of interleukin-6 against dexamethasone-induced apoptosis in multiple myeloma cells. J Biol Chem 275:27845–27850.

Chellaiah MA, Kuppuswamy D, Lasky L, Linder S (2007) Phosphorylation of a Wiscott-Aldrich syndrome protein-associated signal complex is critical in osteoclast bone resorption. J Biol Chem 282:10104–10116.

Chen HC, Appeddu PA, Isoda H, Guan JL (1996) Phosphorylation of tyrosine 397 in focal adhesion kinase is required for binding phosphatidylinositol 3-kinase. J Biol Chem 271:26329–26334.

Chen HC, Appeddu PA, Parsons JT, Hildebrand JD, Schaller MD, Guan JL (1995) Interaction of focal adhesion kinase with cytoskeletal protein talin. J Biol Chem 270:16995–16999.

Chen J, Lu Y, Meng S, Han M-H, Lin C, Wang X (2009) alpha- and gamma-Protocadherins negatively regulate PYK2. J Biol Chem 284:2880–2890.

Cheung R, Ravyn V, Wang L, Ptasznik A, Collman RG (2008) Signaling mechanism of HIV-1 gp120 and virion-induced IL-1beta release in primary human macrophages. J Immunol 180:6675–6684.

Cheung SMS, Ostergaard HL (2016a) Pyk2 Controls Integrin-Dependent CTL Migration through Regulation of De-Adhesion. J Immunol 197:1945–1956.

Cheung SMS, Ostergaard HL (2016b) Pyk2 Controls Integrin-Dependent CTL Migration through Regulation of De-Adhesion. J Immunol 197:1945–1956.

Chieffi P, Barchi M, Di Agostino S, Rossi P, Tramontano D, Geremia R (2003) Prolin-rich tyrosine kinase 2 (PYK2) expression and localization in mouse testis. Mol Reprod Dev 65:330–335.

Chishti AH et al. (1998) The FERM domain: a unique module involved in the linkage of cytoplasmic proteins to the membrane. Trends Biochem Sci 23:281–282.

Choi JH, Yang Y-R, Lee SK, Kim I-S, Ha SH, Kim E-K, Bae YS, Ryu SH, Suh P-G (2007) Phospholipase C-gamma1 potentiates integrin-dependent cell spreading and migration through Pyk2/paxillin activation. Cell Signal 19:1784–1796.

Chung I-C, OuYang C-N, Yuan S-N, Li H-P, Chen J-T, Shieh H-R, Chen Y-J, Ojcius DM, Chu C-L, Yu J-S, Chang Y-S, Chen L-C (2016) Pyk2 activates the NLRP3 inflammasome by directly phosphorylating ASC and contributes to inflammasome-dependent peritonitis. Sci Rep 6:36214.

Cipolla L, Consonni A, Guidetti G, Canobbio I, Okigaki M, Falasca M, Ciraolo E, Hirsch E, Balduini C, Torti M (2013) The proline-rich tyrosine kinase Pyk2 regulates platelet integrin αIIbβ3 outside-in signaling. J Thromb Haemost 11:345–356.

Clarke M et al. (2013) Genome of Acanthamoeba castellanii highlights extensive lateral gene transfer and early evolution of tyrosine kinase signaling. Genome Biol 14:R11.

Cohen E, Paulsson JF, Blinder P, Burstyn-Cohen T, Du D, Estepa G, Adame A, Pham HM, Holzenberger M, Kelly JW, Masliah E, Dillin A (2009) Reduced IGF-1 Signaling Delays Age-Associated Proteotoxicity in Mice. Cell 139:1157–1169.

Combs CK, Johnson DE, Cannady SB, Lehman TM, Landreth GE (1999) Identification of microglial signal transduction pathways mediating a neurotoxic response to amyloidogenic fragments of beta-amyloid and prion proteins. J Neurosci 19:928–939.

Contet C, Goulding SP, Kuljis DA, Barth AL (2016) BK Channels in the Central Nervous System. In, pp 281–342.

Corsi J-M, Houbron C, Billuart P, Brunet I, Bouvrée K, Eichmann A, Girault J-A, Enslen H (2009) Autophosphorylation-independent and -dependent functions of focal adhesion kinase during development. J Biol Chem 284:34769–34776.

Corsi J-M, Rouer E, Girault J-A, Enslen H (2006) Organization and post-transcriptional processing of focal adhesion kinase gene. BMC Genomics 7:198.

Corvol J-C, Valjent E, Toutant M, Enslen H, Irinopoulou T, Lev S, Hervé D, Girault J-A (2005) Depolarization activates ERK and proline-rich tyrosine kinase 2 (PYK2) independently in different cellular compartments in hippocampal slices. J Biol Chem 280:660–668.

Corvol JC, Valjent E, Pascoli V, Robin A, Stipanovich A, Luedtke RR, Belluscio L, Girault JA, Hervé D (2007) Quantitative changes in Gαolf protein levels, but not D1 receptor, alter specifically acute responses to psychostimulants. Neuropsychopharmacology.

Crawford BD, Henry CA, Clason TA, Becker AL, Hille MB (2003) Activity and distribution of paxillin, focal adhesion kinase, and cadherin indicate cooperative roles during zebrafish morphogenesis. Mol Biol Cell 14:3065–3081.

Datta A, Bhasin N, Kim H, Ranjan M, Rider B, Abd Elmageed ZY, Mondal D, Agrawal KC, Abdel-Mageed AB (2015) Selective targeting of FAK-Pyk2 axis by alpha-naphthoflavone abrogates doxorubicin resistance in breast cancer cells. Cancer Lett 362:25–35.

Davidson D, Shi X, Zhong M-C, Rhee I, Veillette A (2010) The Phosphatase PTP-PEST Promotes Secondary T Cell Responses by Dephosphorylating the Protein Tyrosine Kinase Pyk2. Immunity 33:167–180.

Davidson D, Veillette A (2001) PTP-PEST, a scaffold protein tyrosine phosphatase, negatively regulates lymphocyte activation by targeting a unique set of substrates. EMBO J 20:3414–3426.

De Jager PL et al. (2014) Alzheimer's disease: early alterations in brain DNA methylation at ANK1, BIN1, RHBDF2 and other loci. Nat Neurosci 17:1156–1163.

de Pins B, Cifuentes-Díaz C, Farah AT, López-Molina L, Montalban E, Sancho-Balsells A, López A, Ginés S, Delgado-García JM, Alberch J, Gruart A, Girault J-A, Giralt A (2019) Conditional BDNF Delivery from Astrocytes Rescues Memory Deficits, Spine Density, and Synaptic Properties in the 5xFAD Mouse Model of Alzheimer Disease. J Neurosci 39:2441–2458.

Derkinderen P, Enslen H, Girault JA (1999) The ERK/MAP-kinases cascade in the nervous system. Neuroreport 10:R24-34.

Despeaux M, Chicanne G, Rouer E, De Toni-Costes F, Bertrand J, Mansat-De Mas V, Vergnolle N, Eaves C, Payrastre B, Girault J-A, Racaud-Sultan C (2012) Focal adhesion kinase splice variants maintain primitive acute myeloid leukemia cells through altered Wnt signaling. Stem Cells 30:1597–1610.

Dikic I, Dikic I, Schlessinger J (1998) Identification of a new Pyk2 isoform implicated in chemokine and antigen receptor signaling. J Biol Chem 273:14301–14308.

Dikic I, Tokiwa G, Lev S, Courtneidge SA, Schlessinger J (1996) A role for Pyk2 and Src in linking G-protein-coupled receptors with MAP kinase activation. Nature 383:547–550.

Ding L, Guo D, Homandberg GA (2009) Fibronectin fragments mediate matrix metalloproteinase upregulation and cartilage damage through proline rich tyrosine kinase 2, c-src, NF-κB and protein kinase Cδ. Osteoarthr Cartil 17:1385–1392.

Dorostkar MM, Zou C, Blazquez-Llorca L, Herms J (2015) Analyzing dendritic spine pathology in Alzheimer's disease: problems and opportunities. Acta Neuropathol 130:1–19.

Dourlen P et al. (2017) Functional screening of Alzheimer risk loci identifies PTK2B as an in vivo modulator and early marker of Tau pathology. Mol Psychiatry 22:874–883.

Du QS, Ren XR, Xie Y, Wang Q, Mei L, Xiong WC (2001) Inhibition of PYK2-induced actin cytoskeleton reorganization, PYK2 autophosphorylation and focal adhesion targeting by FAK. J Cell Sci 114:2977–2987.

Duan Y, Learoyd J, Meliton AY, Clay BS, Leff AR, Zhu X (2010) Inhibition of Pyk2 Blocks Airway Inflammation and Hyperresponsiveness in a Mouse Model of Asthma. Am J Respir Cell Mol Biol 42:491–497.

Duan Y, Learoyd J, Meliton AY, Leff AR, Zhu X (2012) Inhibition of Pyk2 blocks lung inflammation and injury in a mouse model of acute lung injury. Respir Res 13:4.

Duong LT, Lakkakorpi PT, Nakamura I, Machwate M, Nagy RM, Rodan GA (1998) PYK2 in osteoclasts is an adhesion kinase, localized in the sealing zone, activated by ligation of alpha(v)beta3 integrin, and phosphorylated by src kinase. J Clin Invest 102:881–892.

Duxbury M., Ito H, Zinner M., Ashley S., Whang E. (2004) Focal adhesion kinase gene silencing promotes anoikis and suppresses metastasis of human pancreatic adenocarcinoma cells. Surgery 135:555–562.

Dylla SJ, Deyle DR, Theunissen K, Padurean AM, Verfaillie CM (2004) Integrin engagement-induced inhibition of human myelopoiesis is mediated by proline-rich tyrosine kinase 2 gene products. Exp Hematol 32:365–374.

Edwards SD, Keep NH (2001) The 2.7 A crystal structure of the activated FERM domain of moesin: an analysis of structural changes on activation. Biochemistry 40:7061–7068.

Eleniste PP, Du L, Shivanna M, Bruzzaniti A (2012) Dynamin and PTP-PEST cooperatively regulate Pyk2 dephosphorylation in osteoclasts. Int J Biochem Cell Biol 44:790–800.

Eleniste PP, Patel V, Posritong S, Zero O, Largura H, Cheng Y-H, Himes ER, Hamilton M, Baughman J, Kacena MA, Bruzzaniti A (2016) Pyk2 and Megakaryocytes Regulate Osteoblast Differentiation and Migration Via Distinct and Overlapping Mechanisms. J Cell Biochem 117:1396–1406.

Evangelista V, Pamuklar Z, Piccoli A, Manarini S, Dell'elba G, Pecce R, Martelli N, Federico L, Rojas M, Berton G, Lowell CA, Totani L, Smyth SS (2007) Src family kinases mediate neutrophil adhesion to adherent platelets. Blood 109:2461–2469.

Fairclough SR, Chen Z, Kramer E, Zeng Q, Young S, Robertson HM, Begovic E, Richter DJ, Russ C, Westbrook MJ, Manning G, Lang BF, Haas B, Nusbaum C, King N (2013) Premetazoan genome evolution and the regulation of cell differentiation in the choanoflagellate Salpingoeca rosetta. Genome Biol 14:R15.

Faure C, Corvol J-C, Toutant M, Valjent E, Hvalby O, Jensen V, El Messari S, Corsi J-M, Kadaré G, Girault J-A (2007) Calcineurin is essential for depolarization-induced nuclear translocation and tyrosine phosphorylation of PYK2 in neurons. J Cell Sci 120:3034–3044.

Faure C, Ramos M, Girault J-A (2013) Pyk2 cytonuclear localization: mechanisms and regulation

by serine dephosphorylation. Cell Mol Life Sci 70:137–152.
Felsch JS, Cachero TG, Peralta EG (1998) Activation of protein tyrosine kinase PYK2 by the m1 muscarinic acetylcholine receptor. Proc Natl Acad Sci U S A 95:5051–5056.
Fiedorek FT, Kay ES (1995) Mapping of the focal adhesion kinase (Fadk) gene to mouse chromosome 15 and human chromosome 8. Mamm Genome 6:123–126.
Fisslthaler B, Loot AE, Mohamed A, Busse R, Fleming I (2008) Inhibition of endothelial nitric oxide synthase activity by proline-rich tyrosine kinase 2 in response to fluid shear stress and insulin. Circ Res 102:1520–1528.
Fitzgerald PJ, Pinard CR, Camp MC, Feyder M, Sah A, Bergstrom HC, Graybeal C, Liu Y, Schlüter OM, Grant SG, Singewald N, Xu W, Holmes A (2015) Durable fear memories require PSD-95. Mol Psychiatry 20:901–912.
Florio T, Casagrande S, Diana F, Bajetto A, Porcile C, Zona G, Thellung S, Arena S, Pattarozzi A, Corsaro A, Spaziante R, Robello M, Schettini G (2005) Chemokine Stromal Cell-Derived Factor 1 Induces Proliferation and Growth Hormone Release in GH4C1 Rat Pituitary Adenoma Cell Line through Multiple Intracellular Signals. Mol Pharmacol 69:539–546.
Fox GL, Rebay I, Hynes RO (1999) Expression of DFak56, a Drosophila homolog of vertebrate focal adhesion kinase, supports a role in cell migration in vivo. Proc Natl Acad Sci U S A 96:14978–14983.
Freeman WM, Brebner K, Lynch WJ, Patel KM, Robertson DJ, Roberts DCS, Vrana KE (2002) Changes in rat frontal cortex gene expression following chronic cocaine. Brain Res Mol Brain Res 104:11–20.
Freeman WM, Nader MA, Nader SH, Robertson DJ, Gioia L, Mitchell SM, Daunais JB, Porrino LJ, Friedman DP, Vrana KE (2001) Chronic cocaine-mediated changes in non-human primate nucleus accumbens gene expression. J Neurochem 77:542–549.
Fujimoto J, Sawamoto K, Okabe M, Takagi Y, Tezuka T, Yoshikawa S, Ryo H, Okano H, Yamamoto T (1999) Cloning and characterization of Dfak56, a homolog of focal adhesion kinase, in Drosophila melanogaster. J Biol Chem 274:29196–29201.
Fuortes M, Melchior M, Han H, Lyon GJ, Nathan C (1999) Role of the tyrosine kinase pyk2 in the integrin-dependent activation of human neutrophils by TNF. J Clin Invest 104:327–335.
Furuta Y, Ilić D, Kanazawa S, Takeda N, Yamamoto T, Aizawa S (1995) Mesodermal defect in late phase of gastrulation by a targeted mutation of focal adhesion kinase, FAK. Oncogene 11:1989–1995.
Ganju RK, Brubaker SA, Chernock RD, Avraham S, Groopman JE (2000) Beta-chemokine receptor CCR5 signals through SHP1, SHP2, and Syk. J Biol Chem 275:17263–17268.
Gao Y-Y, Zhang Z-H, Zhuang Z, Lu Y, Wu L-Y, Ye Z, Zhang X-S, Chen C-L, Li W, Hang C-H (2018) Recombinant milk fat globule-EGF factor-8 reduces apoptosis via integrin β3/FAK/PI3K/AKT signaling pathway in rats after traumatic brain injury. Cell Death Dis 9:845.
García MG, Toney SJ, Hille MB (2004) Focal adhesion kinase (FAK) expression and phosphorylation in sea urchin embryos. Gene Expr Patterns 4:223–234.
Garrett AM, Schreiner D, Lobas MA, Weiner JA (2012) γ-protocadherins control cortical dendrite arborization by regulating the activity of a FAK/PKC/MARCKS signaling pathway. Neuron 74:269–276.
Geng W, Ng KTP, Sun CKW, Yau WL, Liu XB, Cheng Q, Poon RTP, Lo CM, Man K, Fan ST (2011) The role of proline rich tyrosine kinase 2 (Pyk2) on cisplatin resistance in hepatocellular carcinoma. Maki CG, ed. PLoS One 6:e27362.
Genua M, Xu S-Q, Buraschi S, Peiper SC, Gomella LG, Belfiore A, Iozzo R V, Morrione A (2012) Proline-rich tyrosine kinase 2 (Pyk2) regulates IGF-I-induced cell motility and invasion of urothelial carcinoma cells. Andre F, ed. PLoS One 7:e40148.
Gil-Henn H, Destaing O, Sims NA, Aoki K, Alles N, Neff L, Sanjay A, Bruzzaniti A, De Camilli P, Baron R, Schlessinger J (2007) Defective microtubule-dependent podosome organization

in osteoclasts leads to increased bone density in Pyk2(-/-) mice. J Cell Biol 178:1053–1064.
Giralt A, Brito V, Chevy Q, Simonnet C, Otsu Y, Cifuentes-Díaz C, de Pins B, Coura R, Alberch J, Ginés S, Poncer J-C, Girault J-A (2017) Pyk2 modulates hippocampal excitatory synapses and contributes to cognitive deficits in a Huntington's disease model. Nat Commun 8:15592.
Giralt A, Coura R, Girault J-A (2016) Pyk2 is essential for astrocytes mobility following brain lesion. Glia 64:620–634.
Giralt A, de Pins B, Cifuentes-Díaz C, López-Molina L, Farah AT, Tible M, Deramecourt V, Arold ST, Ginés S, Hugon J, Girault J-A (2018) PTK2B/Pyk2 overexpression improves a mouse model of Alzheimer's disease. Exp Neurol 307:62–73.
Giralt A, Friedman HC, Caneda-Ferrón B, Urbán N, Moreno E, Rubio N, Blanco J, Peterson A, Canals JM, Alberch J (2010) BDNF regulation under GFAP promoter provides engineered astrocytes as a new approach for long-term protection in Huntington's disease. Gene Ther 17:1294–1308.
Girault JA, Costa A, Derkinderen P, Studler JM, Toutant M (1999a) FAK and PYK2/CAKbeta in the nervous system: a link between neuronal activity, plasticity and survival? Trends Neurosci 22:257–263.
Girault JA, Labesse G, Mornon JP, Callebaut I (1999b) The N-termini of FAK and JAKs contain divergent band 4.1 domains. Trends Biochem Sci 24:54–57.
Gluck SL (2004) Acid sensing in renal epithelial cells. J Clin Invest 114:1696–1699.
Golubovskaya V, Kaur A, Cance W (2004) Cloning and characterization of the promoter region of human focal adhesion kinase gene: nuclear factor kappa B and p53 binding sites. Biochim Biophys Acta - Gene Struct Expr 1678:111–125.
Golubovskaya VM, Cance WG (2011) FAK and p53 protein interactions. Anticancer Agents Med Chem 11:617–619.
Golubovskaya VM, Cance WG (2013) Targeting the p53 Pathway. Surg Oncol Clin N Am 22:747–764.
Gorski JA, Talley T, Qiu M, Puelles L, Rubenstein JLR, Jones KR (2002) Cortical excitatory neurons and glia, but not GABAergic neurons, are produced in the Emx1-expressing lineage. J Neurosci 22:6309–6314.
Grangeasse C, Nessler S, Mijakovic I (2012) Bacterial tyrosine kinases: evolution, biological function and structural insights. Philos Trans R Soc Lond B Biol Sci 367:2640–2655.
Grant SG, Karl KA, Kiebler MA, Kandel ER (1995) Focal adhesion kinase in the brain: novel subcellular localization and specific regulation by Fyn tyrosine kinase in mutant mice. Genes Dev 9:1909–1921.
Grossi M, Bhattachariya A, Nordström I, Turczyńska KM, Svensson D, Albinsson S, Nilsson B-O, Hellstrand P (2017) Pyk2 inhibition promotes contractile differentiation in arterial smooth muscle. J Cell Physiol 232:3088–3102.
Grove M, Brophy PJ (2014) FAK Is Required for Schwann Cell Spreading on Immature Basal Lamina to Coordinate the Radial Sorting of Peripheral Axons with Myelination. J Neurosci 34:13422–13434.
Guan JL, Trevithick JE, Hynes RO (1991) Fibronectin/integrin interaction induces tyrosine phosphorylation of a 120-kDa protein. Cell Regul 2:951–964.
Guignandon A, Boutahar N, Rattner A, Vico L, Lafage-Proust M-H (2006) Cyclic strain promotes shuttling of PYK2/Hic-5 complex from focal contacts in osteoblast-like cells. Biochem Biophys Res Commun 343:407–414.
Guinamard R, Okigaki M, Schlessinger J, Ravetch J V (2000) Absence of marginal zone B cells in Pyk-2-deficient mice defines their role in the humoral response. Nat Immunol 1:31–36.
Gupta A, Lee BS, Khadeer MA, Tang Z, Chellaiah M, Abu-Amer Y, Goldknopf J, Hruska KA (2003) Leupaxin is a critical adaptor protein in the adhesion zone of the osteoclast. J Bone Miner Res 18:669–685.
Haas LT, Salazar S V., Kostylev MA, Um JW, Kaufman AC, Strittmatter SM (2016) Metabotropic

glutamate receptor 5 couples cellular prion protein to intracellular signalling in Alzheimer's disease. Brain 139:526–546.
Haas LT, Salazar S V, Smith LM, Zhao HR, Cox TO, Herber CS, Degnan AP, Balakrishnan A, Macor JE, Albright CF, Strittmatter SM (2017) Silent Allosteric Modulation of mGluR5 Maintains Glutamate Signaling while Rescuing Alzheimer's Mouse Phenotypes. Cell Rep 20:76–88.
Haas LT, Strittmatter SM (2016) Oligomers of Amyloid β Prevent Physiological Activation of the Cellular Prion Protein-Metabotropic Glutamate Receptor 5 Complex by Glutamate in Alzheimer Disease. J Biol Chem 291:17112–17121.
Haglund K, Ivankovic-Dikic I, Shimokawa N, Kruh GD, Dikic I (2004) Recruitment of Pyk2 and Cbl to lipid rafts mediates signals important for actin reorganization in growing neurites. J Cell Sci 117:2557–2568.
Hall JE, Fu W, Schaller MD (2011) Focal adhesion kinase: exploring Fak structure to gain insight into function. Int Rev Cell Mol Biol 288:185–225.
Hamada K, Shimizu T, Matsui T, Tsukita S, Hakoshima T (2000) Structural basis of the membrane-targeting and unmasking mechanisms of the radixin FERM domain. EMBO J 19:4449–4462.
Hamada K, Shimizu T, Yonemura S, Tsukita S, Tsukita S, Hakoshima T (2003) Structural basis of adhesion-molecule recognition by ERM proteins revealed by the crystal structure of the radixin-ICAM-2 complex. EMBO J 22:502–514.
Han H, Fuortes M, Nathan C (2003) Critical role of the carboxyl terminus of proline-rich tyrosine kinase (Pyk2) in the activation of human neutrophils by tumor necrosis factor: separation of signals for the respiratory burst and degranulation. J Exp Med 197:63–75.
Han S, Mistry A, Chang JS, Cunningham D, Griffor M, Bonnette PC, Wang H, Chrunyk BA, Aspnes GE, Walker DP, Brosius AD, Buckbinder L (2009) Structural characterization of proline-rich tyrosine kinase 2 (PYK2) reveals a unique (DFG-out) conformation and enables inhibitor design. J Biol Chem 284:13193–13201.
Hanks SK, Calalb MB, Harper MC, Patel SK (1992) Focal adhesion protein-tyrosine kinase phosphorylated in response to cell attachment to fibronectin. Proc Natl Acad Sci U S A 89:8487–8491.
Hanks SK, Hunter T (1995) Protein kinases 6. The eukaryotic protein kinase superfamily: kinase (catalytic) domain structure and classification. FASEB J 9:576–596.
Hanks SK, Ryzhova L, Shin N-Y, Brábek J (2003) Focal adhesion kinase signaling activities and their implications in the control of cell survival and motility. Front Biosci 8:d982-96.
Hart DL, Heidkamp MC, Iyengar R, Vijayan K, Szotek EL, Barakat JA, Leya M, Henze M, Scrogin K, Henderson KK, Samarel AM (2008) CRNK gene transfer improves function and reverses the myosin heavy chain isoenzyme switch during post-myocardial infarction left ventricular remodeling. J Mol Cell Cardiol 45:93–105.
Hashido M, Hayashi K, Hirose K, Iino M (2006) Ca2+ lightning conveys cell-cell contact information inside the cells. EMBO Rep 7:1117–1123.
Hayashi I, Vuori K, Liddington RC (2002) The focal adhesion targeting (FAT) region of focal adhesion kinase is a four-helix bundle that binds paxillin. Nat Struct Biol 9:101–106.
Heidinger V, Manzerra P, Wang XQ, Strasser U, Yu S-P, Choi DW, Behrens MM (2002) Metabotropic glutamate receptor 1-induced upregulation of NMDA receptor current: mediation through the Pyk2/Src-family kinase pathway in cortical neurons. J Neurosci 22:5452–5461.
Henry CA, Crawford BD, Yan Y-L, Postlethwait J, Cooper MS, Hille MB (2001) Roles for Zebrafish Focal Adhesion Kinase in Notochord and Somite Morphogenesis. Dev Biol 240:474–487.
Hens MD, DeSimone DW (1995) Molecular analysis and developmental expression of the focal adhesion kinase pp125FAK in Xenopus laevis. Dev Biol 170:274–288.
Herzog H, Nicholl J, Hort YJ, Sutherland GR, Shine J (1996) Molecular cloning and assignment of

FAK2, a novel human focal adhesion kinase, to 8p11.2-p22 by nonisotopic in situ hybridization. Genomics 32:484–486.
Hildebrand JD, Schaller MD, Parsons JT (1993) Identification of sequences required for the efficient localization of the focal adhesion kinase, pp125FAK, to cellular focal adhesions. J Cell Biol 123:993–1005.
Hirao M, Sato N, Kondo T, Yonemura S, Monden M, Sasaki T, Takai Y, Tsukita S, Tsukita S (1996) Regulation mechanism of ERM (ezrin/radixin/moesin) protein/plasma membrane association: possible involvement of phosphatidylinositol turnover and Rho-dependent signaling pathway. J Cell Biol 135:37–51.
Hirschler-Laszkiewicz I, Chen S, Bao L, Wang J, Zhang X-Q, Shanmughapriya S, Keefer K, Madesh M, Cheung JY, Miller BA (2018) The Human Ion Channel TRPM2 Modulates Neuroblastoma Cell Survival and Mitochondrial Function through Pyk2, CREB, and MCU Activation. Am J Physiol Physiol:ajpcell.00098.2018.
Hoelzinger DB, Mariani L, Weis J, Woyke T, Berens TJ, McDonough WS, Sloan A, Coons SW, Berens ME (2005) Gene expression profile of glioblastoma multiforme invasive phenotype points to new therapeutic targets. Neoplasia 7:7–16.
Hooper C, Killick R, Lovestone S (2008) The GSK3 hypothesis of Alzheimer's disease. J Neurochem 104:1433–1439.
Horne WC, Sanjay A, Bruzzaniti A, Baron R (2005) The role(s) of Src kinase and Cbl proteins in the regulation of osteoclast differentiation and function. Immunol Rev 208:106–125.
Hsieh H-L, Yang S-H, Lee T-H, Fang J-Y, Lin C-F (2016) Evaluation of Anti-Inflammatory Effects of Helminthostachys zeylanica Extracts via Inhibiting Bradykinin-Induced MMP-9 Expression in Brain Astrocytes. Mol Neurobiol 53:5995–6005.
Hsin H, Kim MJ, Wang C-F, Sheng M (2010) Proline-Rich Tyrosine Kinase 2 Regulates Hippocampal Long-Term Depression. J Neurosci 30:11983–11993.
Huang C, Borchers CH, Schaller MD, Jacobson K (2004) Phosphorylation of paxillin by p38MAPK is involved in the neurite extension of PC-12 cells. J Cell Biol 164:593–602.
Huang Y, Lu W, Ali DW, Pelkey KA, Pitcher GM, Lu YM, Aoto H, Roder JC, Sasaki T, Salter MW, MacDonald JF (2001) CAKbeta/Pyk2 kinase is a signaling link for induction of long-term potentiation in CA1 hippocampus. Neuron 29:485–496.
Hudson KJ, Bliska JB, Bouton AH (2005) Distinct mechanisms of integrin binding by Yersinia pseudotuberculosis adhesins determine the phagocytic response of host macrophages. Cell Microbiol 7:1474–1489.
Hum JM, Day RN, Bidwell JP, Wang Y, Pavalko FM (2014) Mechanical Loading in Osteocytes Induces Formation of a Src/Pyk2/MBD2 Complex That Suppresses Anabolic Gene Expression Leipzig ND, ed. PLoS One 9:e97942.
Hunter T, Cooper JA (1981) Epidermal growth factor induces rapid tyrosine phosphorylation of proteins in A431 human tumor cells. Cell 24:741–752.
Hyun JH, Eom K, Lee K-H, Ho W-K, Lee S-H (2013) Activity-dependent downregulation of D-type K^+ channel subunit Kv1.2 in rat hippocampal CA3 pyramidal neurons. J Physiol 591:5525–5540.
Ilić D, Furuta Y, Kanazawa S, Takeda N, Sobue K, Nakatsuji N, Nomura S, Fujimoto J, Okada M, Yamamoto T, Aizawa S (1995) Reduced cell motility and enhanced focal adhesion contact formation in cells from FAK-deficient mice. Nature 377:539–544.
Ilic D, Furuta Y, Suda T, Atsumi T, Fujimoto J, Ikawa Y, Yamamoto T, Aizawa S (1995) Focal Adhesion Kinase Is Not Essential for in Vitro and in Vivo Differentiation of ES Cells. Biochem Biophys Res Commun 209:300–309.
Ivankovic-Dikic I, Grönroos E, Blaukat A, Barth B-U, Dikic I (2000) Pyk2 and FAK regulate neurite outgrowth induced by growth factors and integrins. Nat Cell Biol 2:574–581.
Jiao B, Liu X, Zhou L, Wang MH, Zhou Y, Xiao T, Zhang W, Sun R, Waye MMY, Tang B, Shen L (2015) Polygenic Analysis of Late-Onset Alzheimer's Disease from Mainland China Yan R,

ed. PLoS One 10:e0144898.
Jimenez JC, Su K, Goldberg AR, Luna VM, Biane JS, Ordek G, Zhou P, Ong SK, Wright MA, Zweifel L, Paninski L, Hen R, Kheirbek MA (2018) Anxiety Cells in a Hippocampal-Hypothalamic Circuit. Neuron 97:670–683.e6.
Jin J, Pawson T (2012) Modular evolution of phosphorylation-based signalling systems. Philos Trans R Soc Lond B Biol Sci 367:2540–2555.
Jones ML, Leonard JP (2005) PKC site mutations reveal differential modulation by insulin of NMDA receptors containing NR2A or NR2B subunits. J Neurochem 92:1431–1438.
Judelson HS, Ah-Fong AM V (2010) The kinome of Phytophthora infestans reveals oomycete-specific innovations and links to other taxonomic groups. BMC Genomics 11:700.
Kacena MA, Eleniste PP, Cheng Y-H, Huang S, Shivanna M, Meijome TE, Mayo LD, Bruzzaniti A (2012) Megakaryocytes Regulate Expression of Pyk2 Isoforms and Caspase-mediated Cleavage of Actin in Osteoblasts. J Biol Chem 287:17257–17268.
Kamboh MI et al. (2012) Genome-wide association study of Alzheimer's disease. Transl Psychiatry 2:e117–e117.
Kamen LA, Schlessinger J, Lowell CA (2011) Pyk2 is required for neutrophil degranulation and host defense responses to bacterial infection. J Immunol 186:1656–1665.
Kamihara Y, Takada K, Sato T, Kawano Y, Murase K, Arihara Y, Kikuchi S, Hayasaka N, Usami M, Iyama S, Miyanishi K, Sato Y, Kobune M, Kato J (2016) The iron chelator deferasirox induces apoptosis by targeting oncogenic Pyk2/β-catenin signaling in human multiple myeloma. Oncotarget 7:64330–64341.
Kaminari A, Giannakas N, Tzinia A, Tsilibary EC (2017) Overexpression of matrix metalloproteinase-9 (MMP-9) rescues insulin-mediated impairment in the 5XFAD model of Alzheimer's disease. Sci Rep 7:683.
Kanazawa S, Ilic D, Noumura T, Yamamoto T, Aizawa S (1995) Integrin Stimulation Decreases Tyrosine Phosphorylation and Activity of Focal Adhesion Kinase in Thymocytes. Biochem Biophys Res Commun 215:438–445.
Kang H, Welcher AA, Shelton D, Schuman EM (1997) Neurotrophins and time: different roles for TrkB signaling in hippocampal long-term potentiation. Neuron 19:653–664.
Katoh K (2017) Activation of Rho-kinase and focal adhesion kinase regulates the organization of stress fibers and focal adhesions in the central part of fibroblasts. PeerJ 5:e4063.
Katsumi A, Orr AW, Tzima E, Schwartz MA (2004) Integrins in Mechanotransduction. J Biol Chem 279:12001–12004.
Kaufman AC, Salazar S V., Haas LT, Yang J, Kostylev MA, Jeng AT, Robinson SA, Gunther EC, van Dyck CH, Nygaard HB, Strittmatter SM (2015) Fyn inhibition rescues established memory and synapse loss in Alzheimer mice. Ann Neurol 77:953–971.
Kedzierska K, Vardaxis NJ, Jaworowski A, Crowe SM (2001) FcgammaR-mediated phagocytosis by human macrophages involves Hck, Syk, and Pyk2 and is augmented by GM-CSF. J Leukoc Biol 70:322–328.
Keogh RJ, Houliston RA, Wheeler-Jones CPD (2002) Human endothelial Pyk2 is expressed in two isoforms and associates with paxillin and p130Cas. Biochem Biophys Res Commun 290:1470–1477.
Kerk D, Templeton G, Moorhead GBG (2008) Evolutionary radiation pattern of novel protein phosphatases revealed by analysis of protein data from the completely sequenced genomes of humans, green algae, and higher plants. Plant Physiol 146:351–367.
Kerstein PC, Patel KM, Gomez TM (2017) Calpain-Mediated Proteolysis of Talin and FAK Regulates Adhesion Dynamics Necessary for Axon Guidance. J Neurosci 37:1568–1580.
Kim S, Cipolla L, Guidetti G, Okigaki M, Jin J, Torti M, Kunapuli SP (2013) Distinct role of Pyk2 in mediating thromboxane generation downstream of both G12/13 and integrin αIIbβ3 in platelets. J Biol Chem 288:18194–18203.
King N (2004) The unicellular ancestry of animal development. Dev Cell 7:313–325.

King N et al. (2008) The genome of the choanoflagellate Monosiga brevicollis and the origin of metazoans. Nature 451:783–788.
King N, Carroll SB (2001) A receptor tyrosine kinase from choanoflagellates: molecular insights into early animal evolution. Proc Natl Acad Sci U S A 98:15032–15037.
King N, Hittinger CT, Carroll SB (2003) Evolution of key cell signaling and adhesion protein families predates animal origins. Science 301:361–363.
Kinoshita Y, Hunter RG, Gray JD, Mesias R, McEwen BS, Benson DL, Kohtz DS (2014) Role for NUP62 depletion and PYK2 redistribution in dendritic retraction resulting from chronic stress. Proc Natl Acad Sci U S A 111:16130–16135.
Kirchner J, Kam Z, Tzur G, Bershadsky AD, Geiger B (2003) Live-cell monitoring of tyrosine phosphorylation in focal adhesions following microtubule disruption. J Cell Sci 116:975–986.
Klaus A, Birchmeier W (2008) Wnt signalling and its impact on development and cancer. Nat Rev Cancer 8:387–398.
Köhler C, Dinekov M, Götz J (2013) Active glycogen synthase kinase-3 and tau pathology-related tyrosine phosphorylation in pR5 human tau transgenic mice. Neurobiol Aging 34:1369–1379.
Kohno T, Matsuda E, Sasaki H, Sasaki T (2008) Protein-tyrosine kinase CAKbeta/PYK2 is activated by binding Ca2+/calmodulin to FERM F2 alpha2 helix and thus forming its dimer. Biochem J 410:513–523.
Kuipers SD, Trentani A, Tiron A, Mao X, Kuhl D, Bramham CR (2016) BDNF-induced LTP is associated with rapid Arc/Arg3.1-dependent enhancement in adult hippocampal neurogenesis. Sci Rep 6:21222.
Kumar S, Avraham S, Bharti A, Goyal J, Pandey P, Kharbanda S (1999) Negative regulation of PYK2/related adhesion focal tyrosine kinase signal transduction by hematopoietic tyrosine phosphatase SHPTP1. J Biol Chem 274:30657–30663.
Kurup PK, Xu J, Videira RA, Ononenyi C, Baltazar G, Lombroso PJ, Nairn AC (2015) STEP $_{61}$ is a substrate of the E3 ligase parkin and is upregulated in Parkinson's disease. Proc Natl Acad Sci 112:1202–1207.
Lakkakorpi PT, Bett AJ, Lipfert L, Rodan GA, Duong LT (2003) PYK2 autophosphorylation, but not kinase activity, is necessary for adhesion-induced association with c-Src, osteoclast spreading, and bone resorption. J Biol Chem 278:11502–11512.
Lakkakorpi PT, Nakamura I, Nagy RM, Parsons JT, Rodan GA, Duong LT (1999) Stable association of PYK2 and p130(Cas) in osteoclasts and their co-localization in the sealing zone. J Biol Chem 274:4900–4907.
Lambert JC et al. (2013) Meta-analysis of 74,046 individuals identifies 11 new susceptibility loci for Alzheimer's disease. Nat Genet 45:1452–1458.
Lawson CD, Ridley AJ (2018) Rho GTPase signaling complexes in cell migration and invasion. J Cell Biol 217:447–457.
Lee G, Newman ST, Gard DL, Band H, Panchamoorthy G (1998) Tau interacts with src-family non-receptor tyrosine kinases. J Cell Sci 111 (Pt 21):3167–3177.
Lee G, Thangavel R, Sharma VM, Litersky JM, Bhaskar K, Fang SM, Do LH, Andreadis A, Van Hoesen G, Ksiezak-Reding H (2004) Phosphorylation of Tau by Fyn: Implications for Alzheimer's Disease. J Neurosci 24:2304–2312.
Lee S, Salazar S V., Cox TO, Strittmatter SM (2019) Pyk2 Signaling through Graf1 and RhoA GTPase Is Required for Amyloid-β Oligomer-Triggered Synapse Loss. J Neurosci 39:1910–1929.
Lev S, Hernandez J, Martinez R, Chen A, Plowman G, Schlessinger J (1999) Identification of a novel family of targets of PYK2 related to Drosophila retinal degeneration B (rdgB) protein. Mol Cell Biol 19:2278–2288.
Lev S, Moreno H, Martinez R, Canoll P, Peles E, Musacchio JM, Plowman GD, Rudy B, Schlessinger J (1995) Protein tyrosine kinase PYK2 involved in Ca(2+)-induced regulation of ion channel and MAP kinase functions. Nature 376:737–745.

Li C, Götz J (2018) Pyk2 is a Novel Tau Tyrosine Kinase that is Regulated by the Tyrosine Kinase Fyn. J Alzheimer's Dis:1–17.
Li J, Davidson D, Martins Souza C, Zhong M-C, Wu N, Park M, Muller WJ, Veillette A (2015) Loss of PTPN12 Stimulates Progression of ErbB2-Dependent Breast Cancer by Enhancing Cell Survival, Migration, and Epithelial-to-Mesenchymal Transition. Mol Cell Biol 35:4069–4082.
Li S, Sato S, Yang X, Preisig PA, Alpern RJ (2004a) Pyk2 activation is integral to acid stimulation of sodium/hydrogen exchanger 3. J Clin Invest 114:1782–1789.
Li W, Lee J, Vikis HG, Lee S-H, Liu G, Aurandt J, Shen T-L, Fearon ER, Guan J-L, Han M, Rao Y, Hong K, Guan K-L (2004b) Activation of FAK and Src are receptor-proximal events required for netrin signaling. Nat Neurosci 7:1213–1221.
Li X, Dy RC, Cance WG, Graves LM, Earp HS (1999) Interactions between two cytoskeleton-associated tyrosine kinases: calcium-dependent tyrosine kinase and focal adhesion tyrosine kinase. J Biol Chem 274:8917–8924.
Li Y-Q, Tan M-S, Wang H-F, Tan C-C, Zhang W, Zheng Z-J, Kong L-L, Wang Z-X, Tan L, Jiang T, Tan L, Yu J-T (2016) Common variant in PTK2B is associated with late-onset Alzheimer's disease: A replication study and meta-analyses. Neurosci Lett 621:83–87.
Lietha D, Cai X, Ceccarelli DFJ, Li Y, Schaller MD, Eck MJ (2007) Structural basis for the autoinhibition of focal adhesion kinase. Cell 129:1177–1187.
Lim S-T, Chen XL, Lim Y, Hanson DA, Vo T-T, Howerton K, Larocque N, Fisher SJ, Schlaepfer DD, Ilic D (2008a) Nuclear FAK promotes cell proliferation and survival through FERM-enhanced p53 degradation. Mol Cell 29:9–22.
Lim S-T, Miller NLG, Nam J-O, Chen XL, Lim Y, Schlaepfer DD (2010) Pyk2 Inhibition of p53 as an Adaptive and Intrinsic Mechanism Facilitating Cell Proliferation and Survival. J Biol Chem 285:1743–1753.
Lim Y, Lim S-T, Tomar A, Gardel M, Bernard-Trifilo JA, Chen XL, Uryu SA, Canete-Soler R, Zhai J, Lin H, Schlaepfer WW, Nalbant P, Bokoch G, Ilic D, Waterman-Storer C, Schlaepfer DD (2008b) PyK2 and FAK connections to p190Rho guanine nucleotide exchange factor regulate RhoA activity, focal adhesion formation, and cell motility. J Cell Biol 180:187–203.
Lim Y, Park H, Jeon J, Han I, Kim J, Jho E-H, Oh E-S (2007) Focal Adhesion Kinase Is Negatively Regulated by Phosphorylation at Tyrosine 407. J Biol Chem 282:10398–10404.
Lin C-F, Tsai C-C, Huang W-C, Wang C-Y, Tseng H-C, Wang Y, Kai J-I, Wang S-W, Cheng Y-L (2008) IFN-gamma synergizes with LPS to induce nitric oxide biosynthesis through glycogen synthase kinase-3-inhibited IL-10. J Cell Biochem 105:746–755.
Lin E, Tsai S-J, Kuo P-H, Liu Y-L, Yang AC, Kao C-F (2017) Association and interaction effects of Alzheimer’s disease-associated genes and lifestyle on cognitive aging in older adults in a Taiwanese population. Oncotarget 8.
Lin K, Wang D, Sadée W (2002) Serum response factor activation by muscarinic receptors via RhoA. Novel pathway specific to M1 subtype involving calmodulin, calcineurin, and Pyk2. J Biol Chem 277:40789–40798.
Lindberg RA, Quinn AM, Hunter T (1992) Dual-specificity protein kinases: will any hydroxyl do? Trends Biochem Sci 17:114–119.
Ling S, Sheng J-Z, Braun AP (2004) The calcium-dependent activity of large-conductance, calcium-activated K+ channels is enhanced by Pyk2- and Hck-induced tyrosine phosphorylation. Am J Physiol Cell Physiol 287:C698-706.
Liou C-J, Yang C-M, Lee T-H, Liu P-S, Hsieh H-L (2019) Neuroprotective Effects of Dehydroepiandrosterone Sulfate Through Inhibiting Expression of Matrix Metalloproteinase-9 from Bradykinin-Challenged Astroglia. Mol Neurobiol 56:736–747.
Lipinski CA, Loftus JC (2010) Targeting Pyk2 for therapeutic intervention. Expert Opin Ther Targets 14:95–108.
Lipinski CA, Tran NL, Bay C, Kloss J, McDonough WS, Beaudry C, Berens ME, Loftus JC (2003)

Differential role of proline-rich tyrosine kinase 2 and focal adhesion kinase in determining glioblastoma migration and proliferation. Mol Cancer Res 1:323–332.
Lipinski CA, Tran NL, Menashi E, Rohl C, Kloss J, Bay RC, Berens ME, Loftus JC (2005) The tyrosine kinase pyk2 promotes migration and invasion of glioma cells. Neoplasia 7:435–445.
Liu BA, Nash PD (2012) Evolution of SH2 domains and phosphotyrosine signalling networks. Philos Trans R Soc B Biol Sci 367:2556–2573.
Liu BA, Shah E, Jablonowski K, Stergachis A, Engelmann B, Nash PD (2011) The SH2 domain-containing proteins in 21 species establish the provenance and scope of phosphotyrosine signaling in eukaryotes. Sci Signal 4:ra83.
Liu G, Guibao CD, Zheng J (2002) Structural insight into the mechanisms of targeting and signaling of focal adhesion kinase. Mol Cell Biol 22:2751–2760.
Liu Y, Hou X-Y, Zhang G-Y, Xu T-L (2003) L-type voltage-gated calcium channel attends regulation of tyrosine phosphorylation of NMDA receptor subunit 2A induced by transient brain ischemia. Brain Res 972:142–148.
Liu Y, Zhang G-Y, Yan J-Z, Xu T-L (2005) Suppression of Pyk2 attenuated the increased tyrosine phosphorylation of NMDA receptor subunit 2A after brain ischemia in rat hippocampus. Neurosci Lett 379:55–58.
Llewellyn RA, Thomas KS, Gutknecht MF, Bouton AH (2017) The nonreceptor protein tyrosine kinase Pyk2 promotes the turnover of monocytes at steady state. J Leukoc Biol 102:1069–1080.
Lobo M, Zachary I (2000) Nuclear localization and apoptotic regulation of an amino-terminal domain focal adhesion kinase fragment in endothelial cells. Biochem Biophys Res Commun 276:1068–1074.
Loftus JC, Yang Z, Kloss J, Dhruv H, Tran NL, Riggs DL (2013) A Novel Interaction between Pyk2 and MAP4K4 Is Integrated with Glioma Cell Migration. J Signal Transduct 2013:956580.
Lombroso PJ, Ogren M, Kurup P, Nairn AC (2016) Molecular underpinnings of neurodegenerative disorders: striatal-enriched protein tyrosine phosphatase signaling and synaptic plasticity. F1000Research 5:2932.
Loving HS, Underbakke ES (2019) Conformational Dynamics of FERM-Mediated Autoinhibition in Pyk2 Tyrosine Kinase. Biochemistry:acs.biochem.9b00541.
Lulo J, Yuzawa S, Schlessinger J (2009) Crystal structures of free and ligand-bound focal adhesion targeting domain of Pyk2. Biochem Biophys Res Commun 383:347–352.
Lynch G, Rex CS, Chen LY, Gall CM (2008) The substrates of memory: Defects, treatments, and enhancement. Eur J Pharmacol 585:2–13.
Lyons PD, Dunty JM, Schaefer EM, Schaller MD (2001) Inhibition of the catalytic activity of cell adhesion kinase beta by protein-tyrosine phosphatase-PEST-mediated dephosphorylation. J Biol Chem 276:24422–24431.
Ma J, Zhang G-Y, Liu Y, Yan J-Z, Hao Z-B (2004) Lithium suppressed Tyr-402 phosphorylation of proline-rich tyrosine kinase (Pyk2) and interactions of Pyk2 and PSD-95 with NR2A in rat hippocampus following cerebral ischemia. Neurosci Res 49:357–362.
Mandelkow E-M, Mandelkow E (2012) Biochemistry and Cell Biology of Tau Protein in Neurofibrillary Degeneration. Cold Spring Harb Perspect Med 2:a006247–a006247.
Manning G, Plowman GD, Hunter T, Sudarsanam S (2002a) Evolution of protein kinase signaling from yeast to man. Trends Biochem Sci 27:514–520.
Manning G, Whyte DB, Martinez R, Hunter T, Sudarsanam S (2002b) The Protein Kinase Complement of the Human Genome. Science (80-) 298:1912–1934.
Manning G, Young SL, Miller WT, Zhai Y (2008) The protist, Monosiga brevicollis, has a tyrosine kinase signaling network more elaborate and diverse than found in any known metazoan. Proc Natl Acad Sci U S A 105:9674–9679.
Manzur MJ, Aguilera MO, Kotler ML, Berón W, Ciuffo GM (2018) Focal adhesion kinase, RhoA,

and p38 mitogen-activated protein kinase modulates apoptosis mediated by angiotensin II AT 2 receptors. J Cell Biochem.

Marhaba R, Mary F, Pelassy C, Stanescu AT, Aussel C, Breittmayer JP (1996) Tyrphostin A9 inhibits calcium release-dependent phosphorylations and calcium entry via calcium release-activated channel in Jurkat T cells. J Immunol 157:1468–1473.

Mariappan MM, Prasad S, D'Silva K, Cedillo E, Sataranatarajan K, Barnes JL, Choudhury GG, Kasinath BS (2014) Activation of glycogen synthase kinase 3β ameliorates diabetes-induced kidney injury. J Biol Chem 289:35363–35375.

Massa A, Casagrande S, Bajetto A, Porcile C, Barbieri F, Thellung S, Arena S, Pattarozzi A, Gatti M, Corsaro A, Robello M, Schettini G, Florio T (2006) SDF-1 controls pituitary cell proliferation through the activation of ERK1/2 and the Ca2+-dependent, cytosolic tyrosine kinase Pyk2. Ann N Y Acad Sci 1090:385–398.

Matsui A, Okigaki M, Amano K, Adachi Y, Jin D, Takai S, Yamashita T, Kawashima S, Kurihara T, Miyazaki M, Tateishi K, Matsunaga S, Katsume A, Honshou S, Takahashi T, Matoba S, Kusaba T, Tatsumi T, Matsubara H (2007) Central role of calcium-dependent tyrosine kinase PYK2 in endothelial nitric oxide synthase-mediated angiogenic response and vascular function. Circulation 116:1041–1051.

Matsuya M, Sasaki H, Aoto H, Mitaka T, Nagura K, Ohba T, Ishino M, Takahashi S, Suzuki R, Sasaki T (1998) Cell adhesion kinase beta forms a complex with a new member, Hic-5, of proteins localized at focal adhesions. J Biol Chem 273:1003–1014.

Meirson T, Samson A, Gil-Henn H (2017) An in silico high-throughput screen identifies potential selective inhibitors for the non-receptor tyrosine kinase Pyk2. Drug Des Devel Ther Volume 11:1535–1557.

Melendez J, Turner C, Avraham H, Steinberg SF, Schaefer E, Sussman MA (2004) Cardiomyocyte apoptosis triggered by RAFTK/pyk2 via Src kinase is antagonized by paxillin. J Biol Chem 279:53516–53523.

Menegon A, Burgaya F, Baudot P, Dunlap DD, Girault JA, Valtorta F (1999) FAK+ and PYK2/CAKbeta, two related tyrosine kinases highly expressed in the central nervous system: similarities and differences in the expression pattern. Eur J Neurosci 11:3777–3788.

Miao L, Xin X, Xin H, Shen X, Zhu Y-Z (2016) Hydrogen Sulfide Recruits Macrophage Migration by Integrin β1-Src-FAK/Pyk2-Rac Pathway in Myocardial Infarction. Sci Rep 6:22363.

Mierke CT, Fischer T, Puder S, Kunschmann T, Soetje B, Ziegler WH (2017) Focal adhesion kinase activity is required for actomyosin contractility-based invasion of cells into dense 3D matrices. Sci Rep 7:42780.

Miller BA, Wang J, Song J, Zhang X, Hirschler Laszkiewicz I, Shanmughapriya S, Tomar D, Rajan S, Feldman AM, Madesh M, Sheu S, Cheung JY (2019) Trpm2 enhances physiological bioenergetics and protects against pathological oxidative cardiac injury: Role of Pyk2 phosphorylation. J Cell Physiol 234:15048–15060.

Miller WT (2012) Tyrosine kinase signaling and the emergence of multicellularity. Biochim Biophys Acta - Mol Cell Res 1823:1053–1057.

Mills RD, Mita M, Nakagawa J, Shoji M, Sutherland C, Walsh MP (2015) A Role for the Tyrosine Kinase Pyk2 in Depolarization-induced Contraction of Vascular Smooth Muscle. J Biol Chem 290:8677–8692.

Milnerwood AJ, Cummings DM, Dallérac GM, Brown JY, Vatsavayai SC, Hirst MC, Rezaie P, Murphy KPSJ (2006) Early development of aberrant synaptic plasticity in a mouse model of Huntington's disease. Hum Mol Genet 15:1690–1703.

Miranda-Saavedra D, Barton GJ (2007) Classification and functional annotation of eukaryotic protein kinases. Proteins Struct Funct Bioinforma 68:893–914.

Mitchell RM, Tajuddin N, Campbell EM, Neafsey EJ, Collins MA (2016) Ethanol preconditioning of rat cerebellar cultures targets NMDA receptors to the synapse and enhances peroxiredoxin 2 expression. Brain Res 1642:163–169.

Mitra SK, Hanson DA, Schlaepfer DD (2005) Focal adhesion kinase: in command and control of cell motility. Nat Rev Mol Cell Biol 6:56–68.
Miyazaki T, Takaoka A, Nogueira L, Dikic I, Fujii H, Tsujino S, Mitani Y, Maeda M, Schlessinger J, Taniguchi T (1998) Pyk2 is a downstream mediator of the IL-2 receptor-coupled Jak signaling pathway. Genes Dev 12:770–775.
Mohanty P, Bhatnagar S (2018) Structure of focal adhesion kinase in healthy heart versus pathological cardiac hypertrophy: A modeling and simulation study. J Mol Graph Model 80:15–24.
Montalban E, Al-Massadi O, Sancho-Balsells A, Brito V, de Pins B, Alberch J, Ginés S, Girault J-A, Giralt A (2019) Pyk2 in the amygdala modulates chronic stress sequelae via PSD-95-related micro-structural changes. Transl Psychiatry 9:3.
Mucke L, Selkoe DJ (2012) Neurotoxicity of amyloid β-protein: synaptic and network dysfunction. Cold Spring Harb Perspect Med 2:a006338.
Murphy KP, Carter RJ, Lione LA, Mangiarini L, Mahal A, Bates GP, Dunnett SB, Morton AJ (2000) Abnormal synaptic plasticity and impaired spatial cognition in mice transgenic for exon 1 of the human Huntington's disease mutation. J Neurosci 20:5115–5123.
Myers MG, Grammer TC, Wang LM, Sun XJ, Pierce JH, Blenis J, White MF (1994) Insulin receptor substrate-1 mediates phosphatidylinositol 3'-kinase and p70S6k signaling during insulin, insulin-like growth factor-1, and interleukin-4 stimulation. J Biol Chem 269:28783–28789.
Nakagawa-Yagi Y, Choi DK, Ogane N, Shimada S, Seya M, Momoi T, Ito T, Sakaki Y (2001) Discovery of a novel compound: insight into mechanisms for acrylamide-induced axonopathy and colchicine-induced apoptotic neuronal cell death. Brain Res 909:8–19.
Naser R, Aldehaiman A, Díaz-Galicia E, Arold S (2018) Endogenous Control Mechanisms of FAK and PYK2 and Their Relevance to Cancer Development. Cancers (Basel) 10:196.
Nesti E, Everill B, Morielli AD (2004) Endocytosis as a mechanism for tyrosine kinase-dependent suppression of a voltage-gated potassium channel. Mol Biol Cell 15:4073–4088.
Nettiksimmons J, Tranah G, Evans DS, Yokoyama JS, Yaffe K (2016) Gene-based aggregate SNP associations between candidate AD genes and cognitive decline. Age (Omaha) 38:41.
Oddo S, Caccamo A, Shepherd JD, Murphy MP, Golde TE, Kayed R, Metherate R, Mattson MP, Akbari Y, LaFerla FM (2003) Triple-transgenic model of Alzheimer's disease with plaques and tangles: intracellular Abeta and synaptic dysfunction. Neuron 39:409–421.
Ohba T, Ishino M, Aoto H, Sasaki T (1998) Interaction of two proline-rich sequences of cell adhesion kinase beta with SH3 domains of p130Cas-related proteins and a GTPase-activating protein, Graf. Biochem J 330 (Pt 3):1249–1254.
Ohmori T, Yatomi Y, Asazuma N, Satoh K, Ozaki Y (1999) Suppression of protein kinase C is associated with inhibition of PYK2 tyrosine phosphorylation and enhancement of PYK2 interaction with Src in thrombin-activated platelets. Thromb Res 93:291–298.
Ohtsu H, Mifune M, Frank GD, Saito S, Inagami T, Kim-Mitsuyama S, Takuwa Y, Sasaki T, Rothstein JD, Suzuki H, Nakashima H, Woolfolk EA, Motley ED, Eguchi S (2005) Signal-crosstalk between Rho/ROCK and c-Jun NH2-terminal kinase mediates migration of vascular smooth muscle cells stimulated by angiotensin II. Arterioscler Thromb Vasc Biol 25:1831–1836.
Okbay A et al. (2016) Genetic variants associated with subjective well-being, depressive symptoms, and neuroticism identified through genome-wide analyses. Nat Genet 48:624–633.
Okenwa C, Kumar A, Rego D, Konarski Y, Nilchi L, Wright K, Kozlowski M (2013) SHP-1-Pyk2-Src protein complex and p38 MAPK pathways independently regulate IL-10 production in lipopolysaccharide-stimulated macrophages. J Immunol 191:2589–2603.
Okigaki M, Davis C, Falasca M, Harroch S, Felsenfeld DP, Sheetz MP, Schlessinger J (2003) Pyk2 regulates multiple signaling events crucial for macrophage morphology and migration. Proc Natl Acad Sci 100:10740–10745.
Okitsu-Sakurayama S, Higa-Nakamine S, Torihara H, Takahashi H, Higashiyama S, Yamamoto H

(2019) Activation of Pyk2 by CaM kinase II in cultured hypothalamic neurons and gonadotroph cells. J Cell Physiol 234:6865–6875.
Oppermann FS, Gnad F, Olsen J V, Hornberger R, Greff Z, Kéri G, Mann M, Daub H (2009) Large-scale proteomics analysis of the human kinome. Mol Cell Proteomics 8:1751–1764.
Orr AW, Murphy-Ullrich JE (2004) Regulation of endothelial cell function BY FAK and PYK2. Front Biosci 9:1254–1266.
Ossovskaya V, Lim S-T, Ota N, Schlaepfer DD, Ilic D (2008) FAK nuclear export signal sequences. FEBS Lett 582:2402–2406.
Otero K, Turnbull IR, Poliani PL, Vermi W, Cerutti E, Aoshi T, Tassi I, Takai T, Stanley SL, Miller M, Shaw AS, Colonna M (2009) Macrophage colony-stimulating factor induces the proliferation and survival of macrophages via a pathway involving DAP12 and beta-catenin. Nat Immunol 10:734–743.
Owen KA, Abshire MY, Tilghman RW, Casanova JE, Bouton AH (2011) FAK regulates intestinal epithelial cell survival and proliferation during mucosal wound healing. Dalmasso G, ed. PLoS One 6:e23123.
Owen KA, Thomas KS, Bouton AH (2007) The differential expression of Yersinia pseudotuberculosis adhesins determines the requirement for FAK and/or Pyk2 during bacterial phagocytosis by macrophages. Cell Microbiol 9:596–609.
Palmer RH, Fessler LI, Edeen PT, Madigan SJ, McKeown M, Hunter T (1999) DFak56 is a novel Drosophila melanogaster focal adhesion kinase. J Biol Chem 274:35621–35629.
Palumbo GA, Yarom N, Gazit A, Sandalon Z, Baniyash M, Kleinberger-Doron N, Levitzki A, Ben-Yehuda D (1997) The tryphostin AG17 induces apoptosis and inhibition of cdk2 activity in a lymphoma cell line that overexpresses bcl-2. Cancer Res 57:2434–2439.
Pandey P, Avraham S, Kumar S, Nakazawa A, Place A, Ghanem L, Rana A, Kumar V, Majumder PK, Avraham H, Davis RJ, Kharbanda S (1999) Activation of p38 mitogen-activated protein kinase by PYK2/related adhesion focal tyrosine kinase-dependent mechanism. J Biol Chem 274:10140–10144.
Paone C, Rodrigues N, Ittner E, Santos C, Buntru A, Hauck CR (2016) The Tyrosine Kinase Pyk2 Contributes to Complement-Mediated Phagocytosis in Murine Macrophages. J Innate Immun 8:437–451.
Park S-Y, Avraham H, Avraham S (2000) Characterization of the Tyrosine Kinases RAFTK/Pyk2 and FAK in Nerve Growth Factor-induced Neuronal Differentiation. J Biol Chem 275:19768–19777.
Park S-Y, Avraham HK, Avraham S (2004) RAFTK/Pyk2 activation is mediated by trans-acting autophosphorylation in a Src-independent manner. J Biol Chem 279:33315–33322.
Park S-Y, Li H, Avraham S (2007) RAFTK/Pyk2 regulates EGF-induced PC12 cell spreading and movement. Cell Signal 19:289–300.
Parsons JT (2003) Focal adhesion kinase: the first ten years. J Cell Sci 116:1409–1416.
Parsons MP, Kang R, Buren C, Dau A, Southwell AL, Doty CN, Sanders SS, Hayden MR, Raymond LA (2014) Bidirectional control of postsynaptic density-95 (PSD-95) clustering by Huntingtin. J Biol Chem 289:3518–3528.
Pearson MA, Reczek D, Bretscher A, Karplus PA (2000) Structure of the ERM protein moesin reveals the FERM domain fold masked by an extended actin binding tail domain. Cell 101:259–270.
Picascia A, Stanzione R, Chieffi P, Kisslinger A, Dikic I, Tramontano D (2002) Proline-rich tyrosine kinase 2 regulates proliferation and differentiation of prostate cells. Mol Cell Endocrinol 186:81–87.
Pincus D, Letunic I, Bork P, Lim WA (2008) Evolution of the phospho-tyrosine signaling machinery in premetazoan lineages. Proc Natl Acad Sci U S A 105:9680–9684.
Plotkin LI, Manolagas SC, Bellido T (2007) Glucocorticoids Induce Osteocyte Apoptosis by Blocking Focal Adhesion Kinase-mediated Survival. J Biol Chem 282:24120–24130.

Polis B, Gil-Henn H (2019) Commentary on Giralt et al.: PTK2B/Pyk2 overexpression improves a mouse model of Alzheimer's disease. Exp Neurol 311:313–317.
Posritong S, Flores Chavez R, Chu T-M, Bruzzaniti A (2019) A Pyk2 inhibitor incorporated into a PEGDA-gelatin hydrogel promotes osteoblast activity and mineral deposition. Biomed Mater.
Posritong S, Hong JM, Eleniste PP, McIntyre PW, Wu JL, Himes ER, Patel V, Kacena MA, Bruzzaniti A (2018) Pyk2 deficiency potentiates osteoblast differentiation and mineralizing activity in response to estrogen or raloxifene. Mol Cell Endocrinol 474:35–47.
Preisig PA (2007) The acid-activated signaling pathway: starting with Pyk2 and ending with increased NHE3 activity. Kidney Int 72:1324–1329.
Raab M, Lu Y, Kohler K, Smith X, Strebhardt K, Rudd CE (2017) LFA-1 activates focal adhesion kinases FAK1/PYK2 to generate LAT-GRB2-SKAP1 complexes that terminate T-cell conjugate formation. Nat Commun 8:16001.
Ren XD, Kiosses WB, Sieg DJ, Otey CA, Schlaepfer DD, Schwartz MA (2000) Focal adhesion kinase suppresses Rho activity to promote focal adhesion turnover. J Cell Sci 113 (Pt 20):3673–3678.
Renaudin A, Lehmann M, Girault J, McKerracher L (1999) Organization of point contacts in neuronal growth cones. J Neurosci Res 55:458–471.
Rhee I, Davidson D, Souza CM, Vacher J, Veillette A (2013) Macrophage Fusion Is Controlled by the Cytoplasmic Protein Tyrosine Phosphatase PTP-PEST/PTPN12. Mol Cell Biol 33:2458–2469.
Rhee I, Zhong M-C, Reizis B, Cheong C, Veillette A (2014) Control of Dendritic Cell Migration, T Cell-Dependent Immunity, and Autoimmunity by Protein Tyrosine Phosphatase PTPN12 Expressed in Dendritic Cells. Mol Cell Biol 34:888–899.
Richter DJ, King N (2013) The Genomic and Cellular Foundations of Animal Origins. Annu Rev Genet 47:509–537.
Rico B, Beggs HE, Schahin-Reed D, Kimes N, Schmidt A, Reichardt LF (2004) Control of axonal branching and synapse formation by focal adhesion kinase. Nat Neurosci 7:1059–1069.
Riggs D, Yang Z, Kloss J, Loftus JC (2011) The Pyk2 FERM regulates Pyk2 complex formation and phosphorylation. Cell Signal 23:288–296.
Roberts WG et al. (2008) Antitumor Activity and Pharmacology of a Selective Focal Adhesion Kinase Inhibitor, PF-562,271. Cancer Res 68:1935–1944.
Robinet C, Pellerin L (2011) Brain-derived neurotrophic factor enhances the hippocampal expression of key postsynaptic proteins in vivo including the monocarboxylate transporter MCT2. Neuroscience 192:155–163.
Roelle S, Grosse R, Buech T, Chubanov V, Gudermann T (2008) Essential role of Pyk2 and Src kinase activation in neuropeptide-induced proliferation of small cell lung cancer cells. Oncogene 27:1737–1748.
Rolls A, Avidan H, Cahalon L, Schori H, Bakalash S, Litvak V, Lev S, Lider O, Schwartz M (2004) A disaccharide derived from chondroitin sulphate proteoglycan promotes central nervous system repair in rats and mice. Eur J Neurosci 20:1973–1983.
Rolón-Reyes K, Kucheryavykh Y V., Cubano LA, Inyushin M, Skatchkov SN, Eaton MJ, Harrison JK, Kucheryavykh LY (2015) Microglia Activate Migration of Glioma Cells through a Pyk2 Intracellular Pathway Castro MG, ed. PLoS One 10:e0131059.
Sahu SN, Nunez S, Bai G, Gupta A (2007) Interaction of Pyk2 and PTP-PEST with leupaxin in prostate cancer cells. Am J Physiol Physiol 292:C2288–C2296.
Saitoh K, Tsuchiya T, Kashiwakura J-I, Muromoto R, Kitai Y, Sekine Y, Oritani K, Matsuda T (2017) STAP-2 interacts with Pyk2 and enhances Pyk2 activity in T-cells. Biochem Biophys Res Commun 488:81–87.
Salazar S V., Cox TO, Lee S, Brody AH, Chyung AS, Haas LT, Strittmatter SM (2019) Alzheimer's Disease Risk Factor Pyk2 Mediates Amyloid-β-Induced Synaptic Dysfunction and Loss. J

Neurosci 39:758–772.
Salter MW, Kalia L V. (2004) Src kinases: a hub for NMDA receptor regulation. Nat Rev Neurosci 5:317–328.
Sasaki H, Nagura K, Ishino M, Tobioka H, Kotani K, Sasaki T (1995) Cloning and characterization of cell adhesion kinase beta, a novel protein-tyrosine kinase of the focal adhesion kinase subfamily. J Biol Chem 270:21206–21219.
Sastry SK, Burridge K (2000) Focal adhesions: a nexus for intracellular signaling and cytoskeletal dynamics. Exp Cell Res 261:25–36.
Sayas CL, Ariaens A, Ponsioen B, Moolenaar WH (2006) GSK-3 is activated by the tyrosine kinase Pyk2 during LPA1-mediated neurite retraction. Mol Biol Cell 17:1834–1844.
Schaap P et al. (2015) The Physarum polycephalum Genome Reveals Extensive Use of Prokaryotic Two-Component and Metazoan-Type Tyrosine Kinase Signaling. Genome Biol Evol 8:109–125.
Schaller MD (2008) Calcium-dependent Pyk2 activation: a role for calmodulin? Biochem J 410:e3–e4.
Schaller MD (2010) Cellular functions of FAK kinases: insight into molecular mechanisms and novel functions. J Cell Sci 123:1007–1013.
Schaller MD, Borgman CA, Cobb BS, Vines RR, Reynolds AB, Parsons JT (1992) pp125FAK a structurally distinctive protein-tyrosine kinase associated with focal adhesions. Proc Natl Acad Sci U S A 89:5192–5196.
Schaller MD, Hildebrand JD, Shannon JD, Fox JW, Vines RR, Parsons JT (1994) Autophosphorylation of the focal adhesion kinase, pp125FAK, directs SH2-dependent binding of pp60src. Mol Cell Biol 14:1680–1688.
Schindler EM, Baumgartner M, Gribben EM, Li L, Efimova T (2007) The Role of Proline-Rich Protein Tyrosine Kinase 2 in Differentiation-Dependent Signaling in Human Epidermal Keratinocytes. J Invest Dermatol 127:1094–1106.
Schlaepfer DD, Hauck CR, Sieg DJ (1999) Signaling through focal adhesion kinase. Prog Biophys Mol Biol 71:435–478.
Schlaepfer DD, Hunter T (1996) Evidence for in vivo phosphorylation of the Grb2 SH2-domain binding site on focal adhesion kinase by Src-family protein-tyrosine kinases. Mol Cell Biol 16:5623–5633.
Schlaepfer DD, Mitra SK (2004) Multiple connections link FAK to cell motility and invasion. Curr Opin Genet Dev 14:92–101.
Seabold GK, Burette A, Lim IA, Weinberg RJ, Hell JW (2003) Interaction of the tyrosine kinase Pyk2 with the N-methyl-D-aspartate receptor complex via the Src homology 3 domains of PSD-95 and SAP102. J Biol Chem 278:15040–15048.
Sebé-Pedrós A, Peña MI, Capella-Gutiérrez S, Antó M, Gabaldón T, Ruiz-Trillo I, Sabidó E (2016) High-Throughput Proteomics Reveals the Unicellular Roots of Animal Phosphosignaling and Cell Differentiation. Dev Cell 39:186–197.
Sebe-Pedros A, Roger AJ, Lang FB, King N, Ruiz-Trillo I (2010) Ancient origin of the integrin-mediated adhesion and signaling machinery. Proc Natl Acad Sci 107:10142–10147.
Segawa Y, Suga H, Iwabe N, Oneyama C, Akagi T, Miyata T, Okada M (2006) Functional development of Src tyrosine kinases during evolution from a unicellular ancestor to multicellular animals. Proc Natl Acad Sci U S A 103:12021–12026.
Shalchian-Tabrizi K, Minge MA, Espelund M, Orr R, Ruden T, Jakobsen KS, Cavalier-Smith T (2008) Multigene Phylogeny of Choanozoa and the Origin of Animals Aramayo R, ed. PLoS One 3:e2098.
Shankar GM, Li S, Mehta TH, Garcia-Munoz A, Shepardson NE, Smith I, Brett FM, Farrell MA, Rowan MJ, Lemere CA, Regan CM, Walsh DM, Sabatini BL, Selkoe DJ (2008) Amyloid-beta protein dimers isolated directly from Alzheimer's brains impair synaptic plasticity and memory. Nat Med 14:837–842.

Sharma D, Kinsey WH (2013) PYK2: a calcium-sensitive protein tyrosine kinase activated in response to fertilization of the zebrafish oocyte. Dev Biol 373:130–140.
Sharma R, Colarusso P, Zhang H, Stevens KM, Patel KD (2015) FRNK negatively regulates IL-4-mediated inflammation. J Cell Sci 128:695–705.
Shattil SJ, Brugge JS (1991) Protein tyrosine phosphorylation and the adhesive functions of platelets. Curr Opin Cell Biol 3:869–879.
Sheehan TP, Neve RL, Duman RS, Russell DS (2003) Antidepressant effect of the calcium-activated tyrosine kinase Pyk2 in the lateral septum. Biol Psychiatry 54:540–551.
Shen T, Guo Q (2018) Role of Pyk2 in Human Cancers. Med Sci Monit 24:8172–8182.
Shen Y, Schaller MD (1999) Focal Adhesion Targeting: The Critical Determinant of FAK Regulation and Substrate Phosphorylation Brugge J, ed. Mol Biol Cell 10:2507–2518.
Shiu S-H, Li W-H (2004) Origins, Lineage-Specific Expansions, and Multiple Losses of Tyrosine Kinases in Eukaryotes. Mol Biol Evol 21:828–840.
Shyu J-F, Shih C, Tseng C-Y, Lin C-H, Sun D-T, Liu H-T, Tsung H-C, Chen T-H, Lu R-B (2007) Calcitonin induces podosome disassembly and detachment of osteoclasts by modulating Pyk2 and Src activities. Bone 40:1329–1342.
Siciliano JC, Toutant M, Derkinderen P, Sasaki T, Girault JA (1996) Differential regulation of proline-rich tyrosine kinase 2/cell adhesion kinase beta (PYK2/CAKbeta) and pp125(FAK) by glutamate and depolarization in rat hippocampus. J Biol Chem 271:28942–28946.
Sieg DJ, Ilić D, Jones KC, Damsky CH, Hunter T, Schlaepfer DD (1998) Pyk2 and Src-family protein-tyrosine kinases compensate for the loss of FAK in fibronectin-stimulated signaling events but Pyk2 does not fully function to enhance FAK- cell migration. EMBO J 17:5933–5947.
Siegrist SE, Doe CQ (2007) Microtubule-induced cortical cell polarity. Genes Dev 21:483–496.
Small DH, Klaver DW, Foa L (2010) Presenilins and the gamma-secretase: still a complex problem. Mol Brain 3:7.
Soe NN, Ishida T, Ishida M, Sawano M, Abe K, Miho N, Chayama K, Kihara Y, Yoshizumi M (2009) Nifedipine interferes with migration of vascular smooth muscle cells via inhibition of Pyk2-Src axis. J Atheroscler Thromb 16:230–238.
Song C, Zhang Y, Parsons CG, Liu YF (2003) Expression of polyglutamine-expanded huntingtin induces tyrosine phosphorylation of N-methyl-D-aspartate receptors. J Biol Chem 278:33364–33369.
Song J-H, Yu J-T, Tan L (2015) Brain-Derived Neurotrophic Factor in Alzheimer's Disease: Risk, Mechanisms, and Therapy. Mol Neurobiol 52:1477–1493.
Soni D, Regmi SC, Wang D-M, DebRoy A, Zhao Y-Y, Vogel SM, Malik AB, Tiruppathi C (2017) Pyk2 phosphorylation of VE-PTP downstream of STIM1-induced Ca2+ entry regulates disassembly of adherens junctions. Am J Physiol Lung Cell Mol Physiol 312:L1003–L1017.
Sorokin A, Kozlowski P, Graves L, Philip A (2001) Protein-tyrosine kinase Pyk2 mediates endothelin-induced p38 MAPK activation in glomerular mesangial cells. J Biol Chem 276:21521–21528.
Souza CM, Davidson D, Rhee I, Gratton J-P, Davis EC, Veillette A (2012) The Phosphatase PTP-PEST/PTPN12 Regulates Endothelial Cell Migration and Adhesion, but Not Permeability, and Controls Vascular Development and Embryonic Viability. J Biol Chem 287:43180–43190.
Stanzione R, Picascia A, Chieffi P, Imbimbo C, Palmieri A, Mirone V, Staibano S, Franco R, De Rosa G, Schlessinger J, Tramontano D (2001) Variations of proline-rich kinase Pyk2 expression correlate with prostate cancer progression. Lab Invest 81:51–59.
Stokes JB, Adair SJ, Slack-Davis JK, Walters DM, Tilghman RW, Hershey ED, Lowrey B, Thomas KS, Bouton AH, Hwang RF, Stelow EB, Parsons JT, Bauer TW (2011) Inhibition of focal adhesion kinase by PF-562,271 inhibits the growth and metastasis of pancreatic cancer concomitant with altering the tumor microenvironment. Mol Cancer Ther 10:2135–2145.
Strappazzon F, Torch S, Trioulier Y, Blot B, Sadoul R, Verna J-M (2007) Survival response-linked

Pyk2 activation during potassium depletion-induced apoptosis of cerebellar granule neurons. Mol Cell Neurosci 34:355–365.
Suga H, Dacre M, de Mendoza A, Shalchian-Tabrizi K, Manning G, Ruiz-Trillo I (2012) Genomic survey of premetazoans shows deep conservation of cytoplasmic tyrosine kinases and multiple radiations of receptor tyrosine kinases. Sci Signal 5:ra35.
Suga H, Sasaki G, Kuma K-I, Nishiyori H, Hirose N, Su Z-H, Iwabe N, Miyata T (2008) Ancient divergence of animal protein tyrosine kinase genes demonstrated by a gene family tree including choanoflagellate genes. FEBS Lett 582:815–818.
Suga H, Torruella G, Burger G, Brown MW, Ruiz-Trillo I (2014) Earliest Holozoan Expansion of Phosphotyrosine Signaling. Mol Biol Evol 31:517–528.
Sun CK, Man K, Ng KT, Ho JW, Lim ZX, Cheng Q, Lo C-M, Poon RT, Fan S-T (2008) Proline-rich tyrosine kinase 2 (Pyk2) promotes proliferation and invasiveness of hepatocellular carcinoma cells through c-Src/ERK activation. Carcinogenesis 29:2096–2105.
Sun CK, Ng KT, Lim ZX, Cheng Q, Lo CM, Poon RT, Man K, Wong N, Fan ST (2011) Proline-rich tyrosine kinase 2 (Pyk2) promotes cell motility of hepatocellular carcinoma through induction of epithelial to mesenchymal transition. Dent P, ed. PLoS One 6:e18878.
Sun Y, Savanenin A, Reddy PH, Liu YF (2001) Polyglutamine-expanded Huntingtin Promotes Sensitization of *N* -Methyl-d-aspartate Receptors via Post-synaptic Density 95. J Biol Chem 276:24713–24718.
Suo L, Lu H, Ying G, Capecchi MR, Wu Q (2012) Protocadherin clusters and cell adhesion kinase regulate dendrite complexity through Rho GTPase. J Mol Cell Biol 4:362–376.
Tachibana K, Sato T, D'Avirro N, Morimoto C (1995) Direct association of pp125FAK with paxillin, the focal adhesion-targeting mechanism of pp125FAK. J Exp Med 182:1089–1099.
Takahashi T, Yamashita H, Nagano Y, Nakamura T, Ohmori H, Avraham H, Avraham S, Yasuda M, Matsumoto M (2003) Identification and characterization of a novel Pyk2/related adhesion focal tyrosine kinase-associated protein that inhibits alpha-synuclein phosphorylation. J Biol Chem 278:42225–42233.
Tang H, Zhao ZJ, Landon EJ, Inagami T (2000) Regulation of calcium-sensitive tyrosine kinase Pyk2 by angiotensin II in endothelial cells. Roles of Yes tyrosine kinase and tyrosine phosphatase SHP-2. J Biol Chem 275:8389–8396.
Thomas JW, Ellis B, Boerner RJ, Knight WB, White GC, Schaller MD (1998) SH2- and SH3-mediated interactions between focal adhesion kinase and Src. J Biol Chem 273:577–583.
Tian D, Litvak V, Lev S (2000) Cerebral ischemia and seizures induce tyrosine phosphorylation of PYK2 in neurons and microglial cells. J Neurosci 20:6478–6487.
Tilghman RW, Slack-Davis JK, Sergina N, Martin KH, Iwanicki M, Hershey ED, Beggs HE, Reichardt LF, Parsons JT (2005) Focal adhesion kinase is required for the spatial organization of the leading edge in migrating cells. J Cell Sci 118:2613–2623.
Tong K, Wang Y, Su Z (2017) Phosphotyrosine signalling and the origin of animal multicellularity. Proc R Soc B Biol Sci 284:20170681.
Tse KWK, Dang-Lawson M, Lee RL, Vong D, Bulic A, Buckbinder L, Gold MR (2009) B cell receptor-induced phosphorylation of Pyk2 and focal adhesion kinase involves integrins and the Rap GTPases and is required for B cell spreading. J Biol Chem 284:22865–22877.
Tse KWK, Lin KBL, Dang-Lawson M, Guzman-Perez A, Aspnes GE, Buckbinder L, Gold MR (2012) Small molecule inhibitors of the Pyk2 and FAK kinases modulate chemoattractant-induced migration, adhesion and Akt activation in follicular and marginal zone B cells. Cell Immunol 275:47–54.
Ueda H, Abbi S, Zheng C, Guan JL (2000) Suppression of Pyk2 kinase and cellular activities by FIP200. J Cell Biol 149:423–430.
Uzoma I, Hu J, Cox E, Xia S, Zhou J, Rho H-S, Guzzo C, Paul C, Ajala O, Goodwin CR, Jeong J, Moore C, Zhang H, Meluh P, Blackshaw S, Matunis M, Qian J, Zhu H (2018) Global Identification of Small Ubiquitin-related Modifier (SUMO) Substrates Reveals Crosstalk

between SUMOylation and Phosphorylation Promotes Cell Migration. Mol Cell Proteomics 17:871–888.
Välimäki E, Miettinen JJ, Lietzén N, Matikainen S, Nyman TA (2013) Monosodium urate activates Src/Pyk2/PI3 kinase and cathepsin dependent unconventional protein secretion from human primary macrophages. Mol Cell Proteomics 12:749–763.
van Buul JD, Anthony EC, Fernandez-Borja M, Burridge K, Hordijk PL (2005) Proline-rich tyrosine kinase 2 (Pyk2) mediates vascular endothelial-cadherin-based cell-cell adhesion by regulating beta-catenin tyrosine phosphorylation. J Biol Chem 280:21129–21136.
van der Horst EH, Weber I, Ullrich A (2005) Tyrosine phosphorylation of PYK2 mediates heregulin-induced glioma invasion: novel heregulin/HER3-stimulated signaling pathway in glioma. Int J cancer 113:689–698.
Vanarotti MS, Finkelstein DB, Guibao CD, Nourse A, Miller DJ, Zheng JJ (2016) Structural Basis for the Interaction between Pyk2-FAT Domain and Leupaxin LD Repeats. Biochemistry 55:1332–1345.
Vanarotti MS, Miller DJ, Guibao CD, Nourse A, Zheng JJ (2014) Structural and mechanistic insights into the interaction between Pyk2 and paxillin LD motifs. J Mol Biol 426:3985–4001.
von Bohlen und Halbach O, von Bohlen und Halbach V (2018) BDNF effects on dendritic spine morphology and hippocampal function. Cell Tissue Res 373:729–741.
von Sengbusch A, Gassmann P, Fisch KM, Enns A, Nicolson GL, Haier J (2005) Focal Adhesion Kinase Regulates Metastatic Adhesion of Carcinoma Cells within Liver Sinusoids. Am J Pathol 166:585–596.
Walker DP et al. (2008) Trifluoromethylpyrimidine-based inhibitors of proline-rich tyrosine kinase 2 (PYK2): structure-activity relationships and strategies for the elimination of reactive metabolite formation. Bioorg Med Chem Lett 18:6071–6077.
Walkiewicz KW, Girault J-A, Arold ST (2015) How to awaken your nanomachines: Site-specific activation of focal adhesion kinases through ligand interactions. Prog Biophys Mol Biol 119:60–71.
Walsh DM, Klyubin I, Fadeeva J V., Cullen WK, Anwyl R, Wolfe MS, Rowan MJ, Selkoe DJ (2002) Naturally secreted oligomers of amyloid β protein potently inhibit hippocampal long-term potentiation in vivo. Nature 416:535–539.
Wang L, Learoyd J, Duan Y, Leff AR, Zhu X (2010a) Hematopoietic Pyk2 regulates migration of differentiated HL-60 cells. J Inflamm (Lond) 7:26.
Wang Q, Xie Y, Du Q-S, Wu X-J, Feng X, Mei L, McDonald JM, Xiong W-C (2003) Regulation of the formation of osteoclastic actin rings by proline-rich tyrosine kinase 2 interacting with gelsolin. J Cell Biol 160:565–575.
Wang X, Bao X, Pal R, Agbas A, Michaelis EK (2010b) Transcriptomic responses in mouse brain exposed to chronic excess of the neurotransmitter glutamate. BMC Genomics 11:360.
Wang X, Lopez OL, Sweet RA, Becker JT, DeKosky ST, Barmada MM, Demirci FY, Kamboh MI (2014) Genetic Determinants of Disease Progression in Alzheimer's Disease. J Alzheimer's Dis 43:649–655.
Wang X, Yang Y, Guo X, Sampson ER, Hsu C-L, Tsai M-Y, Yeh S, Wu G, Guo Y, Chang C (2002) Suppression of Androgen Receptor Transactivation by Pyk2 via Interaction and Phosphorylation of the ARA55 Coregulator. J Biol Chem 277:15426–15431.
Wang Z, Brecher P (2001) Salicylate Inhibits Phosphorylation of the Nonreceptor Tyrosine Kinases, Proline-Rich Tyrosine Kinase 2 and c-Src. Hypertens (Dallas, Tex 1979) 37:148–153.
Watson JM, Harding TW, Golubovskaya V, Morris JS, Hunter D, Li X, Haskill JS, Earp HS (2001) Inhibition of the calcium-dependent tyrosine kinase (CADTK) blocks monocyte spreading and motility. J Biol Chem 276:3536–3542.
Weis SM, Lim S-T, Lutu-Fuga KM, Barnes LA, Chen XL, Göthert JR, Shen T-L, Guan J-L, Schlaepfer DD, Cheresh DA (2008) Compensatory role for Pyk2 during angiogenesis in adult

mice lacking endothelial cell FAK. J Cell Biol 181:43–50.
Weiss A, Littman DR (1994) Signal transduction by lymphocyte antigen receptors. Cell 76:263–274.
Weng H-R, Gao M, Maixner DW (2014) Glycogen synthase kinase 3 beta regulates glial glutamate transporter protein expression in the spinal dorsal horn in rats with neuropathic pain. Exp Neurol 252:18–27.
Wheeler GL, Miranda-Saavedra D, Barton GJ (2008) Genome analysis of the unicellular green alga Chlamydomonas reinhardtii Indicates an ancient evolutionary origin for key pattern recognition and cell-signaling protein families. Genetics 179:193–197.
Whitney GS, Chan PY, Blake J, Cosand WL, Neubauer MG, Aruffo A, Kanner SB (1993) Human T and B lymphocytes express a structurally conserved focal adhesion kinase, pp125FAK. DNA Cell Biol 12:823–830.
Wiese H, Gelis L, Wiese S, Reichenbach C, Jovancevic N, Osterloh M, Meyer HE, Neuhaus EM, Hatt HH, Radziwill G, Warscheid B (2015) Quantitative phosphoproteomics reveals the protein tyrosine kinase Pyk2 as a central effector of olfactory receptor signaling in prostate cancer cells. Biochim Biophys Acta 1854:632–640.
Wiiger MT, Prydz H (2004) The epidermal growth factor receptor (EGFR) and proline rich tyrosine kinase 2 (PYK2) are involved in tissue factor dependent factor VIIa signalling in HaCaT cells. Thromb Haemost 92:13–22.
Williams LM, Ridley AJ (2000) Lipopolysaccharide induces actin reorganization and tyrosine phosphorylation of Pyk2 and paxillin in monocytes and macrophages. J Immunol 164:2028–2036.
Williams MR, Markey JC, Doczi MA, Morielli AD (2007) An essential role for cortactin in the modulation of the potassium channel Kv1.2. Proc Natl Acad Sci U S A 104:17412–17417.
Williamson R, Scales T, Clark BR, Gibb G, Reynolds CH, Kellie S, Bird IN, Varndell IM, Sheppard PW, Everall I, Anderton BH (2002) Rapid tyrosine phosphorylation of neuronal proteins including tau and focal adhesion kinase in response to amyloid-beta peptide exposure: involvement of Src family protein kinases. J Neurosci 22:10–20.
Willuhn I, Steiner H (2009) Skill-memory consolidation in the striatum: critical for late but not early long-term memory and stabilized by cocaine. Behav Brain Res 199:103–107.
Wilson LJ, Linley A, Hammond DE, Hood FE, Coulson JM, MacEwan DJ, Ross SJ, Slupsky JR, Smith PD, Eyers PA, Prior IA (2018) New Perspectives, Opportunities, and Challenges in Exploring the Human Protein Kinome. Cancer Res 78:15–29.
Wu X, Suetsugu S, Cooper LA, Takenawa T, Guan J-L (2004) Focal Adhesion Kinase Regulation of N-WASP Subcellular Localization and Function. J Biol Chem 279:9565–9576.
Xia W, Shen Y, Xie H, Zheng S (2006) Involvement of endoplasmic reticulum in hepatitis B virus replication. Virus Res 121:116–121.
Xiang X, Huang W, Haile CN, Kosten TA (2011) Hippocampal GluR1 associates with behavior in the elevated plus maze and shows sex differences. Behav Brain Res 222:326–331.
Xie Z, Sanada K, Samuels BA, Shih H, Tsai LH (2003) Serine 732 phosphorylation of FAK by Cdk5 is important for microtubule organization, nuclear movement, and neuronal migration. Cell 114:469–482.
Xiong W, Parsons JT (1997) Induction of apoptosis after expression of PYK2, a tyrosine kinase structurally related to focal adhesion kinase. J Cell Biol 139:529–539.
Xiong WC, Macklem M, Parsons JT (1998) Expression and characterization of splice variants of PYK2, a focal adhesion kinase-related protein. J Cell Sci 111 (Pt 14):1981–1991.
Xu C-S, Wang Z-F, Huang X-D, Dai L-M, Cao C-J, Li Z-Q (2015) Involvement of ROS-alpha v beta 3 integrin-FAK/Pyk2 in the inhibitory effect of melatonin on U251 glioma cell migration and invasion under hypoxia. J Transl Med 13:95.
Xu J et al. (2014) Inhibitor of the tyrosine phosphatase STEP reverses cognitive deficits in a mouse model of Alzheimer's disease. Khosla C, ed. PLoS Biol 12:e1001923.

Xu J, Kurup P, Azkona G, Baguley TD, Saavedra A, Nairn AC, Ellman JA, Pérez-Navarro E, Lombroso PJ (2016) Down-regulation of BDNF in cell and animal models increases striatal-enriched protein tyrosine phosphatase 61 (STEP $_{61}$) levels. J Neurochem 136:285–294.

Xu J, Kurup P, Bartos JA, Patriarchi T, Hell JW, Lombroso PJ (2012) Striatal-enriched Protein-tyrosine Phosphatase (STEP) Regulates Pyk2 Kinase Activity. J Biol Chem 287:20942–20956.

Yamamoto S, Shimizu S, Kiyonaka S, Takahashi N, Wajima T, Hara Y, Negoro T, Hiroi T, Kiuchi Y, Okada T, Kaneko S, Lange I, Fleig A, Penner R, Nishi M, Takeshima H, Mori Y (2008) TRPM2-mediated Ca2+influx induces chemokine production in monocytes that aggravates inflammatory neutrophil infiltration. Nat Med 14:738–747.

Yan X-L, Liu D-H, Zhang G-L, Hu S-Q, Chen Y-G, Xu T (2015) S-Nitrosylation of proline-rich tyrosine kinase 2 involves its activation induced by oxygen–glucose deprivation. Neurosci Lett 597:90–96.

Yan Z, Feng J, Fienberg AA, Greengard P (1999) D(2) dopamine receptors induce mitogen-activated protein kinase and cAMP response element-binding protein phosphorylation in neurons. Proc Natl Acad Sci U S A 96:11607–11612.

Yang S, Roselli F, Patchev A V, Yu S, Almeida OFX (2013) Non-receptor-tyrosine kinases integrate fast glucocorticoid signaling in hippocampal neurons. J Biol Chem 288:23725–23739.

Yi XP, Wang X, Gerdes AM, Li F (2003) Subcellular redistribution of focal adhesion kinase and its related nonkinase in hypertrophic myocardium. Hypertens (Dallas, Tex 1979) 41:1317–1323.

Ying Z, Giachini FRC, Tostes RC, Webb RC (2009) Salicylates dilate blood vessels through inhibiting PYK2-mediated RhoA/Rho-kinase activation. Cardiovasc Res 83:155–162.

Yoshii A, Constantine-Paton M (2007) BDNF induces transport of PSD-95 to dendrites through PI3K-AKT signaling after NMDA receptor activation. Nat Neurosci 10:702–711.

Yoshii A, Constantine-Paton M (2014) Postsynaptic localization of PSD-95 is regulated by all three pathways downstream of TrkB signaling. Front Synaptic Neurosci 6:6.

You K, Huang Y, Zhang M-C, Hao J (2015) Control and prevention of myocardial fibrosis using Pyk2-related non-kinase. Int J Clin Exp Med 8:18284–18292.

Yu H, Li X, Marchetto GS, Dy R, Hunter D, Calvo B, Dawson TL, Wilm M, Anderegg RJ, Graves LM, Earp HS (1996) Activation of a novel calcium-dependent protein-tyrosine kinase. Correlation with c-Jun N-terminal kinase but not mitogen-activated protein kinase activation. J Biol Chem 271:29993–29998.

Yu XM, Askalan R, Keil GJ, Salter MW (1997) NMDA channel regulation by channel-associated protein tyrosine kinase Src. Science 275:674–678.

Yue Y, Li Z-N, Fang Q-G, Zhang X, Yang L-L, Sun C-F, Liu F-Y (2015) The role of Pyk2 in the CCR7-mediated regulation of metastasis and viability in squamous cell carcinoma of the head and neck cells in vivo and in vitro. Oncol Rep 34:3280–3287.

Yuki D, Sugiura Y, Zaima N, Akatsu H, Takei S, Yao I, Maesako M, Kinoshita A, Yamamoto T, Kon R, Sugiyama K, Setou M (2014) DHA-PC and PSD-95 decrease after loss of synaptophysin and before neuronal loss in patients with Alzheimer's disease. Sci Rep 4:7130.

Zacchia M, Tian X, Zona E, Alpern RJ, Preisig PA (2018) Acid Stimulation of the Citrate Transporter NaDC-1 Requires Pyk2 and ERK1/2 Signaling Pathways. J Am Soc Nephrol 29:1720–1730.

Zachary I (1997) Focal adhesion kinase. Int J Biochem Cell Biol 29:929–934.

Zaidel-Bar R, Ballestrem C, Kam Z, Geiger B (2003) Early molecular events in the assembly of matrix adhesions at the leading edge of migrating cells. J Cell Sci 116:4605–4613.

Zalewska T, Bielawski A, Stanaszek L, Wieczerzak K, Ziemka-Nałęcz M, Nalepa I (2016) Imipramine administration induces changes in the phosphorylation of FAK and PYK2 and modulates signaling pathways related to their activity. Biochim Biophys Acta - Gen Subj 1860:424–433.

Zhang C, Qiu HE, Krafft GA, Klein WL (1996) A beta peptide enhances focal adhesion

kinase/Fyn association in a rat CNS nerve cell line. Neurosci Lett 211:187–190.
Zhang S, Guo D, Jiang L, Zhang Q, Qiu X, Wang E (2008a) SOCS3 inhibiting migration of A549 cells correlates with PYK2 signaling in vitro. BMC Cancer 8:150.
Zhang S, Qiu X, Gu Y, Wang E (2008b) Up-regulation of proline-rich tyrosine kinase 2 in non-small cell lung cancer. Lung Cancer 62:295–301.
Zhang X, Wright C V, Hanks SK (1995) Cloning of a Xenopus laevis cDNA encoding focal adhesion kinase (FAK) and expression during early development. Gene 160:219–222.
Zhang Y et al. (2014) Pyk2 promotes tumor progression in multiple myeloma. Blood 124:2675–2686.
Zhao C, Du C-P, Peng Y, Xu Z, Sun C-C, Liu Y, Hou X-Y (2015) The upregulation of NR2A-containing N-methyl-D-aspartate receptor function by tyrosine phosphorylation of postsynaptic density 95 via facilitating Src/proline-rich tyrosine kinase 2 activation. Mol Neurobiol 51:500–511.
Zhao J, Bian ZC, Yee K, Chen BPC, Chien S, Guan J-L (2003) Identification of transcription factor KLF8 as a downstream target of focal adhesion kinase in its regulation of cyclin D1 and cell cycle progression. Mol Cell 11:1503–1515.
Zhao JH, Reiske H, Guan JL (1998) Regulation of the cell cycle by focal adhesion kinase. J Cell Biol 143:1997–2008.
Zhao M, Finlay D, Zharkikh I, Vuori K (2016) Novel Role of Src in Priming Pyk2 Phosphorylation. Buday L, ed. PLoS One 11:e0149231.
Zhao T, Bokoch GM (2005) Critical role of proline-rich tyrosine kinase 2 in reversion of the adhesion-mediated suppression of reactive oxygen species generation by human neutrophils. J Immunol 174:8049–8055.
Zheng C, Xing Z, Bian ZC, Guo C, Akbay A, Warner L, Guan JL (1998) Differential regulation of Pyk2 and focal adhesion kinase (FAK). The C-terminal domain of FAK confers response to cell adhesion. J Biol Chem 273:2384–2389.
Zhu X, Bao Y, Guo Y, Yang W (2018) Proline-Rich Protein Tyrosine Kinase 2 in Inflammation and Cancer. Cancers (Basel) 10:139.
Zhu X, Boetticher E, Wang L, Duan Y, Learoyd J, Leff AR (2008) Proline-rich tyrosine kinase 2 regulates spreading and migration of eosinophils after beta2-integrin adhesion. Am J Respir Cell Mol Biol 39:263–269.
Zrihan-Licht S, Avraham S, Jiang S, Fu Y, Avraham HK (2004) Coupling of RAFTK/Pyk2 kinase with c-Abl and their role in the migration of breast cancer cells. Int J Oncol 24:153–159.
Zwick E, Wallasch C, Daub H, Ullrich A (1999) Distinct calcium-dependent pathways of epidermal growth factor receptor transactivation and PYK2 tyrosine phosphorylation in PC12 cells. J Biol Chem 274:20989–20996.

Abstract

In metazoans, phosphotyrosine signaling mediates cell-cell communication and contributes to the development of multicellularity. Proline-rich tyrosine kinase 2 (Pyk2) is a calcium-dependent non-receptor tyrosine kinase of the focal adhesion kinase (FAK) family, enriched in forebrain neurons. Pyk2 activation involves autophosphorylation of Tyr-402, which recruits and activates Src family kinases (SFKs). Pyk2 can also interact with many other molecular partners, in particular through its proline-rich (PR) motifs, which bind SH3 domains. Pyk2 can thus activate, depending on the cell type, different signaling pathways. In the central nervous system, Pyk2 is particularly abundant in neurons of the cerebral cortex, the striatum and the hippocampus where it plays a role in synaptic plasticity.

In this thesis, I studied Pyk2 in neuropathological conditions *in vivo*, using total or conditional knock-out mice. Pyk2 deficit in the hippocampus resulted in alterations of NMDA receptors, PSD-95 and dendritic spines. These defects were associated with an impairment of CA1 LTP and hippocampal-related learning thus confirming the crucial importance of Pyk2 in the expression of synaptic plasticity. Huntington's and Alzheimer's diseases were associated with decreased in total Pyk2 or its activated forms in hippocampus, which contributed to the phenotype of mouse models of these diseases. Overexpression of Pyk2 using adeno-associated virus (Pyk2-AAV) rescued synaptic properties and memory deficits. In parallel with this main project, we showed the efficacy of astrocytic delivery of BDNF (a known activator of Pyk2) in a mouse model of Alzheimer's disease. Conversely, deletion of Pyk2 in the amygdala prevented spine alterations and development of depressive-like symptoms induced by chronic unpredictable stress. Finally, in the striatum, Pyk2 deficiency was not associated with the synaptic defects observed in other brain areas. However, it decreased locomotor response to acute cocaine injection without altering locomotor sensitization and conditioned place preference. This phenotype was recapitulated by deletion of Pyk2 in the nucleus accumbens or in D1 receptor-expressing neurons suggesting a specific role of Pyk2 in these neurons.

Taken together this work supports an important role for Pyk2 in synapses and shows that its alteration contributes to the development of neurological disorders.